

# **FRICTION AND THE TEXTURE OF AGGREGATE PARTICLES USED IN THE ROAD SURFACE COURSE**

---

**ALAN DUNFORD**

Thesis submitted to the University of Nottingham for the  
degree of Doctor of Philosophy

April 2013

---



## **Abstract**

---

Skid resistance, the road surface's contribution to friction, is a crucial property of a road surface course required to maintain a safe and serviceable road network.

Measurement of skid resistance is restricted by the need to measure the forces acting on a rubber wheel or slider while it is dragged across the surface. If the skid resistance of the road could be determined without the need for contact then measurement could be cheaper and more thorough.

One route to achieving this goal is by measurement of the texture of the road that generates the friction experienced by a sliding tyre. However, the form and scale of the texture required is not well defined.

The work presented in this thesis attempts to establish a robust methodology for measurement of texture on the surfaces of aggregate particles (the main constituent of the road surface course) so that it can be compared with friction. The stages of development are described in detail and the methodology is employed to examine the changing texture on two types of aggregate.

The mechanisms by which these aggregates polish, methods for characterising their surface texture, and the consequences for the friction they are able to generate are explored.

---





## Publications

---

Where experiments described in this thesis have been published elsewhere, references are given in the text. In addition, elements of the work presented in Chapters 5, 6 and 7 of this thesis have been published as follows.

Dunford, A. (2010). *PPR538. Measuring skid resistance without contact; 2009-2010 progress report*. Crowthorne: TRL.

Dunford, A. M., Parry, A. R., Shipway, P. H., & Viner, H. E. (2012). Three-dimensional characterisation of surface texture for road stones undergoing simulated traffic wear. *Wear* 292, 188-196.

---



## Acknowledgements

---

There are a great many people to acknowledge and I have run out of words to thank them all properly so they appear here as a list of names.

Dunfords: Catherine, Raspberry, Diana, Bryan, Daniel, Mary

Supervisors: Tony Parry, Helen Viner, Phil Shipway

TRL and (in alphabetical order) Emma Benbow, Stuart Brittain, Nathan Dhillon, Kevin Green, Martin Greene, Rod Kimber, Richard Lodge, Stuart McRobbie, Derek Meachen, Neil Paulley, Peter Roe, Peter Sanders, Richard Woodward, Alex Wright, Dean Wright

NPL and Richard Leach, Claudiu Giusca, James Claverley

UoN and Nigel Neate, Nick Thom

Highways Agency and Louise Caudwell, Ramesh Sinhal

Lafarge and Paul Edwards, John Harris, Robert Gossling

David Woodward and Richard Ellis of University of Ulster

---



# Contents

---

<b>1</b>	<b>Introduction</b>	<b>1</b>
1.1	Background	2
1.2	Research aims	5
1.3	Description of following chapters	6
1.4	References	8
<b>2</b>	<b>Literature review</b>	<b>9</b>
2.1	Friction theory	11
2.1.1	Classical friction	11
2.1.2	Rubber friction	12
2.1.3	Lubrication	20
2.1.4	Summary	22
2.2	Road surface texture	24
2.3	Measuring texture	30
2.3.1	Standard methods for measuring road surface texture	30
2.3.2	Less common or future field measurement techniques	31
2.3.3	Laboratory techniques for measurement of surface texture	35
2.4	Texture characterisation	39
2.4.1	Standard characterisation of road surface texture	39
2.4.2	Experimental characterisation of road surface texture	41
2.4.3	Laboratory	49
2.5	Factors affecting skid resistance	57
2.5.1	Surface texture	57
2.5.2	Other factors affecting skid resistance	63
2.6	Aggregates	67
2.6.1	Specification of road stones	67
2.6.2	Geology of typical road stones	71
2.7	Summary	75
2.8	References	78
<b>3</b>	<b>Feasibility studies</b>	<b>85</b>
3.1	Collecting information about road surface texture	86
3.2	Using information contained in high resolution images of aggregate surfaces	91
3.3	Developing a methodology for measuring and characterising aggregate surface texture	98
3.3.1	Texture measurements	98
3.3.2	Characterising texture	100

3.3.3	Comparing texture and friction	104
3.4	Discussion	107
3.5	References	109
<b>4</b>	<b>First attempts at an improved methodology for examination of surface texture changes</b>	<b>111</b>
4.1	Methodology	112
4.1.1	Specimen	112
4.1.2	Polishing	114
4.1.3	Photography	115
4.1.4	Surface replication	115
4.1.5	Scanning electron microscopy	116
4.1.6	Surface texture measurement	117
4.2	Photography	118
4.3	Scanning electron microscopy	123
4.4	Surface texture measurements	128
4.4.1	Analysis using raw data and Microsoft Excel	128
4.4.2	Texture analysis using data visualisation software	129
4.4.3	Texture analysis using bespoke software	134
4.5	Discussion	137
4.6	References	139
<b>5</b>	<b>Development of a robust methodology to examine surface texture changes</b>	<b>141</b>
5.1	Polishing in the laboratory	142
5.1.1	Methodology for comparing W-S polishing with traffic polishing	142
5.1.2	Progressive polishing of aggregate specimens	147
5.2	Measuring friction in the laboratory	149
5.2.1	Friction measurement using the Wehner-Schulze machine	149
5.2.2	Details of the W-S friction measurement system	150
5.2.3	Measurements of friction for comparison with surface texture	152
5.3	Texture measurement areas and alignment	155
5.4	Texture measurement	161
5.5	Paint erosion	164
5.6	Aggregates	166
5.7	References	168
<b>6</b>	<b>Qualitative analysis of changes in texture during simulated polishing</b>	<b>169</b>
6.1	Friction measurements	170
6.2	Changes observable on whole stone faces	171
6.2.1	Photographic evidence	171
6.2.2	Topographical evidence	175

6.3	Changes that become apparent when considering smaller areas of surface	179
6.4	Analysis in two dimensions	184
6.5	Discussion	187
<b>7</b>	<b>Quantitative analysis of changes in texture during polishing</b>	<b>189</b>
7.1	Development of model profiles against which to examine the surface characterisation techniques	191
7.2	Manual analysis	194
7.3	Power Spectral Density	199
7.4	Fractal analysis	207
7.5	Introduction to roughness parameters	212
7.6	Height parameters	216
7.7	Peak height and peak density	226
7.8	Peak gradient	233
7.9	Volumetric parameters	235
7.10	Height distribution	239
7.11	Correlation between roughness parameters and friction	244
7.12	Inclusion of results from dolerite surfaces	248
7.13	Discussion	250
7.14	References	252
<b>8</b>	<b>Summary and discussion</b>	<b>255</b>
8.1	Introduction	256
8.2	Literature review	257
8.3	Feasibility studies	258
8.4	First attempts at an improved methodology	259
8.5	Development of a robust methodology	260
8.6	Qualitative analysis of changes in texture	261
8.7	Quantitative analysis of changes in texture	262
8.8	General discussion	264
8.9	References	265
<b>9</b>	<b>Conclusions and recommendations for further work</b>	<b>267</b>
9.1	Conclusions	268
9.2	Recommendations for further work	271
9.3	References	273





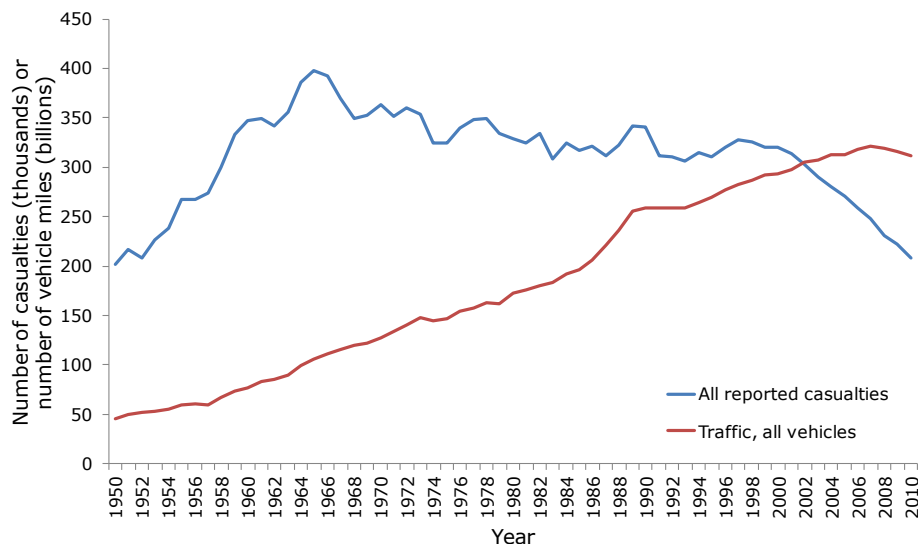
# **1 Introduction**

---

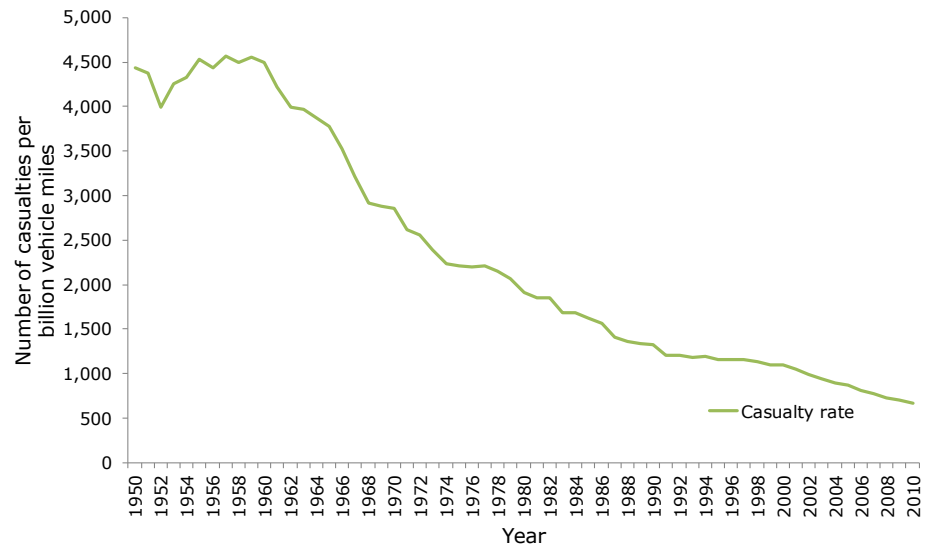
This chapter introduces the work described in this thesis. A background to the project is given by way of justification for the work before broad research questions and specific research aims are presented.

## 1.1 Background

The number of road accidents and casualties reported in the UK has not changed as much, in the last sixty years, as the length of our roads and the number of vehicles using them; Figure 1.1 shows the relatively small fluctuations in thousands of casualties and the substantial increase in billions of vehicle miles. Accident statistics are therefore often presented in terms of a casualty rate per billion vehicle miles (Figure 1.2), which demonstrates a significant reduction so that, despite the increase in road traffic, travel seems to be getting safer (Department for Transport, 2011). The general improvement is often attributed to government safety campaigns (seatbelt and drink-drive campaigns for example) and improved vehicle safety features such as anti-lock braking. Although often uncredited, developments in road surfacing, condition monitoring and policies have played an important part in reducing skidding accidents. In particular, it has been shown that skid resistance is linked to accident risk. For example, Rogers and Gargett (1991) demonstrated an increase in risk for road sites with lower skid resistance and Viner et al (2005) analysed skid resistance and accident data and made conclusions including "For dual carriageways there is a statistically significant trend for accident risk to increase at locations with lower skid resistance".



**Figure 1.1 Number of road casualties and number of vehicle miles in the UK**



**Figure 1.2 UK casualty rate**

In England, the Highways Agency has responsibility for providing a safe and serviceable trunk road network (i.e. motorways and most major roads) and one crucial element of this is to ensure that the roads have adequate skid resistance. For more than two decades, the Agency’s “skid policy” has been to monitor the skid resistance of the network by carrying out thorough routine measurements (Design Manual for Roads and Bridges, 2004). The same, or a similar, policy has typically been adopted by those authorities with responsibility for all other parts of the UK road network. Investigation of better ways to make measurements of skid resistance is where the work described in this thesis began.

Skid resistance can be measured by various types of equipment, but all devices suitable for routine use rely on measuring the forces generated when a rubber tyre or slider is dragged across a wetted surface. The logistics of measuring using specialist devices means that surveys are costly and time consuming. There are other major disadvantages to making measurements in this way:

- For logistical and legal reasons measurements are confined to a small proportion of the road width, generally a single, continuous line in the nearside wheel path of lane 1. Although this is generally supposed to be the area of lowest skid resistance it is possible that other areas of low skid resistance may go undetected.

- Skid resistance measurements made through physical contact vary with the speed of measurement (the friction/speed relationship is described in more detail in Section 2.5). Measurement errors can be introduced when measurement vehicles are unable to maintain a constant speed amongst live traffic, typically for safety reasons.

If skid resistance could be measured, or at least estimated, without contact, then these limitations could be avoided, potentially improving safety. A better, or more complete, understanding of the condition of the road network could lead to improved targeting of maintenance which, in turn, could lead to increased sustainability and cost benefit.

It is thought that the skid resistance of a road is affected by its surface texture, and in particular, by texture with wavelengths less 10 mm. It is already possible to measure texture without contact for wavelengths of 2 mm and higher, but these features are thought, and have been shown empirically, to determine the rate of change in skid resistance with speed (as mentioned above). The actual level of skid resistance is supposedly related to texture on a somewhat finer scale and, unfortunately, this conjecture is almost as far as the theory goes. To complicate matters further, a road's skid resistance is not a constant property, not least because the surface's component parts (mainly the coarse aggregate used in construction) respond to the polishing action of traffic in conjunction with the prevailing weather conditions.

The subject of this thesis is the investigation of aggregate particle (road stone) surface texture, with particular reference to the influence of this texture on the skid resistance of the road pavement and the way it changes as it is polished, either by traffic or in the laboratory. As the work progressed it became clear that there was a need to first develop a robust methodology and so the experimental work described in later chapters is of a practical nature.

## **1.2 Research aims**

Setting aside the technical difficulty with measuring detailed texture of sufficiently small wavelengths at sufficiently high speeds, there are a number of distinct questions to answer before contactless measurement of skid resistance is possible:

- Which wavelengths of texture are important? There may be limits above or below which the texture is less important, or a continuum may be required.
- What form does the texture take? This may be different for the numerous different types of materials used to make road surfaces.
- How can the relevant texture be numerically characterised?
- What is the link between texture and skid resistance?

Devising a robust methodology for proper investigation is a crucial step which has to be undertaken first. The aims of the research presented in the following chapters can be summarised as follows:

- Develop a methodology that will allow observation of changes in surface texture on aggregate particle surfaces as they are polished in the laboratory
- Observe changes in texture on more than one type of aggregate and compare the forms of the texture present and the mechanisms by which texture changes
- Evaluate several numerical methods for their ability to characterise the texture found on aggregate particle surfaces.

### **1.3 Description of following chapters**

This thesis is split into nine chapters. Their titles and contents are as follows:

#### **1. Introduction**

The current chapter introduces the topic of study and states the general questions and specific aims of the research presented in subsequent chapters.

#### **2. Literature review**

Discusses theories proposed for friction generation, methods for measurement and characterisation of texture and concentrates on research undertaken attempting to relate the texture of road stones to friction.

#### **3. Feasibility studies**

Relating primarily to the practical implementation aspects of this project, the experiments described in this chapter explore the feasibility of measuring texture at traffic speed and the feasibility of characterising texture using measurements made in the laboratory.

#### **4. First attempts at an improved methodology for examination of surface texture changes**

Describes an experiment using an early incarnation of the robust methodology described in the next chapter and justifies the need for careful development of such a methodology.

#### **5. Development of a robust methodology to examine surface texture changes**

Describes in detail the methodology developed, including comparisons between polishing in the laboratory and polishing by traffic, and friction testing in the laboratory and skid resistance measurement on in-service roads.

#### **6. Qualitative analysis of changes in texture during simulated polishing**

Observations about the apparent changes in texture on the surfaces of two aggregates as they are polished in the laboratory are presented.

## **7. Quantitative analysis of changes in texture during polishing**

Explains the attempts made to characterise the surface texture of aggregate surfaces and the potential for development of a numerical relationship between texture and friction.

## **8. Summary and discussion**

Collates the findings from preceding chapters and discusses their implications.

## **9. Conclusions and recommendations for further work**

Discusses the research presented in this thesis in the context of the research questions and the research aims posed at outset. This chapter also proposes further work that should be carried out to advance the understanding of the relationship between friction and the texture of aggregate particle surfaces.

## 1.4 References

- Design Manual for Roads and Bridges. (2004, August). *Volume 7 Section 3, HD28/04, Skid resistance*. London: The Stationery Office.
- Department for Transport. (2011, December 15). *RAS40007 Reported road accidents and casualties: 1950 onwards*. Retrieved July 20, 2012, from DfT Transport Statistics:  
<http://www.dft.gov.uk/statistics/tables/ras40007/>
- Rogers, M. P., & Gargett, T. (1991). A skidding resistance standard for the national road network. *Highways And Transportation*, 38, 10-16.
- Viner, H. E., Sinhal, R., & Parry, A. R. (2005). Linking road traffic accidents with skid resistance - recent UK developments. *International Safer Roads Conference*. Cheltenham.



## 2 Literature review

---

The first research aim is to develop a robust methodology for observation of aggregate particle surface texture during polishing in the laboratory. In order to tailor the methodology to allow investigation of the most pertinent features of aggregate surfaces it is necessary to develop an understanding of a range of subjects. This chapter therefore presents a review of available literature with particular attention to the topics listed below.

### 1. Friction theory

The mechanisms involved in opposing the movement of one body sliding against another. There are many theories about friction interaction, rigorously debated and without general consensus, and some elements are likely to be useful when considering what characteristics of a pavement surface effect and affect its skid resistance.

### 2. Road surface texture

Definitions of various scales of texture such as macrotexture and microtexture, the need for pavement microtexture and methods used to measure pavement texture. It has been well established that the surface texture of a pavement is a critical element of the road/tyre interaction and there exist several commonly used descriptions of surface texture. Empirical evidence has suggested that the various discrete scales of texture influence various performance criteria. The smallest scale of texture, microtexture, has the greatest influence on slow speed skid resistance in the wet, and macrotexture (the next size up) influences the speed dependence of friction seen by a sliding tyre. Macrotexture is routinely measured on pavement surfaces, but microtexture is not (although low speed skidding resistance is measured directly).

### 3. Texture measurement

Methods used to measure surface texture. Surface texture plays a vital role in many applications, particularly when considering machine components, and its measurement has therefore been an important exercise for many decades. Measurement of pavement surface texture is somewhat newer and there are several common techniques used in both fields.

#### 4. Texture characterisation

Methods used to describe a surface's texture. There are well established methods of characterising a pavement's macrotexture, and there are standard parameters used in engineering to describe elements of a surface's roughness. While some researchers have attempted to characterise microtexture of pavement surfaces there is no established methodology for doing so.

#### 5. Factors (including texture) affecting skid resistance

Attempts to compare texture and skid resistance, or estimate skid resistance based on texture measurements alone. The relationship between macrotexture and the friction/speed curve has been well documented. Researchers have frequently attempted (with some success) to calculate the skid resistance expected on a surface at any speed given its skid resistance at one speed and a measure of macrotexture. However, partly because of the relative difficulty of measuring microtexture and the lack of an established method for microtexture characterisation, the link between microtexture and skid resistance is less well understood.

#### 6. Aggregates

Characteristics of a variety of rocks used as aggregate in UK roads and standardised methods to measure their polish resistance. Different stones react to the action of polishing by traffic, and to other external factors, differently depending on their geological makeup. It will be important to consider an aggregate's mineralogy and expected behaviour when studying its surface texture.

## 2.1 Friction theory

The research carried out for this PhD is primarily concerned with the skid resistance of the road surface (i.e. the road's contribution to road/tyre interaction and the resultant friction force) and the characterisation of texture that affects skid resistance. To a certain extent it is independent of the added complications of tyre rubber's behaviour and of the hydrodynamic flow of water that is frequently present on the road surface. However, in order to understand the features of road surfaces that will contribute to its skid resistance, it is necessary to first explore mechanisms of friction as a whole. Note, therefore, that this section deals primarily with theory as examined in the laboratory using idealised rubber compounds and idealised surfaces. Comments about the relevance of the theory for tyre/road interaction are made at the end of the section.

### 2.1.1 *Classical friction*

The laws of friction, as taught in schools, can be found in many texts, the first reference source in this literature review is from a well-known online encyclopaedia.

Guillaume Amontons published his laws of friction in 1699, based on notes made by Leonardo da Vinci, and they were amended by Charles-Augustin de Coulomb and Leonhard Euler. The resulting three laws of friction, which apply in dry conditions, can be summarised as (Wikipedia):

- The force of friction is directly proportional to the applied load (Amontons's 1st Law)
- The force of friction is independent of the apparent area of contact (Amontons's 2nd Law)
- Kinetic friction is independent of the sliding velocity (Coulomb's Law).

Through mathematical description of the interactions, Euler also contributed a further observation:

- Static friction is greater than kinetic friction.

Amontons's two laws are summarised by the equation:

$$F = \mu N \quad 2.1$$

where  $F$  is the force due to friction,  $N$  is the normal force and  $\mu$  is the coefficient of friction.  $\mu$  is specific to the two materials in contact, is dimensionless, and can only be found empirically.

Substantial further work to develop the understanding of friction was carried out by Bowden and Tabor, and they popularised the adhesion model of friction: “the frictional resistance between un-lubricated metals is due primarily to the shearing of the metallic junctions formed by adhesion and welding at the points of contact” (Bowden & Tabor, Mechanism of metallic friction, 1942). A further theory, demonstrated experimentally and published in 1950 (Bowden & Tabor, The friction and lubrication of solids, 1950), suggested that the true area of contact, being only a proportion of the apparent area of contact, even for apparently smooth surfaces, increases with increasing normal force as more asperities come into contact and those already in contact plastically deform.

David Tabor, incidentally, was part of the committee that proposed the term ‘tribology’ for the study of frictional interaction between solids (Field, 2008).

The field of study for frictional interaction between metals and other plastically deforming materials is large. Any further review of literature not dealing with rubber could be considered unproductive because rubber (and therefore any vehicle tyre) does not obey any of the above described ‘laws’ of friction. The concept of friction due to adhesion forces, and the work of Tabor, is relevant.

### **2.1.2 Rubber friction**

Being one half of the tyre/road interaction, the properties of tyres (i.e. rubber) are very important. Rubber, both natural and synthetic, is composed of polymers (long chains of molecules linked by covalent bonding); it is a viscoelastic material. Its viscoelasticity has a direct bearing on the various theories governing frictional forces experienced when rubber is involved.

Kummer (1966) presented a generalised model for sliding tyres:

$$F_T = F_A + F_{Hb} + F_C \quad 2.2$$

where  $F_T$  is the total frictional resistance developed between a sliding tyre and a dry pavement,  $F_A$  is the frictional contribution from adhesion of the two surfaces,  $F_{Hb}$  is the frictional contribution from bulk deformation hysteresis in the rubber and  $F_C$  is a contribution from rubber wear. He

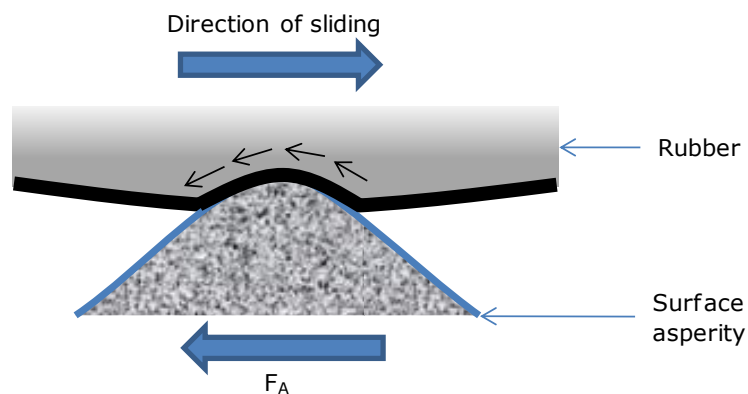
considered the force due to wear to be 'intrinsic' and relatively small (1-2%) in all non-emergency braking. Even in emergency braking situations, where  $F_C$  is more significant, it will depend largely on the tyre composition and is likely to be highest on those surfaces already providing high  $F_A$  and  $F_{Hb}$ .

Roth, Driscoll and Holt (1942) carried out experiments to investigate the friction between rubber and hard surfaces. They used rubber specimens and testing surfaces, prepared in the laboratory, set up on a horizontal track system. The rubber specimens had a similar composition to soft rubber compounds used in vehicle tyres. Various loads were applied to the sliding rubber specimens and it was found that the coefficient of friction (Equation 2.1) decreased with increasing load. They also found that different specimen sizes exhibited different friction coefficients, so that  $\mu$  appeared to be area dependent.

Similar experiments by Thirion (1946) led to the same conclusions: that  $\mu$  decreases with load and is area dependent. The concept of adhesion was used to explain the friction between rubber and the smooth glass plates used.

#### 2.1.2.1 Adhesion

The friction force due to adhesion is due to a molecular interaction at the sliding interface - molecular chains (polymers) in the rubber surface attempt to link with molecules in the hard surface and the bonding, stretching and breaking cycle results in a retarding force. Figure 2.1 shows a standard diagrammatic representation of the adhesion component of friction.



**Figure 2.1 Friction force due to adhesion**

Adhesion can be considered as a sum of forces between individual points of contact so that:

$$F_A = \sum_i n_i j_i \quad 2.3$$

where  $n_i$  is the number of molecular junctions between the surfaces at location  $i$  and  $j_i$  is the effective junction or bond strength. So, the more points of contact, the greater the adhesive friction.

The conflict between this interpretation and Amontons's laws was resolved for plastic deformation: the true area of contact, which, due to the presence of small asperities is smaller than the apparent area of contact, is proportional or nearly proportional to the load applied (Bowden & Tabor, 1950). This is further expanded by researchers such as Shallamach (1952) who showed that frictional force is dependent on the true area of contact and that, for rubbers, its variation with load is consistent with Hertz's formula:

$$d = 2.2 \left( \frac{Wr}{2E} \right)^{\frac{1}{3}} \quad 2.4$$

where  $d$  is the diameter of a circle formed when an elastic sphere is flattened against a hard surface,  $W$  is the normal load,  $r$  is the sphere's radius and  $E$  is Young's modulus of the sphere. So that the coefficient of friction becomes:

$$\mu = cW^{-\frac{1}{3}} \quad 2.5$$

where  $c$  is a factor to be determined empirically.

Lorenz et al. (2010), who note that a full comprehension of contact between randomly rough surfaces has not yet been achieved, present two theories governing separation of two surfaces, including the difference between actual and apparent contact, when two solids are squeezed together. A simple experiment, whereby a near-elastic rubber block was pressed against an asphalt block and a concrete block in turn, showed that increasing squeezing pressure caused an exponential decrease in surface separation.

#### 2.1.2.2 *Hysteresis*

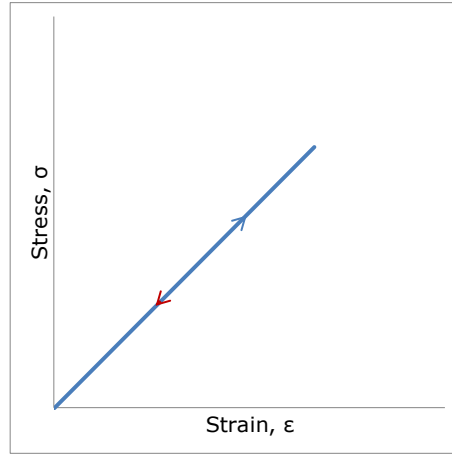
Friction caused by hysteresis (Kummer, 1966) comes into play when demonstrating that rubber does not obey the third law of friction (Coulomb's), that friction is independent of sliding velocity.

When a viscoelastic material deforms it exhibits properties of both viscous materials and elastic materials. To differentiate between viscous, elastic and viscoelastic, it is necessary to consider stress and strain. Strain,  $\epsilon$ , is a measure of the relative displacement between particles in a material body in response to the application of some force, or stress,  $\sigma$ . Strain is unitless: the length of deformation per length of original size. Stress, with units of  $\text{Nm}^{-2}$ , is measured in relation to the unit area to which it is applied.

- Viscous materials deform linearly with time under a given stress: the longer the stress is present, the greater the strain. Viscous materials do not return to their original shape when the stress is removed.
- Elastic materials deform instantaneously when stress is applied and can return to their original shape when the stress is removed.
- Viscoelastic materials have properties of both; the relationship between stress and strain is dependent on time and the material can return to its original shape when the stress is removed.

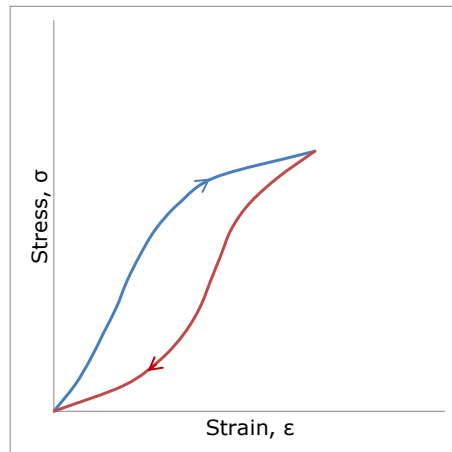
Tabor (1955) carried out experiments using smooth steel spheres, of various radii, rolling in rubber grooves. He found that a considerable friction force still acted even when lubricants were present separating the surfaces (so preventing, or at least suppressing, adhesion). He concluded that there must be another mechanism acting to oppose the motion of the spheres and that it must be related to the work done compressing or stretching the rubber.

When stress is applied to a purely elastic material, the material deforms instantly, and it also deforms linearly with the amount of stress applied. When the stress is removed, the material instantly returns to its original form. This can be shown in a stress-strain curve, as in Figure 2.2, which shows the stress required for any given strain (or the strain achieved at any given stress) and is the same whether loading or unloading is being performed.



**Figure 2.2 Elastic stress-strain**

When stress is applied to rubber, because it is viscoelastic, the deformation is not proportional to the amount of stress applied. Furthermore, as the stress is removed, the reformation of the material is neither proportional to the amount of stress, nor opposite to the amount of deformation that occurred when the stress was applied. This can be represented in a typical hysteresis loop as in Figure 2.3. As more and more stress is applied, the amount of deformation (measured by strain) increases non-linearly along the blue, loading, path (top). As stress is removed, the amount of deformation reduces more slowly at first, along the red, unloading, path (bottom).



**Figure 2.3 Viscoelastic stress-strain hysteresis loop**

The area under stress-strain curves is given by:

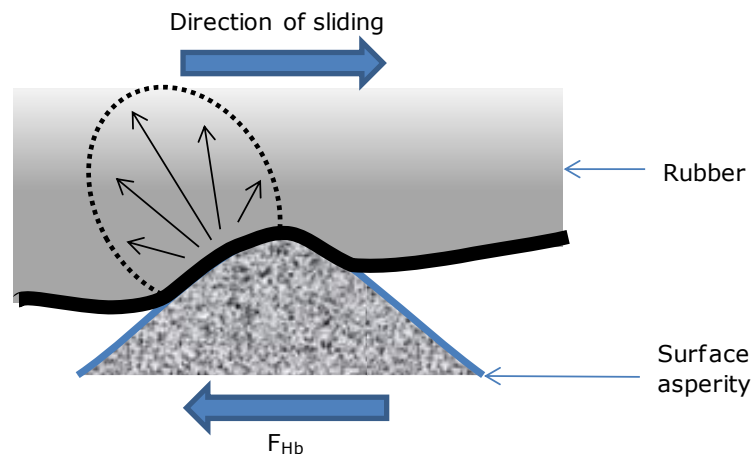
$$\int_0^{\epsilon} \sigma d\epsilon = \int \frac{F}{A} \frac{dl}{l} = \frac{1}{V} \int F dl \quad 2.6$$

where  $F$  is the force applied per area  $A$  of material (stress) and  $dl$  is the amount of deformation in the material relative to its original size,  $l$  (strain). So, the area under the curve is equal to amount of work done (force



multiplied by distance moved) per unit volume of material. In a hysteresis loop, the amount of energy required to deform the material (area under the blue curve) is greater than the energy released when the material reforms (area under the red curve). The difference in energy is dissipated as heat. Energy is lost as a tyre rolls over a rough surface (as in Tabor's experiments) when the surface causes a deformation.

Because reformation is slower than deformation, when surface roughness exists, the motion of a sliding tyre causes an asymmetrical draping of rubber over a surface asperity. The rubber tends to pile up on the leading edge of the asperity and break contact with trailing edge of the asperity at a higher point. In this way, a pressure distribution is formed that has a net opposition to the direction of sliding, shown diagrammatically in Figure 2.4.



**Figure 2.4 Friction force due to hysteresis**

A more detailed analysis of hysteresis includes consideration that, for rubber, when a stress is applied the resulting strain can become out of phase (Roch, 1994). At low temperatures (below the 'glass transition temperature') polymer chains in rubber will not move about freely. At high temperatures, polymer chains are able to move and the rubber becomes almost elastic. In between these two temperatures polymer chains can move but only if there is space available to do so, which depends on the movement of other polymer chains. So, when a stress is applied it takes time for the polymer chains to align in the direction of that stress and deformation therefore lags behind the stress applied. The effect can be observed by application of a sinusoidal stress to a rubber specimen: the deformation will also be sinusoidal, but will lag behind by a phase angle. It has been shown that the hysteretic loss in the rubber is related to the tangent of this phase angle. As the frequency of the stress applied

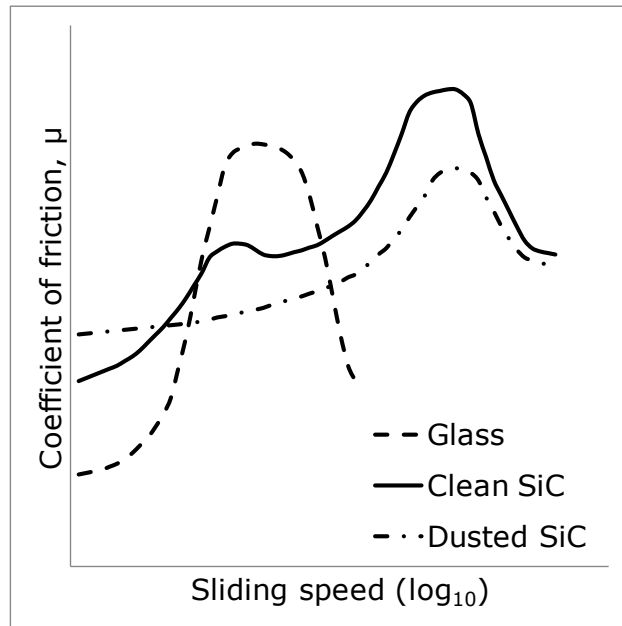
increases, so too does the phase angle. For a sliding rubber block, the frequency of the stress applied is related to the speed of sliding and the size and spacing of surface asperities.

It is possible, apparently, to optimise the damping properties of rubber tyres so that they provide improved wet skid resistance without detrimental increase in rolling resistance (a factor not covered in this review but which is undesirable from an efficiency and environmental point of view). Rubber polymers have been developed that are tuned to generate hysteretic loss under different conditions. So, when the tyre is sliding, hysteretic loss will be greater because tyre deformations occur at higher frequencies than when the tyre is rolling (Roch, 1994).

#### *2.1.2.3 Adhesion and hysteresis together, and further possible mechanisms*

To further investigate hysteretic bulk deformation theories, Grosch (1963) carried out experiments by sliding various surfaces at different speeds against five types of rubber. While carefully controlling temperature and measuring the forces generated, he pressed flat rubber specimens against a moving track surface using a dead load suspended below. The surfaces included silicon carbide paper and smooth, but wavy, glass; the experiment was repeated for each of these surfaces after coating in a fine magnesium powder (separating rubber from the surface and suppressing adhesion).

Grosch plotted master curves, using results corrected to a reference temperature, for coefficient of friction,  $\mu$ , against the logarithm of the test surface sliding speed. He found that, on the glass surface,  $\mu$  increased to a maximum at a particular speed, and then decreased. He noted that when the experiment was repeated on a glass surface dusted with magnesium powder, the friction measured remained almost constant over the range of speeds. For the rough silicon carbide paper surface, the  $\mu$ -speed curve exhibited a significant peak at higher speeds, and often, a smaller peak at a lower speed, coinciding with the one found on un-dusted glass. When silicon carbide surfaces were dusted, the higher speed peak was reduced, and the lower peak was eliminated. The graph in Figure 2.5 gives a graphical representation of the approximate results.



**Figure 2.5 Coefficient of friction against speed**

It is thought that the adhesive interaction relies on bonds between the surface and the rubber forming and breaking. The rate at which this can occur is limited by the size of bonds and the size of polymer chains in the rubber. The maximum adhesive friction is therefore experienced at relatively low speed. Friction due to hysteretic losses depends on the frequency of application of the stress and this is related to the sliding speed and the size/spacing of asperities on the surface, which is a lot larger than the size of polymer chains. The speed at which hysteretic friction reaches a maximum is therefore generally higher. The exact speed at which these maxima occur is governed by the properties of the rubber.

Savkoor (1965), Kummer (1966) and Yandell (1970), amongst others, also suggested the existence of a fourth mechanism of friction. The mechanism arises because macroscopically smooth surfaces can be microscopically rough, and micro-asperities on a rubber surface could interact with the micro-asperities on the hard surface, causing surface (as opposed to bulk-) hysteresis or '*microhysteresis*',  $F_{Hs}$ .

In his recent book, Smith (2008) summarises the results from a number of experiments looking at the mechanisms of friction (as above) and performs back-calculations using the results. He shows that, in the majority of cases, when the total frictional force is considered in its component parts, there is a remaining unaccounted-for component. This fourth component, also attributed to '*microhysteresis*', is independent of applied load, and is proportional to the contact area.

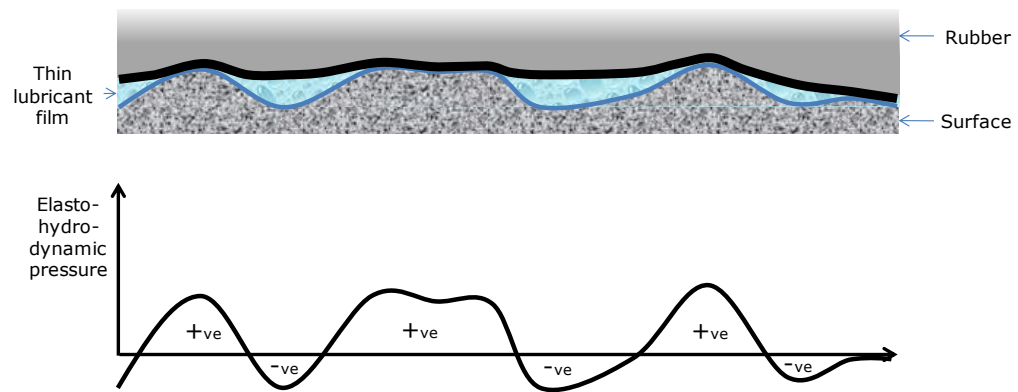
Using finite element analysis and considering either rigid spheres indenting rubber surfaces or rubber spheres sliding on rigid surfaces, Gabriel et al. (2010) suggested an additional frictional force,  $F_{Geometry}$ , that exists in the former but not in the latter. The magnitude of this additional mechanical force is dependent on the penetration of the rigid body into the elastomer. Further work will consider more complicated, multi-asperity surface interactions such as that of the tyre and road.

Using rubber spheres sliding on a hard surface, Schallamach (1971) observed that rather than slipping past one another, folds are generated within the contact area, known as waves of detachment (or *Schallamach waves*). The waves run from the front to the rear edge of the 'sliding' rubber and, as with a fold in a rug that moves over a floor, the rubber can become displaced relative to the hard surface without truly sliding against it. In a more recent paper, Fukahori et al. (2010) cites a number of attempts to specifically investigate Schallamach waves. Amongst other observations it is noted that the frequency of the waves is dependent on sliding speed, Schallamach waves are not observed below a certain critical sliding velocity, and the presence of these waves reduces contact area.

It should be noted, however, that the Schallamach waves are generally only observed when the elastomeric compound is very soft and the surfaces generate a very high level of friction. It has therefore been suggested that the waves are strictly an effect of friction rather than a cause of it (Savkoor A. R., 1987).

### **2.1.3      *Lubrication***

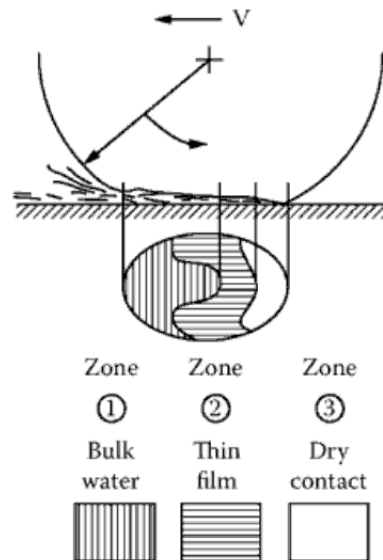
The introduction of a lubricating film between two surfaces will generally reduce the coefficient of friction, and therefore the frictional force experienced. When the two surfaces are rigid the forces experienced can be modelled using Navier-Stokes and Reynolds's equations. Once again, rubber makes things more complicated. Except in flooded conditions, rubber will drape over asperities in a rigid surface so that there is more separation (filled with the lubricating film) in some regions than in others. Moore (1975) presents a diagrammatic representation of rubber draping, and the resulting 'elastohydrodynamic' pressures involved, similar to Figure 2.6. Positive pressure outweighs negative pressure and there is a net separating effect.



**Figure 2.6 Elastohydrodynamic separating effect in lubricated sliding**

The diagram above appears to show a boundary lubrication condition, where some of the rubber is in contact with lubricant and some is in contact with the solid surface. However, during sliding, because of the flowing action of the rubber, some of the lubricant is also dragged over the asperity tips. If the asperities are smooth and rounded, complete separation may occur, drastically reducing the coefficient of friction. If there is some roughness at the asperity tips, the lubricant film is broken and adhesion can occur. This theory that road surface roughness is required to break through a lubricating film of water is revisited in Section 2.2.

If there is sufficient water on the surface (the lubricant in the case of tyre/road interaction is generally water), there are likely to be regions where the tyre does not contact the road at all. It is thought that, when a tyre rolls or slides over a wet road surface, there are three distinct zones of contact (Gough, 1974) and (Moore, 1975). The tyre squeezes water out in front of it and the front part of the tyre, in zone 1, floats on an unbroken thin film of water. Further back, in zone 2, the tyre is able to drape over the larger asperities and will begin to make actual contact with the smaller asperities. In zone 3, only a thin film of water may remain, and in this area the tyre makes contact with the surface through the film. The relative size of these three zones depends on speed, and above a critical speed there may be no contact with the pavement leading to hydroplaning.



**Figure 2.7 Three zone contact concept**  
*from (Smith, 2008)*

#### **2.1.4 Summary**

Considerable work has been carried out by the tyre manufacturing industry to study the mechanisms of friction between the road and their product. Indeed, a number of the papers referred to above are the result of research funded by rubber and tyre producers.

The literature has shown, as expected, that tyre/road interaction is a complex phenomenon, further complicated by the unusual and less predictable (through classical mechanics at least) behaviour of viscoelastic rubber. Smith (2008) neatly summarises results from a large number of rubber friction experiments and shows that in the vast majority, the laws of (metallic) friction do not apply.

When considering the way in which surface texture effects a road's skid resistance, three of the well documented rubber-friction phenomena will be of particular interest:

- The coefficient of friction is related to the true area of contact.
- The coefficient of friction is dependent on asperity distribution leading to:
- The friction force generated is dependent on sliding speed.

It may also be useful to bear in mind that the coefficient of friction reaches a maximum as the true contact area saturates, and that there is normally a peak in friction at a given sliding speed which is dependent on material properties.

The remainder of this review will deal with the other half of the tyre/road interaction problem, (i.e. the road surface) and the next section discusses road surface texture.

## 2.2 Road surface texture

The previous section started with a brief review of classical friction theory. However, it was noted that the application of that theory, where the properties of rubber had not been taken into account, is not necessarily relevant to the study of tyre/road interaction. Similarly, research dealing with idealised surfaces created in the laboratory or surfaces existing only in theory, may not apply to road or aggregate surfaces.

In his thesis dealing with the dry adhesive friction of elastomers, Savkoor (1987) notes:

"...it may be argued from experience that when the many surfaces which may not be "smooth textured" initially, do become so after having "run-in" for some time so that the shapes of their asperity tips are most likely to be smooth and convex. Such smooth and convex shapes can be represented generally by a curved surface having two principal radii of curvature..."

Savkoor goes on to restrict his theoretical work to the case of ideal spherical asperities.

Another frequently used simplification is that of a self-affine fractal surface (Persson, 2001). In these surfaces, given the correct scale transformation, very fine texture has the same form as texture on a larger scale, which in turn has the same form as texture on a larger scale again. Fractal dimensions will be discussed in more detail when considering methods for characterisation of surface texture.

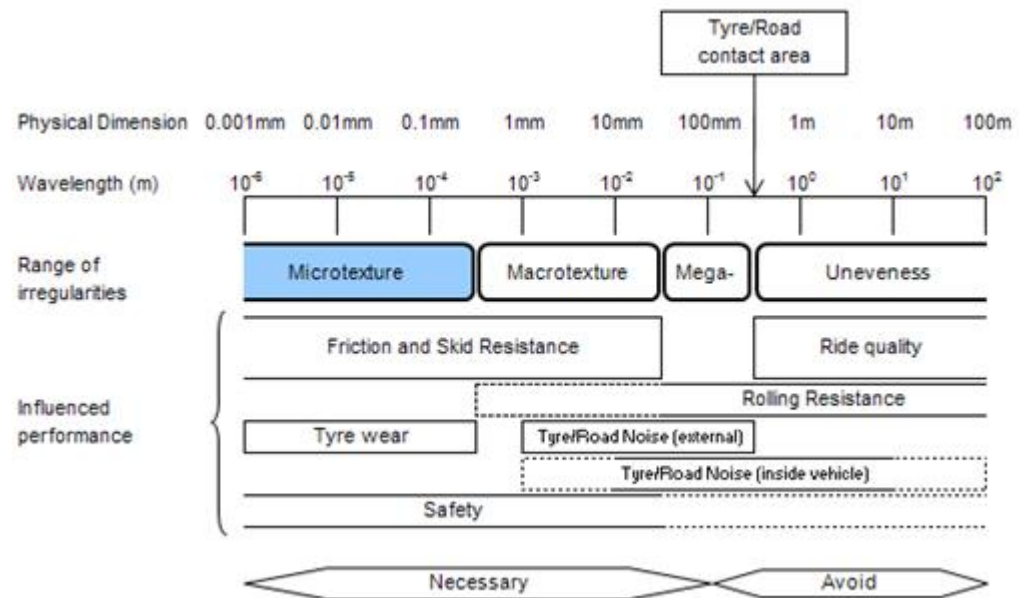
These are common, and perhaps necessary, assumptions because rubber friction is complicated enough without also dealing with surface texture. However, since the research presented in this thesis is aimed at measurement and characterisation of surface texture (rather than a study of friction) this section skips over theoretical treatments of surface texture straight to a review of accepted definitions of road surface texture and its perceived necessity.

The geometric profile of the road in the vertical plane has traditionally been divided into different scales depending on the dynamic response of interest to vehicles or vehicle passengers e.g. ride comfort, skidding resistance, rolling noise, and vehicle operating cost factors.

Figure 2.8 shows the range of each surface characteristic as expanded from those defined by PIARC in the report of the Brussels Congress (PIARC,



1987). It should be noted that, in general, large amplitudes are desirable when wavelengths are below 10 mm and small amplitudes are desirable for wavelengths above 10 mm. The surface characteristics are divided into four general pavement surface features – unevenness, megatexture, macrotexture and microtexture – which are discussed below.



**Figure 2.8 Surface texture characteristics**




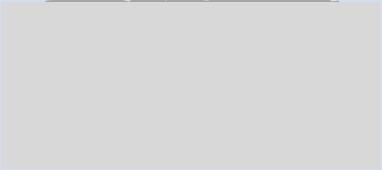
- The *unevenness* of the road surface, with wavelengths from 0.5 m to 50 m, is associated with longitudinal profiles larger than the tyre footprint. It affects vehicle dynamics, ride quality, dynamic loads, and drainage. In extreme cases, unevenness can lead to loss of contact with the surface, and it is normally caused either by poor initial construction or deformation caused by loading.
- The road's *megatexture* refers to deviations with wavelengths from 50 mm to 500 mm. Examples of megatexture include ruts, potholes, major joints and cracks. It affects vibration in the tyre walls but not the vehicle suspension, and it is therefore strongly associated with noise and rolling resistance. Although megatexture generally has larger dimensions than those which affect skid resistance, it is possible that this scale of texture could influence tyre/road contact.
- *Macrotexture* is the amplitude of deviations with wavelengths from 0.5 mm to 50 mm, and is effected by the size, shape, spacing and arrangement of coarse aggregate particles. Macrotexture affects

mainly tyre noise and water drainage from the tyre footprint. This scale of texture is thought to be important for hysteretic friction, especially at high speed.

- *Microtexture* is the amplitude of deviations with wavelengths less than or equal to 0.5 mm. This scale of texture is measured on the micron scale, and is typically found on the surfaces of coarse aggregate particles (rather than being due to the gaps between them as in macrotexture) or the texture of bituminous mortar and fine material. Microtexture is frequently therefore a function of aggregate particle mineralogy and petrology and is affected by climate/weather effects and traffic action. The microtexture of the road surface is thought to affect skid resistance at all speeds for dry and wet conditions.

The scales of surface irregularities that affect skid resistance are illustrated in Table 2.1 along with terms used to describe them .

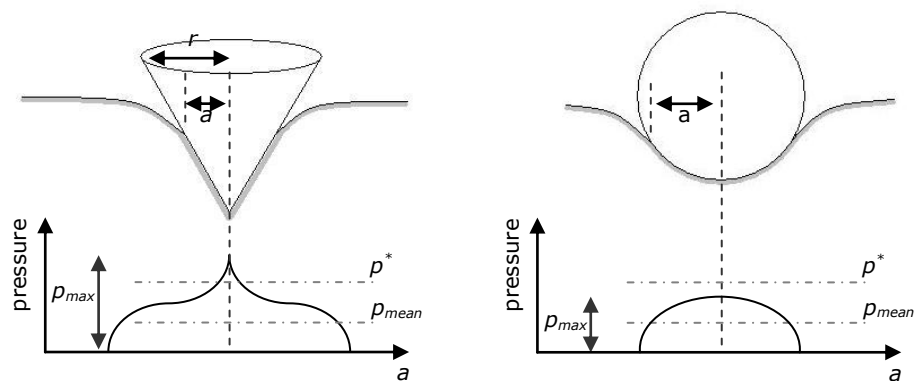
**Table 2.1 Illustration of terms used to describe road surface texture**

Surface	Scale of texture	
	Macro (large)	Micro (fine)
A 	Rough	Harsh
B 	Rough	Polished
C 	Smooth	Harsh
D 	Smooth	Polished

Experimental results show that surfaces with harsh microtexture, but smooth macrotexture, have high skid resistance at low speed, but the rate at which friction reduces with increasing speed is greater than for surfaces with rough macrotexture – this is expanded in Section 2.5.

Considering a pavement under wet conditions, the presence of a thin film of water obscuring contact between the tyre and surface drives the requirement for roughness, and the shape of roughness required. The following is an analysis of the requirement for pavement roughness in wet conditions from Moore (1975).

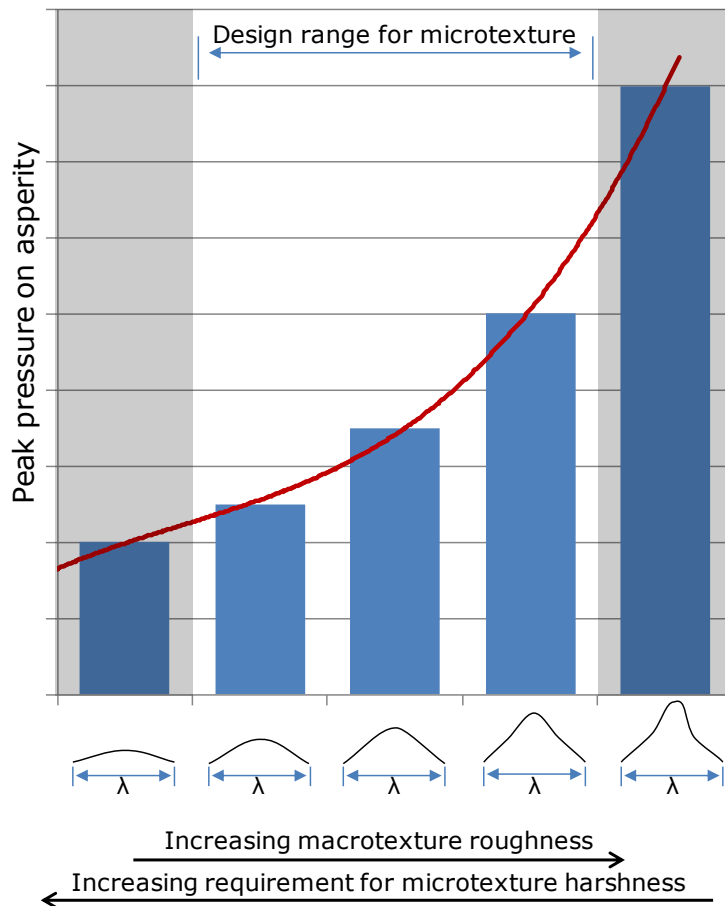
Two extreme examples of roughness shape, the cone and the sphere, are illustrated in Figure 2.9. Let  $p^*$  be the minimum pressure required to break through the water film on the surface. If a load is applied to the cone shape such that the maximum pressure exerted on the tyre,  $p_{max}$ , is just more than  $p^*$ , then the same load applied to the sphere will result in a maximum pressure exerted which is less than  $p^*$  and no penetration of the water film can occur. However, since the cone would be subject to severe wear at its peak, a compromise between the two shapes is required.



**Figure 2.9 Examples of pressure distribution in tyre surface**

It is generally agreed that surface macrotexture is required in wet conditions so that the bulk of water present can be drained away and also to generate friction through tyre deformation and therefore bulk hysteresis. A surface requires microtexture so that it can break through any remaining film of water. The graph in Figure 2.10 demonstrates the trade-off between macrotexture and microtexture. On the extreme left of the graph, if the pavement has relatively smooth macrotexture, then the surface will have insufficient drainage and there will be little or no contact with the tyre regardless of the amount of microtexture present. On the extreme right of the graph, the shape of asperities and therefore the roughness of the

macrotexture is sufficient by itself to break through any water present on the surface; again microtexture is not necessary. Most pavement surfaces will have macrotexture somewhere in between these two extremes and microtexture, therefore, will be required for adequate friction in wet conditions.



**Figure 2.10 Microtexture requirements for pavement design**

Sabey (1958) investigated the friction between rubber and various sliding shapes under wet conditions. Her tests showed that the coefficient of friction under wet conditions is closely related to the pressure over the contact area between the sliders and the rubber. It was concluded that, to ensure good skid resistance in wet conditions, surface asperities should be such that average pressures of  $1000 \text{ lb in}^{-2}$  (approximately 6.9 MPa) are set up on them, and that individual projections should have angles at their tips of  $90^\circ$  or less.

Experiments carried out in the laboratory to investigate the influence on friction of water depth determined a critical water depth at the transition between boundary and mixed lubrication regimes (Do, Cerezo, Beautru, & Kane, 2013). During friction testing it is supposed that the test slider is

partly supported by asperities emerging through the water film and partly supported by the water film itself (see Section 2.1.3). Consideration of the theoretical deformation of the rubber slider alone could not differentiate between surfaces with and without microtexture and so it was concluded that an adhesion component of force, relating to the contact between the slider and the emerging asperities was required.

## **2.3 Measuring texture**

The texture that is generally believed to have the greatest effect on a road's skid resistance has wavelengths lower than 50 mm and amplitudes are typically less than 5 mm (PIARC, 1987) i.e. macrotexture and microtexture. Clearly there are additional practical considerations driving the techniques that are suitable for measurement in the field, including speed, robustness and accuracy.

However, since the intention of this project is to make detailed measurements of surface texture, any device or technique that is capable of measuring texture within the specified range is potentially of relevance. This section first describes the techniques that are well established for measurement of road surface texture, then techniques that may be useful for field measurement in the future, and finally techniques that will probably only ever be possible under controlled laboratory conditions.

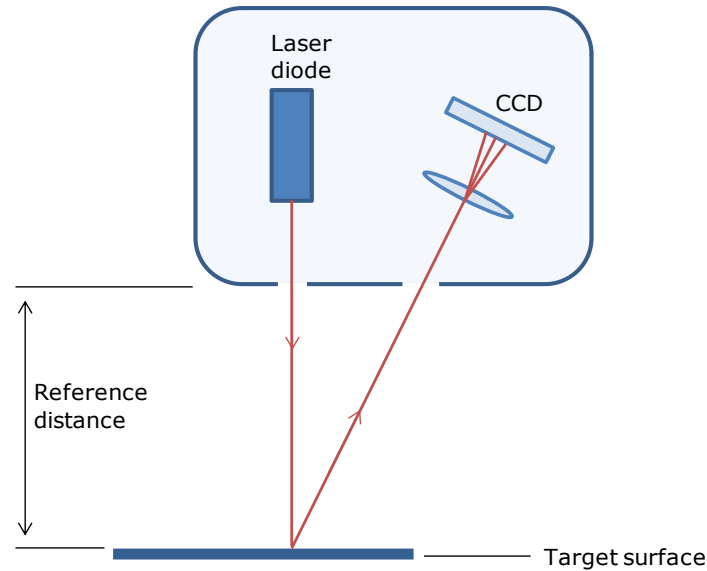
Macrotexture is routinely measured on in-service roads and although there have been various methods employed in the past, in the UK macrotexture is now almost exclusively measured using the volumetric patch technique or using distance measuring lasers.

### **2.3.1 *Standard methods for measuring road surface texture***

The volumetric patch technique is documented in a British Standard (British Standards, 2010). A known volume of sand (or glass beads) is spread evenly over the surface to be measured, in a circular pattern. The diameter of the resulting circle of sand is measured and used to estimate the mean texture depth (MTD) of the surface. This method is accurate and repeatable and, importantly, gives a direct measurement of surface texture, but requires a stationary operator and a traffic-free road. In the UK, it is still used for new surfacing before the road is opened to traffic, and when the road is closed for other reasons (such as when cores are taken to assess structural condition). However, for large scale measurements and traffic speed surveys, distance measuring lasers are used to produce a surface profile from which texture depth can be estimated by calculation.

The lasers employed use triangulation to measure distance - a laser spot or line is projected onto the surface and its reflection from the surface is focused onto an optical detector. If the angles between the laser source and the detector are known, then the height of the surface can be

calculated. Servo systems are often installed in the measuring device to keep the laser at a known reference distance from the surface, allowing the small changes in distance due to surface asperities to be measured. This type of laser system is represented in Figure 2.11.



**Figure 2.11 Laser triangulation**

The distances measured by the laser are then used to calculate either 'Sensor Measured Texture Depth' (SMTD) or 'Mean Profile Depth' (MPD), discussed in Section 2.4, which are used as measures of macrotexture.

### **2.3.2 Less common or future field measurement techniques**

One technique that is frequently examined for use in measurement of road surface texture is that of profile projection. Essentially, light, in a straight line, is projected onto a surface at an angle, and then photographed. The resulting image of the straight line can be used to measure surface profile directly (Forster, 1989), although the resolution of this technique depends on the image resolution and the method of measurement. The method employed by Forster is as follows: the surface is coated with white paint and a semi circle of light is projected onto the surface at an angle of  $45^\circ$  so that a straight line is sharply focussed on the surface. Viewed from above, the straight line traces the vertical profile of the surface which can then be photographed and measured using a microscope or by projection onto a screen with a calibrated scale.

A study to assess laser triangulation under structured lighting as a potential method for determination of road surface microtexture was carried out by Demeyere and Eugène (2004). The method described,

which also had applications in several areas of general metrology, used a laser to cast a line onto a road surface under test, which is observed using a digital camera. The 3D coordinates of each point on the laser curve were calculated leading to determination of the road microprofile with a claimed accuracy of approximately 10  $\mu\text{m}$ .

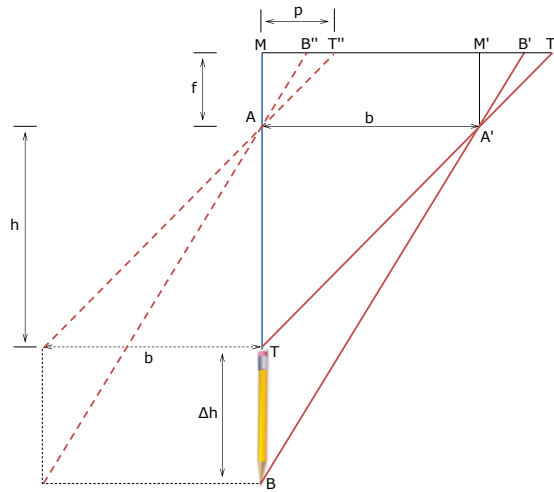
Another commonly investigated technique is stereopsis, which is a field of photogrammetry, also referred to as stereo-photogrammetry or stereovision. Sabey and Lupton (1967) describe the technique and prototype equipment used to capture texture information about asphalt surfaces. Figure 2.12 shows a copy of the simple ray diagram they used to explain the principle. If a pencil, standing on its end, is photographed from directly above and from a position slightly displaced, the two images created when they are superimposed will also be slightly displaced. The top (T) and bottom (B) of the pencil will superpose in an image taken from directly above, at position M, when the camera lens is at position A. If the camera lens is moved a distance  $b$  to the right, to position A', the images of the top and bottom of the pencil appear at T' and B' respectively. The displacement of the lens to the right is equivalent to a displacement of the pencil the same distance,  $b$ , to the left; the dashed lines show how the images of the ends of the pencil would appear at T'' and B'' if this were the case. When the second image is superimposed on the first, its displacement, to the right, is called its parallax.

If the parallax of the top of the pencil, the distance, MT'', is called  $p$  then

$$\frac{p}{b} = \frac{f}{h} \quad 2.7$$

where  $b$  is the distance between the two lens position,  $f$  is the distance between the lens and the photographic plate (or CCD sensor in a modern camera) and  $h$  is the vertical distance between the lens and the object.





**Figure 2.12 Schematic for stereovision**

From the ray diagram, it's clear that this follows from observations of similar triangles. By finding the equivalent relationship for the bottom of the pencil, or by differentiation with respect to  $p$ ,

$$\Delta p = -\frac{bf}{h^2} \Delta h \quad 2.8$$

where  $\Delta h$  is the height of the pencil and  $\Delta p$  is the difference in parallax, which is negative because points further away from the lens will create a displaced image closer to the original.

Millar and Woodward (2010) used a stereo vision technique to generate three-dimensional models of various road surfaces on a trip between Torino and Calais. Road surface texture measured using the models compares well with measurements made of the same surface using the volumetric patch technique. The same researchers went on to use the technique, and three-dimensional models of asphalt surfaces, to investigate tyre contact and its effect on wear and asphalt durability (2011).

A similar technique was used effectively by researchers at the SIC laboratory of the University of Poitiers and the LCPC through development of a transportable system for capturing pavement images (Slimane, Koudeir, Brochard, & Do, 2008). In this case, rather than moving the camera a known distance and taking two photographs, a camera in a fixed position was surrounded by three separate light sources. Three photographs, lit from different angles, were taken and used to calculate surface relief. A brief description of the system, and calculations, follows.

The amount of light reflected by a surface element in the direction of the camera will depend on its specularity, its angle in relation to the camera

and its colour. Colour digital images contain information about hue, saturation and intensity for each individual pixel - this is the HSI model (Wyszecki, 1982). All of this information can be used for analysis of the surface being photographed.

The assumption was made that, for surfaces of uniform colour, variations in grey-level in images were equivalent to variations in relief. This is an important assumption that will be revisited in Chapter 4. The technique using stereovision with three lighting angles was developed to improve performance on surfaces that were not uniform in colour. The images, with resolution of approximately 50  $\mu\text{m}$  per pixel, were taken in turn with lighting positioned at 120° angles around the camera and focused on the image area so that the light incident on the surface was at the same angle from vertical.

It was assumed that the surface was Lambertian - light falling on the surface is diffusely reflected in such a way that the apparent brightness of the surface to an observer is the same regardless of the observer's angle of view - and that the intensity of light reaching the camera lens is expressed by:

$$I(x, y) = \frac{L(x, y)}{r^2} \cos\phi(x, y) \quad 2.9$$

where  $\phi(x, y)$  is the incidence angle of light related to the reflecting facets of the surface,  $r$  is the distance between the lighting source and the reflecting facet and  $L(x, y)$  describes the colour properties of the surface at any point.

It is then shown that the angle of incidence of light related to the reflecting facet,  $\phi(x, y)$ , can be expressed in terms of the angle of incidence of light related to the surface plane,  $\theta_i$  (for  $i = 1, 2$  or  $3$  for each light source), the angle of incidence of light related to the x-axis,  $\phi_i$  (0°, 120° and 240° as described), and the gradients of the surface facets.

Since there is one such equation,  $I_1(x, y)$ ,  $I_2(x, y)$  and  $I_3(x, y)$ , for each of the three lighting angles, they can be solved to cancel the colour information  $L(x, y)$  and yield the gradients of the surface facets for each pixel in the images:

$$\frac{dz}{dx} = -\frac{(2I_1 - I_2 - I_3)\cos\theta}{(I_1 + I_2 + I_3)\sin\theta} \quad 2.10$$

$$\frac{dz}{dy} = -\frac{\sqrt{3}(-I_2 + I_3)\cos\theta}{(I_1 + I_2 + I_3)\sin\theta} \quad 2.11$$

### **2.3.3      *Laboratory techniques for measurement of surface texture***

Several of the most common techniques are described in some detail in a book on the subject of optical measurement of surface topography (Leach, 2011). It is pointless to reproduce full descriptions of all of them here. Stylus instruments are mentioned below for context and for reference when surface texture characterisation is discussed in Section 2.4. Three other techniques (laser triangulation, focus variation and scanning electron microscopy), and specific examples of the equipment using them, are discussed because they will be used in the experiments described in Chapters 3, 4 and 5.

Stylus instruments are the oldest method for measurement of surface texture: a stylus is dragged across the surface and its vertical motion is used to describe a profile along individual lines. Devices for measurement of longitudinal road profile, or for detection of rutting, such as the rolling straight edge (Young, 1977), are not entirely dissimilar, but this type of technique is unlikely to be of any practical use for measurement on scales smaller than 'megatexture'. In particular, stylus instruments do not cope well with voids or steep slopes, and they are limited by the size of the stylus tip (too large a radius gives poor resolution, and too small a radius can damage the surface through ploughing).

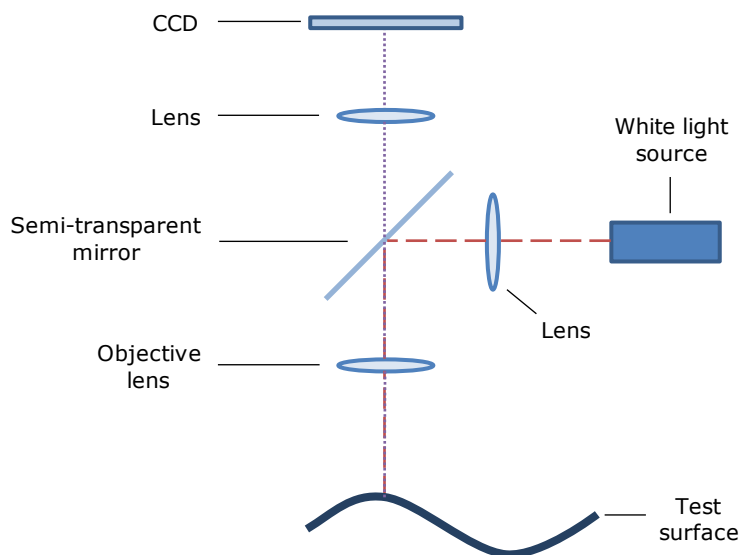
The Talysurf CLI 1000, made by Taylor Hobson, can be fitted with confocal, laser triangulation and stylus gauges. In the feasibility study described in Chapter 3, a laser triangulation gauge was used, and the basic principle for this technique is described in Section 2.3.1. The gauge is positioned over the test surface and can move up and down to facilitate height measurements. The test surface, placed on a moving stage, is moved laterally, along the x-axis, to build up a series of height measurements along a profile. A three dimensional surface can be scanned by moving incrementally along the y-axis so that a number of parallel profiles can be built up. The specifications for the laser triangulation gauge define its vertical resolution as 1  $\mu\text{m}$  and lateral resolution as 30  $\mu\text{m}$  and a speed of measurement up to 30 mm per second (Taylor Hobson, 2004).

Focus variation, as used by the Alicona Infinite Focus (Alicona, 2011), Figure 2.13, combines the small depth of field of an optical system with vertical scanning to provide topographical information derived from the variation in focus (as the name would suggest).



**Figure 2.13 Alicona Infinite Focus microscope**

Using a beam splitting mirror, light emerging from a white light source is inserted into the optical path of the system and focused onto the specimen via the objective lens. Light rays reflecting from the specimen and entering the objective lens are gathered by a light sensitive sensor behind the beam splitting mirror. Due to the small depth of field of the optics, only small regions of the specimen are sharply imaged when the lens is at any given height. The lens is moved vertically along the optical axis while continuously capturing data from the surface until each region of the specimen has been imaged in sharp focus (Helmli, 2011). Figure 2.14 shows a schematic diagram of a focus variation instrument.



**Figure 2.14 Schematic for focus-variation instruments**

The degree of focus at the CCD sensor varies from low to high and back again as the surface and the objective lens move closer or further apart. Analysis of the contrast in the captured images allows calculation of the position at which focus was at its best, and therefore, for each lateral

position, the topography of the surface. One method to measure focus is to calculate the standard deviation in the variation of intensity in small groups of pixels surrounding the pixel at the centre. If the focus is poor, the intensity of the surrounding pixels is almost identical, and the standard deviation is low. When the focus is good, the contrast between adjacent pixels, and therefore the standard deviation of their intensities, is at a maximum.

As with a conventional microscope, the objective lens can be interchanged and so the resolution of the device depends on the lens used. The specification for the Alicona Infinite Focus device, using a 20X objective lens, suggests lateral resolution of 438 nm and vertical resolution of 10 nm. Speed of measurement also depends on the objective lens and the vertical resolution required (the number of steps or slices can be increased or decreased) but, because an area is captured in one scanning pass, rather than having to build up a series of parallel lines, measurement can be considerably faster than with laser triangulation.

It's worth noting that measurement using the limited depth of field of an objective lens is possible without use of modern image analysis. An optical microscope can be focussed by eye first on the peak of an asperity, and then on the base, and, if the vertical movement in the objective lens is instrumented (perhaps with a micrometer screw gauge), the surface's topography can be laboriously calculated.

In a scanning electron microscope (SEM), an electron beam is produced at the top of the microscope column by an electron gun. The beam proceeds vertically down through the microscope, which is held in vacuum, through electromagnetic lenses which focus the beam onto a sample surface. When the beam hits the sample, electrons and X-rays are ejected from the surface. Detectors in the microscope collect the scattered electrons and generate signals which correspond to the topography of the sample surface. The X-rays can also be used to examine the composition and relative abundance of elements on the sample surface. SEMs can achieve much greater magnification (up to 250,000X) and higher depth of field than conventional light microscopes. Because of the need for high vacuum, samples to be inspected must be inserted into a vacuum chamber and sample size is typically restricted. The sample must be electrically conductive and anything that is not is generally coated with a very thin layer of material that is (e.g. gold, platinum, graphite etc.).

The SEM used to make qualitative analyses of surfaces in those experiments described later is a Philips/FEI XL30 with a tungsten filament electron source.

The SEM is essentially a two-dimensional technique, but as with cameras, three-dimensional information can be gained by tilting the sample, or by using techniques similar to stereoscopy.

## **2.4 Texture characterisation**

The information that follows, relating to the characterisation of surface texture, can also be categorised, as before, into current techniques used on the road, techniques that have been tried on the road, and techniques that are generally only used in the laboratory.

“Characterisation of road texture requires several parameters, but it doesn’t necessarily matter what parameters are used so long as there are enough of them and there are no duplicates” (Moore, 1975). This general statement holds true for any scale of surface texture and typical sets of parameters may be the size, shape and spacing of asperities along with the asperity height distribution, or the height, width and angularity of asperities along with the spacing density.

### **2.4.1 *Standard characterisation of road surface texture***

For road surface macrotexture, there are several well defined and frequently used methods for characterisation. The three most commonly used in the UK are mean texture depth (MTD), sensor measured texture depth (SMTD) and Mean Profile Depth (MPD). If the volumetric patch measurement technique is used (see Section 2.3.1) then texture is measured almost directly and a simple formula (Equation 2.12) relates the measurements made (volume of sand and diameter of resulting sand circle) to the mean texture depth (British Standards, 2010). If a laser based system is used to generate a set of measurements making up a surface profile then an algorithm is used to summarise the data into a single average. Specifications for macrotexture on roads in the UK typically refer to SMTD (DfT, 2009) and European specifications typically refer to MPD (British Standards, 2004) which are calculated using Equations 2.13 and 2.14 respectively. SMTD is a root mean square (rms) measure of the texture above and below a mean level, and MPD measures the heights of the highest peaks above the mean level. All are expressed in millimetres.

$$MTD = \frac{4V}{\pi d^2} \quad 2.12$$

where  $V$  is the volume of sand poured onto the surface and  $d$  is the diameter of the area covered by the sand after it has been spread.

$$SMTD = \frac{n \sum y^2 - (\sum y)^2 - \{12(\sum xy)^2 + P\} - (n^2 - 1)}{n^2} \quad 2.13$$

$$\text{for } P = \frac{5\{(n^2-1)\sum y - 12\sum x^2 y\}^2}{4(n^2-4)}$$

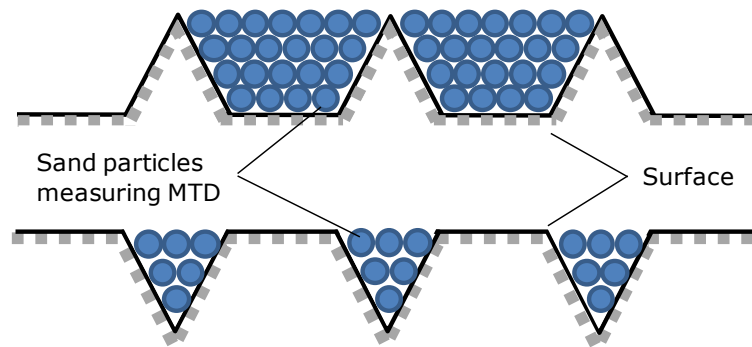
where  $n$  is the number of measurements in 300 mm length and is always forced to be odd,  $y$  is the height measurement measured by the laser and  $x$  is the nominal scaled distance between measurements ranging from  $-\frac{1}{2}(n-1)$  to  $\frac{1}{2}(n-1)$  over the 300 mm length.

$$MPD = \frac{y_1 + y_2}{2} \quad 2.14$$

where  $y_1$  is the height of the highest peak in the first half of a 100 mm length of profile, and  $y_2$  is the height of the highest peak in the second half of the 100 mm profile. Note that this method relies on either digital high pass filtering over the continuous profile to remove wavelengths above 100 mm, or subtraction of a least squares fit from the continuous profile to remove the slope and offset.

A very important point to note is that, given identical road surfaces, and even identical sets of height measurements, the reported value for macrotexture will be different depending on which characterisation algorithm is used. Furthermore, the response of the algorithms to different forms or shapes of surface varies, so that they will not always characterise surfaces in the same way, and may fail to give a full representation of a surface. Figure 2.15 shows an example of how macrotexture measurements on two surfaces may vary (McGhee & Flintsch, 2003). In this example, the surfaces are idealised and inverted versions of one another, the top one is referred to as having positive texture, and the bottom as having negative texture. Both surfaces would have identical SMTD, but the top surface would have a much higher MPD, and MTD, than the bottom surface – the latter demonstrated by the ‘sand particles’ shown in the diagram.



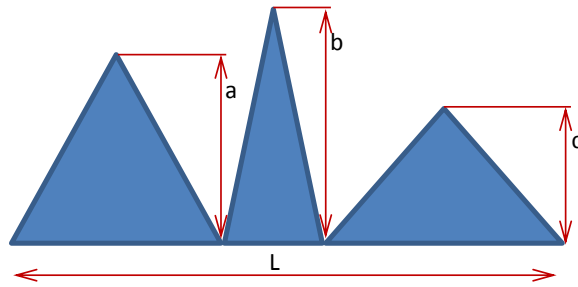


**Figure 2.15 Positive and negative texture and texture measurements**

There are no equivalent standardised measurements of pavement microtexture, although the measurements from skid resistance devices such as the portable skid resistance tester have sometimes erroneously been referred to as microtexture on the basis that it is the microtexture that supposedly affects low speed friction (Section 2.2). A range of published attempts to characterise road surface microtexture are reviewed in the following section.

#### **2.4.2 Experimental characterisation of road surface texture**

When Forster (1989) made measurements of surface texture using profile projection (Section 2.3.2) he considered three descriptors of the surface: average asperity density, height and shape (as shown in Figure 2.16), and demonstrated that shape provided the closest link to friction. He further noted that the optimum asperity height was between 0.01 mm and 0.1 mm and the belief that the density component was important because this drove the amount of adhesion. In order to improve the correlation between texture and friction he investigated the shape factor within the contact area only by using paint transfer from a rubber pad to identify areas of rubber contact. He found that using the percentage contact area – i.e. the percentage of the pavement area highlighted by paint transfer – gave a slight improvement in the correlation coefficient.



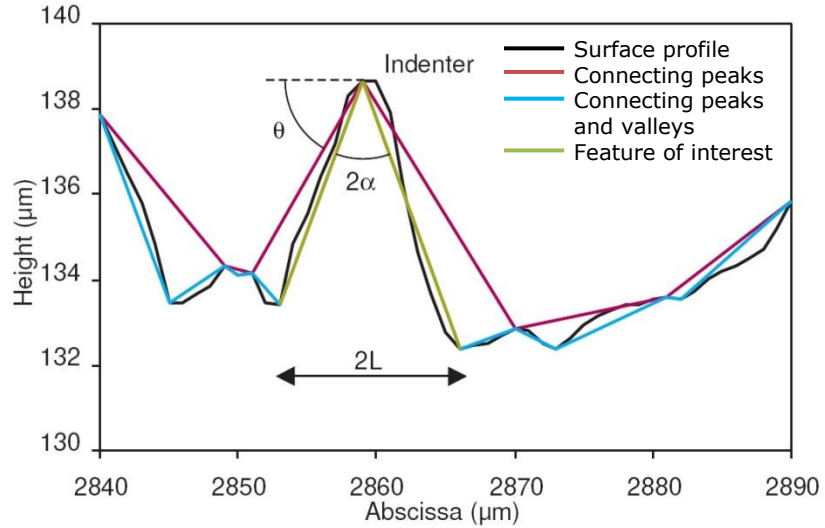
**Figure 2.16 Descriptors for microtexture**

$$\text{Average asperity height} = \frac{a+b+c}{3} \quad 2.15$$

$$\text{Average asperity density} = \frac{3}{L} \quad 2.16$$

$$\text{Average shape factor} = \frac{\frac{a+b+c}{3}}{\frac{L}{3}} \quad 2.17$$

Do (2005) has also attempted to describe the shape of the surface from microtexture measurements. The main observation is that tyre/pavement contact is not established at all points on the surface, but only at certain asperities called 'indenters' which deform the tyre. So, emphasis has been put on characterising the 'indenters' portion of the surface in order to correlate with friction measurements. The diagram in Figure 2.17 shows a typical indenter, and the method used to describe its shape, indenter density and relief, following Forster. The black line in the diagram represents the actual surface profile, the green line highlights the indenter of interest and the red and blue lines are construction lines used in characterisation with the red line connecting only the peaks, and the blue line connecting all peaks and valleys. Indenter shape is defined by the angle  $2\alpha$  at the peak, density is calculated from the number of indenters per unit length of profile, using the width of the indenter,  $2L$ , and the third parameter,  $\theta$ , defines the relief of the surface, being the angle formed by the segment connecting the peaks of two consecutive indenters with the horizontal.



**Figure 2.17 Shape measurements made to correlate with friction  
reproduced from (Do M. T., 2005)**

$$\theta = \tan^{-1} \left| \frac{z_{i+1} - z_i}{x_{i+1} - x_i} \right| \quad 2.18$$

$$\alpha = \frac{1}{2} \left[ \tan^{-1} \left| \frac{x_i - x_{i-1}}{z_i - z_{i-1}} \right| + \tan^{-1} \left| \frac{x_{i+1} - x_i}{z_{i+1} - z_i} \right| \right] \quad 2.19$$

The paper also offers a definition of peaks and valleys as follows. If a profile contains  $N$  points then point  $i$  (for  $i$  between 2 and  $N-1$ ) at position  $x_i$  with altitude  $z_i$ , is deemed a peak if  $z_{i-1} < z_i$  and  $z_{i+1} < z_i$  and as a valley if  $z_{i-1} > z_i$  and  $z_{i+1} > z_i$ . The point must be taller or shorter than both the points either side. This is a straightforward statement, but it is a very important definition and alteration of the definition will have a significant impact on the characterisation of the surface.

Several researchers have used Fourier analysis to examine the topography of road and aggregate surfaces. The analysis relies on the theory that any function (in this case a surface profile) can be described by a combination of an infinite number of harmonic or trigonometric functions. Hecht (1987) delivers a well-regarded explanation of Fourier transforms for the subject of optics, describing them initially as a “new bag of analytic toys”. It should be noted that the technique is frequently used to study electronic signals, where information is spread across time at a fixed point in space, whereas optics is generally concerned with information spread across a region of space at a fixed location in time. Hecht’s descriptions therefore lend themselves well to the study of topography which is height information, instead of intensity information, spread across a region of space.

In several experiments, where change in surface texture is observed, the power spectrum of a surface profile has been used to determine whether certain wavelengths change more than others. If the surface profile can be represented by a function  $f(x)$  then its Fourier transform,  $F(k)$ , equates to the spatial frequency spectrum of that profile and the energy per unit spatial frequency interval is proportional to  $|F(k)|^2$ .

Another way to consider the power spectrum is via the profile's autocorrelation function, as follows. If an apparently random profile has some hidden periodicity within it (such as a sine wave obscured by a large amount of noise) then it is possible to reveal that periodicity using autocorrelation. The profile is multiplied by a version of itself that is shifted laterally by some small amount,  $\delta$ . The area under the resulting product function (i.e. its integral) will be larger if, for example, peaks in the original profile and its shifted version coincide for that small shift. The function generated when those integral values are plotted against every  $\delta$ , is called the autocorrelation function  $C_{ff}(\delta)$ . If there is some periodicity in the original profile, then peaks will be present in the autocorrelation function at the appropriate values of  $\delta$ , revealing the wavelength of that periodicity. A Fourier transform of the autocorrelation function generates the equivalent function in the frequency domain and is called the power spectrum – peaks in the power spectrum occur if there is a dominant frequency in the original profile.

It can be shown that

$$\mathfrak{F}\{C_{ff}(\delta)\} = |F(k)|^2 \quad 2.20$$

where  $\mathfrak{F}$  denotes the Fourier transform.

In New Zealand, digital images of chipseal surfaces were analysed using fast Fourier transforms (FFT) to see if it was possible to duplicate results of volumetric patch (macrottexture) measurements (Pidwerbesky, Waters, Gransberg, & Stemprok, 2008). Digital images and volumetric patch measurements were taken at identical locations on several surfaces. A good correlation was demonstrated between patch measurements and parameters calculated using FFT analysis of the variation in pixel intensities within the digital images.

Using surface profiles measured with two laser-triangulation sensors, researchers in Italy claimed to characterise various asphalt surfaces using PSD curves, although no clear explanation of the technique is offered (Cigada, Mancosu, Manzoni, & Zappa, 2010).

In addition to calculating MPD and a newly proposed, but apparently identical parameter, PDI (see Section 2.5.1), for profiles measured on asphalt specimens, Himeno et al. (2000) also carried out some analysis using power spectral density. The description of the results and the interpretation is almost indecipherable and a vague conclusion, that “the most influential wavelength range was found to be 0.01~1 mm”, is given.

In experiments similar to those that will be described in Chapters 4 and 5, Chen and Wang (2011) used a Wehner-Schulze machine (Section 2.6) to polish aggregate surfaces before measuring friction and texture at a range of stages of polishing. Three surface profiles, 100 mm in length, were measured using a non-contact profilometer at each stage of polishing. The profiles were automatically aligned in an attempt to better compare the surface condition at each polishing stage and one of the techniques used to analyse the profiles was spectral analysis. It is reported that changes in the PSD curve are apparent for wavelengths shorter than 150 µm and even more significant variances occur at wavelengths shorter than 40 µm, which corresponds to the mean particle size of the polishing agent. The published results are not immediately compelling: the automatic alignment of profiles suggests material loss without loss of surface texture and the PSD curves for different stages of the polishing are almost indistinguishable. The paper recommends further analysis to consider the combined effects of mineralogy and texture variation. As part of the same work, fractal analysis was also applied to the same profiles.

Fractal analysis is used in a great many fields where characterisation of structures is needed. Its use to measure the roughness of a surface profile generally relies on the fractal dimension of that profile, using the following theory. Lewis Fry Richardson is often cited as the originator of the concept of the fractal dimension. While studying the causes of war he noted that published lengths of international borders varied greatly and he went on to investigate how the total length of a border increases when the unit of measurement used decreases. Richardson’s empirical studies were expanded by Mandelbrot, who coined the term “fractal” and offered a relationship between the length of a coast line or border and the length of the unit used to measure it:

$$L(G) = MG^{1-D} \quad 2.21$$

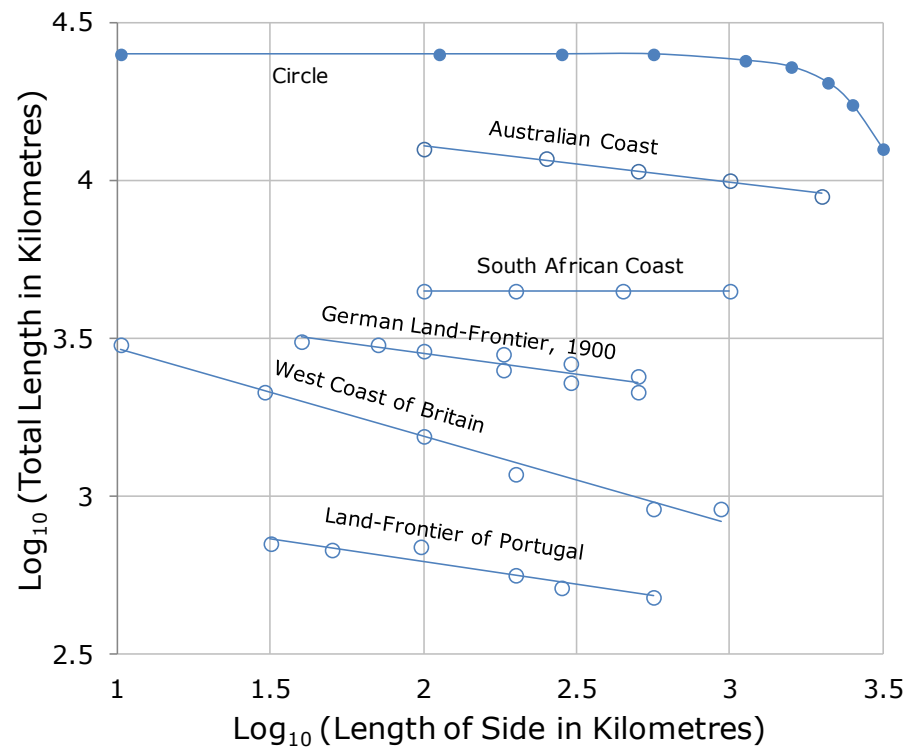
where  $L$  is the length of the coastline or border,  $M$  is a positive constant,  $G$  is the length of measurement unit and  $D$  is a characteristic of the border,

at least equal to unity (Mandelbrot, 1967). The diagram in Figure 2.18 is a rough reproduction (using Microsoft's Clipart) of a popularly displayed illustration of the concept for the measurement of the coastline of Great Britain. As the length of the measuring stick is reduced, more of the detail in the coastline is included in the measurement and so the total measured length increases.



**Figure 2.18 Coastline of Great Britain measured using successively smaller units**

If the logarithm of the measured length ( $L$ ) is plotted against the logarithm of the size of measuring unit ( $G$ ), as in Figure 2.19, the negative slope, equal in magnitude to  $D-1$ , is steeper for more complicated borders – the South African coast is a lot smoother than the west coast of Britain.  $D$  is the fractal dimension of that border.



**Figure 2.19 Measurements of geographical curves  
reproduced from (Mandelbrot, 1967)**

In Euclidean geometry, points have dimension of 0, lines have dimension 1 (length), surfaces have dimension 2 (length and width), and volumes have dimension 3 (height, length and width). The fractal dimension allows distinction between two lines depending on how complicated they are. In the graph in Figure 2.19, the slope of the data for the South African coast is about 0.02, so its fractal dimension is 1.02, almost the same as for a geometrically smooth line. Whereas, the negative slope of the data for the west coast of Britain is about 0.25, and its fractal dimension is therefore 1.25: somewhere between a line and a surface. Fractal analysis is particularly useful for characterisation of profiles that exhibit self-similarity and appear the same under any magnification. The Koch curve (or snowflake) has an infinite length because it always has some variation no matter how much you 'zoom in', but it has a fractal dimension of approximately 1.26.

An important feature that will come up during later analysis is demonstrated by the data for the circle. The total length measured tends towards a limit ( $10^{4.4}$  km as shown) as the length of the measuring unit tends to zero. In this example, once the measurement length is less than  $10^3$  km, the total length measured does not change by very much. So the circle must be smooth and its diameter must be sufficiently large that

chords of length 1000 km ( $10^3$  km) approximate its true circumference. For a non-smooth line this behaviour could indicate the wavelength of the smallest scale of roughness or the resolution limit of the measuring instrument: if total length does not increase for measurement unit lengths below a certain value then the scale of texture on that line must be larger than that value.

Fractal analysis can be undertaken for surfaces (as opposed to lines/coasts/profiles) by counting the number of boxes of ever decreasing size required to trace the contours of that surface. Surfaces have fractal dimensions between 2 and 3.

Chen and Wang's work (2011) did not show any change in fractal dimension with polishing. However, they refer to an alternative fractal parameter,  $C$ , proposed by Ganti and Bhushan (1995), which relates to the amplitude of surface frequencies. The derivation of  $C$  is generated from consideration of the power spectrum of the surface profile, although it is difficult to follow from either paper. It is linked to the variance of surface profiles.

In contrast, Carr et al. (1990) provide a clear explanation of the potential to use fractal dimension to characterise the roughness of aggregate particles. They used silhouettes of various aggregate particles and manually calculated the fractal dimension of each by walking dividers, opened to different ruler lengths, around the aggregate perimeters. Results from a small sample size show, with statistical significance, that the more angular (harsh) the texture on the surface of aggregate particles, the higher the fractal dimension.

A fractal texture model for pavement surfaces is presented in a conference paper (Radó, 1996) along with a stochastic-viscoelastic contact model. The first topic was developed in response to observation that pavement surface texture was difficult to characterise because new roughness, with different properties, presents itself with increasing magnification. A scale independent method of surface characterisation would therefore be useful. The treatment in the paper is very similar to that of Ganti and Bhushan (1995) and uses surface profile PSDs as well as fractal dimension. The fractal parameters were used to estimate the height variation of a set of profiles, measured by laser on a number of pavements. The estimated variation in height correlated well with the variation in height calculated



more conventionally by the measurement equipment (which gives an output similar to SMTD – Section 2.3.1).

### **2.4.3 Laboratory**

In addition to the literature based on road research and attempts to characterise pavement microtexture, there are a great many methods of texture characterisation from the fields of metrology (the science of measurement) and mechanical engineering where roughness measurements are routinely made of machine parts in attempts to minimise wear.

In the introduction to a chapter on surface topography characterisation Leach (2010) quotes a reference to the proliferation of surface texture parameters as 'parameter rash', and there are indeed many from which to choose. Some are summarised here to give an idea of the way metrologists treat surface characterisation. Before doing so, however, it is necessary to discuss some common terms. It is simplest to consider profiles before thinking about surfaces; in general, addition of a third dimension only slightly alters the principles applied.

Profile parameters are normally calculated for a given 'sampling length' and then averaged over the total 'evaluation length'. The evaluation length is normally equal to five times the sampling length (unless otherwise indicated). The choice of sampling length, as per the governing Standard (British Standards, 1998), depends on the surface roughness – it is recommended that rougher surfaces use longer sampling lengths. The choice of sampling length, in a sense, acts like a filter – a parameter calculated over 0.08 mm will not necessarily give the same result as when it is calculated over 0.8 mm.

Filtering of the surface profile is therefore a very important consideration. Aside from the selection of an appropriate sampling length, it is normal practice to apply a filter to a measured surface profile so that the correct scale of texture is examined (depending on the desired outcome). In metrological study of surface texture, as for pavement texture, there are two distinct scales of texture: short wavelengths are called roughness and long wavelengths are called waviness. The wavelength boundary between the two is not defined in general because it depends on the surface in question – one surface's roughness is another's waviness. For digital surface texture measurement, the appropriate filter for surface profile

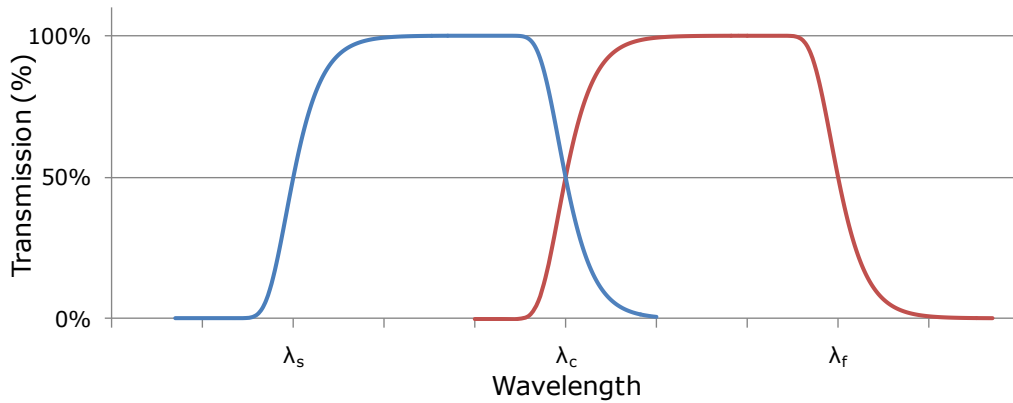
information is Gaussian with 50 % transmission at the cut-off wavelength (British Standards, 1998).

The Gaussian weighting function has the form:

$$s(x) = \frac{1}{\alpha\lambda_i} e^{-\pi\left(\frac{x}{\alpha\lambda_i}\right)^2} \quad 2.22$$

$$\alpha = \sqrt{\frac{\ln 2}{\pi}} \approx 0.47$$

where  $\lambda_i$  is the minimum cut-off wavelength of the filter; if  $\lambda_i$  is the maximum wavelength of interest then the filter has the form  $1-s(x)$ . The effect on the measured profile is that amplitudes of various wavelengths are attenuated according to the graph in Figure 2.20. At the cut-off wavelength, the transmission is 50 % (this avoids any confusing artefacts that would be generated if the filter attenuated to zero transmission at the cut-off). In the example shown, reproduced from (Leach, 2010) and (British Standards, 2000), the measured profile can be split into three components: wavelengths above  $\lambda_s$  constitute the *primary profile*, wavelengths between  $\lambda_s$  and  $\lambda_c$  constitute the *roughness profile* and wavelengths between  $\lambda_c$  and  $\lambda_f$  constitute the *waviness profile* of the surface.



**Figure 2.20 Attenuation of wavelengths according to Gaussian filter**

There are a range of profile parameters, and these are denoted  $P$ ,  $R$  and  $W$  depending on whether they are applied to the primary, roughness or waviness profiles respectively. The appropriate parameter depends on the desired outcome for its use. For example,  $R_p$ , the maximum profile peak height simply returns the height of the highest peak in the roughness profile. This parameter does not give much information about the texture of the surface but may be of some use to detect an abnormally large burr on a newly produced metal sheet. Similarly, the maximum profile valley

depth,  $R_v$ , could be used to detect an abnormally large dent. Some of the other commonly used profile roughness parameters, defined in the Standard (British Standards, 2000), are described in Table 2.2.

Most of the parameters require a definition of 'peak' or 'valley'. The definition in the Standard is similar to that given in the paper by Do (2005): a peak is the highest part of the profile above the mean line, between successive crossings of the mean line and a valley is the lowest part of the profile below the mean line between successive crossings of the mean line. Additionally, some of the parameters require height and spacing discrimination, which is a requirement for the minimum height and minimum spacing of profile peaks or profile valleys; this helps to ignore slight fluctuations where the profile crosses the mean line and immediately crosses back. By default, the minimum height (or depth) required for a fluctuation to be called a peak (or valley) is 10 % of  $R_z$ , and the minimum spacing between peaks (or valleys) is 1 % of the sampling length.

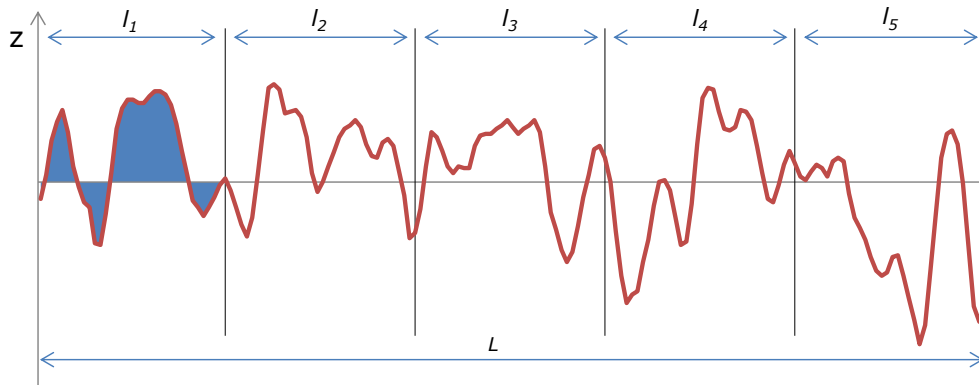
**Table 2.2 Common profile roughness parameters**

Parameter	Description
$R_z$	Maximum height of the profile. Sum of the largest profile peak, $R_p$ , and the largest profile valley, $R_v$ , within the <b>sampling length</b> .
$R_t$	Total height of the profile. Sum of the height of the largest profile peak and the depth largest profile valley within the <b>evaluation length</b> . Note that $R_t \geq R_z$ .
$R_a$	Arithmetical mean deviation of the assessed profile. Formula and graphical description below.
$R_q$	Root mean square deviation of the assessed profile. Formula below.
$R_{sk}$	Skewness of the assessed profile. Measure of the symmetry of the profile about the mean line.
$R_{ku}$	Kurtosis of the assessed profile. Measure of the sharpness of the distribution of the profile about the mean line.
$R_{Sm}$	Mean width of profile elements. Mean distance between successive positive crossings of the mean line.

$$R_a = \frac{1}{l} \int_0^l |z(x)| dx \quad 2.23$$

$$R_q = \sqrt{\frac{1}{l} \int_0^l z^2(x) dx} \quad 2.24$$

where  $z$  is a height measurement at position  $x$  and  $l$  is the sampling length.



**Figure 2.21 Area under the curve, used in calculation of  $R_a$  for each sampling length  $l_i$  in evaluation length  $L$**

There are other standard parameters and techniques defined in the literature. Of particular interest is the material ratio or Abbot-Firestone curve; this will be discussed in relation to surface texture characterisation in three dimensions.

The characterisation of texture on a surface, as opposed to a line profile taken from the surface, is referred to as 'areal' surface texture characterisation. The development of parameters for areal surface texture characterisation is relatively new – the final ISO standard describing areal texture parameters was published recently (British Standards, 2012). A major European initiative, led by a research group at Birmingham University, resulted in the first recognised set of 3D surface parameters in 1996. The "Birmingham 14" parameters included  $S_{qr}$ ,  $S_{zr}$ ,  $S_{skr}$  and  $S_{kur}$  the 3D equivalents of  $R_q$ ,  $R_z$ ,  $R_{sk}$  and  $R_{ku}$ . A further project, "SURFSTAND" looked at the practical application of these parameters and tightened up their definitions (Blunt & Jiang, 2003).

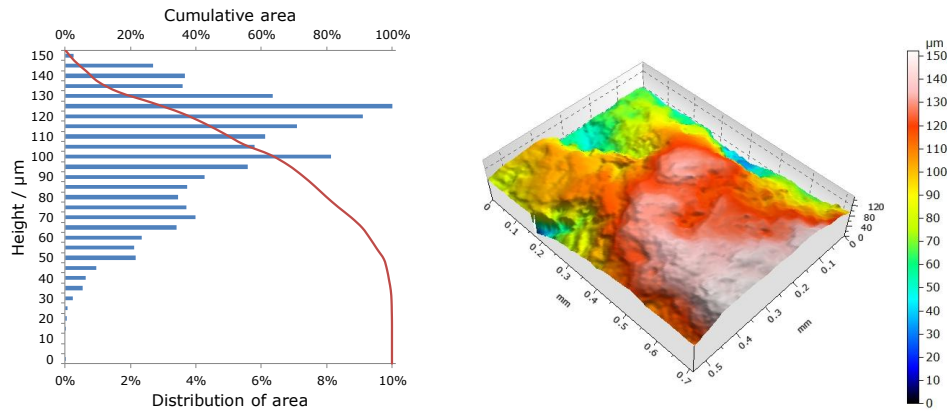
Following from that project, the current ISO document defines 'field parameters' and 'feature characterisation': a "toolbox of pattern recognition techniques that can be used to characterise specified features..." (British Standards, 2012).

Areal parameters are not separately denoted for primary, roughness and waviness ( $P$ ,  $R$  and  $W$ ) characterisation as for profile parameters. Instead there is a single nomenclature,  $S_q$ , for example, whose meaning depends on the filtering applied, which must be explicitly stated. The filtering is broadly analogous however. An S-filter is applied to remove small scale lateral components from the measured surface (this results in a primary surface), an L-filter is applied to remove large scale lateral components from the primary surface and an F-operator is applied to remove the nominal form from the primary surface. An S-F surface is the result of applying an S-filter and then removing form with an F-operation. An S-L surface is derived from the S-F surface by removing large-scale components using an L-filter; an S-L surface is the 3D equivalent of the roughness profile. Both S-F and S-L surfaces are called 'scale-limited surfaces'. The scale of the S-, or L-filter is controlled by the nesting index applied for each. The nesting index is equivalent to the cut-off wavelengths used in 2D filtering and is specified in terms of a wavelength. The Gaussian filter is commonly applied in 3D, and is derived by convolution of the filter defined in Equation 2.22 applied in turn to columns and then rows of measured data.

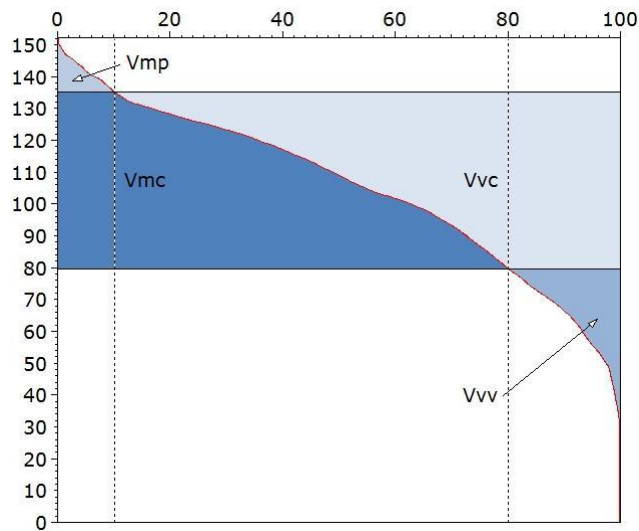
There are three-dimensional, areal, equivalents for most of the parameters listed in Table 2.2. Rather than providing another exhaustive list here, parameters will be defined when they are used in analysis of experimental work (mainly Chapter 7) – this is in the spirit of only considering parameters that have a practical application, in line with the SURFSTAND project described above. However, the concepts for the volumetric field parameters, calculated using the material volume or Abbott-Firestone curve, are explored in more detailed in the following paragraphs.

The Abbott-Firestone curve (also called the bearing area curve, presumably because of its use in understanding the properties of bearing surfaces) is, mathematically, the cumulative probability density function of the surface's height. The graph on the left of Figure 2.22 shows the distribution of heights for the example aggregate surface shown on the right. The bars indicate the percentage of surface area at heights within the range of bins (in this case bins of width 5  $\mu\text{m}$  between 0  $\mu\text{m}$  and 150  $\mu\text{m}$ ) and the superimposed line shows the cumulative height distribution. The curve is the Abbott-Firestone curve and it can be used to calculate four distinct parameters, as shown in Figure 2.23 and described in Table 2.3. Note that the distribution in Figure 2.22 indicates that this surface will have a

negative value for  $S_{sk}$  (the distribution is skewed towards higher values) and a positive value for  $S_{ku}$  (the distribution peak is sharper and its tails are longer than the normal distribution).



**Figure 2.22 Height distribution (left) for aggregate surface (right)**



**Figure 2.23 Example Abbott-Firestone curve and volumetric parameters**

**Table 2.3 Parameters calculated from the Abbott-Firestone curve**

Parameter	Description
$V_{mp}$	Peak material volume of the scale-limited surface. This is the volume of material within the top $p$ percent of the surface. The default value of $p$ , as shown in the graph, is 10 %.
$V_{mc}$	Core material volume of the scale-limited surface. This is the volume contained within the material ratios $p$ and $q$ . By default, and as shown this will be the volume of surface with height lower than the top 10 % but higher than the bottom 20 %.
$V_{vc}$	Core void volume of the scale-limited surface. Volume of the void not occupied by the material bounded by the material ratios $p$ and $q$ , again by default 10 % and 80 % respectively.
$V_{vv}$	Dale void volume of the scale-limited surface. Volume of the void not occupied by the material contained within its dales.

Feature characterisation is described in the literature in several places in addition to the Standard (British Standards, 2012), mainly by people who were involved in the SURFSTAND project. Scott (2009) summarises the process in five steps:

1. Selection of the type of texture feature

There are three main types of feature and selection of the correct type is important if characterisation is to be relevant to the function of the surface. Features are either areal (hills and dales), line (course and ridge lines) or point (peaks, pits and saddle points).

2. Segmentation

Features on the surface are identified using an automatic method and this is the most involved step in the feature characterisation process. The whole surface is divided into regions consisting of hills (where maximum uphill paths lead to a peak) and regions consisting of dales (where maximum downhill paths lead to a pit). In addition to hills and dales that affect the function of the surface, this will probably result in a large number of very small, unwanted, regions where noise in the measurement data has created small hills or dales with little functional significance. So, the number of hills and dales is reduced, or pruned, so that small regions are combined with neighbouring, functionally significant regions. A popular pruning method is Wolf pruning (Wolf, 1991), (Scott P. J., 2004), and this is often directly applied by proprietary surface analysis software.

### 3. Determining significant features

This step is designed to differentiate features identified by segmentation that are significant for the function of the surface from those features that are not significant. This is again an automatic function, normally applied by analysis software, and an example of function might be "feature is significant if not connected to the edge at a given height".

### 4. Selection of feature attributes

This step implements the advice given by Moore (1975), paraphrased as "Characterisation of texture requires several parameters, but it doesn't necessarily matter what parameters are used so long as there are enough of them and there are no duplicates". Most attributes are a measure of feature size (length, height, or volume) or feature density.

### 5. Quantification of feature attribute statistics

The final step is to calculate a statistic based on the selected feature attributes, or a feature parameter or a histogram of attribute values.



## **2.5 Factors affecting skid resistance**

Several experiments have been carried out to investigate the link between measurements of a surface's texture and its skid resistance; it is well documented that low speed skid resistance relies on surface microtexture and that the friction-speed behaviour of a surface is dependent on its macrotexture. In the context of a road surface, skid resistance is almost always measured in wet conditions because, generally, the friction generated between the road surface and a sliding tyre is worse in the wet. Additionally, because most measurement systems add water prior to testing, some control over the amount of water present is possible and measurement can be undertaken in a wider range of conditions (e.g. dry testing requires the surface to be dry, which is a severe restriction to routine skid resistance monitoring). Unless otherwise specified, where skid resistance has been measured as part of the experiments described below, it has been measured in wet conditions.

The first few paragraphs in this section review various experiments that deal with macrotexture and skid resistance and those that compare microtexture with skid resistance. Some of the experiments have been mentioned in earlier sections of this review when describing methods used for measurement or characterisation of texture. For completeness, at the end of this section, other factors that are known to affect skid resistance are also reviewed.

### **2.5.1 Surface texture**

One of the most popular and enduring models relating macrotexture to skid resistance was developed at Pennsylvania State University (Leu & Henry, 1978). The Penn State model is designed to describe the variation of skid resistance with vehicle speed and it incorporates constants dependent on both macrotexture and microtexture. It was to be used theoretically to predict skid resistance at any speed using measurements of macrotexture alone given an initial measurement of skid resistance on the surface in question. The model was empirically derived using results from skid resistance testing at various speeds and the theory that the gradient of a line fitted to these results is dependent on the macrotexture of the surface. The experimental, 'Skid Number' ( $SN$ ), data was produced using a locked wheel friction tester, and features of the data such as the Skid Number Gradient ( $SNG$ ) with respect to the speed of testing,  $V$ , and Percentage

Skid Number Gradient ( $PSNG$ , which is simply  $SNG$  divided by  $SN$ , and multiplied by -100 because the gradient is always negative) are used to derive the model as follows:

$$PSNG = -\frac{100}{SN} \frac{d(SN)}{dV} \quad 2.25$$

$$\frac{d(SN)}{SN} = -\frac{PSNG}{100} dV \quad 2.26$$

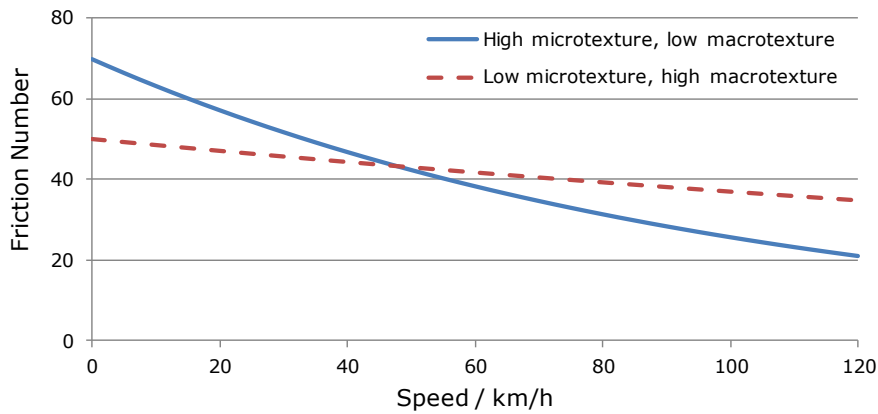
Integrating this from zero to any speed, and assuming  $PSNG$  is independent of speed:

$$\ln\left(\frac{SN_V}{SN_{V=0}}\right) = -\frac{PSNG}{100} V \quad 2.27$$

And this yields the Pennsylvania State University model for skid resistance-speed behaviour:

$$SN = c_0 e^{c_1 V} \quad 2.28$$

where  $c_0$  is  $SN_0$ , the skid resistance at zero (or, practically speaking, low) speed, which is thought to be related to microtexture, and  $c_1$  is  $\frac{PSNG}{-100}$ , the percentage skid number gradient, which is independent of speed and is related to surface macrotexture. Curves using this model, which have been fitted to experimental data, are similar to those shown in Figure 2.24. The behaviour is in part because the surface's ability to remove water from the contact area becomes crucial as the test speed increases and the time available to remove water is reduced.



**Figure 2.24 Friction speed curves using the Penn State model**

Researchers went on to demonstrate experimentally that numerical values for the two constants  $c_0$  and  $c_1$  could be found using microtexture and macrotexture parameters respectively. For macrotexture, two parameters were considered: root mean square height from profiles of the surface and sand-patch mean texture depth ( $MTD$ ). These two parameters were shown

to be correlated to one another and a reasonable non-linear relationship with  $c_1$  was found:

$$c_1 = -0.041.MTD^{-0.47} \quad 2.29$$

For microtexture, values of root mean square height, calculated from surface profiles, were compared with measurements made with the portable skid resistance tester. The root mean square heights were calculated as a function of the longest wavelength and a range of different wavelength cut-offs were examined. The best correlation was obtained for a cut-off wavelength of 0.5 mm.

Forster's experiments with microtexture measurement using white light line projection (1989) have been mentioned already. He measured surface profiles on 87 samples of asphalt and Portland cement concrete taken from in-service roads and demonstrated a correlation (with correlation coefficient of 0.73) between shape factor (Equation 2.17) and skid resistance, measured using the portable skid resistance tester. It is noted that 100 profiles, each approximately 2 mm long, are sufficient to characterise the microtexture of each sample. The correlation was improved by additional consideration of the percentage contact area between the tester's rubber slider and the sample surfaces, he concluded that a combination of microtexture and macrotexture characterisation was required to properly estimate skid resistance.

In a joint programme of research investigating the relation between skid resistance and microtexture of pavement surfaces (Himeno, Nakamura, Kawamura, & Saito, 2000) used 17 specimens, measuring 300 mm × 300 mm × 30 mm (height × width × depth), which were prepared from asphalt mixes of varying aggregate gradings. Friction on each specimen surface was measured using a Dynamic Friction Tester (DFT) and the microtexture of the surface of each specimen was measured over four 30 mm lengths, along the path of the rubber tips of the DFT, using a laser profiler (10 µm horizontal and 1 µm vertical resolution). The profiles were characterised using Mean Profile Depth (MPD) and a newly proposed parameter, Profile Depth Index (PDI). PDI is defined as a "weighted average of frequency of the wave" and further description of the parameter is very poor, although it is apparently very similar to MPD because its relationship with friction is nearly identical. The results of the dynamic friction tests found that the friction coefficients of the specimens ranged between 0.47 and 0.81 and there was an inverse relation between the

measured dynamic friction coefficient and both the MPD and PDI. In both cases a correlation coefficient,  $r$ , of 0.72 was reported.

Work at LCPC, using the indenter model (Figure 2.17) found that  $\theta$  and  $\alpha$ , calculated from sets of 13 surface profiles, 80 mm in length measured on each of approximately 20 asphalt samples, using Equations 2.18 and 2.19, could be correlated with measurements of  $\mu$  with correlation coefficients ( $R^2$ ) of 0.64 and 0.51 respectively. The work was extended to make use of a model defining the area of contact between a rubber tyre and a rough surface (Do, Marsac, & Delanne, 2004). Friction was calculated and compared against British Pendulum Number and peak friction from vehicle braking tests. It was concluded that, generally, the comparison was fair but that the scatter in the results showed that efforts are still needed before the prediction of friction from surface microtexture is solved. Some analysis of where improvements can be made is also presented: the resolution of the profile, at 10  $\mu\text{m}$ , is sufficient but the shape and relief descriptors of the microtexture ( $\alpha$  and  $\theta$ ) could be improved. The comparison between texture and friction was improved when only the upper part of the profile is considered (roughly 0.5 mm to 1 mm) and the mathematical process of filtering the profile to achieve this should be improved and some physical proof or justification should be sought.

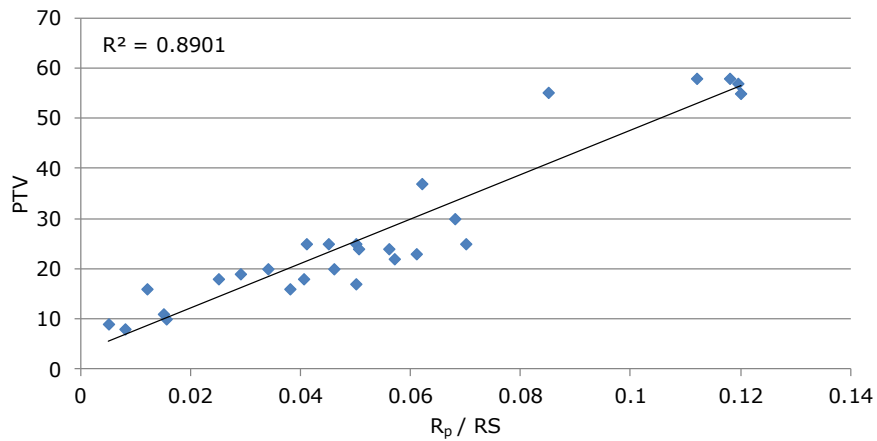
More recent work by the same research group (Do, Tang, Kane, & de Larrard, 2009) also included use of the indenter model. They measured 15 surface profiles, 76 mm in length, at only three stages during a polishing process using a Wehner-Schulze machine (Section 2.6) on two different aggregates: rhyolite and limestone. In addition to the indenter model, the standard roughness parameter  $R_q$  was used to characterise the surface texture in relation to the friction measured in the Wehner-Schulze machine. Comparisons showed that a reduction in friction on the aggregate surfaces was accompanied by a reduction in roughness as characterised by both methods. The polishing action affected each of the two aggregates differently and two different polishing mechanisms were proposed: for the rhyolite aggregate, polishing affected asperity height, whereas for the limestone aggregate, polishing affected both asperity height and asperity shape. The composition of the aggregates was considered to be a significant factor. Limestone is predominantly made up of only one mineral (calcite) and so the whole surface is abraded in equal amounts leading to a 'general polishing' behaviour. Conversely, rhyolite is made up of several

different minerals and a 'differential polishing' behaviour may occur whereby soft minerals are abraded more than hard minerals.

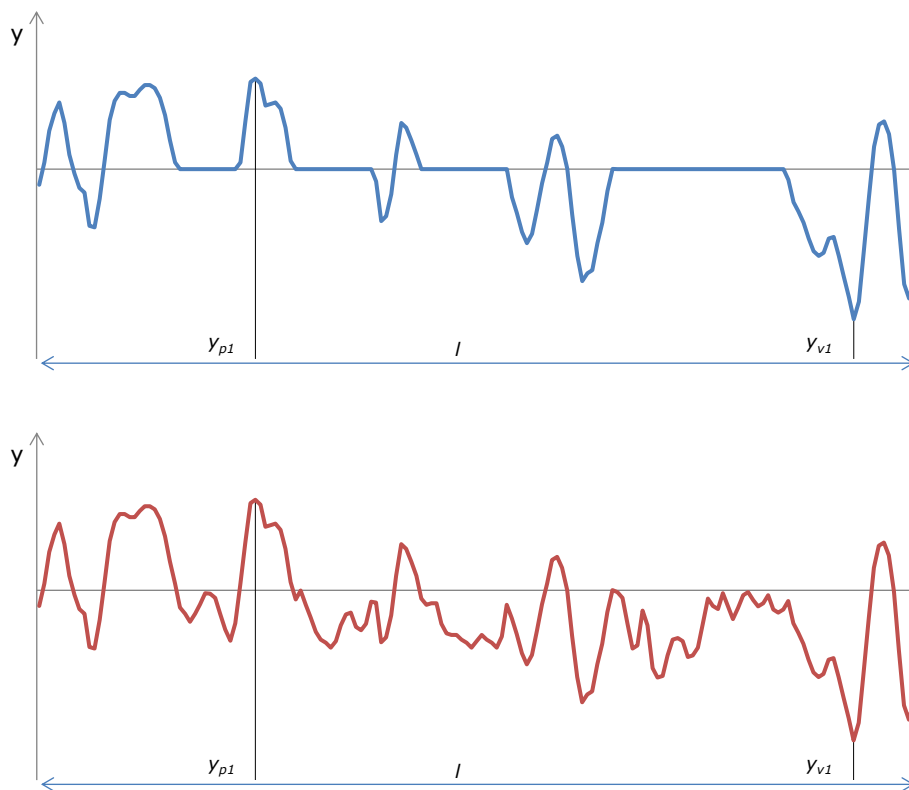
The Health and Safety Executive (HSE) carried out an investigation into slips and trips, the most common cause of major injuries in the work place, and the interaction of a pedestrian's heel with the floor surface (Shaw, 2007). At present, the HSE use two primary measurements to help assess the slip resistance of floor surfaces - coefficient of friction, determined by portable skid resistance tester (PSRT, aka the pendulum test), and  $R_z$  surface microroughness. The  $R_z$  component is supposed to provide an indicator of how a surface is likely to perform when it is contaminated; it is typically measured by means of a portable roughness device using a stylus. The development of affordable and portable roughness instruments has made it possible to measure a wider range of parameters on site than was traditionally available. So, the purpose of the investigation was to study the relationships between different roughness parameters and wet PSRT values to determine whether any of the other parameters could be used in the determination of surface slip resistance.

The HSE investigation recorded 11 roughness parameters on a number of floor samples in laboratory conditions. Parameter values were plotted against measured pendulum test values (PTV) in turn with varying degrees of agreement. Six roughness parameters showed some correlation with PTV and  $R_p$ , the maximum profile peak height, gave the best correlation, with an  $R^2$  value of 0.5967 compared to the correlation for  $R_z$  of 0.5012. It was observed that, when surfaces were acid etched, PTV increases were not usually accompanied by corresponding increases in  $R_z$ , but were accompanied by a reduction in  $RS$ , the mean distance between profile peaks. When  $R_z/RS$  was plotted against PTV an improved  $R^2$  value of 0.6311 was found and when  $R_p/RS$  was plotted, the correlation coefficient was 0.8901 – the highest correlation ever seen by HSE between wet PTV and another surface test. The graph is reproduced below in Figure 2.25. Other spacing parameters were also used in place of  $RS$  but the correlation was not equalled. When the surface is artificially roughened, the highest peaks (and deepest troughs) may not necessarily be removed, and indeed may remain the highest peaks within the sampling length so parameters like  $R_z$  or  $R_p$  would not change. However, the roughening process is likely to introduce more peaks (and troughs) within each sampling length so  $RS$  would decrease. Figure 2.26 shows two example surfaces that have the

same  $R_z$  and  $R_p$  but different  $RS$ , the bottom one, in red, having lower  $RS$  perhaps representing the effect of acid etching.



**Figure 2.25 Relationship between portable skid resistance tester values and composite roughness parameters**



**Figure 2.26 Two surfaces with identical  $R_p$  and  $R_z$  but differing  $RS$**

In experiments considering the measurement of surface texture of stones with particular regard to the effect on their frictional properties, Yandell (1970) concluded that there did not exist a single parameter for

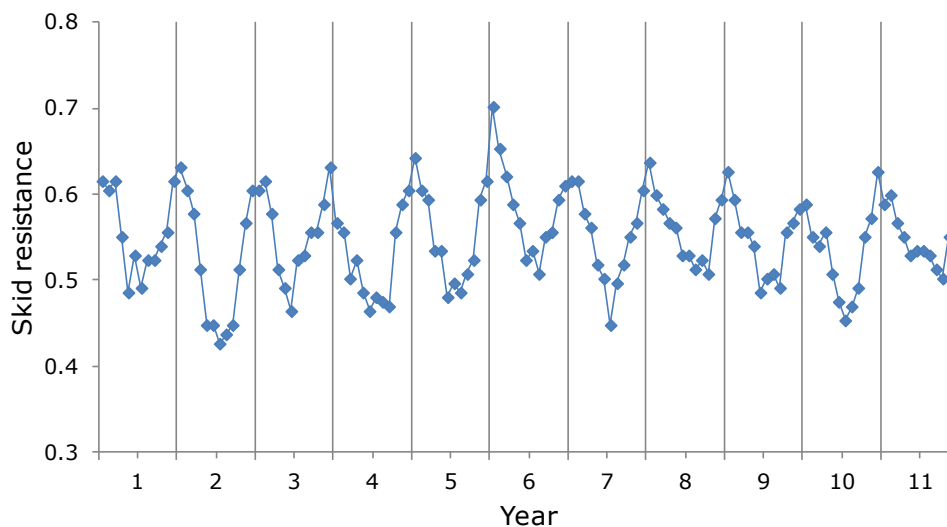
characterising roughness for all applications. For example, a parameter that characterises two surfaces as equally rough may be sufficient for a structural chemist looking at bonding calculations because the heights of asperities are important, but insufficient for a mechanical engineer looking at wear because the shape and density of the asperities is important. However, it was possible to relate the texture of surfaces to the generated skid resistance, and a mechano-lattice analogy was developed to analyse the stresses and strains on a surface and predict hysteretic friction. The experimental work was carried out primarily on dry, polished, roadstones and in this case it was noted that the friction between roadstones and sliding rubber is attributable to the energy losses in the deforming tyre.

### **2.5.2      *Other factors affecting skid resistance***

Hosking and Woodford (1976) describe a number of factors that affect the slipperiness of a road surface, including: the presence of water or some contaminant; seasonal variation; temperature; age; traffic density and road geometry. For some of the factors, the reason for the effect on slipperiness is well established and can be demonstrated both empirically and theoretically. For example, as temperature rises, rubber resilience increases and hysteresis losses are reduced, leading to a small reduction in skid resistance. In locations where traffic exerts a greater horizontal force, such as braking areas approaching roundabouts and junctions, or on bends and slopes, the polishing effect of traffic is amplified and the skid resistance tends to be lower. This is why different aggregates are specified for different locations (see Section 2.6).

Perhaps the most significant affect that is still only hypothetically explained is that of seasonal variation. On most roads, the lowest skid resistance is generally measured in the wet during the summer. In fact, the skid resistance of any given road, all other factors being equal, is approximately sinusoidal with time. Figure 2.27 shows data from skid resistance measurements (measured using a device called SCRIM) taken on a well-established road over the course of several years. Although not conforming to a perfect sine wave, it is clear that the skid resistance dips during the summer months in the middle of the year, and is highest at the start and end of each year. For road maintenance purposes, skid resistance measurements are made during the summer season (May to September) each year in order to capture the lowest point in the cycle.

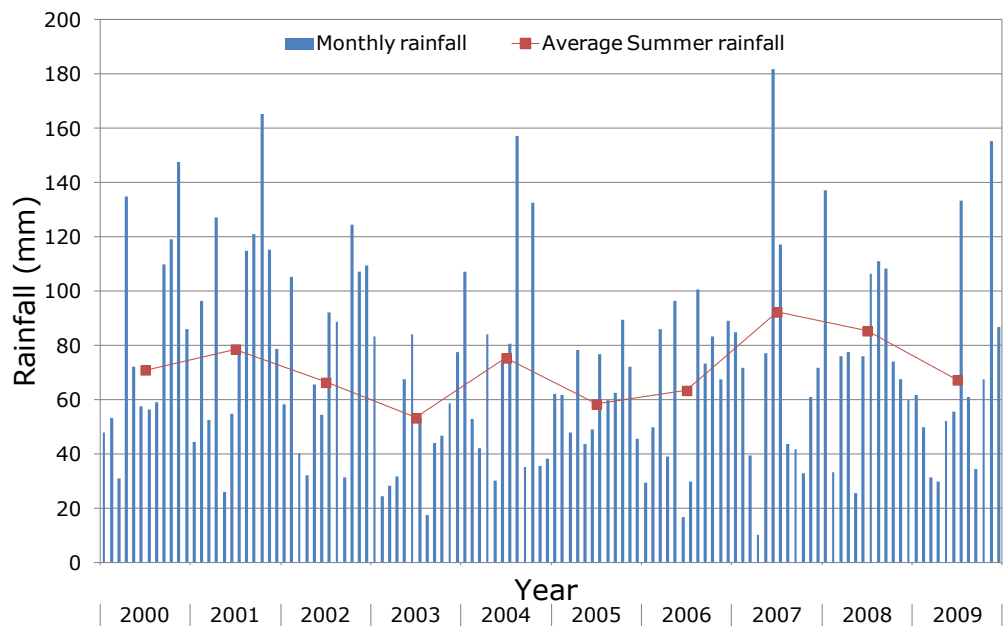
The accepted reason for the seasonal effect is that during the summer, when it is generally drier, the detritus on the road is in the form of fine dust which, with the action of passing traffic, polishes the aggregate particles in the road surface and reduces surface microtexture. After sufficient rain however, the fines are removed and the remaining detritus is larger and grittier, which will roughen the surface of aggregate particles and lead to a recovery of skid resistance over the winter period. Additional grit may be applied during winter to reduce ice formation and, where localised freezing does occur, this will also roughen the aggregate surfaces.



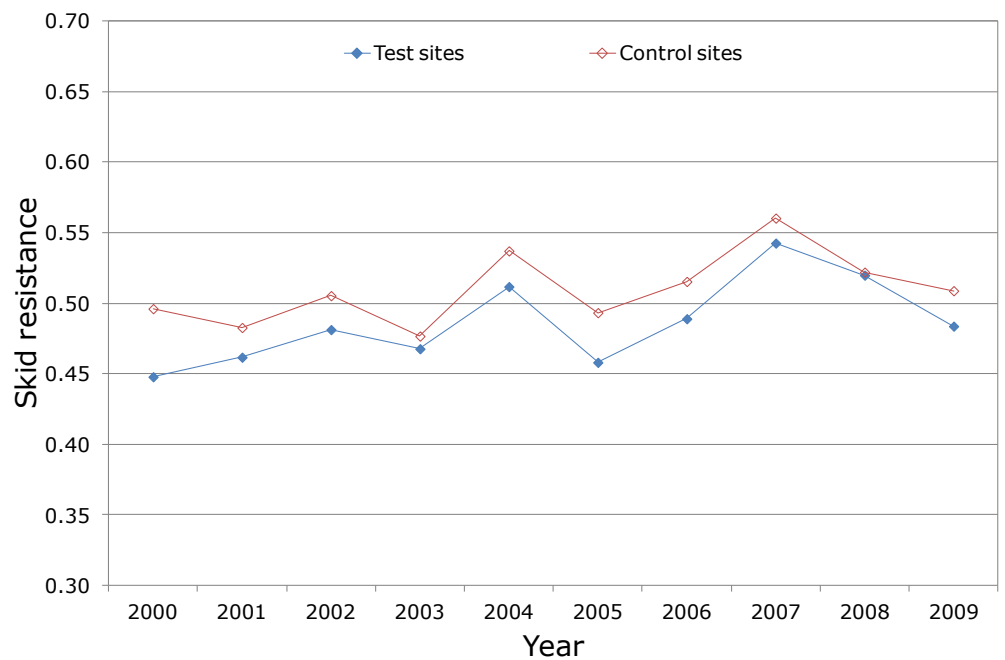
**Figure 2.27 Long term variation in skid resistance**  
***Reproduced using published data (Hosking & Woodford, 1976)***

The between-year element of seasonal variation is also explained using the same principles. On years where the summer is wet and relatively cold, skid resistance is generally higher. The graph in Figure 2.28 shows rainfall amounts for the East and North East region of the UK. The blue columns show monthly rainfall and the overlaid red points show the average summer rainfall (average rainfall during May – September). The graph in Figure 2.29 shows average skid resistance measured, during the summer period, on roads within the same region, as part of a monitoring project (Dunford, BOS Slag: 10 years of monitoring, 2012). From 2002 onwards there is a noticeable similarity between the summer rainfall pattern and the variations in skid resistance.





**Figure 2.28 Average rainfall for East and North East region (Met Office, 2009)**



**Figure 2.29 Average summer skid resistance on roads in East and North East region**

At present, because of the need to preserve skid resistance at speed, the macrotexture of new road surfaces is specified above a certain level. The required macrotexture currently precludes the use of smaller aggregate sizes in thin surfacings. However, historic research has shown that surfaces with smaller aggregate particles actually provide higher skid resistance. A programme of work investigated whether an increase in low

speed skid resistance on surfaces using smaller aggregate particles is sufficient to offset the expected more rapid reduction in skid resistance at increasing speed (Roe, Dunford, & Crabb, PPR324, 2008), (Roe & Dunford, 2012) (Woodward, Woodside, Ellis, Phillips, & Walsh, 2008). The wider use of finer-sized thin surfacing products would permit the use of smaller fractions (such as 6 mm material) that were a by-product of normal aggregate production and stockpiled.

## **2.6 Aggregates**

A good aggregate can be graded so it allows good macrotexture and will be able to provide adequate resistance to environmental exposure, abrasion and impact so retaining macrotexture. Furthermore, a good aggregate will have good initial microtexture and will provide adequate resistance to polishing so retaining microtexture (Anderson & Henry, 1979).

Topics of geology such as petrography (detailed description of the mineral content and the textural relationships within rocks) and mineralogy (study of mineral origin, formation and geological distribution) have been studied in great depth. In understanding the link between surface texture and friction on road surface aggregates it will be important to consider the ways the various types of aggregate provide texture in the first place, and the ways the texture is likely to change as it is polished by the action of traffic.

### **2.6.1 Specification of road stones**

In the UK, the polish resistance of aggregate used in the surface course of a road is measured using the polished stone value (PSV) test (British Standards, 2009). An aggregate's PSV gives an approximate prediction of its resistance to the polishing action of vehicle tyres under conditions designed to be similar to those occurring on the road surface. The PSV test is used internationally and, since 1976, has been an integral part of the UK specifications used in the selection of aggregates for use in surface courses on new road surfacings.

The PSV test uses small curved test specimens made from single-size aggregate particles placed by hand in a mould and fixed using a resin. These are subjected to polishing under controlled conditions on a purpose-made accelerated polishing machine. In this process, the test specimens are fixed in pairs to the rim of a test wheel which is rotated by an electric motor. A solid rubber-tyred wheel is loaded on to the specimen surfaces and water and corn emery are fed into the interface between the rubber tyre and the wheel to simulate the polishing action of traffic.

The polishing machine is operated in two stages; an initial "conditioning" stage using coarse emery, followed by a polishing stage using fine emery. After a fixed interval, the specimens are removed from the machine, washed, and the skid resistance of each is determined using a Portable Skid Resistance Tester (PSRT, aka British pendulum). Two of the test specimens are made from a standard "control stone" and the results from

these are used to confirm that an appropriate level of polishing action has been applied and to adjust the results from the remaining specimens to calculate the PSV.

The results are used to specify the type of aggregate that should be used for road surfaces in various locations and under various levels of traffic. Table 2.4 is an extract, reproduced from a table in the Design Manual for Roads and Bridges (Design Manual for Roads and Bridges, 2006); it shows only the first two site categories from the complete table. The numbers are the minimum PSVs required for an aggregate to allow its use in the surface course in each given situation. Although this table is provided for guidance, it is generally used as an absolute requirement in the construction of the majority of UK roads. Note that the more traffic on the road (measured as commercial vehicles per lane per day), or the more complicated the geometry, the higher resistance to polishing the aggregate must have. IL stands for Investigatory Level and, in this context, is the minimum level of skid resistance, as measured by SCRIM, that one should expect to achieve by using the aggregate specified in each given situation.

**Table 2.4 Recommended PSV for aggregates in road surfaces**

Site category	Site description	IL	Minimum PSV required for given IL, traffic level and type of site									
			Traffic (cv/lane/day) at design life									
			0-250	251-500	501-750	751-1000	1001-2000	2001-3000	3001-4000	4001-5000	5001-6000	Over 6000
A1	Motorways where traffic is generally free-flowing on a relatively straight line	0.30	50	50	50	50	50	55	55	60	65	65
		0.35	50	50	50	50	50	60	60	60	65	65
A2	Motorways where some braking regularly occurs	0.35	50	50	50	55	55	60	60	65	65	65
B1	Dual carriageways where traffic is generally free-flowing on a relatively straight line	0.30	50	50	50	50	50	55	55	60	65	65
		0.35	50	50	50	50	50	60	60	60	65	65
		0.40	50	50	50	55	60	65	65	65	65	68+
B2	Dual carriageways where some braking regularly occurs	0.35	50	50	50	55	55	60	60	65	65	65
		0.40	55	60	60	65	65	68+	68+	68+	68+	68+

An alternative tool, also designed to apply a controlled amount of polishing in the laboratory, is the Wehner-Schulze (W-S) machine. An important difference between the PSV test and the procedure using the W-S machine, however, is that the latter uses large, flat specimens (usually 225 mm diameter) that can be obtained from actual road surfaces, asphalt test specimens manufactured in the laboratory or laboratory-manufactured test plates using aggregate alone. The test is carried out using a purpose-designed machine, shown in Figure 2.30, which meets the specification outlined in a draft Standard (British Standards, 2011) and is available commercially.



**Figure 2.30 Wehner-Schulze machine**

Specimens are held in an aluminium mould and attached firmly to the mounting table in the machine so that the table and specimen surfaces are accurately parallel. The mounting table can slide between the friction testing station and the polishing station.

Polishing is achieved in the Wehner-Schulze machine by lowering a polishing head consisting of three independently suspended conical rubber rollers so that they are forced into contact with the test surface. Each roller is 56 mm long, with a base diameter of 80 mm and an apex diameter of 36 mm; they are aligned so that their axes of rotation are approximately  $21^\circ$  to horizontal and contact in the plane of the test plate is 60 mm long. The polishing head is rotated at a speed of 500 rpm in a clockwise direction while a suspension of silicon dioxide in water is pumped onto the surface to act as a polishing medium. The suspension consists of 2.4 kg of quartz with nominal particle size of  $40\ \mu\text{m}$  suspended in 40 litres of water (giving 6 % concentration quartz in water by mass). The suspension is contained in a tank to the side of the machine and is continually agitated to distribute the quartz powder. During polishing, the suspension is pumped onto the centre of the test plate at a rate of 5 litres per minute; it is then collected under the test plate and is recycled into its tank. The quartz suspension is

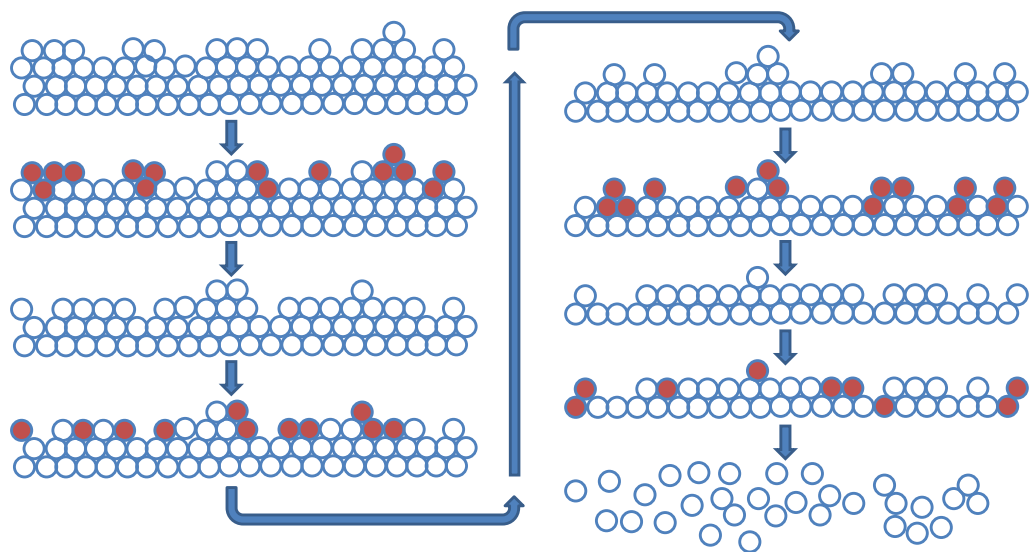
replaced after five test plates have been polished, or sooner if the suspension appears to be contaminated with detritus washed from the test specimen. The polishing head has a mass of 40 kg and, according to calculations made by researchers in Germany (Huschek, 2004), this results in each roller being independently loaded onto the test surface with an average contact pressure of approximately  $0.4 \text{ N mm}^{-2}$ , equivalent to 4 bar (58 psi), typical of the tyre pressures of a commercial vehicle. The same research has suggested that, although the rollers are free to rotate, there is some drag due to the mounting bearings, giving a slight slip of 0.5 % to 1.0 %. Eight grooves, 3.5 mm wide and 4.5 mm deep, are cut into the rubber from base to apex, to simulate tyre treads. The roller rubber is specified to have Shore hardness  $65 \pm 3^\circ$ .

Friction is calculated from measurements of torque imparted to the test surface when the test head, comprising three separate rubber sliders, and rotating at a pre-defined speed, is dropped onto the surface and allowed to slide to a halt under its own mass. The test head has diameter of 180 mm and each rubber slider is 30 mm long and 14.5mm wide; the rubber used has Shore hardness  $65 \pm 3^\circ$ . In the standard test, the measuring head is accelerated until it is rotating at 3000 rpm, which is equivalent to a tangential speed for the rubber sliders of 100 km/h. Just before the head is dropped onto the test surface, water is sprayed on to the test surface at a rate of 20 litres per minute to attain a theoretical water film thickness of 0.5 mm until the test has finished. The test head has a mass of 26 kg and it has been calculated that each rubber slider imparts a static pressure of approximately  $0.2 \text{ N mm}^{-2}$ , equivalent to 2 bar (29 psi) in tyre pressure (Huschek, 2004). The friction test value normally recorded,  $\mu_{\text{PWS } 60}$ , is the friction calculated when the friction head has slowed to 60 km/h.

The W-S machine has been used in the experiments described in Chapters 4 and 5 and its use and capabilities are examined further in Chapter 5. Its use in various experiments to examine the changing texture of aggregate has already been described in this Chapter (Section 2.4). It has also been used to investigate the properties of asphalt designs of different composition (Allen, Phillips, Woodward, & Woodside, 2008), (Dunford, 2012). Its correlation with the PSV test has been demonstrated by various researchers (Dames, Huschek, & Lindner, 1997), (Arampamoorthy & Patrick, 2011), but some researchers regard its ability to predict in-service performance, especially when used to measure properties of asphalt rather

than just coarse aggregate alone, to be superior (Artamendi, Phillips, Allen, & Woodward, 2012).

Another test, complementary to the PSV, is the Aggregate Abrasion Value (AAV) test. It is detailed in the same Standard documentation and measures (as the name suggests) an aggregate's resistance to abrasion. A known mass of aggregate chippings are set into a small flat resin plate and subjected to abrasion on a grinding apparatus that is fed with a known type of sand. The loss in mass of the aggregate after a specified time as a percentage of the original mass is the AAV. An aggregate with a high AAV may well have a high PSV because the surface is constantly renewed as it is polished by the action of traffic but it may come at the cost of the overall longevity of the road surface. A balance between the two values is often sought. The sequence of diagrams in Figure 2.31 shows how an aggregate particle, made up from grains of some mineral, may retain its surface texture and therefore have high PSV but be rapidly worn away rendering it undesirable for use in the road surface course.



**Figure 2.31 Aggregate abrasion with retention of microtexture**

### **2.6.2 Geology of typical road stones**

In an attempt to find an alternative to calcined bauxite, the increasing price of which was making high friction surfacings costly, researchers studied “the factors which cause some materials to remain non-skid” (James, 1967). They concluded that stones fell into one of five categories, listed as follows:

### 1. Extremely hard materials

Angular stones made of uniform, hard (measured on Moh's scale), material. If oriented correctly, with a sharp point uppermost, then these materials could be suitable for road surfacing. The hardest materials include diamond or, more realistically, artificial abrasives such as aluminium oxide and silicon carbide. Orientation is difficult, particle sizes are typically too small and the material cost is too high.

### 2. Conglomerations of small hard particles

Minerals of intermediate hardness (e.g. quartz) bonded together by a softer siliceous or calcareous material. Although quartz is not as hard as the hard materials above, provided the bond between particles is weak enough, slow attrition can occur under traffic and fresh particles are continually exposed allowing the stone to maintain a harsh surface texture. Sandstones and gritstones fall into this category, but the requirement for an inter-particle bond that is neither too strong nor too weak limits the number of suitable stones.

### 3. Dispersions of hard particles in a softer matrix

The binding, inter-particle, material dominates over the abrasive particles, such as gritty limestones. Stones in this category could be used in the surface providing the matrix erodes slowly enough and the particles are abrasive enough.

### 4. Materials which fracture in an irregular manner

Some stones that would normally flake to leave rounded edges (e.g. flint) can be altered, through heating (calcined to about 1000 °C), so that they become more crystalline and fracture more irregularly thus giving a higher resistance to polishing.

### 5. Vesicular materials

Rocks combining numerous small cavities. Typically resistance to polishing is good, but crushing strength is quite poor. Steel slag falls into this category.

Most naturally occurring aggregates used in road surface courses in the UK are combinations of categories 2 and 3.

There are around 2000 rock forming minerals but most rocks are primarily formed from a dozen minerals (Duff, 1998). Chief amongst these (in terms of the aggregates used for making road surfaces) are quartz, feldspars, micas, olivines and pyroxenes. These are all silicate minerals and they



share a common crystal structure: a tetrahedral arrangement of four oxygen ions around a single silicon ion. The numerous ways in which these tetrahedron structures combine with other ions to balance their charge (one  $\text{Si}^{4+}$  and four  $\text{O}^{2-}$  ions results in a net 4- charge) result in the different minerals.

Feldspars consist of  $\text{SiO}_4$  and  $\text{AlO}_4$ , in tetrahedral frameworks, with ions of potassium ( $\text{KAlSi}_3\text{O}_8$ ), sodium ( $\text{NaAlSi}_3\text{O}_8$ ) or calcium ( $\text{CaAl}_2\text{Si}_2\text{O}_8$ ). The presence of these components can have an effect on the way in which the rock reacts to external forces. For example, the potassium based component, which is also called orthoclase feldspar, is the pinkish or cream-coloured mineral in granite. When it breaks, orthoclase 'cleaves' along parallel planes to leave a smooth surface. There are two sets of cleavage planes, arranged at right angles, which is where its name originates (Greek *orthos*, normal or right; *klastos*, broken).

In quartz (also 'framework silicates'), the excess charge from the four oxygen ions is neutralised by sharing of silicon ions; pure quartz is  $\text{SiO}_2$ . Quartz, which is resistant to weathering and has no planes of cleavage, is a major constituent of sandstone. Micas are 'hydrous alumina-silicates of potassium' and come in two main varieties: white mica, or muscovite, and dark mica or biotite. Mica is a 'sheet silicate' and it consists of tetrahedral sheets bound in layers by ions such as aluminium (Al), magnesium (Mg) or iron ( $\text{Fe}^{2+}$ ) and it cleaves easily along the weak intermediate ion layers. Olivines and pyroxenes are called ferromagnesian or mafic minerals because they contain magnesium and iron. Rock-forming olivine, such as in basalt and gabbro, tends to contain more magnesium than iron and is formed from separate  $\text{SiO}_4$  tetrahedra, held together by ions such as  $\text{Mg}^{2+}$ , without any sharing of oxygen ions – an 'island silicate'. Pyroxenes, also found in basalts, are 'chain silicates' consisting of single chains of  $\text{SiO}_4$  tetrahedra formed by sharing of two oxygen ions.

As part of work investigating the sustainable use of high specification aggregates in the UK, a list of quarries providing aggregate for use in road surface courses was drawn up (Thompson, Burrows, Flavin, & Walsh, 2004). The list of 337 quarries is not comprehensive, and may now require updating, but it does give an indication of the types of rock available for use in the more demanding traffic-loading situations. The rock types with the four largest numbers of quarries are basalt (46 quarries), dolerite (63 quarries), granite (15 quarries) and greywacke (96 quarries).

Basalt is an extrusive volcanic rock and it is usually grey to black in colour and fine-grained due to rapid cooling of lava. It may be porphyritic (containing porphyry – a variety of igneous rock) containing larger crystals in a fine matrix, or it may be vesicular.

Dolerite is a similar, igneous, rock. Dolerite normally has a fine but visible texture comprising silicate crystals set in a finer matrix of silicate mineral (clinopyroxene), and its texture is termed interstitial.

Granite, another intrusive, igneous rock, typically has a medium to coarse texture, occasionally with some individual crystals larger than its finer matrix. Granites can be pink to dark grey or black, depending on their chemistry and mineralogy.

Greywacke (German *grauwacke*, signifying a grey, earthy rock) is a variety of sandstone generally characterized by its hardness, dark colour, and poorly-sorted, angular grains of quartz, feldspar, and small rock fragments set in a compact, clay-fine matrix. It is a sedimentary rock and its component particles are not normally very rounded or polished. Other sedimentary rocks with similar structure include gritstone (which could be argued as another name for the same thing), sandstone, as mentioned, and siltstone. The main difference between these types of rock is the size of particles from which they are composed.

Another important rock type, for inclusion in this short list, is limestone. Limestone is not used as aggregate in road surface courses because it is very susceptible to polishing, although it is used in lower layers of pavement construction. However, it has been used in previous polish inspection experiments (Do, Tang, Kane, & de Larrard, 2009) because of its relative simplicity, and in part because its polish susceptibility allows a wide range of friction levels. Limestone is typically very homogenous, predominantly composed of a single mineral (calcite –  $\text{CaCO}_3$ ), with only small amounts of secondary minerals such as quartz or feldspars. The surface texture of limestone should be amongst the simplest to interpret of any aggregate type.

## **2.7 Summary**

There is some accord about mechanisms that underlie friction interactions with rubber, at least insofar as it is complicated and does not follow Amontons's and Coulomb's classic laws of friction. Research is still ongoing, especially in tyre and rubber seal/bearing industries, and there are still some significant gaps in this large and old topic of research. For the purposes of characterising surface texture, and its contribution to a surface's skid resistance it may be sufficient to know the fundamental mechanisms: adhesion, which is dependent on contact area and applied load, and hysteresis, which is dependent on speed and asperity distribution.

Qualitative descriptions of road surface texture have been well established. Theories relating the physical size (wavelength and amplitude) of surface deviations to resulting physical phenomena have also been published prolifically. Treatments, such as Moore's (1975) suggesting that the need for surface texture on different scales relates to the bulk removal of water and the pressure required to break through a thin film of water, seem sound.

Texture measurement is also a well-established field and it is possible to measure texture on different scales. Generally though, practical measurement of the texture of road surfaces is restricted to scales of macrotexture and larger. If it can be shown that measurement of smaller texture scales is informative with regard to skid resistance, then there is scope for improvement to existing measurement systems by increasing the resolution of high-speed systems or increasing the speed of high-resolution systems. This is the subject of research that has been carried out in conjunction with the main surface texture characterisation investigations presented later in this thesis; it is summarised in Chapter 3.

Surface texture characterisation is an important field of study in a range of industrial situations and the advent of three-dimensional (areal) parameters opens up a range of possibilities for functional characterisation. The majority (and, as far as the author can tell at the time of writing, all) of the research into the surface texture of aggregates used in the road surface has used two-dimensional texture profiles. It was demonstrated that the principles of measurement and characterisation in two-dimensions are generally applicable (with only small amendments) when a third dimension is added. Accordingly, it will be important to bear in mind those

techniques that have already shown (or have been ascribed) some promise such as fractal and Fourier analysis. There is some agreement on which parameters are the most useful for associating surface texture with skid resistance, although nomenclature is often different. Forster (1989) uses a shape factor, Do (2005) uses the angle of asperity indenters, and Shaw (2007) uses standard roughness parameters. All of these are essentially some measurement of asperity height divided by asperity width or spacing. Given the complexity of aggregate mineralogy and the various polishing mechanisms proposed, however, it is unlikely that a one-size-fits-all characterisation solution exists.

There are several factors that affect the skid resistance of road surfaces; its texture, on all scales, is critical. In fact, some of the other factors, such as weather and polishing susceptibility, are also reliant on surface texture creation or destruction. The way surface texture changes when aggregates are used in the pavement surface, and the resulting changes in measured skid resistance, is key to the investigation of the link between the two. The feasibility study described in the following chapter indicates that polishing mechanisms are likely to be different for different rock types, probably because of differing mineralogy. The various aspects of the field of geological study are old and well documented. It will be informative to refer to the mineralogical composition of any stones used in future experimental work as a means of explaining the polishing behaviour exposed.

There are a number of avenues of study that might be pursued in developing the understanding of skid resistance. A review of available literature has shown that some are already well covered, leaving relatively little room for new discovery except in minutiae, such as rubber friction theory and geology. Others are slightly less pinned down, such as the still hypothetical understanding of seasonal variation in skid resistance (which is, albeit, actually related to surface texture anyway). Some of the experiments, already published, looking at aggregate texture have suffered greatly, in my opinion, from a deficiency of data and difficulty in interpretation.

For example, it could be argued that Forster (1989) was limited by the relatively primitive (by today's standards) technology available, making measurement and analysis a laborious process: he measured one hundred 2 mm profiles on each of 87 specimens, presumably using drawing tools

(i.e. a ruler) to measure photographs taken through a microscope. And yet, 11 years later Himeno et al. (2000) used a triangulation laser to measure surface profiles directly but only measured four 30 mm lengths on each sample (80 mm less profile length per sample than Forster). Chen and Wang (2011), 11 years later again, only measured a total profile length of 300 mm. Also using measurements made by laser-triangulation, Do et al. (2004) and (2009) at least attempted to make use of the labour saving advantages offered by measuring a total profile length of approximately 1000 mm on each surface.

If only a small number of surface profiles have been measured, it is difficult to get an idea of the form of a surface and it is almost impossible to align data with sufficient accuracy to enable inspection of the effect of polishing on an aggregate surface. This is demonstrated by the attempts at alignment made by Chen and Wang (2011) that, as presented, suggest an impossible polishing mechanism for all of the aggregates analysed.

All of the above-mentioned studies have recommended further study. One way to immediately address the data deficit and significantly aid interpretation is by measurement in three-dimensions. The recent progress made in the development of areal characterisation parameters is timely and researchers in that field often request case studies so that their work can find practical application.

The crux of the research presented in the remainder of this thesis is therefore concerned with development of a robust methodology for measurement, in three-dimensions, of aggregate surfaces. Having developed a methodology, the measurements will be used to examine, first qualitatively, and then quantitatively, the differences in texture between aggregate surfaces.

## 2.8 References

Design Manual for Roads and Bridges. (2006, November). *Volume 7 Section 5, HD36/06, Surfacing materials for new and maintenance construction*. London: The Stationery Office.

Alicona. (2011). *Focus-variation for surface measurement in research and production*. Retrieved April 28, 2012, from <http://www.alicon.com/home/products/InfiniteFocus/Focus-Variation.en.php>

Allen, B., Phillips, P., Woodward, D., & Woodside, A. (2008). Prediction of UK surfacing skid resistance using Wehner-Schulze and PSV. *International Safer Roads Conference*. Cheltenham.

Anderson, D. A., & Henry, J. J. (1979). *Synthetic Aggregates for skid resistant surface courses*. Washington: Transportation Research Board.

Arampamoorthy, H., & Patrick, J. (2011). *Potential of the Wehner-Schulze test to predict the on-road friction performance of aggregate*. Wellington: NS Transport Agency.

Artamendi, I., Phillips, P., Allen, B., & Woodward, D. (2012). An assessment of the evolution of the skid resistance of proprietary asphalt surfacings in the UK. *5th Eurasphalt and Eurobitume Congress*. Istanbul.

Blunt, L., & Jiang, X. (2003). *Advanced Techniques for Assessment Surface Topography: development of a basis for 3D surface texture standards "surfstand"*. London: Kogan Page Science.

Bowden, F. P., & Tabor, D. (1942). Mechanism of metallic friction. *Nature* 3798, 197-199.

Bowden, F. P., & Tabor, D. (1950). *The friction and lubrication of solids*. New York: Oxford University Press.

British Standards. (1998). *BS EN ISO 11562. Geometric Product Specifications (GPS) - Surface texture: Profile method - Metrological characteristics of phase correct filters*. London: BSi.

British Standards. (1998). *BS EN ISO 4288. Geometric Product Specification (GPS) - Surface texture - Profile method: Rules and procedures for the assessment of surface texture*. London: BSi.

British Standards. (2000). *BS ISO 4287. Geometrical product specification - surface texture: profile method - terms, definitions and surface texture parameters*. London: BSi.

British Standards. (2004). *BS EN ISO 13473-1. Characterisation of pavement texture by use of surface profiles. Part 1: Determination of Mean Profile Depth*. London: BSi.

British Standards. (2009). *BS EN 1097-8:2009, Tests for mechanical and physical properties of aggregates - Part 8: Determination of the polished stone value*. London: BSi.

British Standards. (2010). *BS EN 13036-1. Road and airfield surface characteristics - Test methods. Part 1: Measurement of pavement surface macrotexture depth using a volumetric patch technique*. London: BSi.

British Standards. (2011). *BS EN 12697-49. Bituminous mixtures. Test methods for hot mix asphalt. Part 49. Determination of friction after polishing*. London: BSi.

British Standards. (2012). *BS EN ISO 25178-2. Geometrical product specifications (GPS) - Surface texture: Areal. Part 2: Terms, definitions and surface texture parameters*. London: BSi.

Carr, J. R., Norris, G. M., & Newcomb, D. E. (1990). Characterisation of aggregate shape using fractal dimension. *Transportation Research Record 1278*, 43-50.

Chen, X. H., & Wang, D. W. (2011). Fractal and spectral analysis of aggregate surface profile in polishing process. *Wear 271*, 2746-2750.

Cigada, A., Mancosu, F., Manzoni, S., & Zappa, E. (2010). Laser-triangulation device for in-line measurement of road texture at medium and high speed. *Mechanical Systems and Signal Processing 24*, 2225-2234.

Dames, J., Huschek, S., & Lindner, J. (1997). *Untersuchungen ueber den Einfluss unterschiedlicher Mineralstoffe auf das Gebrauchsverhalten von Asphaltdeckschichten hinsichtlich Griffigkeit, Querebenheit und Reifengeraeuschen*. Bonn: Typo-Druck und Verlagsgesellschaft (Forschung Strassenbau und Strassenverkehrstechnik, 754).

Demeyere, M., & Eugène, C. (2004). *Determination of road surface microtexture by laser triangulation under structured lighting: a feasibility study*. Université Catholique de Louvain.

- DfT. (2009). *SCANNER specification 2009, Vol 5 - Technical requirements: SCANNER survey parameters and accreditation*. UK Roads Board and TRL.
- Do, M. T. (2005). Relationship between microtexture and skid resistance. *BLPC 255*, 117-136.
- Do, M. T., Marsac, P., & Delanne, Y. (2004). Prediction of tire/wet road friction from road surface microtexture and tire rubber properties. *Proceedings of the 5th symposium on pavement surface characterisitcs*. Toronto.
- Do, M. -T., Tang, Z., Kane, M., & de Larrard, F. (2009). Evolution of road-surface skid-resistance and texture due to polishing. *Wear* 266, 574-577.
- Do, M.-T., Cerezo, V., Beautru, Y., & Kane, M. (2013). Modeling of the connection road surface microtexture/water depth/friction. *Wear*, In Press.
- Duff, D. (1998). *Holmes' principles of physical geology (fourth edition)*. Cheltenham: Stanley Thornes.
- Dunford, A. (2012). *BOS Slag: 10 years of monitoring*. Crowthorne: TRL - In Press.
- Dunford, A. (2012). *PPR605. Use of the Wehner-Schulze machine to explore better use of aggregates with low polishing resistance. 2: Experiments using the Wehner-Schulze machine*. Crowthorne: TRL.
- Field, J. (2008). David Tabor 23 October 1913 - 26 November 2005. *Biographical memoirs of fellows of the Royal Society* 54, 425-459.
- Forster, S. W. (1989). Pavement microtexture and its relation to skid resistance. *Transportation Research Record* 1215.
- Fukahori, Y., Gabriel, P., & Busfield, J. J. (2010). How does rubber truly slide between Schallamach waves and stick-slip motion? *Wear*, 854-866.
- Gabriel, P., Thomas, A. G., & Busfield, J. J. (2010). Influence of interface geometry on rubber friction. *Wear* 268, 747-750.
- Ganti, S., & Bhushan, B. (1995). Generalised fractal analysis and its application to engineering surfaces. *Wear* 180, 17-34.
- Gough, V. (1974). A tyre engineer looks critically at current traction physics. In D. F. Hays, & A. L. Browne, *The Physics of Tire-Traction and Practice*. New York: Plenum Press.
- Grosch, K. (1963). The relation between the friction and visco-elastic properties of rubber. *Proc. Roy. Soc., A*, 274, 21.



- Hecht, E. (1987). *Optics 2nd Ed.* Addison Wesley.
- Helmli, F. (2011). Focus variation instruments. In R. Leach, *Optical measurement of surface topography* (pp. 131-166). Berlin: Springer.
- Himeno, K., Nakamura, Y., Kawamura, A., & Saito, K. (2000). Skid resistance of asphalt pavement surfaces related to their microtexture. . *Proceedings of the international symposium on pavement surface characteristics of roads and airfields*. Nantes: PIARC.
- Hosking, J. R., & Woodford, G. C. (1976). *LR738 Measurement of skidding resistance. Part II. Factors affecting the slipperiness of a road surface*. Crowthorne: TRL Ltd.
- Huschek, S. (2004). Experience with skid resistance prediction based on traffic simulation. *5th symposium of pavement surface characteristics*. Toronto.
- James, J. G. (1967). *Calcined Bauxite and other atificial, polish resistant, roadstones*. Road Research Laboratory.
- Kummer, H. (1966). Unified theory of rubber and tyre friction. *Engineering Research Bulletin, Pennsylvania Satate University*, B-94.
- Leach, R. (2010). *Fundamental principles of engineering nanometrology*. Oxford: Elsevier.
- Leach, R. (2011). *Optical measurement of surface topography*. Berlin: Springer.
- Leu, M. C., & Henry, J. J. (1978). *Prediction of skid resistance as a function of speed from pavement texture measurements*. Washington: Transportation Research Board.
- Lorenz, B., Carbone, G., & Schulze, C. (2010). Average separation between a rough surface and a rubber block: Comparison between theories and experiments. *Wear* 268, 984-990.
- Mandelbrot, B. (1967). How long is the coast of Britain? Statistical Self-Similarity and Fractal Dimension. *Science* 156, 636-638.
- McGhee, K. K., & Flintsch, G. W. (2003). *High-speed texture measurement of pavements*. Charlottesville: Virginia Transportation Research Council.
- Met Office. (2009). *Regional weather datasets*. Retrieved February 11, 2010, from <http://www.metoffice.gov.uk/climate/uk/datasets/>

Millar, P., & Woodward, D. (2010, January). Close up and dirty: a whistle-stop tour of European highway surface textures. *Asphalt Professional*, pp. 14-17.

Millar, P., Woodward, D., & Friel, S. (2011). Mapping interfacial stress distributions to digital surface microtopography. *3rd International surface friction conference*. Gold Coast, Australia.

Moore, D. (1975). *The friction of pneumatic tyres*. Amsterdam: Elsevier Scientific Publishing Company.

Persson, B. N. (2001). Theory of rubber friction and contact mechanics. *The Journal of Chemical Physics*, 115, 3840-3861.

PIARC. (1987). *Report of the Committee on Surface Characteristics*. Brussels: XVIII World Road Congress.

Pidwerbesky, B., Waters, J., Gransberg, D., & Stempok, R. (2008). Road surface texture measurement using digital image processing and information theory. *International Safer Roads Conference 2008*. Cheltenham.

Radó, Z. (1996). Fractal characterisation of road surface texture for analysis of friction. *International symposium on pavement surface characteristics* (pp. 101-132). Christchurch New Zealand: ARRB.

Roch, P. (1994). Compounding for wet grip. *Proceedings of Tyretex '94*. Munich: Rapra Technology.

Roe, P. G., & Dunford, A. (2012). *PPR564. The skid resistance behaviour of thin surface course systems. HA/MPA/RBA collaborative programme 2008-11: topic 1 final report*. Crowthorne: TRL.

Roe, P. G., Dunford, A., & Crabb, G. I. (2008). *PPR324, HA/QPA/RBA Collaborative Programme 2004/2007: Surface requirements for asphalt roads*. Crowthorne: TRL.

Roth, F., Driscoll, R., & Holt, W. (1942). Frictional properties of rubber. *Journal of Research of the National Bureau of Standards*, 28, 439.

Sabey, B. E. (1958). Pressure distributions beneath spherical and conical shapes pressed into a rubber plane, and their bearing on coefficients of friction under wet conditions. *Proc. Phys. Soc.* 71 979, 979-988.

Sabey, B. E., & Lupton, G. N. (1967). *LR57 Measurement of road surface texture using photogrammetry*. Crowthorne: Road Research Laboratory.

- Savkoor, A. (1965). On the friction of rubber. *Wear*, 8, 222.
- Savkoor, A. R. (1987). *Dry adhesive friction of elastomers - a study of the fundamental mechanical aspects (PhD thesis)*. Delft: Technische Universiteit Delft.
- Schallamach, A. (1971). How does rubber slide? *Wear*, 301-312.
- Scott, P. J. (2004). Pattern analysis and metrology: the extraction of stable features from observable measurements. *Proc. R. Soc. Lond. A* 460, 2845-2864.
- Scott, P. J. (2009). Feature Parameters. *Wear* 266, 548-551.
- Shallamach, A. (1952). The load dependence of rubber friction. *Proc. Phys. Soc. B* 65 657, 657-661.
- Shaw, R. (2007). *An examination of novel roughness parameters to be used in conjunction with the HSE slips assessment tool (SAT)*. London: Health and Safety Executive (HSE).
- Slimane, A. B., Koudeir, M., Brochard, J., & Do, M. T. (2008). Characterisation of road microtexture by means of image analysis. *Wear* 264, 464-468.
- Smith, R. (2008). *Analyzing friction in the design of rubber products and their paired surfaces*. London: CRC Press.
- Tabor, D. (1955). The mechanism of rolling friction. *Proc. Roy. Soc.*, A229, 198.
- Taylor Hobson. (2004). *Talysurf CLI 3D surface profiling systems*. Retrieved April 28, 2012, from [http://www.f-di.hu/cli\\_systems.pdf](http://www.f-di.hu/cli_systems.pdf)
- Thirion, P. (1946). Les coefficients d'adherence du caoutchouc. *Rev. Gen. Caoutch*, 23, 101.
- Thompson, A., Burrows, A., Flavin, D., & Walsh, I. (2004). *The Sustainable Use of High Specification Aggregates for Skid Resistant Road Surfacing in England*. East Grinstead: Capita Symonds Ltd.
- Wikipedia. (n.d.). Retrieved April 12, 2012, from Friction: <http://en.wikipedia.org/wiki/Friction>
- Wolf, G. W. (1991). A Fortran subroutine for cartographic generalisation. *Computers and Geosciences* 17, 1359-1381.

Woodward, D., Woodside, A., Ellis, R., Phillips, P., & Walsh, I. (2008). The effect of aggregate type and size on the performance of thin surfacing materials. *International Safer Roads Conference*. Cheltenham.

Wyszecki, G. (1982). *Colorscience concepts and methods, quantitative data and formulae*. Wiley-Interscience.

Yandell, W. O. (1970). *The measurement of surface texture of road stones with particular regard to the effect on the frictional properties of road surfaces*. University of New South Wales.

Young, J. C. (1977). *SR290 Calibration, maintenance and use of the rolling straightedge*. Crowthorne: TRRL.

### 3 Feasibility studies

---

The body of work presented in this thesis was begun to investigate the possibility of enhancing existing skid resistance measurement techniques by making measurements without requiring physical contact with the road. Although this is still a long-term objective it is already clear that a solid theoretical understanding of the mechanisms involved in the generation of friction, or the way that a road's surface texture is related to its skid resistance, is required before it can be achieved. This chapter presents a summary of trial experiments carried out to explore the feasibility of collecting useful information about the road surface at speeds that are sufficiently high to allow some practical implementation on the road network, and to develop methods for improving the understanding of the mechanisms involved in friction generation.

The three sections demonstrate:

- It is possible, or likely to be possible in the near future, to collect useful information about the microtexture of the road surface at traffic speeds.
- It appears to be possible to analyse that information in such a way as to discern something about the road's skid resistance, but there are a number of unknown quantities that require further study.
- It is possible to make surface texture measurements in the laboratory that appear to distinguish the skid resistance properties of aggregates although some refinement to the methodology is required.

### 3.1 Collecting information about road surface texture

The available literature (Section 2.3) suggests that the only practical means of collecting information about the texture of the road surface at sufficiently high resolution as well as sufficiently high speeds is likely to involve image capture. This may be in conjunction with line projection (Forster, 1989), (Demeyere & Eugène, 2004) or by using stereovision (Slimane, Koudeir, Brochard, & Do, 2008). Two of the reasons for image capture being so practically appealing are:

- High resolution is already achievable, although whether it is *sufficiently* high remains a matter for investigation and the consumer market drives a desire for ever-increasing camera resolution.
- The technology to achieve sufficiently high speeds (i.e. capture at traffic speed) is in development. There is a commercial need for fast image capture because, for example, it is used on production lines for automatic inspection of machined parts.

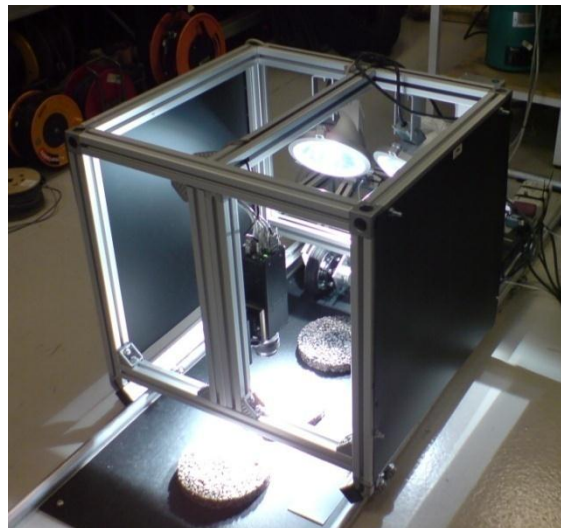
As part of a project for Highways Agency that was already running at the start of the PhD study reported in this thesis (Brittain & Dunford, 2007), a prototype system was developed to assess the possibility of collecting high resolution images at traffic speed. The project and its technical content was managed and supervised by the author, but much of the technical work was carried out by a project team at TRL, largely by Stuart Brittain, with technical input from Helen Viner. In the first instance, equipment was mounted to a trolley structure and then an attempt was made to mount the same equipment onto a vehicle. The project is briefly summarised in the following paragraphs to put into context the potential for practical application of the laboratory studies presented in subsequent chapters.

In addition to analysis hardware, software and associated media onto which to record collected images, there are three critical components to a system for taking continuous images of the road surface, and these directly determine its performance:

- Camera. In principle, any camera could be used, provided it could be programmed to take a series of images as it is moved along the road surface. In the case of the prototype system, a line-scan camera was used, specifically a Dalsa Trillium TR-33 colour linescan camera.

- Lighting. The amount of light available is critical. Images need to be well lit so that exposure time can be reduced and capture speed can consequently be maximised. It is also important that images are lit uniformly, although it may be possible to correct for systematic lighting variation. Narrow beam high pressure discharge lamps (SIL projectors) were used on the prototype system.
- Distance measurement or triggering mechanism. It is clearly necessary to be able to assign a location to any captured image so that, if it can be used for surface characterisation, that output can be put to good use. To avoid taking pictures of the same bit of surface over and over again, the camera needs to be triggered so that images are only captured when it is pointing at a new view.

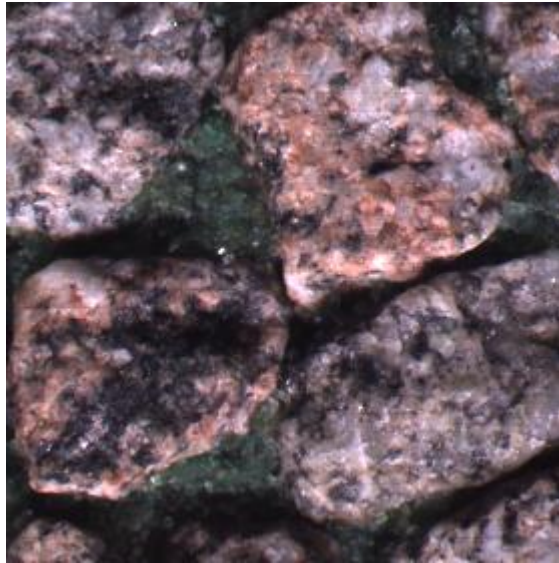
The prototype system is shown in Figure 3.1.



**Figure 3.1 Prototype imaging system**

The camera scans a line of 2048 pixels. The transverse resolution of captured images depends on the lens used and the camera's proximity to the surface. The camera is triggered to scan a line of image using a mechanical rotary shaft encoder mounted onto the hub of a wheel that rotates as the trolley is moved forward. The size of the wheel and the shaft encoder specifications determine the triggering distance/frequency. On the prototype trolley, the distance measurement wheel was 160 mm in diameter and the encoder provides 20,000 output signals per wheel revolution which gives approximately one pulse for every 25  $\mu\text{m}$  movement of the trolley. This is well within the suggested range for road surface 'microtexture', which is defined as texture with wavelengths less than 0.5 mm (Section 2.2).

The camera is connected, via an interface box, to a computer with a frame grabber board (Horizon 4LC by i2S-linescan, Pessac France) that receives the digital information. Software on the computer controls the camera (CAP, by i2S-linescan) and stitches individual scanned lines together to create contiguous images that are automatically stored to the hard disc (ImageCapture by Softronic Systems). The photograph in Figure 3.2 shows granite aggregate particles embedded in a green sand matrix, used as a sample subject for testing the system.



**Figure 3.2 Typical output from prototype image capture system**

Various camera or system settings affect the quality of the image output, and the ease with which the image can be captured. There are several main performance factors to be considered: resolution, depth of field, exposure, focus and the possible speed of capture. The performance factors are all inter-related; improving one has the effect of degenerating another.

Resolution is affected by the quality of the camera, the quality or resolving power of the lens, and the distance between the camera and its subject, called the standoff of the camera. Since the camera and lens remain constant, the resolution in the prototype system can be controlled by increasing or decreasing the standoff. However, altering the standoff has an effect on the depth of field. Since aggregate particle surfaces vary in height, the camera must be able to keep a range of heights in focus, in addition to compensating for the range of movement of the camera as it travels over the surface. It was found that a transverse resolution of



50  $\mu\text{m}$  was achievable when the camera standoff is approximately 215 mm, which in turn gives a depth of field of approximately 4 mm.

However, the depth of field is also affected by the f-stop setting of the lens, which controls the size of the aperture on the lens - a high f-stop corresponds to a small aperture, and a low f-stop corresponds to a large aperture. Decreasing the size of the aperture increases the depth of field but decreases the amount of light travelling through the lens. The decrease in light can be counteracted by increasing the exposure time settings of the camera. The above stated resolution and depth of field were achieved using f-stop 5.6 and an exposure time of 250  $\mu\text{s}$ , and this generated images that were bright enough to easily distinguish surface features. The amount of light available determines the exposure time, which in turn determines the f-stop, depth of field, camera stand-off and resolution. Lighting mechanisms are available that focus light in a line to coincide with the linescan camera and these would improve performance substantially.

The speed capability of the prototype system can be adjusted slightly, by sub-sampling scanned lines for example, but it was ultimately limited by the equipment used. It was determined that the maximum speed of the prototype system, for capture of useable images, was approximately 8 km/h, which is hardly traffic-speed. However, the equipment used was not purchased specifically for this feasibility study (new equipment being a large capital expenditure). At the time of the study it was determined that camera apparatus was already available to increase the maximum potential capture speed to almost 50 km/h, and at the time of writing the same manufacturer makes a camera with sufficiently high linescan rate to allow a theoretical maximum speed of 80 km/h. Provision of sufficiently intense light may still be a limiting factor but it is not unreasonable to expect development in this field to match that of camera speed enhancement.

As an exercise to investigate the further technical issues that might result from mounting the equipment on a vehicle, the trolley prototype was dismantled and its components were mounted on the rear structure of a highways survey vehicle. The survey vehicle (the Highways Agency Road Research Information System, HARRIS) already has on-board computers, power and lighting for the purposes of capturing its own, somewhat lower resolution, images that are used for analysis of surface condition such as cracking. Although these features simplified the system it was immediately

apparent that two additional technical difficulties would need to be overcome before the system can be used on the public road network: proximity of the equipment to the road and focus control or depth of field to cope with vertical movement associated with vehicle suspension.

### **3.2 Using information contained in high resolution images of aggregate surfaces**

In other project work at TRL, this time both led and undertaken by the author with assistance from Clint Mays and Nathan Dhillon, images of aggregate particles were analysed in attempts to characterise their surfaces in relation to friction. This is the direct precursor to the in-depth comparative analysis of aggregate surface microtexture and measured friction that is presented in Chapter 4 onwards, although the work described below was more focussed on practical application.

It had already been determined that image capture is the only method likely to be suitable for capturing high resolution information about the road surface at sufficiently high speeds. So, it was decided that, in parallel to developing equipment that might eventually be able to capture the required images, methods should be sought that could use the information contained in the images.

In order to relate changes observed in the images with changes in skid resistance measured, surfaces with a range of skid resistances must be used. This is common to all of the experimental work described in the following chapters. While a range of levels could be achieved by using a variety of materials – smooth glass or polished limestone compared with freshly quarried granite for example – in order to reduce the number of variables arising from differing material structures, in this work the range of levels has been achieved using one material at a time, polished to different extents. Polishing has been applied using the Highways Agency's Wehner-Schulze machine, the basic operation of which is described in Section 2.6.

The specimens used for the first experiment of its type, attempted as part of the present study, had been prepared as part of work to commission Highways Agency's Wehner-Schulze (W-S) polishing machine in the UK (Woodbridge, Dunford, & Roe, 2006). The three specimens were asphalt discs prepared in the laboratory using three different coarse aggregates, gritstone, granite and limestone, which were chosen because they represent a wide mineralogical and polish resistance range (the latter being measured using the polished stone value test - see Section 2.6).

Aggregate particles in the available asphalt specimens were still coated with bitumen - the preparation process in the laboratory involving

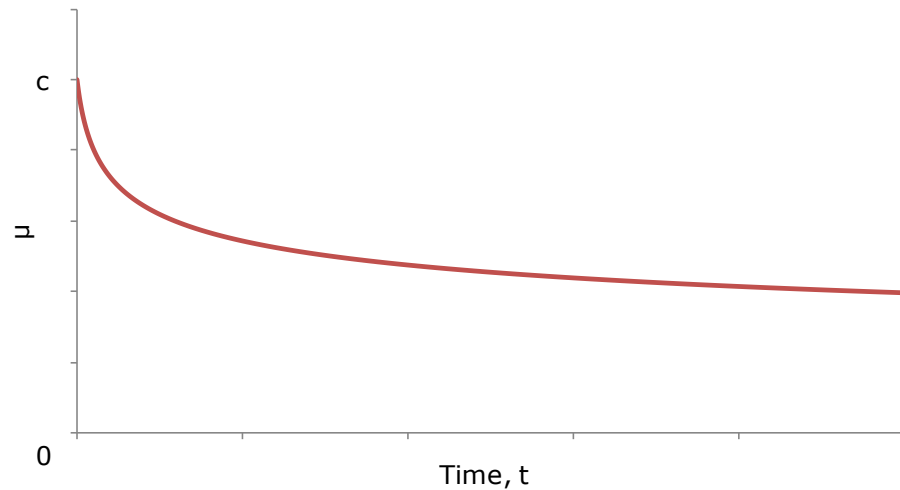
combining aggregate and hot bitumen in a large mixer before compacting slabs of material and allowing the bitumen to cool and bind all the components together. In order to reveal the aggregate particles, the specimen surfaces were subjected to gritblasting and this had the combined effect of clearing the majority of the bitumen and roughening the aggregate surfaces. Friction tested on all three specimens was similar, despite being prepared from three different aggregate types. In order to examine surfaces representing a range of friction levels, the specimens were incrementally polished using the W-S machine.

Note that, while the majority of the text up to this point has used the term 'skid resistance' to refer to a property of a surface that contributes to friction, the Wehner-Schulze machine reports its results as 'friction'. 'Skid resistance' is normally measured via analysis of forces acting on a sliding rubber block or tyre and can only really be considered as a property of the surface if all other factors (i.e. the measurement technique) are kept constant. It would be valid to say "skid resistance measured using the W-S machine" but since the W-S machine reports friction,  $\mu$ , it is that term that will be used for the remainder of this thesis when referring to measurements made in the laboratory.

Huschek (2004) proposed, under polishing, both in the laboratory and by traffic, the friction generated when testing asphalt or aggregate develops according to a power law:

$$\mu = c(t + 1)^b \quad 3.1$$

where  $\mu$  is friction at time  $t$ ,  $c$  is the initial friction and  $b$  is a factor to be determined by adjustment. It has also been suggested that the effect of other external factors must also be overlaid (e.g. seasonal variation – see Section 2.5) but, typically, the underlying evolution of skid resistance has the form shown in Figure 3.3.

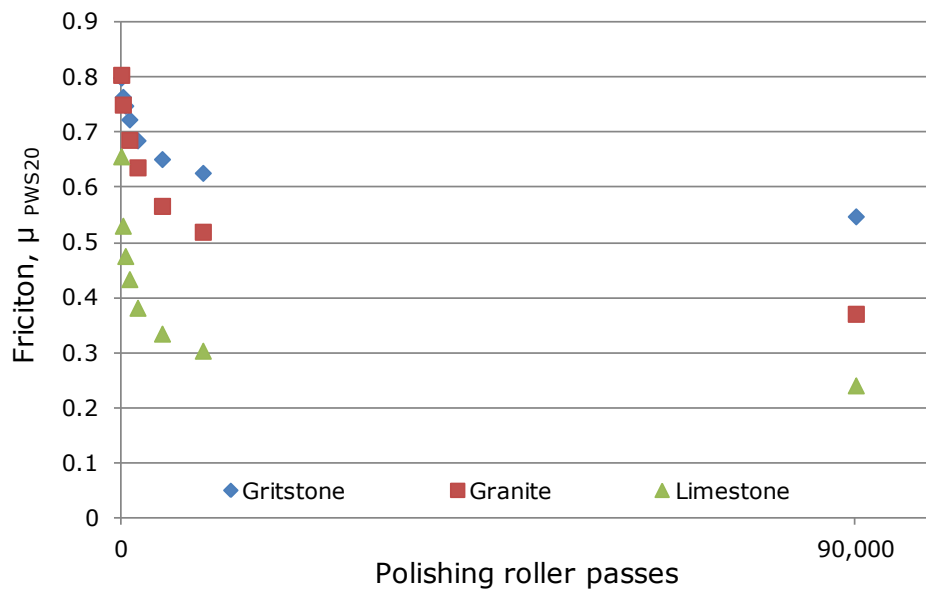


**Figure 3.3 Evolution of friction for asphalt or aggregate undergoing polishing**

For polishing in the Wehner-Schulze machine, this evolution in friction, to an almost asymptotic level, occurs during the manufacturer-specified polishing duration of 90,000 roller passes (which takes an hour). Consequently, in order to capture images of the aggregate surfaces while their frictional properties were changing, the polishing process was carried out in an intermittent fashion with friction tests made and images taken during the earliest part of the process. The state of the surfaces was studied at eight levels of polishing, with 0; 200; 500; 1,000; 2,000; 5,000; 10,000 and 90,000 cumulative passes of the polishing rollers.

Standard operating procedure for the W-S machine involves testing friction with an initial test head speed of 100 km/h, taking the value calculated from measured torque at 60 km/h. However, it is known that the action of friction testing is quite abrasive, which is why tests often include a 'test to the limit' stage after all polishing has been applied. In order to mitigate the potential uncontrolled polishing effect of the friction test itself the initial test speed was reduced to 50 km/h and the friction at 20 km/h was used as a metric. A short experiment demonstrating the validity of this approach is described in Chapter 5.

The graph in Figure 3.4 shows the friction measurement made at each polishing stage for each of the three asphalt specimens.



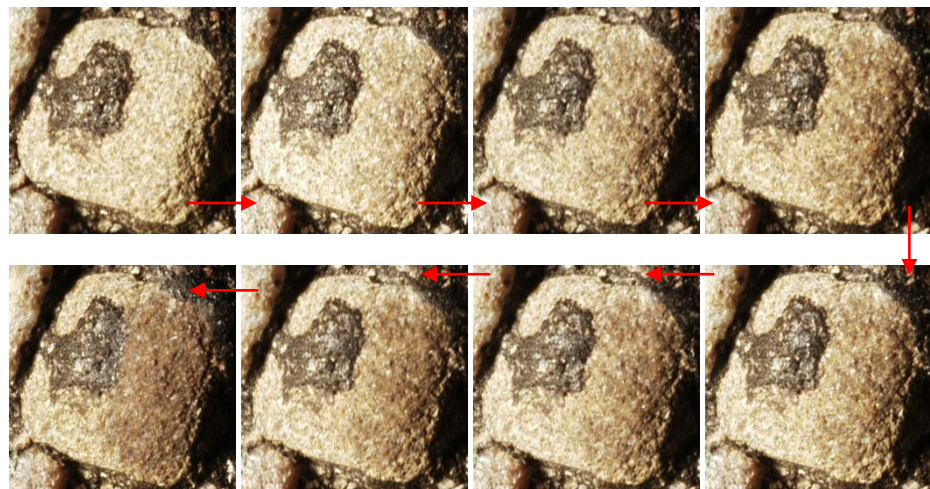
**Figure 3.4 Evolution of friction for three asphalt specimens**

After each polishing stage, a set of photographs was taken. A digital camera with a 55 mm macro lens at a stand-off of 150 mm was used to provide an image area of 45 mm by 30 mm, sufficient to cover several aggregate particles. The samples were lit at an angle of 45° to horizontal using a metal halide discharge lamp encompassing a large floodlight reflector – the same light source used on the prototype trolley equipment described in Section 3.1. To assist photography, the asphalt specimens were positioned under the camera equipment using a simple wooden turntable. The edges of the asphalt specimens were marked (with permanent marker pen) to coincide with marks on the turntable platen and, in turn, the platen was marked so that it could be rotated and accurately lined up with marks on the turntable base. In this way, the same area of each specimen could be photographed after each polishing stage.

On each specimen surface, seven rectangular areas, distributed along the wear path of the W-S machine's polishing rollers, were photographed. Figure 3.5 is an example of one of the photographs taken, while Figure 3.6 shows, clockwise from top left, the changing appearance of a single, gritstone, aggregate particle surface as it was polished. For further analysis, six 'polished' areas were selected on each of the seven photographs. The right hand side of the aggregate particle shown in Figure 3.6, for example, was selected as a 'polished area'.



**Figure 3.5 Photograph of polished asphalt specimen**



**Figure 3.6 Photographs of aggregate particle in asphalt specimen showing changing appearance with polishing**

It can be seen that the polishing process causes the aggregate particles to darken in appearance. Before this structured experiment had been carried out it was expected that the topography of the surface might be revealed in photographs by the shadows projected by surface asperities. Consequently, the first analysis method attempted was designed to examine the length of shadows on the surface. To do this, the number of contiguous pixels that fell below a defined intensity threshold, along each horizontal line within the images, was counted and an average 'shadow length' for each image was calculated.

Each image was processed using bespoke software (Imageviewer, by Alex Wright, Peter Watson, Clint Mays, TRL, Crowthorne) to convert pixel

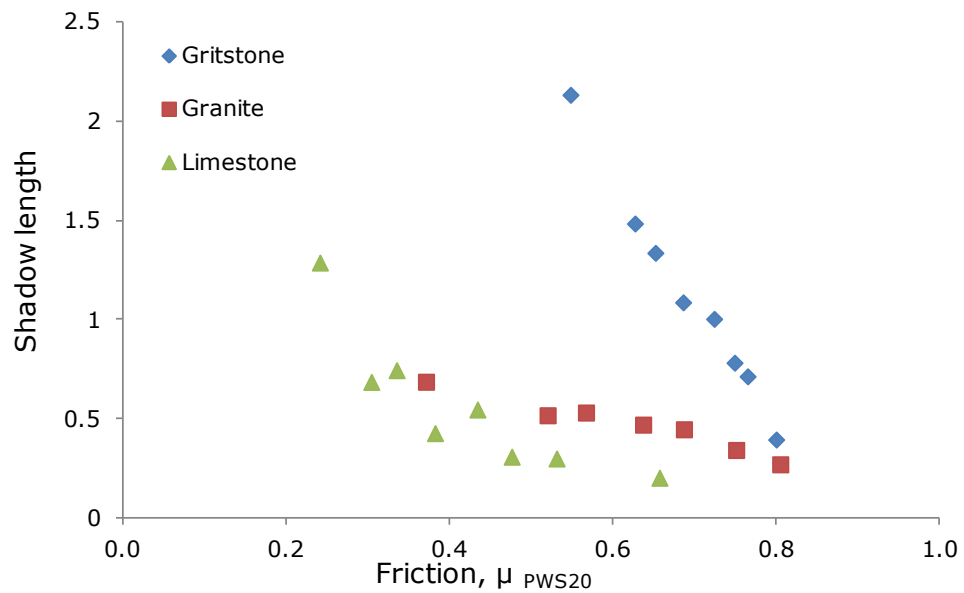
intensities into a matrix of values that could be loaded into a spreadsheet package. Using Microsoft Excel, the average shadow length for each small image section is easily calculated, and a simple method for doing so is described below for a very small example area just 10 pixels wide and 10 pixels tall.

- Transpose the matrix of pixel intensities so that horizontal lines in the image appear as columns in the spreadsheet, in cells A1:J10.
- In cell A12 insert the formula “=IF(A1<=\$L\$1, 1, 0)” and copy this formula right to fill a row of ten cells (A12:J12). This converts the pixel intensity values in the first row of the pixel intensity matrix into 1s if it is below some threshold intensity, which is written into cell L1.
- In cell A13 insert the formula “=IF(A1<=\$L\$1, A12+1, 0)” and copy this formula to fill the remaining block of 10x10 cells. If the next cell in the column of intensity values also falls below the defined threshold, the count of ‘shadow length’ in that column increases.
- In cell A23 insert the formula “=IF(A12>A13,A12)” and copy this down and across to fill the next block of 10x10 cells (A23:J32). This will create a third and final matrix that consists only of maximum values for the number of contiguous cells which fall below the defined threshold and FALSE responses.
- In cell A34 insert the formula “=AVERAGE(A23:J32)”. This will give the average length of contiguous pixels that fall below the defined threshold or the average ‘shadow length’ for that section of the image.

It was discovered that the easiest way to set an appropriate pixel intensity threshold was to calculate the 60<sup>th</sup> percentile intensity for each image under analysis. This helps to account for any slight variation in lighting or other equipment set up between the photographs taken at different stages of the polishing process.

An average shadow length was calculated for each of the ‘polished’ sections of the photographs of each specimen, taken at each of the eight polishing increments. The graph in Figure 3.7 shows average ‘shadow length’ against friction.





**Figure 3.7 Average length of contiguous pixels falling below a 60<sup>th</sup> percentile intensity for photographs of polished areas on asphalt specimens**

It is clear that the name given to this analysis is inappropriate: as friction is reduced, the average length of contiguous pixels falling below a given threshold increases. This is counter to the theory that shadows are cast by asperities in the surface and, in fact, this is plain to see in the images in Figure 3.6. However, the findings may still be of some practical benefit if the interpretation is slightly altered. Areas (or lines) of pixel intensities that become more homogenous probably correspond to a surface topography that is also becoming more homogenous, hence smoother, hence effecting less available friction.

It is clear that the relationship is different for different aggregate types. So, while there does seem to be potential for practical application, it will first be necessary to determine why the appearances of the surfaces of different aggregate types change differently as they polish. In order to do this, it was necessary to move away from studying the potential for practical application and begin to make real measurements of surface texture. The following section describes work in this field that was carried out by TRL and SWPE (now URS) during 2008 under a project for Highways Agency.

### **3.3 Developing a methodology for measuring and characterising aggregate surface texture**

The work described in this chapter was carried out by a team of researchers. The majority of the measurements were made at the University of Nottingham by SP Chong of SWPE Ltd. Measurement methodologies were developed by SP Chong and the author and the analysis presented here was undertaken by the author with input from Tony Parry (University of Nottingham), Alistair Hunter (SWPE Ltd) and Peter Roe (TRL Ltd). The project for which this work was carried out aimed to establish an explanation for the observed uplift in skid resistance that occurs when thin surface course systems (the top layer of the road over which vehicles travel) are prepared with a maximum particle size of 6 mm, as opposed to 10 mm or 14 mm. Consequently, the specimens studied used aggregates of those sizes and the work aimed to compare their surface texture. As such, the outcomes are not tailored to the present PhD study, but there is significant relevance in the development of surface texture measurement and analysis methodologies.

Three specimen types were used in the study: cores taken from the road, aggregate-only mosaics and aggregate-only plaques used for measuring polish resistance in the polished stone value (PSV) test (see Section 2.6).

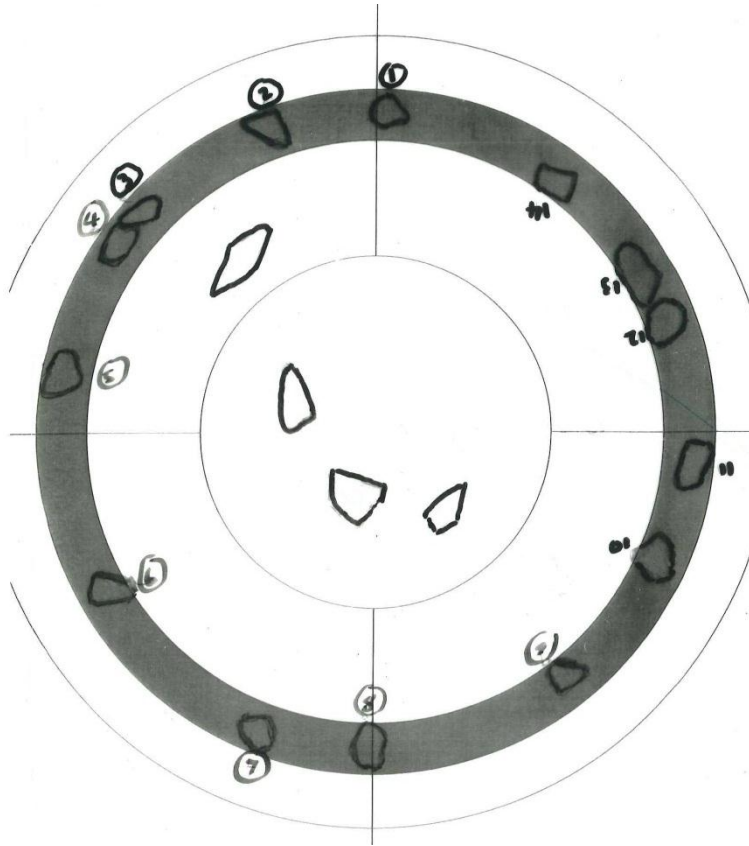
Surface texture was measured on each specimen using a Talysurf CLI 1000 (manufactured by Taylor Hobson), which is described in Section 2.3. Friction was measured, using the Wehner-Schulze machine, on the cores extracted from the road and on the aggregate-only mosaics prepared for polishing in the same machine – for the latter, friction was measured before and after polishing. No friction measurements were made on the PSV test plaques before they were polished, but the polished stone value for the aggregate, as measured with the portable skid resistance tester, was reported.

#### **3.3.1 Texture measurements**

The Talysurf CLI 1000 laser profiler uses a non-contact laser triangulation measurement system. The test specimen is moved under the point of focus of the laser using a servo-controlled platform. The specimen is moved in the X-direction to build up a line of height measurements. When a complete line of measurements has been recorded, the specimen is moved incrementally in the Y-direction and returned to zero in the X-

direction in order to scan the next line. For this experiment, measurement spacing was set to 1  $\mu\text{m}$  in the X-direction and to 20  $\mu\text{m}$  in the Y-direction. On the specimens with 14 mm aggregate particle size, areas of 2 mm square were scanned, and on specimens with 6 mm and 10 mm particle sizes, rectangular areas of 2 mm (X-direction) by 1 mm (Y-direction) were scanned. The different sample distances in the Y-direction were driven by the ability to fit the scanned area onto the aggregate surfaces. Note, however, that the length of scan in the X-direction remained the same throughout and this simplifies texture characterisation, as described below.

To identify and record the locations of the scanned areas on each specimen, and so that the same surfaces could be measured before and after polishing, transparent films were used to mark (using permanent marker pen) the relative positions of the aggregate particles. An example of one of the films, for the 10 mm aggregate-only mosaic, is shown in Figure 3.8. The outer ring has diameter 225 mm, the same as the circular mosaics and cores taken from the road and the shaded annulus marks the approximate sweep of the friction measuring feet in the Wehner-Schulze machine. The outlines of four particles in the centre are marked to assist with aligning the transparency on the specimen and the outlines of fourteen aggregate particles, where texture measurements were made, are marked around the circumference of the friction measurement area.



**Figure 3.8 Copy of transparency used to record aggregate particle positions on aggregate-only mosaic**

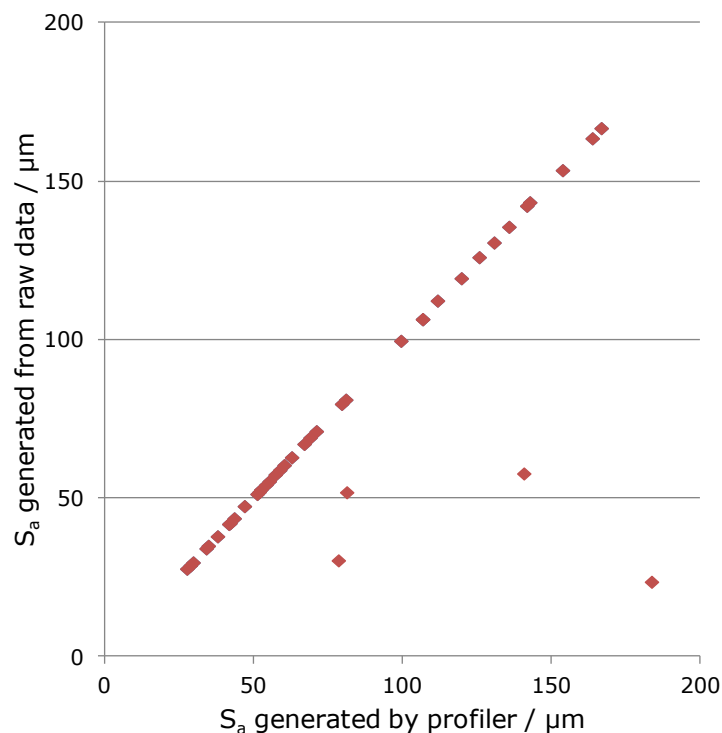
Depending on the size of the individual aggregate particles, two or three areas were scanned on each surface. The number of aggregate particles, and areas measured, was limited by the time available for use of the laser profiler. Generally, for each specimen (in each state of polish), a day was spent making measurements of surface texture on aggregate particles distributed approximately evenly around the specimen.

### **3.3.2 Characterising texture**

The laser profiler allows the user to select from a range of roughness parameters, which can be calculated from profile measurements, in order to characterise the surface. For each of the measured areas, the following parameters were calculated by the profiler software:  $S_a$ ,  $S_q$ ,  $S_z$ ,  $R_a$ ,  $R_q$  and  $R_z$ . Definitions and equations for calculating these parameters are presented in Section 2.4. In addition, raw measurements were output from the laser profiler to plain text files (.csv, comma separated value) so that manual calculation of these parameters could be attempted.

Due to operator error, additional settings such as the cut-off lengths used for roughness parameters calculated by the profiler were not recorded.

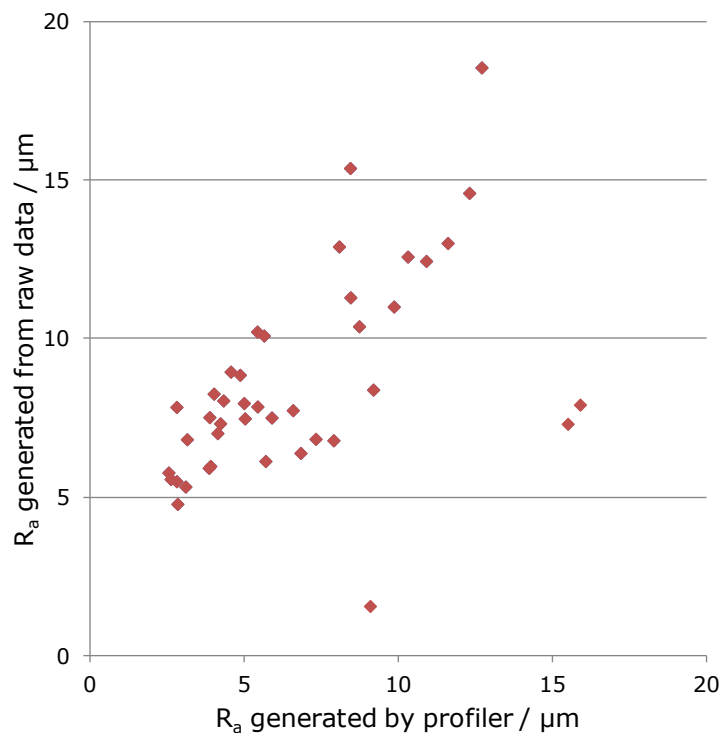
However, it is possible to determine them by comparison with the 'manually' calculated parameters, which were generated using spreadsheet package Microsoft Excel and a simple visual basic macro. The graph in Figure 3.9 shows the relationship between  $S_a$  calculated by the profiler and  $S_a$  calculated using the raw data, both from measurements made on the core extracted from the road with 14 mm maximum particle size. Aside from a few outlying points, the relationship is exactly 1:1. Since the manual calculation used all the raw data, without applying a cut-off length, it can be deduced that the laser profiler also used no additional cut-off or that the cut-off length applied was longer than the longest dimension of the scanned areas (2 mm).



**Figure 3.9 Comparison between profiler calculated and manually calculated areal roughness parameter**

While the areal parameters ( $S_a$  etc.) output by the machine are calculated using the whole area, the profile parameters ( $R_a$  etc.) are calculated using a single arbitrarily chosen scan line scanned in the x-direction, which has the highest resolution. Consequently, when roughness parameters calculated manually were compared with those values given by the profiler, a better correlation was obtained for the areal parameters than for the profile parameters. The exact line used for calculation by the profiler was not recorded and no attempt was made, by comparing manual to profiler calculated parameters, to determine which line was used. The 'manual'

calculation was carried out for each scanned line in turn, and an average profile roughness returned for the whole area. The relationship between  $R_a$  calculated by the profiler and  $R_a$  calculated using the raw data, both from measurements made on the core, as above, is shown in Figure 3.10. It was found that, by manually calculating  $R_a$  with a number of different cut-off lengths including 10  $\mu\text{m}$ , 25  $\mu\text{m}$ , 100  $\mu\text{m}$ , 250  $\mu\text{m}$ , 1000  $\mu\text{m}$  and 2000  $\mu\text{m}$ , the best correlation between manual and profiler generated  $R_a$  was for 250  $\mu\text{m}$ . It is likely that the profiler was set for this cut-off length, which, as was later discovered, is recommended in the measurement standard (British Standards, 1998).



**Figure 3.10 Comparison between profiler calculated and manually calculated profile roughness parameter**

Most of the outliers from the trends for both areal and profile roughness parameters are either due to corrupt or incorrectly saved raw data. Some of the outliers cannot be readily explained by interrogation of the data, but may be due to measurement variability. To examine this further, some tests for repeatability (where the scan was repeated without moving the specimen) and reproducibility (where the specimen was removed and replaced as accurately as possible between successive scans) were made. Table 3.1 shows the parameters  $S_a$  and  $R_a$  for the same area on the 14 mm core specimen, calculated by the profiler, without moving the specimen

(columns on the left, for three scan areas) and when the specimen was removed and replaced (columns on the right for one scan area).

It can be seen that overall repeatability does not account for outlying measurements. However, insofar as it is possible to observe very large variation in measured parameters when the specimen is moved, reproducibility and specimen positioning might. It is likely that, for the profile parameter case, where the specimen is locally very rough, variation across a scanned area may lead to disparity between profiler calculated values (using a single line) and manually calculated values (using an average of all scanned lines). Further, the profiler may automatically exclude measurement points from its calculation of the areal parameter if they are individually outlying, whereas the manual calculation did not. To mitigate the effect of high reproducibility or surface variability on overall texture characterisation, it was deemed important to make enough roughness measurements to ensure that any calculated roughness parameters are representative of the whole surface.

**Table 3.1 Measurement variability for laser profile scanning**

Test label	Repeatability						Reproducibility	
	Area 1		Area 2		Area 3		$S_a$	$R_a$
	$S_a$	$R_a$	$S_a$	$R_a$	$S_a$	$R_a$		
a	47.6	2.5	183	9.1	52.8	8.9	115.0*	12.2*
b	47.3	2.5	184	9.1	52.6	8.8	57.0	8.6
c	47.3	2.5	184	9.1	52.6	8.8	47.6	10.4
d	47.2	2.7	184	9.1	52.6	8.7	48.3	10.7
e	47.1	2.7	184	9.1	52.6	8.7	53.9	8.4
f	47.1	2.9	184	9.1	52.6	8.7		
g	47.0	2.9	184	9.1	52.6	8.7		
h	47.0	3.0	184	9.1	52.6	8.6		
i	46.9	3.0	184	9.1	52.7	8.7		
j	46.9	3.1	184	9.1	52.6	8.6		
$\sigma$	0.22	0.23	0.32	0.01	0.07	0.09	28.58	1.58
r	0.60	0.62	0.88	0.04	0.19	0.26	-	-
R	-	-	-	-	-	-	79.22	4.43
*If the highlighted values are considered outliers then ignoring them yields:								
$\sigma$							4.52	1.19
r							-	-
R							12.58	3.37

### 3.3.3 Comparing texture and friction

Table 3.2 shows the average  $S_a$ , calculated across all scanned areas, for each of the aggregate mosaic specimens, both before and after polishing in the Wehner-Schulze machine and for each of the cores taken from the road sites. Table 3.2 also shows the friction measured on each of these samples using the Wehner-Schulze machine. From these measurements, it is apparent that:

- The relationship between  $S_a$  and friction is not very strong - compare the 14 mm mosaic and the 14 mm core from the road.
- Where specimens have been polished in the laboratory both friction and average roughness have reduced.

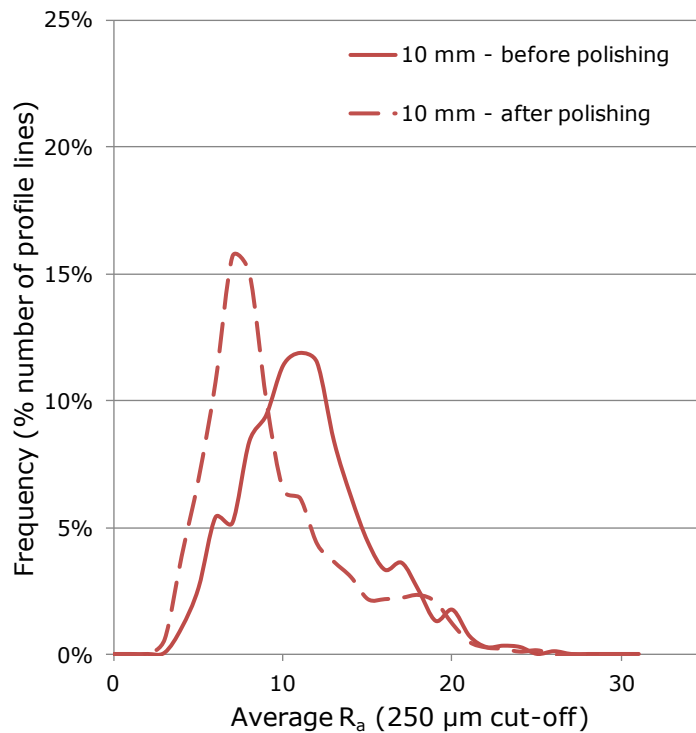


A simple calculation of average  $S_a$ , with no filtering, does not sufficiently characterise surface friction as a standalone measurement but it does appear to indicate that a change has occurred.

**Table 3.2  $S_a$  and friction for mosaics and road cores**

Specimen		$S_a / \mu\text{m}$	Friction, $\mu_{\text{PWS60}}$
Mosaic before polishing	6 mm	44.6	0.43
	10 mm	61.3	0.48
	14 mm	80.6	0.49
Mosaic after polishing	6 mm	36.9	0.43
	10 mm	51.8	0.44
	14 mm	67.0	0.37
Cores from road site	6 mm	61.5	0.47
	10 mm	45.6	0.42
	14 mm	83.8	0.39

A similar conclusion can be reached by making use of more of the raw data. Figure 3.11 shows the distribution of  $R_a$  values, which were calculated for each line within each scanned area on each specimen, for the 10 mm specimen, before and after polishing in the laboratory. The distributions have been normalised to the number of profile lines scanned and are shown against bin size  $1 \mu\text{m}$ . As a result of polishing, the distribution of profile roughness shifts towards lower values. A similar behaviour holds for each of the other specimens, with 6 mm and 14 mm aggregate particles sizes.



**Figure 3.11 Change in distribution of  $R_a$  due to polishing**

To check the significance of this result, a brief statistical analysis was carried out. The software package SPSS 14.0 was used and, because the distributions are all skewed, and probably not normal, non-parametric tests were used to give an indication of the difference between two compared distributions. For the Mann-Whitney, Wilcoxon W, Moses extreme reaction, two sample Kolmogorov-Smirnov and Wald-Wolfowitz tests, a significance level of less than 0.05 demonstrates that the distributions (measurements of  $R_a$ ) appear to come from the same parent population in fewer than 5% of instances. For the distributions shown in Figure 3.11, the significance value was 0.000 – the distributions are indeed different.

### **3.4 Discussion**

The three experiments described in this chapter were carried out in the early stages of study and they all help to inform the work presented in the following chapters.

It is theoretically possible to capture high resolution information about the road surface, either now or at least in the near future. This is an important consideration because the possibility of practical implementation not only provides a *raison d'être* but has made possible the funding and interest for more laboratory studies to come.

It has been shown that the information collected, in the form of high resolution photographs, should enable some characterisation of the surface in a way that relates to its skid resistance. The experiments carried out in the laboratory to investigate the changing appearance of the surface have developed appropriate methods for polishing and friction testing that allow investigation of discrete friction levels. The way in which aggregate surfaces change during the polishing process seems to be dependent on aggregate mineralogy.

Surface profile measurements made on a range of aggregate and asphalt specimens demonstrate that it is possible to make meaningful measurements on specimens of this type, which are generally much rougher than would normally be examined in the laboratory. Experience with the measurement technique has given confidence that, in general, texture measurements are accurate, but that a large number of measurements should be made in order to properly characterise the surface. Raw data can be manipulated to calculate a range of roughness parameters and the application of filtering is likely to be important in the future. Broad characterisation of roughness and relating it to friction is not straightforward but the comparison of the same surface before and after polishing seems to be the most promising approach for future work.

The methodology, and its development, presented in the following chapters uses the experience of the experiments above by:

- Making measurements of texture at several stages of polishing, rather than just before- and after-polishing.
- Taking photographs of surfaces so that qualitative observations of changing texture can be made.

- Measuring as much of the surface area as time will allow.
- Collecting as much data as possible, by increasing resolution along the Y-axis.
- Reducing the amount of corrupt data by careful measurement and handling of data.

### 3.5 References

- British Standards. (1998). *BS EN ISO 4288:1998, Geometric Product Specification (GPS) - Surface texture - Profile method: Rules and procedures for the assessment of surface texture*. London: BSi.
- Brittain, S., & Dunford, A. (2007). *Development and optimisation of a prototype microtexture capture system*. Crowthorne: TRL.
- Demeyere, M., & Eugène, C. (2004). *Determination of road surface microtexture by laser triangulation under structured lighting: a feasibility study*. Université Catholique de Louvain.
- Forster, S. W. (1989). Pavement microtexture and its relation to skid resistance. *Transportation Research Record 1215*.
- Huschek, S. (2004). Experience with skid resistance prediction based on traffic simulation. *5th symposium of pavement surface characteristics*. Toronto.
- Slimane, A. B., Koudeir, M., Brochard, J., & Do, M. T. (2008). Characterisation of road microtexture by means of image analysis. *Wear 264*, 464-468.
- Woodbridge, M. E., Dunford, A., & Roe, P. G. (2006). *PPR144, Wehner-Schulze machine: First UK experiences with a new test for polishing resistance in aggregates*. Crowthorne: TRL.



## **4 First attempts at an improved methodology for examination of surface texture changes**

---

This chapter describes experiments carried out to develop the methodologies explored in the feasibility studies (Chapter 3). Using an aggregate specimen prepared specifically for the purpose, the changing appearance of aggregate surfaces as they are polished in the laboratory was monitored using high resolution photography and an attempt to measure changing texture was made using optical microscopy. The work was sponsored by the Transport Research Foundation and has been reported elsewhere (Dunford, 2010). All work was carried out by the author with assistance from staff at the University of Nottingham (scanning electron microscopy), the National Physical Laboratory (texture measurements) and TRL (use of IDL visualisation software for analysis).

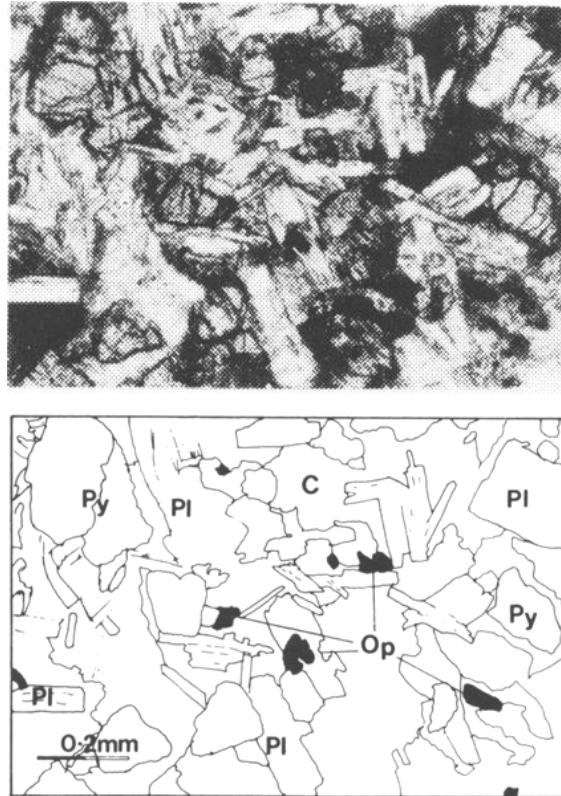
## **4.1 Methodology**

In a similar fashion to that described in Section 3.2, the Wehner-Schulze (W-S) machine was used to polish the surface of an aggregate specimen. As before, polishing in a staged fashion provides a series of similar surfaces with a range of levels of friction (as measured using the W-S machine).

### **4.1.1 Specimen**

To reduce the number of variables, and obviate the need for prior gritblasting to remove a bitumen coating, an aggregate mosaic that could be polished in the W-S machine, was prepared using a dolerite aggregate. The dolerite aggregate was chosen because of the relative abundance of this type of aggregate in the UK (Thompson, Burrows, Flavin, & Walsh, 2004) and because the particular aggregate was readily available at TRL, having been used, between 1983 and 2011, as the control stone in the PSV test. Consequently, petrographic information is available in the public domain (West & Sibbick, 1988). The stone "is composed mainly of plagioclase feldspar, an opaque mineral and pyroxene ... these minerals together constitute 99 % of the total rock". It is noted that the feldspars (62 % by volume) have maximum grain size 0.6 mm long and 0.1 mm wide, the pyroxenes (23 % by volume) have maximum grain size 1.5 mm and the opaque minerals (14 % by volume) have maximum grain size 0.6 mm. For completeness, the photomicrographs presented by West and Sibbick, and the line-drawn interpretation, from which the mineral composition was determined, are shown in Figure 4.1. The abbreviations used in the line drawing are: Py, pyroxene; Pl, plagioclase; C, chlorite; Op, opaque minerals.





**Figure 4.1 Photomicrograph and line-drawn interpretation of quartz dolerite aggregate**

Figure 4.2 shows a photograph of one area of the mosaic specimens prepared using the aggregate.



**Figure 4.2 Dolerite aggregate specimen prepared for polishing**

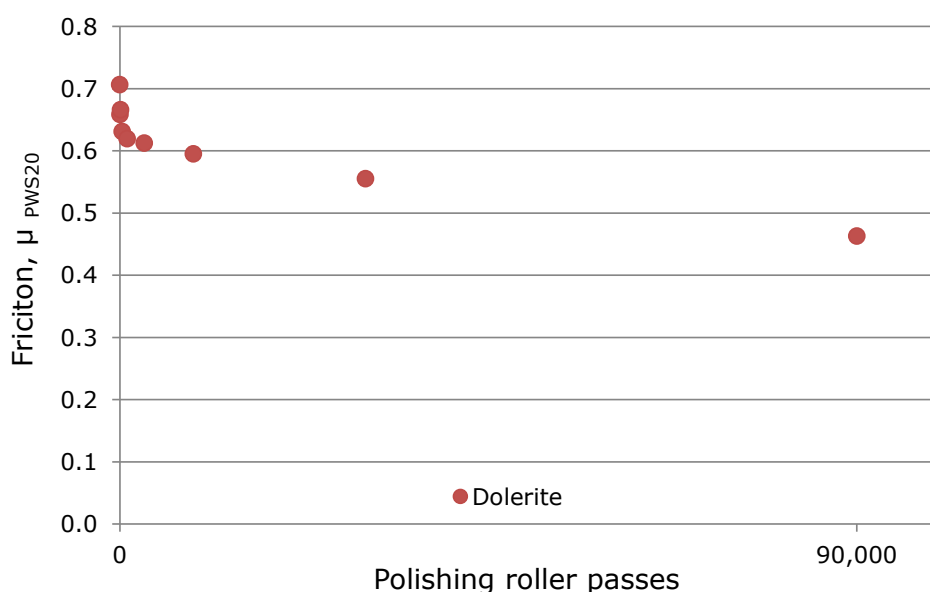
In the case of the aggregate mosaic, instead of bitumen, aggregate particles are stuck together using epoxy resin and sand, which is green. The uppermost surfaces of the aggregate particles are nominally flat

because the mosaic is prepared in such a way as to maximise the surface area that comes into contact with the W-S machine's polishing rollers.

#### 4.1.2 Polishing

In the feasibility study, the change in friction with polishing appeared to conform to a logarithmic pattern, so the polishing regime was altered to be structured in the same manner: polishing was applied in nine stages with measurements being made after cumulative passes of the polishing rollers amounting to 30; 90; 300; 900; 3,000; 9,000; 30,000 and 90,000, in addition to the initial state. These nine discrete levels of polishing are referred to by number (0-8) for the rest of the chapter. Because the surface was not coated in bitumen there was no need to reveal aggregate surfaces with gritblasting.

The graph in Figure 4.3 shows the friction measurements against the number of polishing roller passes.



**Figure 4.3 Evolution of friction on dolerite aggregate mosaic**

At each polishing level (including before-polishing), a set of photographs of the specimen surface and a set of three replicas of the specimen surface were taken before friction was measured using the Wehner-Schulze machine. The replication technique is described in more detail in Section 4.1.4. Replicas of the surface were taken so that measurements of surface texture could be made more easily (the equipment used to measure surface texture being in a different place to the Wehner-Schulze machine), and so that a scanning electron microscope could be used to examine the

surface (the whole aggregate specimen being too large to fit in the microscope chamber).

#### **4.1.3      *Photography***

In order to take photographs of identical areas of the specimen surface at sufficient resolution to track any changes occurring to the surface texture as the specimen was polished, the following equipment was used:

- Nikon D200 10 megapixel digital SLR
- Sigma 50 mm F2.8 DG macro lens
- Copy stand
- Specimen mounting turntable
- Flash lamp set to evenly illuminate the area of interest on the specimen.

The specimen was mounted into the turntable and carefully marked so that its position could be accurately repeated with respect to the camera position in subsequent photographs. Photographs were taken of six areas of the surface around the circumference of the aggregate specimen within the area swept by the polishing rollers of the Wehner-Schulze machine. Each photographed area encompassed at least 5 aggregate particles so that a total of 30 individual aggregate surfaces could be analysed.

#### **4.1.4      *Surface replication***

In order to examine the surface texture within the same area of aggregate before and after polishing, and to retain a record of the polishing state, replicas of the surface were made at each level of polishing. A commercial replication compound, designed for engineering inspection purposes, (Microset Products Ltd, Nuneaton) was used. This two part polymer system is mixed as it is dispensed onto the surface from a cartridge to form a semi-viscous liquid which cures quickly to form a flexible solid compound that can be peeled from the surface to give an inverse relief (mirror image) replica. Normally used to perform metallography of machine components such as inspection of microstructure, micro-cracking and pitting, the replicating compound has better than 0.1  $\mu\text{m}$  resolution, according to the manufacturer.

At each stage of polishing, three areas were replicated. This was achieved by surrounding the area of interest with a plastic ring of diameter 50 mm and flooding the surface within the ring with replicating compound. The

working life of the compound is 30 seconds which was sufficient time for it to coat the surface within the ring and also self-level to give a flat base to the finished (inverted) plaque. Figure 4.4 shows one of the prepared plaques; the replicated surface texture of each aggregate particle can be seen easily. Note that between aggregate particles there are 'walls' of replication material formed when the compound flowed between particles on the mosaic surface.



**Figure 4.4 Replicated aggregate specimen**

When each replica plaque was removed from the surface, the area with which it had been in contact was darker than the surrounding aggregate. This was queried with the manufacturer who thought it could either be that a 'monomolecular layer of silicon compound' had been left on the surface, or that the replica plaque had removed very fine detritus from the surface leaving behind an intricately cleaned area. The replicated areas can be seen clearly on the aggregate specimen shown in Figure 4.5.



**Figure 4.5 Aggregate specimen used in experiment**

#### **4.1.5 Scanning electron microscopy**

The technique of scanning electron microscopy (SEM) is described in Section 2.3. It was initially used to compare the surfaces of aggregate particles and their replicas in order to validate the replication technique. It

was then used to qualitatively examine the changing texture of the aggregate (as recorded by replication) as the specimen was polished in the laboratory. The specific microscope used was a Philips/FEI XL30 with a tungsten filament electron source and assistance in its operation and preparation of specimens was given by Nigel Neate. When trying to compare specific areas of the surface, either between aggregate and replica, or before and after polishing, a navigation technique was developed, which is described further in Section 5.3 because it was used later to track specific areas for texture measurement.

#### **4.1.6      *Surface texture measurement***

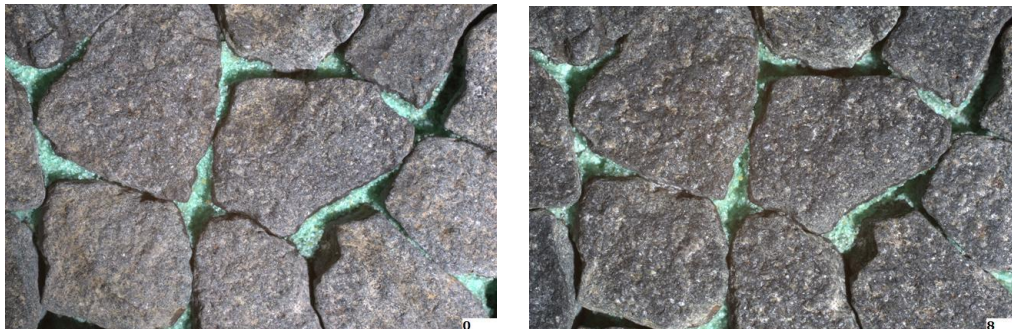
Texture measurements were made on the replicated surfaces of aggregate particles at each of the nine polishing levels using an Alicona Infinite Focus microscope at the National Physical Laboratory (NPL). The microscope's method of operation is described in Section 2.3.

Following from the feasibility study, surface texture was measured on a number of replicas of aggregate particles within the area swept by the W-S machine's polishing rollers. The 3D surface profile in three arbitrarily selected rectangular areas was scanned at three positions on each aggregate particle. Each rectangular area had dimensions of approximately 2.8 mm by 2.2 mm. According to settings on the microscope, minimum spacing between measurement points within the scanned areas was 3.5  $\mu\text{m}$  in all three dimensions. Five aggregate particles were selected within each of the three replicated areas so that, for each polishing level, surface texture was measured in 45 individual areas.

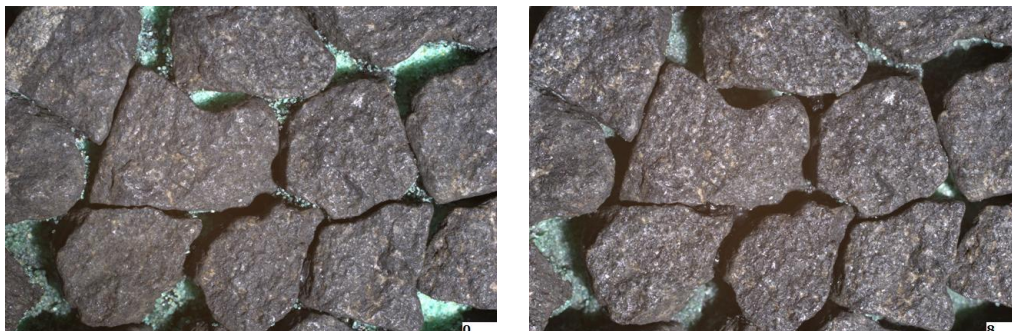


## 4.2 Photography

Six areas of the aggregate specimen were photographed, three of which were replicated, as described in Section 4.1. Figure 4.6 shows two images of the specimen surface before polishing (left) and after all polishing (right), for one of the three areas that were photographed but not replicated. Figure 4.7 shows a similar pair of images for one of the three areas that were replicated. In the first pair of images, from a non-replicated area, the aggregate surfaces appear darker after polishing (i.e. the image on the right is darker). In the second pair, the difference between the two images is less marked, in fact both appear darker than the image of the unpolished, non-replicated area (top left). The lighting was sufficiently well controlled to give confidence that the darkening effect observed (or not observed when comparing the second pair of photographs) is due to the changing surfaces rather than changes in ambient lighting. It has already been noted that the replicating compound leaves behind a darkened area (Figure 4.5).



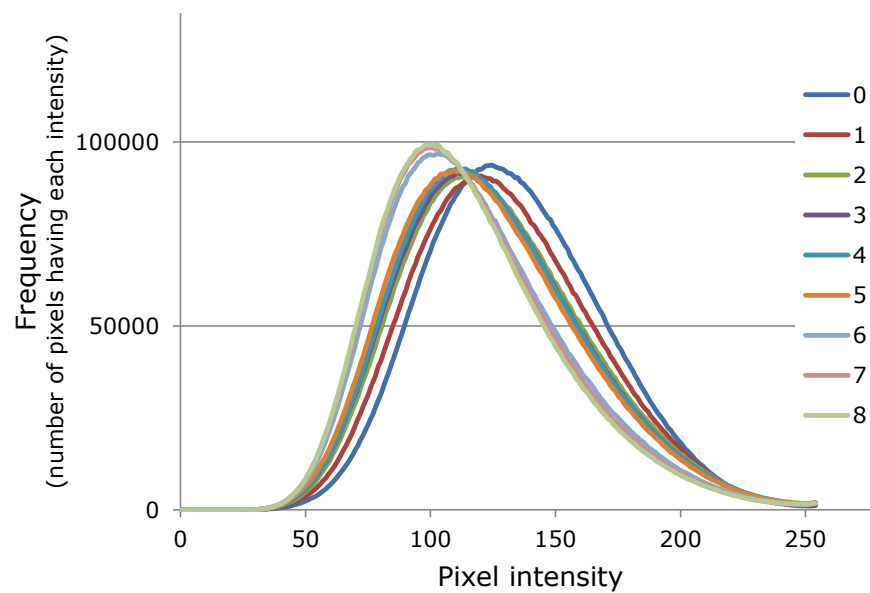
**Figure 4.6 Images from non-replicated areas before (left) and after all polishing**



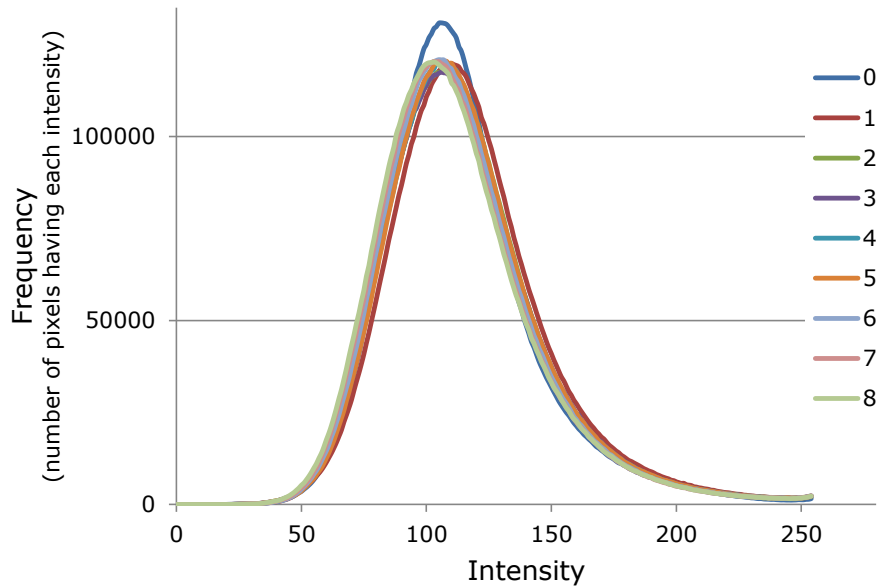
**Figure 4.7 Images from replicated areas before (left) and after all polishing**

Figure 4.8 shows pixel intensity histograms for photographs taken at each of the polishing levels 0 to 8 within the non-replicated areas. Figure 4.9 shows equivalent pixel intensity histograms for photographs of the

replicated areas. Each photograph has just over 10 million pixels, and each pixel can have a discrete intensity value from 0 to 255. The graphs show a smoothed representation of the number of pixels with each level of intensity, averaged over the three photographs taken at each polishing level. In the non-replicated areas, the distribution skews towards lower pixel intensities (darker images) with polishing, but in the replicated areas, the distribution of pixel intensities remains broadly the same throughout the polishing process. Note also that the non-replicated areas are lighter before polishing, and contain a broader range of pixel intensities (the replicated areas are darker and more homogenous). These measurements are consistent with observations based on the images above and suggest that the action of replicating the surface masks the effect of polishing that can be visibly observed. In turn, if the replication process does clean the surface by removing microscopic detritus, this suggests that the visible effect of polishing might be due to a change in the amount of detritus present – perhaps a rougher surface can trap more detritus, which is visible because it contrasts with the aggregate, than can a polished surface.



**Figure 4.8 Intensity histograms for non-replicated areas.**



**Figure 4.9 Intensity histograms for replicated areas**

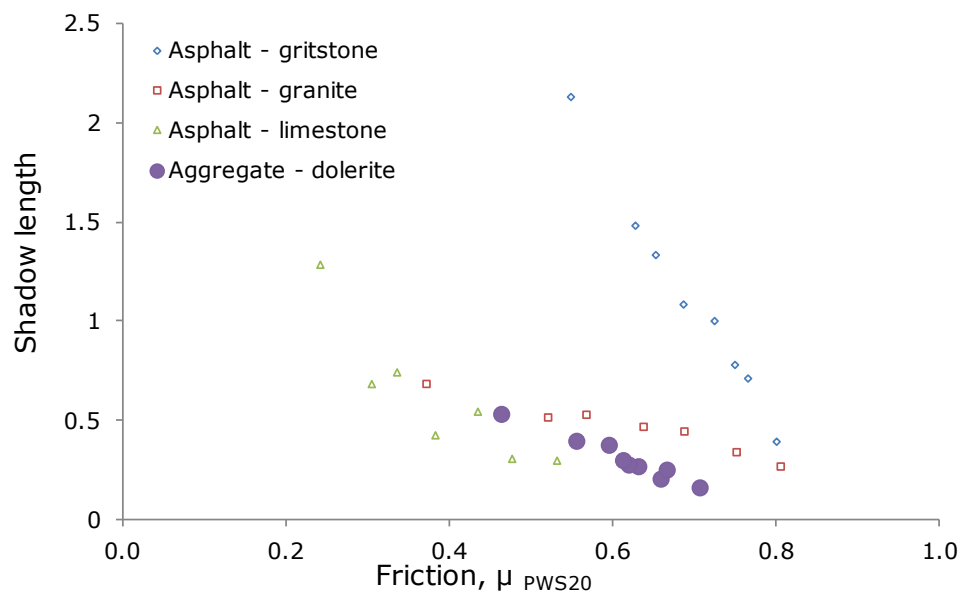
Image processing analysis algorithms were developed in the feasibility study already presented (Section 3.2). On this specimen, because it was not necessary to choose bitumen-free areas, as before, the aggregate sections were segregated from the sand filled gaps in between by manually masking each photograph (see Figure 4.10) before any further image analysis was carried out.



**Figure 4.10 Dolerite aggregate photograph masked to segregate aggregate from sand-filled gaps**



The 'shadow length' algorithm, giving the average length of contiguous pixels with intensity lower than the images' 60<sup>th</sup> percentile, was then applied as in the previous feasibility study. When applied to the replicated areas it was found that the parameters did not vary with polishing level. When applied to the non-replicated areas, the 'shadow length' increases with polishing, and therefore with decreasing friction; this is shown in Figure 4.11 using purple filled circles. Results from the asphalt specimens used in the feasibility study are shown for reference using small, unfilled symbols.



**Figure 4.11 Average length of contiguous pixels falling below a 60th percentile intensity for photographs of polished areas on dolerite aggregate specimen**

For all specimens the average length of contiguous pixels falling below an intensity threshold increases with decreasing friction (reading the x-axis from right to left according to the polishing applied in the laboratory). If longer 'shadows' appear because the surface is becoming more homogenous, i.e. smoother, then this stands to reason.

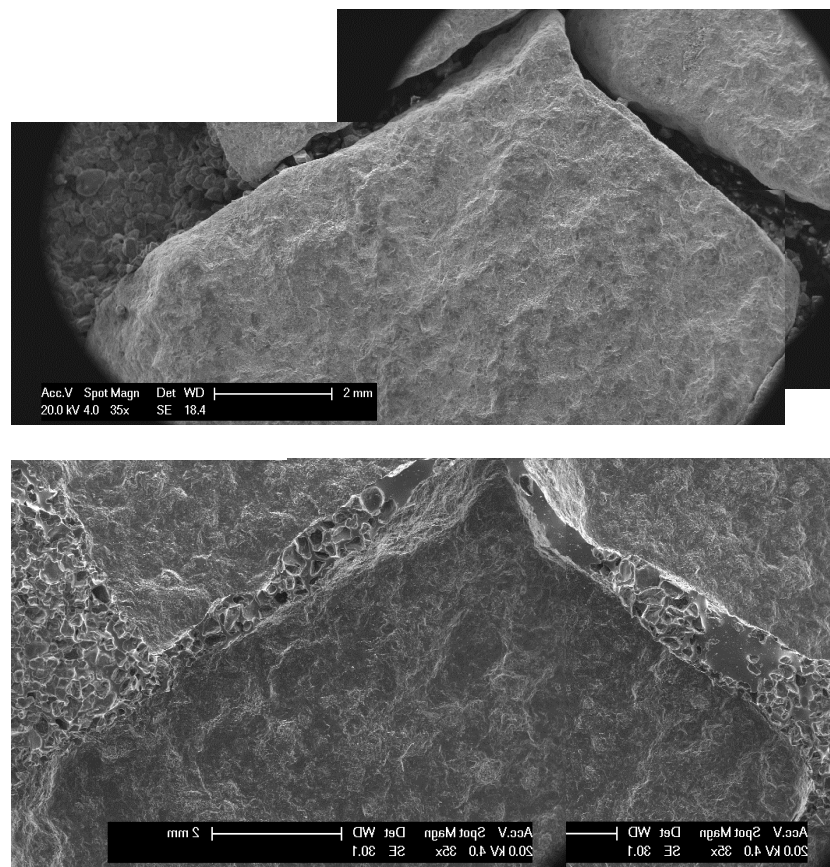
It is useful to observe that results from the dolerite specimen are most similar to the results from the granite specimen in terms of the range of friction measured and the range of 'shadow length' determined from photographs of the surfaces. The range of friction observed is similar because the two aggregates nominally have similar performance according to measurements made using the polished stone value test, as reported by the quarries from which the aggregates were taken. The range of average 'shadow length' measured may be similar because the two aggregates have

similar mineralogical composition. Both are igneous rocks consisting of dispersions of hard particles in a softer matrix (James, 1967). It is difficult to compare the other aggregates: for a given friction, say 0.6, the 'shadow length' on the gritstone is considerably higher than on the dolerite (1.7 compared with 0.4). If longer shadows imply smoother surfaces then the dolerite is generating the same friction with a rougher surface. There may be different relationships with friction for different wavelengths of texture, and the different mineralogies of the aggregates may result in different friction mechanisms.

### 4.3 Scanning electron microscopy

Scanning electron microscopy was used first to check the fidelity of surface replication. It was then used to examine the surfaces before and after polishing to gain a qualitative assessment of the polishing process.

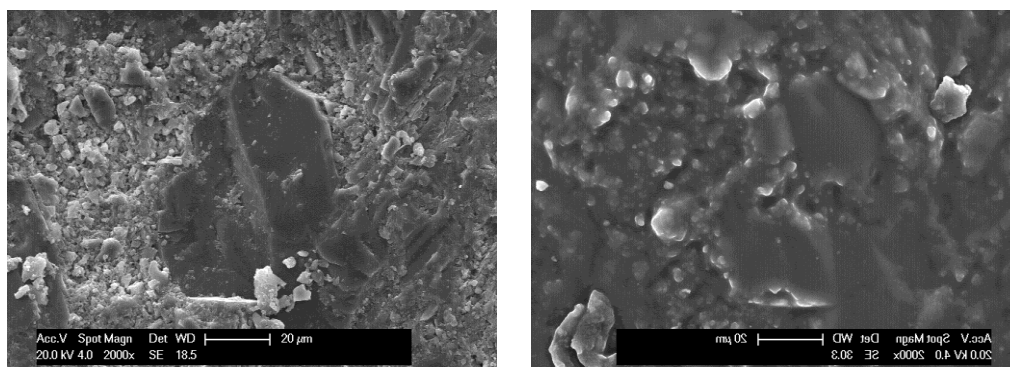
To check the fidelity of replication, a small disc (50 mm diameter) was cut from an additional aggregate specimen, and the replicating compound was applied to its surface using a plastic ring to form a boundary so that the replication liquid could pool over the whole area. Scanning electron microscopy (SEM) was then used to compare the replica to the aggregate surface. Figure 4.12 shows low magnification (composite) images of a stone (top) and its replica (bottom). Because the replication process provides a 'mirror image' of the surface, the SEM images of the replica have been transposed left-right so that the orientation matches.



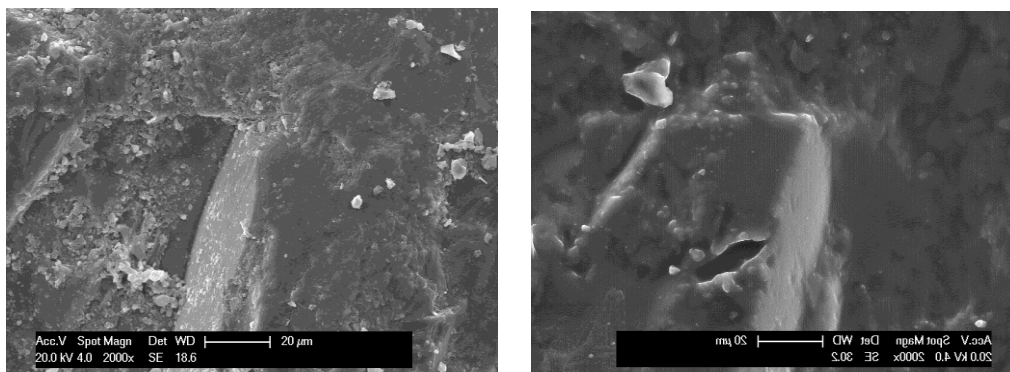
**Figure 4.12 Low magnification images of stone (top) and replica (bottom)**

Using the shape of the stone and its edges for navigation, several corresponding positions were found on both the stone and on the replica. Figure 4.13 and Figure 4.14 show two features of the surface which are

clearly visible and easily identifiable on both the stone (left) and the replica (right). The scale information in the black bar on the bottom of each image indicates a length of 20  $\mu\text{m}$ .



**Figure 4.13 Feature 1 – stone (left) and replica (right)**



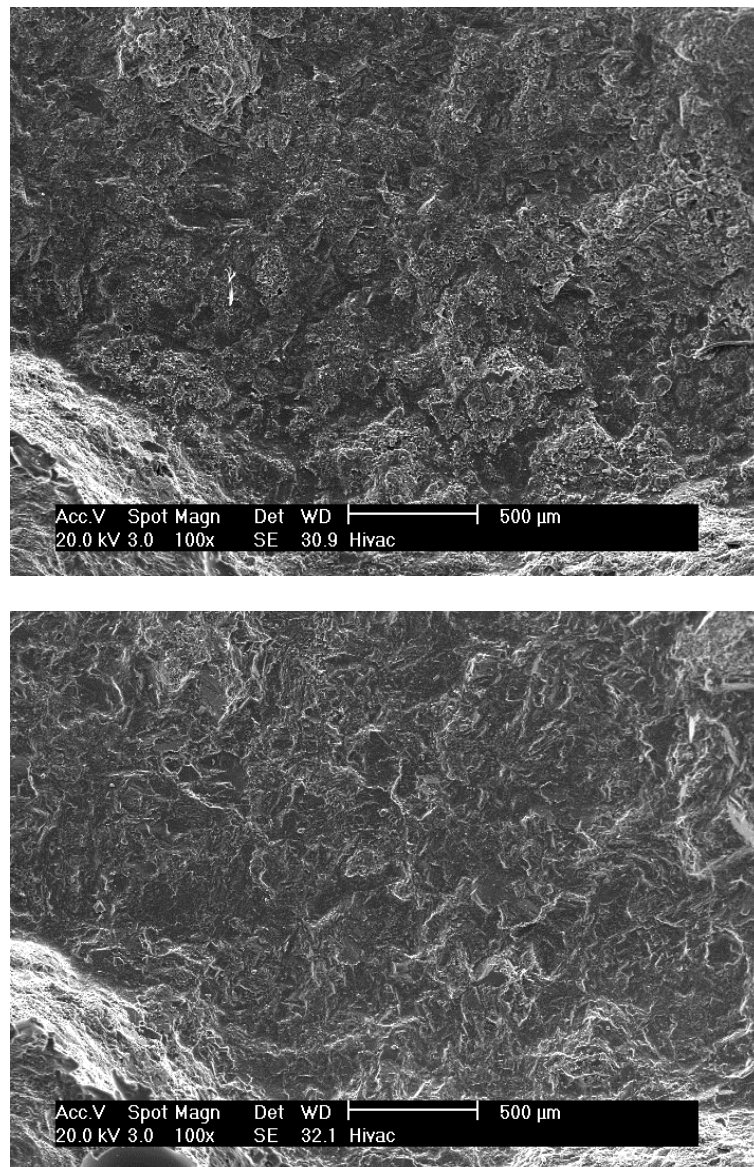
**Figure 4.14 Feature 2 – stone (left) and replica (right)**

This preliminary experiment allows some confidence in the replication technique for aggregate surfaces, and shows that small features between 5  $\mu\text{m}$  and 10  $\mu\text{m}$  are definitely replicated. However, there is some loss of definition on the smallest features suggesting that the resolution of the replication compound may not be as high as 0.1  $\mu\text{m}$  when measuring this type of surface.

In order to directly compare the aggregate surfaces before and after polishing, a similar technique was used to identify specific features on the before-polishing replica and then find the same features on the after-polishing replica.

Scanning electron microscope images of the surface from replica plaques of the before- and after-polishing states can be difficult to interpret because the replica surface is in negative relief. The changes expected due to polishing are presumed to primarily affect the uppermost surfaces of the stone; these surfaces will be represented by the lowermost surfaces of the replica plaques. When comparing SEM images collected before and after

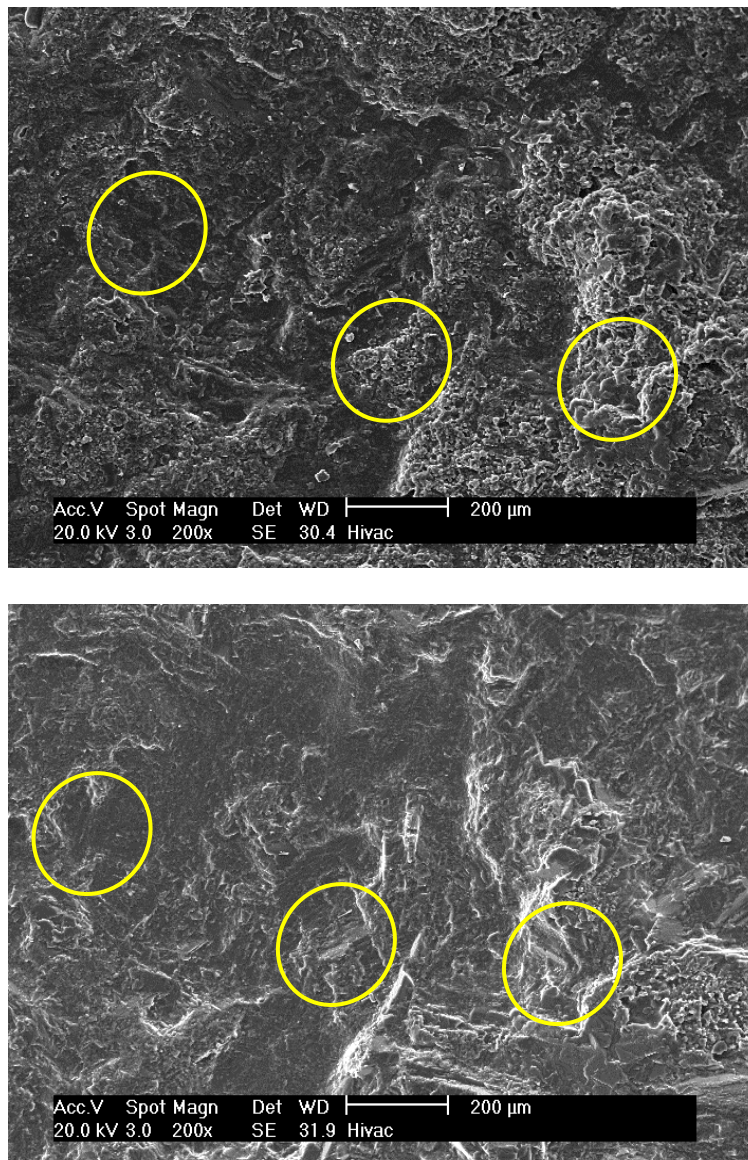
polishing, there are some very clear changes in the texture of the surface. Figure 4.15 shows a section of replica surface, at relatively low magnification, on the plaques before (top) and after polishing. Subjectively, the image after polishing appears smoother in general. It is possible to identify specific areas of the images that appear to show change on different scales (a length of 500  $\mu\text{m}$  is indicated in the black information bar at the bottom of each image).



**Figure 4.15 Texture changes between before-polishing (top) and after-polishing (bottom) at 100x magnification**

Higher magnification images are shown in Figure 4.16 for a second area of the surface. Again, the general smoothness of the after-polishing surface compared to the before-polishing surface is apparent. There are several distinct planes in the image, and the effect of the polishing process is

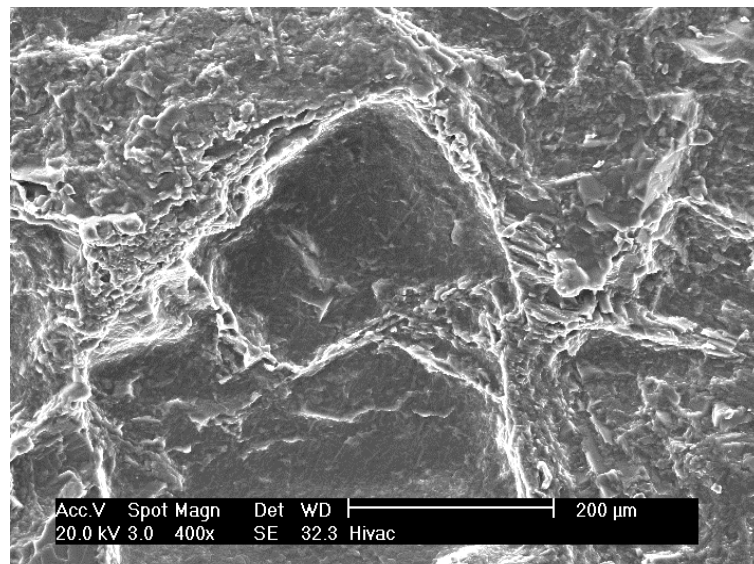
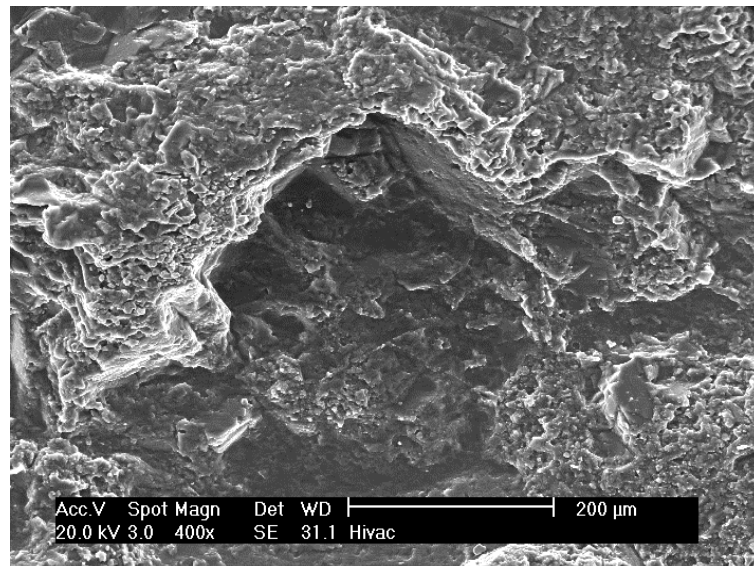
noticeable across their full width – examples highlighted with yellow ovals are clearly smoother in the image after polishing.



**Figure 4.16 Texture changes between before-polishing (top) and after-polishing (bottom) at 200x magnification**

The images in Figure 4.17 show a particular feature that has clearly changed on more than one scale. The edges of the triangular plane have become more rounded while the surfaces are distinctly smoother, and an additional fracture line has appeared horizontally across its centre.





**Figure 4.17 Texture changes between before-polishing (top) and after-polishing (bottom) at 400x magnification**

## 4.4 Surface texture measurements

Analysis of surface texture measurements made using the focus variation scanning microscope was undertaken using three different software packages: Microsoft Excel, data visualisation software IDL by ITT Visual Information Systems, and bespoke texture analysis software MountainsMap by Digitalsurf. The three sub-sections that follow describe the analysis undertaken using these three tools, the last two being carried out simultaneously in an attempt to improve on the results generated by calculation in Excel.

### 4.4.1 Analysis using raw data and Microsoft Excel

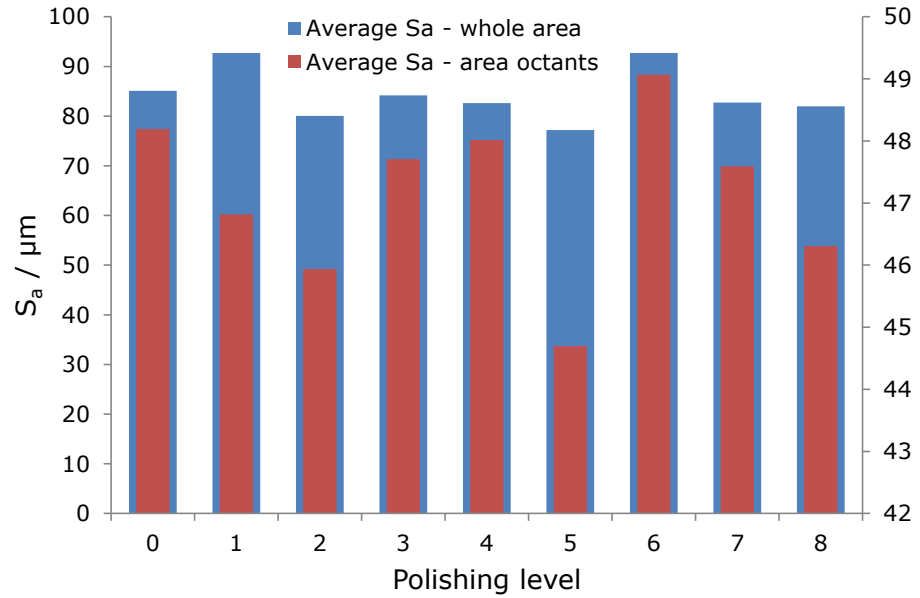
Excel was used to calculate a basic version of the roughness parameter,  $S_a$ , which is the arithmetic mean of absolute departures of a surface from a mean plane (British Standards, 2008). Equation 4.1 is the standard notation for calculation of  $S_a$ .

$$S_a = \frac{1}{A} \int_0^{l_y} \int_0^{l_x} |z(x,y)| dx dy \quad 4.1$$

In the first instance, assessment lengths  $l_x$  and  $l_y$  were set to be the extent of the area measured: 2.8 mm and 2.2 mm respectively. In practice, the value of  $S_a$  was calculated by taking the average of all height measurements within each area and then summing the absolute differences between each measurement and this average before finally dividing by the number of points.

Each scanned area was divided into eight equal portions (octants) and the same basic calculation was repeated. This effectively applies a basic filter by setting the assessment lengths  $l_x$  and  $l_y$  to 0.7 mm and 1.1 mm respectively. The graph in Figure 4.18 shows the average calculated  $S_a$  for each polishing level for the full areas (blue columns in the background using the axis on the left) and for the area octants (red columns in the foreground using the axis on the right).





**Figure 4.18 Basic calculations of  $S_a$  for each polishing level**

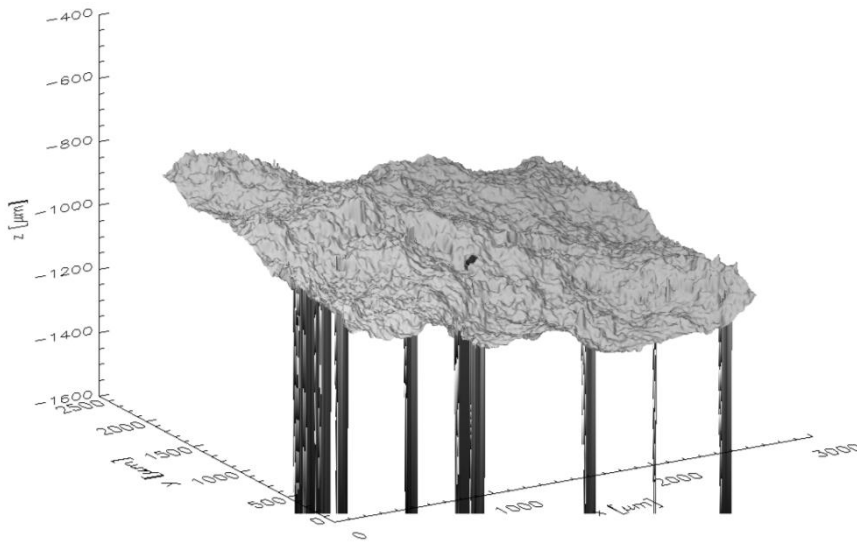
There is no clear relationship between the calculated values of  $S_a$  and the level of polishing, regardless of the use of octants. Values of  $S_a$  calculated using whole areas were approximately twice the values of  $S_a$  calculated using octants of the same areas. The reason for this difference is probably that that long wavelength features contribute to the calculated roughness parameter  $S_a$ . It will be important, therefore, to apply filters to the data in order to isolate the scale of texture responsible for changes in friction from the underlying shape.

#### **4.4.2 Texture analysis using data visualisation software**

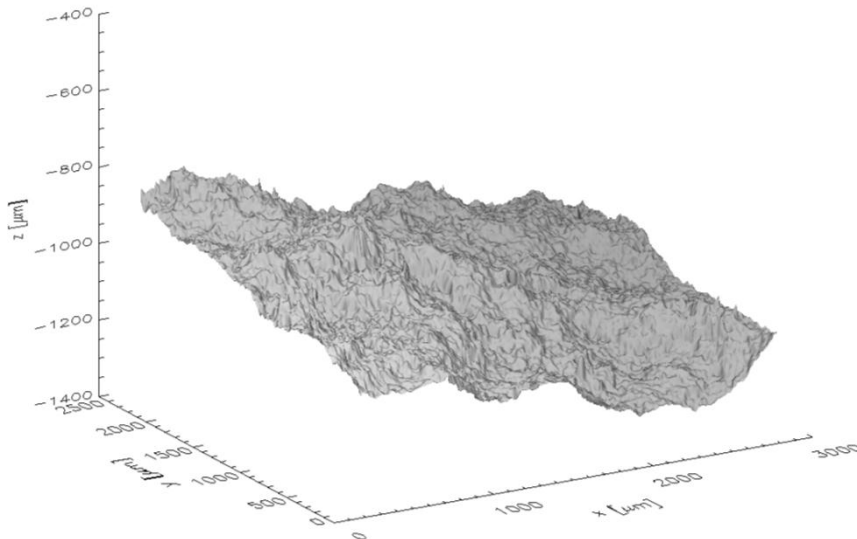
In order to apply more complex filtering to the texture data, IDL data visualisation software was used to plot 3D representations of the measured surfaces and apply simple filters before calculating roughness parameters such as  $S_a$ ,  $S_q$  and  $S_p$  (British Standards, 2008). The processing was carried out by Nathan Dhillon but subsequent analysis of calculated values was carried out by the author.  $S_q$ , defined by Equation 4.2, is an RMS equivalent to  $S_a$ , and for normally distributed texture they are linearly related.  $S_p$  reports the maximum peak height above the average surface plane.

$$S_q = \sqrt{\frac{1}{A} \int_0^{l_y} \int_0^{l_x} z^2(x, y) dx dy} \quad 4.2$$

Figure 4.19 shows an example of one of the 45 areas scanned at polishing level zero (before polishing). It was found that corrupt data points were present, probably due to highly reflective spots or other features causing the microscope's measurement software to fail. The software has displayed the corrupt data points with surface heights of -9999 in Figure 4.19. Figure 4.20 shows the same surface with the corrupt data points replaced by interpolated values. All filters and calculations reported herein were applied to these 'cleaned' versions of each surface area.

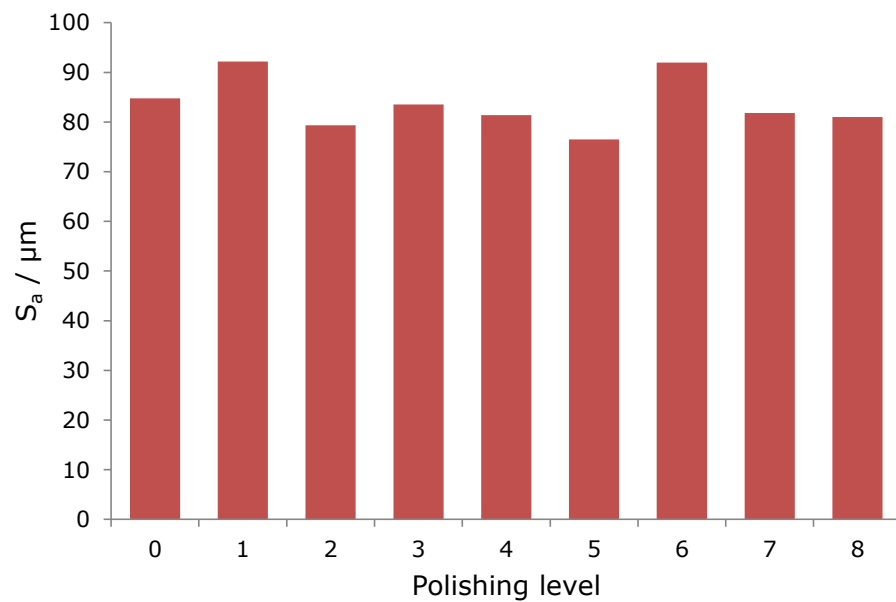


**Figure 4.19 Measured surface profile before polishing**



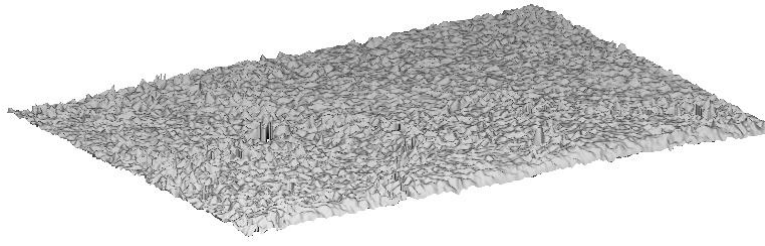
**Figure 4.20 Cleaned version of surface profile before polishing**

A calculation of  $S_a$  on the whole of each surface area before any filtering was applied, shows similar results to those obtained using Microsoft Excel, as would be expected (Figure 4.21).

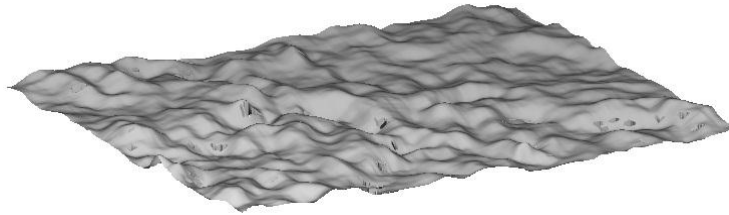


**Figure 4.21 Average  $S_a$  calculated using IDL for all areas before filtering**

The additional functionality of IDL, compared with Excel, was used to apply several filters to the surfaces, with wavelengths based on the standard sampling lengths recommended in ISO4288: 0.08 mm, 0.25 mm and 0.8 mm (British Standards, 1998) with an additional intermediate wavelength of 0.5 mm. Figure 4.22 shows, for example, the same surface from Figure 4.20, with a 0.08 mm moving average filter applied. This is a low pass filter in the wavelength domain (i.e. wavelengths less than 0.08 mm pass). Figure 4.23 shows the same surface again with a 0.08 mm to 0.25 mm moving average bandpass filter applied. Note that the size of the area scanned limits the size of the filter that can be applied and the larger the wavelength, the smaller the remaining useable dataset.



**Figure 4.22 Surface profile with 0.08 mm moving average low pass filter applied**



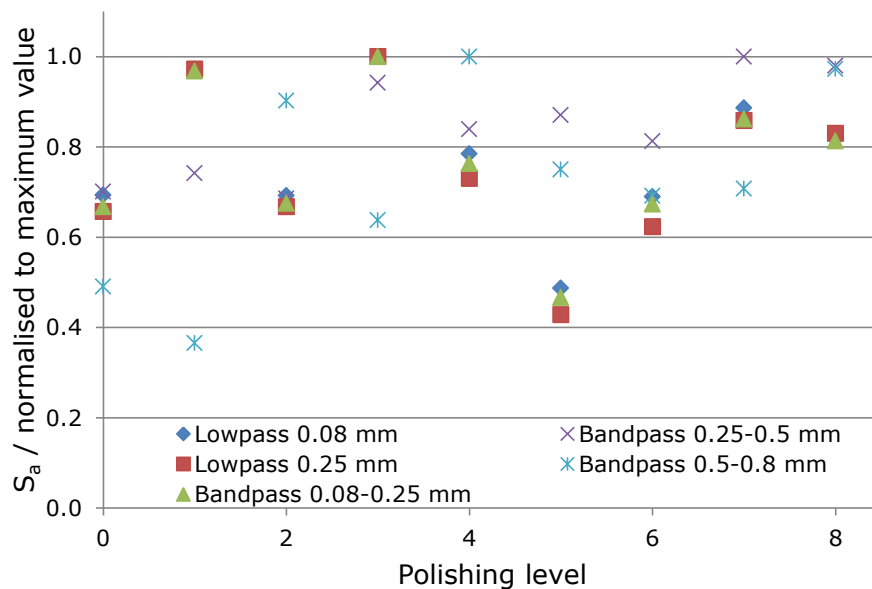
**Figure 4.23 Surface profile with 0.08-0.25 mm moving average bandpass filter applied**

Roughness parameters were calculated for every surface area at each polishing level for each filter applied. Table 4.1 shows the average calculated parameter values.

**Table 4.1 Calculated parameters for all filtered surface areas**

		Lowpass		Bandpass		
	Polishing level	0.08 mm	0.25 mm	0.08-0.25 mm	0.25-0.5 mm	0.5-0.8 mm
<b>S<sub>a</sub></b>	0	29	70	42	162	262
	1	41	103	62	171	195
	2	29	71	43	158	482
	3	43	106	64	218	341
	4	33	77	48	194	534
	5	20	45	29	201	401
	6	29	66	43	188	369
	7	38	91	55	231	378
	8	35	88	52	226	520
<b>S<sub>q</sub></b>	0	32	71	46	163	263
	1	44	104	65	172	196
	2	32	72	46	159	482
	3	45	107	67	218	341
	4	36	79	52	195	534
	5	23	47	33	202	401
	6	32	67	46	188	370
	7	40	92	58	231	378
	8	38	89	55	227	520
<b>S<sub>p</sub></b>	0	75	114	101	197	293
	1	100	165	124	208	224
	2	40	38	40	176	512
	3	103	176	137	263	376
	4	47	63	61	210	566
	5	71	108	86	238	432
	6	80	124	101	226	402
	7	92	162	129	271	411
	8	71	105	85	263	551

The values for  $S_a$ , normalised to maximum values, for each of the filters are plotted in Figure 4.24. There are no discernible trends for changing roughness for increased polishing, and the same is true for  $S_q$  and  $S_p$  which exhibit very similar patterns.



**Figure 4.24 Average normalised  $S_a$  for surfaces after application of filters**

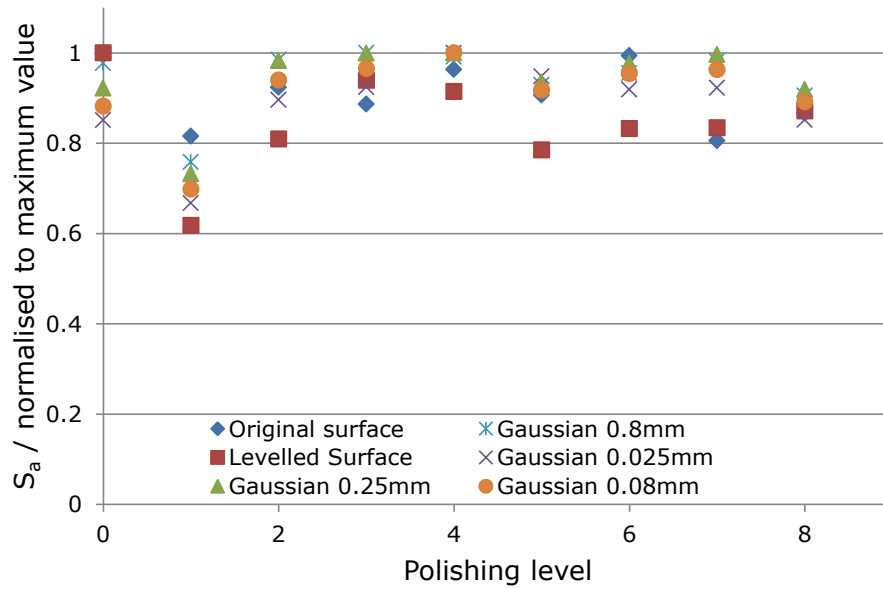
#### 4.4.3 Texture analysis using bespoke software

A commonly used, industry standard, texture analysis software package, MountainsMap by Digitalsurf was used to calculate a wider range of roughness, spacing and surface volume parameters using a number of similar surface filters. Some of the parameters calculated are shown in Table 4.2. Two types of filter were used: a surface levelling filter using subtraction from a fitted least square plane; and Gaussian low pass filters with upper wavelengths 0.025 mm, 0.08 mm, 0.25 mm and 0.8 mm.

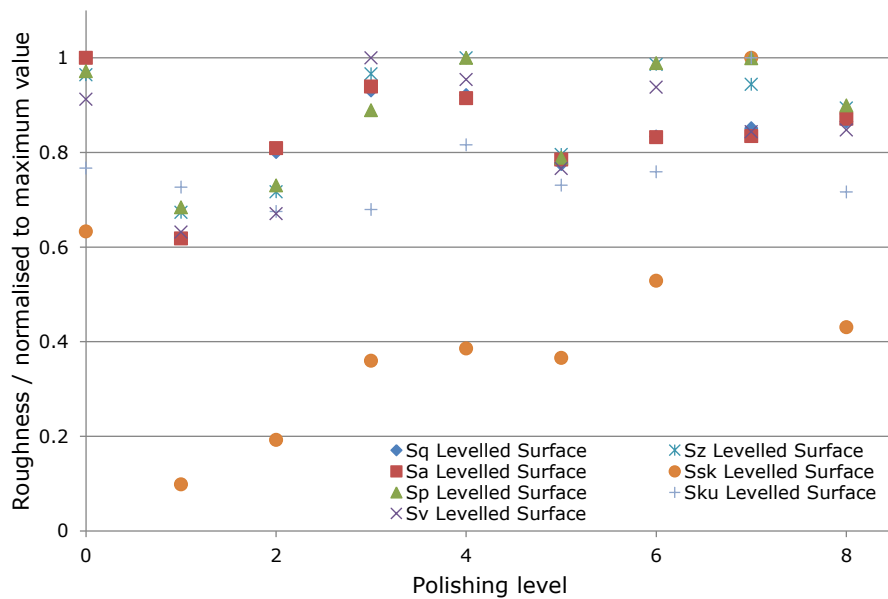
**Table 4.2 Roughness and spatial parameters calculated using MountainsMap**

Parameter	Description
$S_q$	Root mean square height of the surface
$S_{sk}$	Skewness of height distribution
$S_{ku}$	Kurtosis of height distribution
$S_p$	Maximum height of peaks
$S_v$	Maximum height of valleys
$S_z$	Maximum height of the surface
$S_a$	Arithmetical mean height of the surface
$S_{pd}$	Density of peaks – number of local maxima per areas

The graph in Figure 4.25 shows average values of  $S_a$  measured at each polishing level for all the filters applied, normalised to the maximum value of  $S_a$ . As observed in the previous sections, there are no clear trends for changes in  $S_a$  with increased polishing, regardless of the filter applied. The graph in Figure 4.26 shows normalised values for all calculated parameters measured on the software levelled surfaces. The pattern of changing roughness with polishing is similar for all but the skewness measure ( $S_{sk}$ ), and to a lesser extent, the kurtosis measure ( $S_{ku}$ ). However, the difference in the apparent trend is largely attributable to an outlying average value at polishing level 7.



**Figure 4.25 Average normalised  $S_a$  for each polishing level after application of various filters**



**Figure 4.26 Average normalised roughness parameters for each polishing level on software levelled surfaces**



## 4.5 Discussion

Analysis of high resolution photographs taken of aggregate surfaces as they were polished in the laboratory demonstrated that changes in pixel intensities could be linked to the amount of polishing applied. However, the analysis was only successful when areas of the surface that had not been replicated were considered. If the effect of replication is simply to clean the aggregate surface then the implication is that image analysis only works because texture is highlighted by contrasting detritus trapped within the aggregate texture. Although in-service roads are not likely to be clean, this phenomenon could present issues for calibration and consistency when using images of the road in a practical system. This experiment has not allowed further investigation of the link between visual and physical changes because surface texture measurements (and SEM analyses) were carried out on replicas of the surface in areas that presented no obvious visual change. Consequently, although this part of the experiment supports the potential for use of image analysis in the long-term it has not provided information about polishing mechanisms and the differences between aggregate types.

Scanning electron microscopy was used to verify the fidelity of replication and then to compare identical areas from the replica of the before-polishing surface with the replica of the after-polishing surface to observe changes in the surface texture as it is polished. This was achieved by using prominent features of the surface (such as stone edges or distinctive ridges) for navigation so the exact location could be compared (either stone to replica or before- to after-polishing). Although the resolution of replication was not as high as the manufacturer's claim, features as small as 5  $\mu\text{m}$  were easily identifiable. Qualitative observations of changes to surface texture before and after polishing are the most compelling outcome from this work even though the intention was simply to illustrate the sorts of texture change that would subsequently be measured using three dimensional focus variation microscopy.

Quantitative measurements of surface texture were made on the replica plaques by scanning a large number of discrete areas with a focus variation measurement microscope. Standard roughness parameters, calculated without prior filtering, did not demonstrate a change in surface roughness due to polishing. Various filters were applied to the surface in an attempt

to discount the effect of surface form but no trends in the data became apparent.

The methodology assumed that a sufficiently large number of measurements would allow characterisation of the surface as a whole. Although an approximate record of the location of each measured area was kept, no attempt was made to undertake surface texture measurements on the specific areas that had been viewed by SEM. It is difficult to verify that the areas measured were replicated from parts of the aggregate surface that came into contact with the W-S machine's polishing rollers. It was assumed that some trend would be immediately apparent in any measure of surface roughness without the need to first identify suitable parameters based on observed changes. Furthermore, the type of aggregate used may polish in a more complicated way than can be easily characterised using simple roughness parameters.

The replication technique was convenient, allowing experimental work to be carried out in several laboratories with a minimum amount of travel and the easy use of SEM (the aggregate specimen being too big to fit in the microscope chamber), but its use adds a potential source of error, even though its fidelity was demonstrated. So, instead of carrying out any further analysis with the data from this experiment it seemed more sensible to refine the data collection methodology. If qualitative and quantitative analysis of the same areas, throughout the polishing process, can be achieved then identification of appropriate characterisation parameters might be made easier. Furthermore, if it can be verified that the polishing rollers in the W-S machine actually come into contact with the surfaces measured then there can be more confidence in the dataset.

The next chapter describes in detail a new, refined, methodology. It uses aggregates with simpler mineralogy, surface navigation techniques developed for inspection by SEM above, measurements made on aggregate surfaces rather than on replicas and a paint removal technique that identifies the areas of aggregate surface that come into contact with the W-S machine's polishing rollers.

## 4.6 References

- British Standards. (1998). *BS EN ISO 4288. Geometric Product Specification (GPS) - Surface texture - Profile method: Rules and procedures for the assessment of surface texture*. London: BSi.
- British Standards. (2008). *BS ISO 25178-2. Geometric Product Specification (GPS) - Surface texture: Areal. Part 2: Terms, definitions and surface texture parameters*. London: BSi.
- Dunford, A. (2010). *PPR538. Measuring skid resistance without contact; 2009-2010 progress report*. Crowthorne: TRL.
- James, J. G. (1967). *Calcined Bauxite and other artificial, polish resistant, roadstones*. Road Research Laboratory.
- Thompson, A., Burrows, A., Flavin, D., & Walsh, I. (2004). *The Sustainable Use of High Specification Aggregates for Skid Resistant Road Surfacing in England*. East Grinstead: Capita Symonds Ltd.
- West, G., & Sibbick, R. G. (1988). Petrographical comparison of old and new control stones for the accelerated polishing test. *Quarterly Journal of Engineering Geology*, 21, 375-378.



## **5 Development of a robust methodology to examine surface texture changes**

---

It has been established that it is, or will be, possible to collect information about the road surface from which friction could, potentially, be determined, and that it is possible to measure the surface texture of aggregate particles. However, characterisation of the surface texture is not straightforward and the reliability of data collected is very important.

This chapter will give details of a series of experiments carried out in the laboratory. The Wehner-Schulze machine was used again to polish aggregate specimens and to measure friction on their surfaces. The methodology is described in some detail and the mechanisms employed by both functions of the machine are discussed in the context of polishing by traffic and measurement of skid resistance on roads, respectively. The improved techniques for collection of surface texture information are presented, along with methods for ensuring that changes to the same surface area can be tracked and that observations are made on parts of the surface that are subjected to polishing.

Details of the various analyses carried out, and characterisation strategies examined, follow in the next two chapters, although some are introduced here. In particular, to illustrate some points, examples of measurements made on a limestone aggregate specimen are discussed below.

## **5.1 Polishing in the laboratory**

The experiment described in this chapter used the Wehner-Schulze machine to provide aggregate particle surfaces with a range of friction levels. Some of the advantages of examining a single specimen that has been progressively polished in the laboratory have already been mentioned (changes to the same surface can be observed and some external factors can be controlled) and the operation of the Wehner-Schulze machine has been introduced (Sections 2.6, 3.2, and 4.1). If this experiment is to be more than a purely theoretical exercise in surface texture examination, it would be useful if the polishing applied by the Wehner-Schulze machine bore some resemblance to the polishing applied by traffic using the UK road network. Section 5.1.1 summarises work carried out to compare the effect of polishing by the Wehner-Schulze machine with the effect of polishing by traffic. Section 5.1.2 describes the methodology used to provide a series of surfaces with a range of levels of friction.

### **5.1.1 *Methodology for comparing W-S polishing with traffic polishing***

As part of a project to examine the capabilities of the Wehner-Schulze machine for Highways Agency, polishing in the Wehner-Schulze machine was compared with polishing by traffic. The work is described in detail in a published project report (Dunford & Roe, 2012); practical work was carried out by a project team at TRL and the majority of the analysis was undertaken by the present author, with assistance from Peter Sanders and Peter Roe. For ease of reference the following paragraphs summarise the project; additional analysis that was not part of the project is then described.

210 slabs of asphalt were prepared in the laboratory, using one basic asphalt design with fourteen different combinations of coarse and fine aggregates, including different gritstones, granites and one limestone. The slabs were cut into discs to fit the W-S machine and the majority were embedded in road sites, while some of the specimens were just polished in the W-S machine.

Following, and adapting, a method developed in the 1960s (Hosking, 1967), four discs of each mix design (i.e. the same coarse aggregate, fine aggregate and bitumen content) were embedded into the wheel paths of each of three trial sites in August 2007. Fifty six holes were cored in the

wheel paths at each site to receive the prepared asphalt discs, which were fixed in place using a two component adhesive system (Triflex 238 and 239) that is used for bonding frames for reflective studs into road surfaces. The photographs in Figure 5.1 show some of the discs immediately before and after embedment into the outside wheel path of the third trial site.

The trial sites were used in a parallel project and details of the amount of traffic passing each was well known. Asphalt discs were installed in the nearside wheelpath in lane 1 of the A14 near Stanford, in the nearside wheelpath in lane 1 of the A5 near Gibbet Hill and in the outside wheelpath in lane 2 at the same location. The three sites carry approximately 4500, 1200 and 200 commercial vehicles per day (CVD) respectively, corresponding to high, medium and low traffic levels.

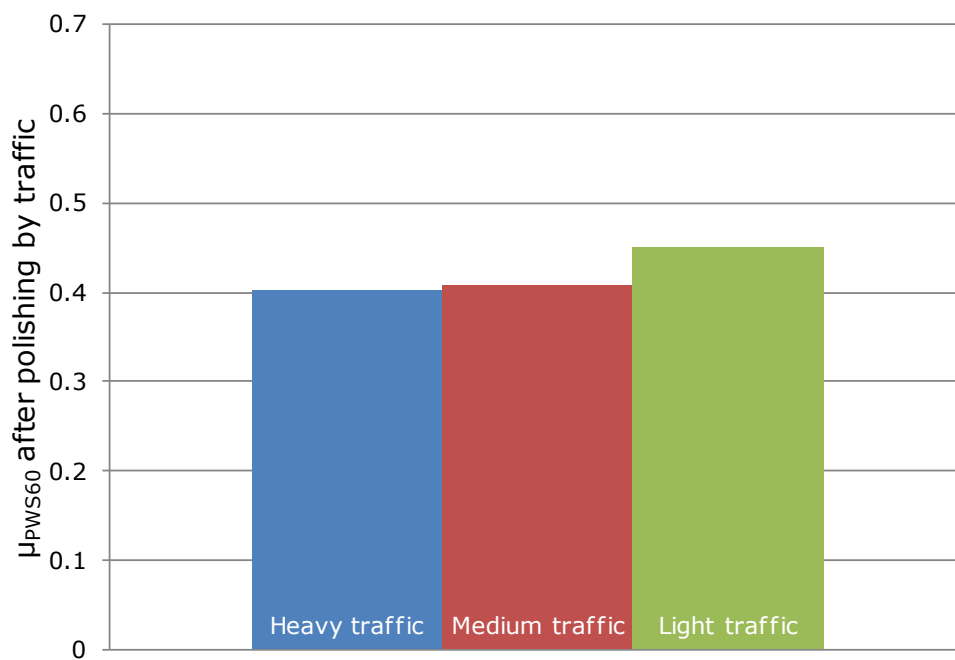


**Figure 5.1 Asphalt discs in lane 2 of the A5 sites, about to be installed (left) and shortly after installation (right)**

Although the intention was to retrieve one specimen of each mix design from each site at six month intervals, due to unforeseen circumstances specimens were removed in a more ad-hoc manner. Specimens were retrieved on four occasions: after they had been in place for 8, 14, 20 and 24 months. On the second occasion, 14 months after embedment, only those specimens from the most heavily trafficked site were retrieved.

Friction was measured, using the W-S machine, on each specimen after it had been removed from its trial site and, on those specimens that were just polished using the W-S machine. These friction measurements can be used to examine the effect of traffic volume, the effect of seasonal variation and, most importantly, the ability of the W-S machine to simulate polishing by traffic.

The graph in Figure 5.2 shows the average friction measured on asphalt discs retrieved from each of the three sites after they had been in place for 24 months. It can be seen that heavy traffic results in a lower average friction, while average friction on the specimens retrieved from the site with the lightest traffic is significantly higher; this is the same as the pattern that would be expected on a road surface (Hosking & Woodford, 1976).

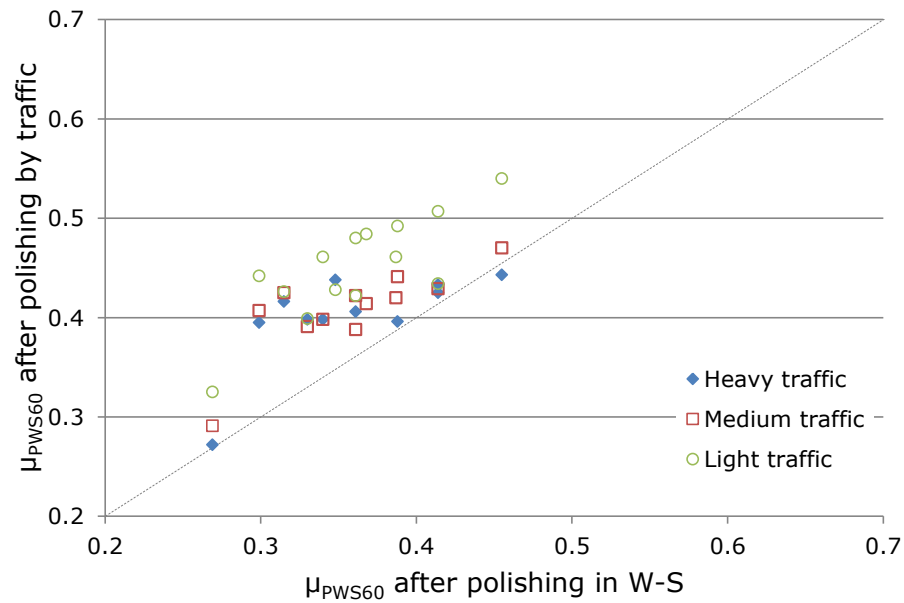


**Figure 5.2 Average friction measured on asphalt specimens extracted from trial sites after 24 months**

If the friction measured on each of the 14 specimens retrieved from each site after 24 months is compared with the friction measured on each of the 14 specimens that were polished in the W-S machine (Figure 5.3) then it is clear there is some correlation between the two. A broken line of unity is shown in the graph for reference. Generally, the polishing effect of traffic is less harsh than that of the W-S machine because friction is lower after polishing in the W-S machine than after polishing by traffic (the points are all above the line of unity). However, the specimens prepared with

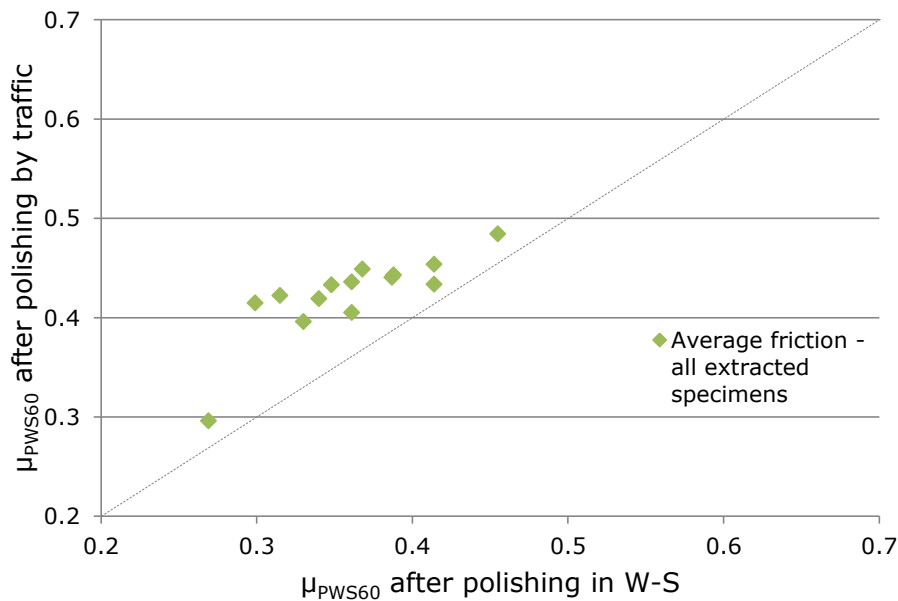


limestone coarse aggregate, with the lowest measured friction, have been polished more aggressively by traffic, relative to the other specimens, even in the most lightly trafficked trial site. The effect of different traffic densities is still evident: friction on the specimens extracted from the most lightly trafficked site is generally higher than on the specimens extracted from the other two sites.



**Figure 5.3 Comparison between friction measured after polishing by traffic and friction measured after polishing by W-S machine**

The correlation between the two polishing mechanisms is easier to see if the average of all friction measurements on the extracted specimens (from the most recent extraction date) is compared with friction measurements made on the equivalent specimens polished by the W-S machine (Figure 5.4).



**Figure 5.4 Comparison between average friction measured after polishing by traffic and friction measured after polishing by W-S machine**

The practical application of this information is limited. With more data it may be possible to develop a relationship, using the correlation between friction measured after polishing in the machine and friction measured after polishing by traffic, to directly predict the friction expected when an aggregate (or asphalt mix design) is used in service, especially if the effect of traffic volume is also taken into account. In this experiment the specimens were inserted into the surface courses of straight, non-event, sections of road. It is therefore not possible to compare the effect of polishing in the machine with the effect of the more aggressive polishing that is likely to be experienced by a surface course on a roundabout approach or tight bend etc.

However, the experiment does demonstrate that:

- There is a correlation between the polishing applied by W-S machine and the polishing applied by traffic.
- When two aggregates are compared, if one has lower skid resistance after polishing by W-S machine, it is likely to have lower skid resistance after polishing by traffic.
- The range of friction measured after polishing by W-S machine is greater than the range of friction measured after polishing by traffic.

- Relative to other aggregates, limestone appears to be more susceptible to polishing by traffic than to polishing by W-S machine.

### **5.1.2 Progressive polishing of aggregate specimens**

The intention of the experiment was to make measurements of texture on the surfaces of aggregate particles as they were polished in the laboratory. The surface texture measurement equipment is located at the National Physical Laboratory in Teddington, while the polishing equipment is located at TRL in Crowthorne. In order to make the experiment more efficient, and minimise the amount of travelling, the polishing regime already trialled (Section 4.1) was reduced. Five discrete levels of friction, or “stress levels” were targeted and surface texture was measured before polishing and after 90, 900, 9,000 and 90,000 cumulative passes of the W-S machine’s polishing rollers.

Also following the trial experiment, aggregate specimens were prepared using graded nominal 10 mm aggregate particles<sup>1</sup>, bound together with sand and epoxy resin. The limestone specimen prepared for this experiment is shown in Figure 5.5.

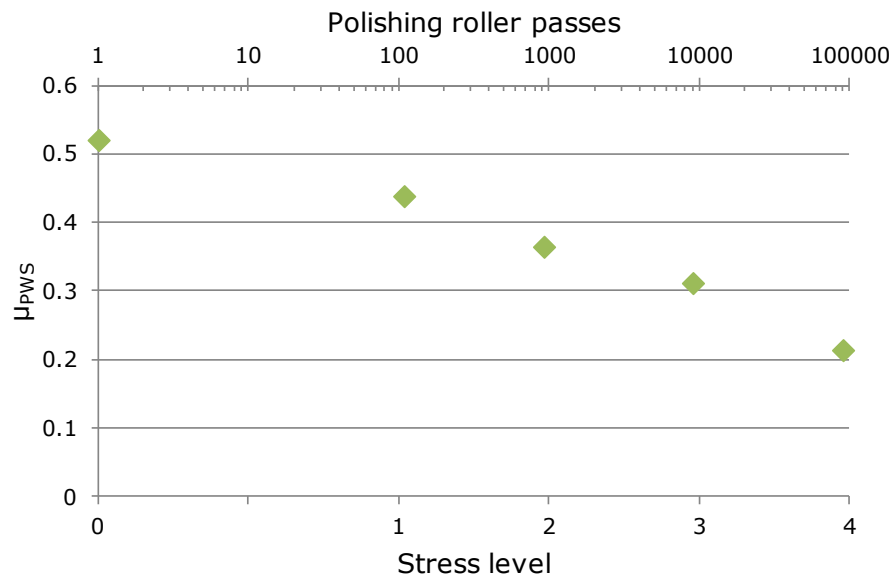


**Figure 5.5 Limestone aggregate test specimen**

Texture measurements were made in at least three locations on one stone in each of two areas (see Section 5.4). Measurements of friction were made on the aggregate specimen before it was polished to the next stress level.

<sup>1</sup> Aggregate sieved to pass 10 mm square sieve and retained on a 14/10 flakey sieve (having rectangular slots 7.2 mm wide and 40 mm long)

Figure 5.6 shows the friction measured at each stress level and the number of roller passes is indicated on a logarithmic scale at the top of the graph (for display purposes, stress level zero has been shown with 1 polishing roller pass instead of 0 passes).



**Figure 5.6 Friction measured on limestone test specimen as a function of polishing in the W-S machine**

## **5.2 Measuring friction in the laboratory**

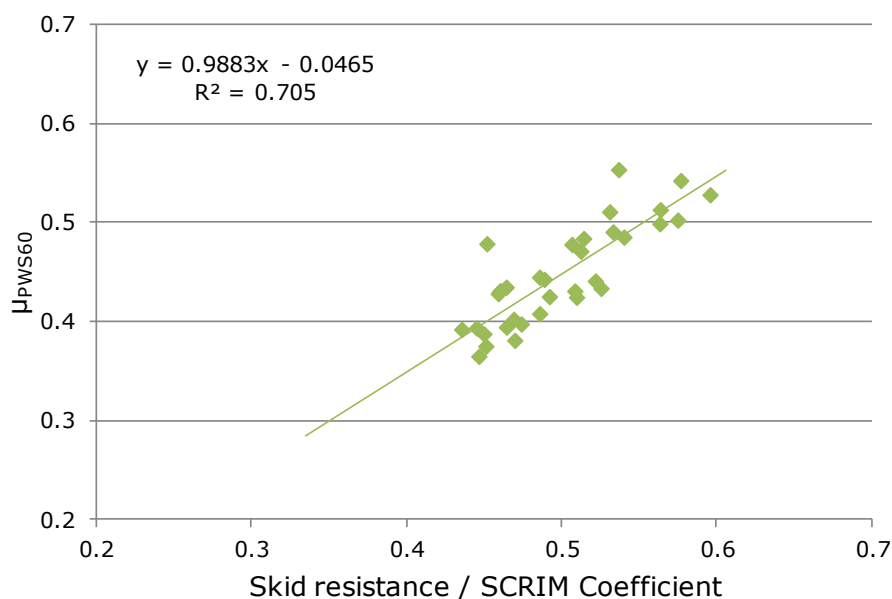
In the same way that it is useful to show that there is a link between the polishing applied by the W-S machine and the polishing applied by traffic, it is also reassuring to demonstrate that measurements of friction made using the machine bear some relation to measurements of skid resistance commonly used by road maintenance practitioners. The first of the following three sections therefore describes such a correlation, the second section details the way friction is measured in the machine and the third section gives details of the friction measurements made during the experiment in hand.

### **5.2.1 Friction measurement using the Wehner-Schulze machine**

The effect of coarse aggregate size in thin surface course systems was investigated as part of a programme of work sponsored by the Highways Agency, Mineral Products Association and Refined Bitumen Association. A number of trial sites were laid and skid resistance was measured on site over a period of more than three years. The Sideway-force Coefficient Routine Investigation Machine (SCRIM) was used to provide a measurement of low-speed skid resistance on the trial sites. SCRIM is used to measure skid resistance across the whole trunk road network, and much of the road network managed by local authorities. It is the de facto standard for measurement of skid resistance of in-service roads in the UK and the values recorded (SCRIM Coefficient) are used to monitor asset condition. Towards the end of the work programme, cores were taken from each trial site so that more in-depth study could be carried out in the laboratory. There were 66 cores (two from each of 33 trial site sections) and friction was measured on each using the Wehner-Schulze machine. Site measurements, core extraction and friction measurements made in the laboratory were carried out by a team of researchers at TRL, supervised by the present author; all subsequent analysis was carried out by the present author. The programme of work is reported in a published project report, PPR564, (Roe & Dunford, 2012) but the following comparison between friction measurement methods is not given in detail.

The graph in Figure 5.7 shows the average friction measured on each pair of cores against the skid resistance measured on site, using SCRIM. The site measurement is the one made at the time closest to core extraction. There is a good linear correlation between the two measurement methods.

In the HA/MPA/RBA programme of work this correlation was used to demonstrate that the cores extracted from the trial sites were representative of the trial sites themselves. The friction measured in the laboratory is based on the surfaces of two 225 mm diameter cores and the skid resistance measured on site is an average over at least 100 m; the good correlation suggests that the trial sites were generally homogenous along their lengths.



**Figure 5.7 Relationship between friction measured by W-S machine and skid resistance measured by SCRIM**

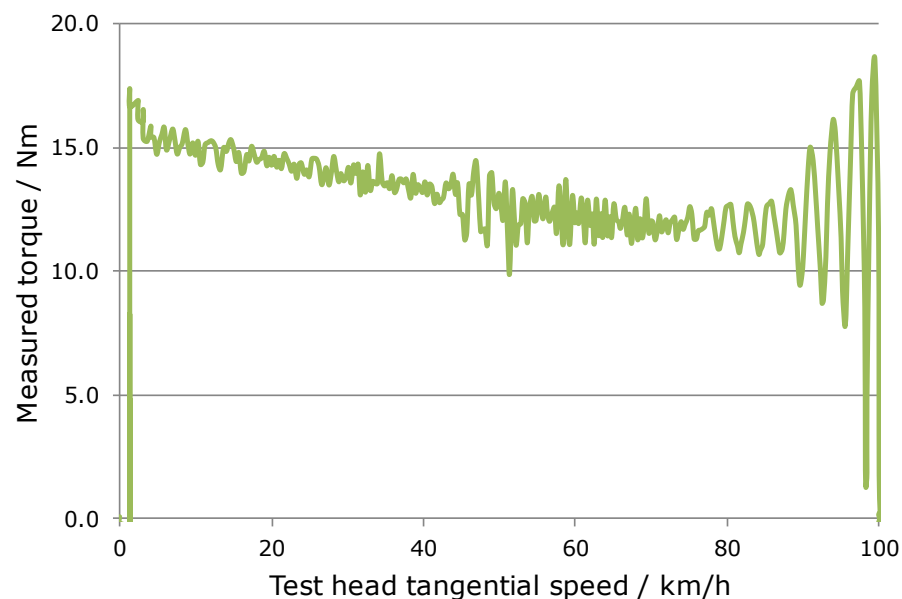
Similar relationships between friction measured by the W-S machine and skid resistance measured by SCRIM (or its European equivalent) have been shown before (Huschek, 2004). It is likely, however, that exact relationships are specific to each W-S machine/SCRIM combination. Whilst SCRIM devices used in the UK are routinely compared (so that they should be interchangeable) the same is not true across all SCRIM devices used in Europe and the reproducibility of the W-S machine has been shown to be questionable at this stage in the device's development (Dunford & Roe, 2012). Nonetheless, friction measurements made in the W-S machine are relevant and are related to the skid resistance performance experienced by vehicles when aggregates are used in service.

### **5.2.2 Details of the W-S friction measurement system**

Friction is calculated in the Wehner-Schulze machine by measuring the torque imparted to the specimen surface when the test head, comprising three rubber sliders mounted in a circle of radius 90 mm, having been

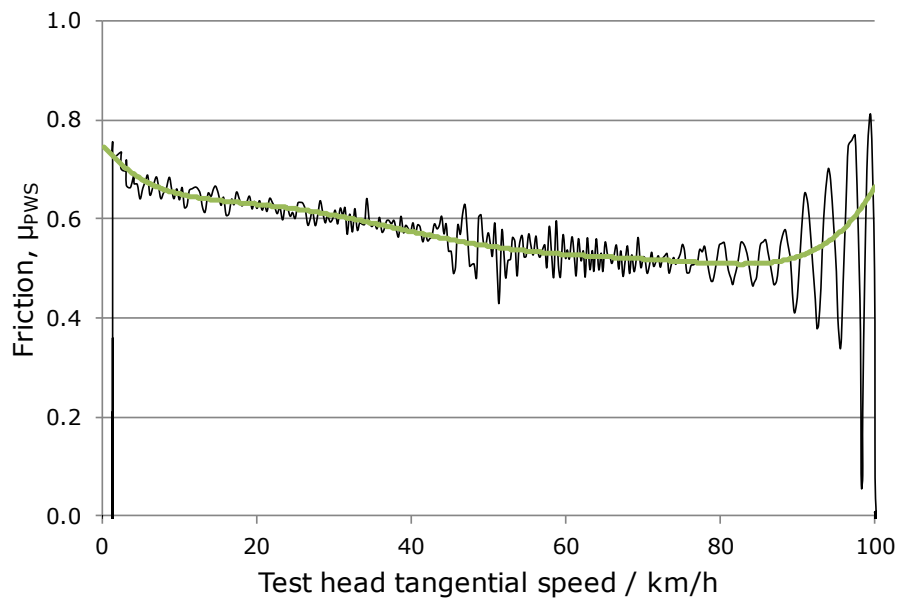
accelerated to a known rotating speed, is dropped and allowed to slide to a halt under its own weight. The torque is measured using torque sensors in the test table, to which the specimen is fixed, every 8 thousandths of a second.

The graph in Figure 5.8 shows the torque measured during a test carried out on a gritstone aggregate specimen with an initial tangential rotation speed of 100 km/h, against the speed of the rotating (slowing) test head. Note that there is a significant amount of noise, especially when the test head is first dropped and when the test head comes to a complete stop.



**Figure 5.8 Torque measured during a friction test using the W-S machine**

Friction is calculated by dividing this measured torque by the vertical force (weight of the test head) and the radius of the test head. In order to remove the noise, a line of best fit (least squares, sixth order polynomial) is superimposed onto the friction values calculated for test head speeds between 5 km/h and 95 km/h. Calculated friction is shown, against the speed of the rotating test head in Figure 5.9. During normal operation, when the initial tangential speed is set to 100 km/h, the reported value of friction (as in Figure 5.7) is the value calculated, from the polynomial fit, when the test head has slowed to a tangential speed of 60 km/h. For the example shown, friction,  $\mu_{\text{PWS60}}$ , would be 0.529, to three decimal places as reported by the machine.



**Figure 5.9 Friction calculated during a friction test using the W-S machine**

To determine the repeatability of measurements made using the W-S machine, 21 aggregate specimens were prepared using three different aggregate sources (nine limestone specimens, nine granite specimens and three gritstone specimens). After polishing in the W-S machine (one hour, 90,000 polishing roller passes), friction was tested using the standard procedure, described above. The standard deviation between these measurements was used to calculate repeatability of 0.02. This is the maximum difference one would expect to see between identical specimens in 95 % of tests carried out in the same laboratory under identical conditions. It should be noted that this is the repeatability of the whole test, and variability includes aggregate sampling, specimen preparation, polishing and the friction test itself. It is likely that the accuracy of the friction test alone is somewhat better this, but, for reference, this is a useful upper limit.

### **5.2.3 *Measurements of friction for comparison with surface texture***

As described previously, a reduced initial test head speed, and corresponding friction calculation speed, was used throughout all progressive polishing experiments. The reason for doing so is because the friction test itself is likely to have an abrasive effect on the aggregate surfaces. In fact, the standard operating procedure ends with a 'test to the limit' stage where friction tests are repeated until no further change is



observed. During the initial stages of the polishing experiment, when the amount of polishing applied is from only 90 or 900 cumulative passes of the polishing rollers, a standard friction test with initial test head speed of 100 km/h may result in:

- Masking of the effect of polishing on surface texture - if texture measurements are made within the annulus scribed by the friction test sliders then the observed texture form may be as a result of friction tests rather than controlled polishing.
- A disconnection between the measured value of friction and the actual state of the whole surface - the friction test is strictly only representative of the annulus scribed by the test sliders if that area has received additional polishing by previous friction tests.

A short experiment was carried out to determine whether useable results could be obtained while testing at reduced initial test head and measurement speeds. Using one asphalt specimen (prepared in the laboratory using gritstone aggregate) friction tests were made 'to the limit' as in the standard operating procedure and then tests were made at a range of initial test head speeds. The values in Table 5.1 show the friction measured,  $\mu_{PWS\ x}$ , using torque measurements taken when the test head had slowed to speed  $x$  for speeds 20, 40, 60 and 80 km/h, from initial rotation speeds between 30 km/h and 100 km/h. Again, because the machine reports friction to three decimal places, the results are shown to three decimal places here.

**Table 5.1 Friction measurements from the W-S machine with a range of initial test head speeds**

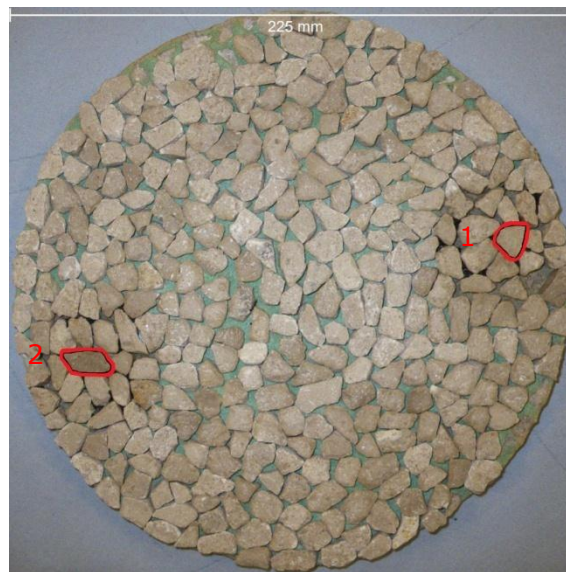
Initial test head speed (km/h)	$\mu_{PWS\ 20}$	$\mu_{PWS\ 40}$	$\mu_{PWS\ 60}$	$\mu_{PWS\ 80}$
100	0.451	0.411	0.381	0.367
90	0.447	0.410	0.384	0.376
80	0.450	0.411	0.385	-
70	0.451	0.414	0.391	-
60	0.452	0.423	-	-
50	0.446	0.411	-	-
40	0.451	-	-	-
30	0.476	-	-	-

It can be seen that, for friction calculated from torque measurements at speed  $x$ , the speed at which the test head is dropped does not significantly affect the friction measured. A lower initial test head speed will provide useable results with a lower abrasive impact on the surface; for the rest of this experiment friction was measured at 20 km/h after an initial speed of 50 km/h. It should be noted, however, that these friction measurements cannot be compared with measurements made using the standard operating procedure because torque information at 60 km/h is not available (60 km/h being above the chosen initial test head speed).

### 5.3 Texture measurement areas and alignment

On each specimen, two aggregate particles that fall within the path of the polishing rollers and within, or close to, the path of the friction testing sliders, were chosen. Their positions were recorded by marking an overlaid acetate sheet with the outlines of these particles and several others.

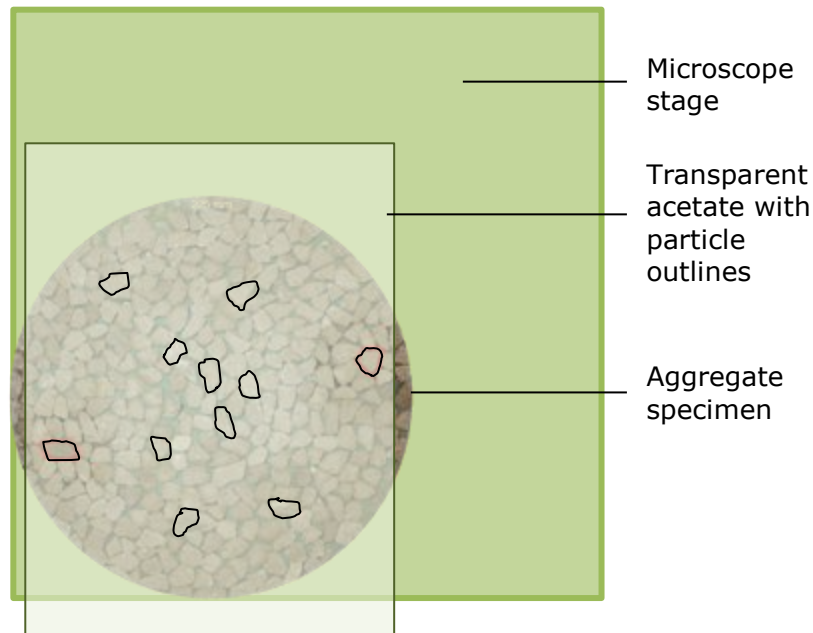
Measurements of the surface profile on each aggregate particle surface were made using the Alicona InfiniteFocus microscope and details of the measurement technique are described in the next section. In each case, the first measurements made encompassed the whole surface of the aggregate particle. To make it easier to inspect the same area of surface at each stress level, the specimen was carefully aligned under the microscope's objective lens. The acetate overlay was used again to assist with this process. Figure 5.10 shows the limestone specimen again, with the two aggregate particles that were inspected highlighted with a red outline and labelled "1" and "2".



**Figure 5.10 Limestone aggregate specimen with inspected aggregate particles marked**

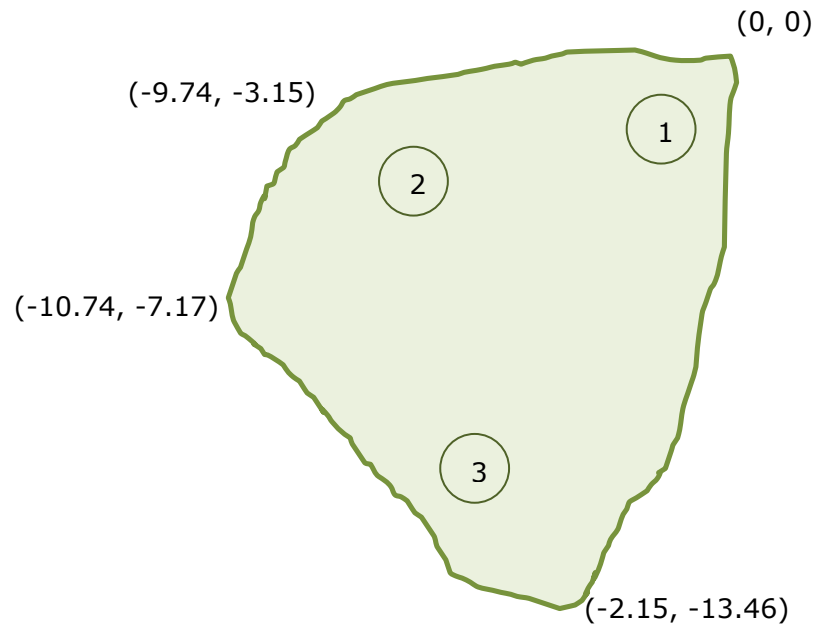
The stage of the Alicona microscope is square and the specimen was placed on the stage in the orientation shown in the photograph, ensuring the edges of the rectangular acetate were parallel with the sides of the microscope stage. The outer circumference of the specimen was aligned as closely as possible with two edges of the microscope stage. The diagram in Figure 5.11 shows the arrangement of the aggregate specimen for measurement of surface texture on particle 1. Note that, for making measurements on particle 2, the whole specimen was moved to the top

right corner of the microscope stage. This is because the maximum lateral travel of the microscope stage, compared to the separation of the two aggregate particles, is not sufficient to allow measurement on both without moving the specimen relative to the stage.



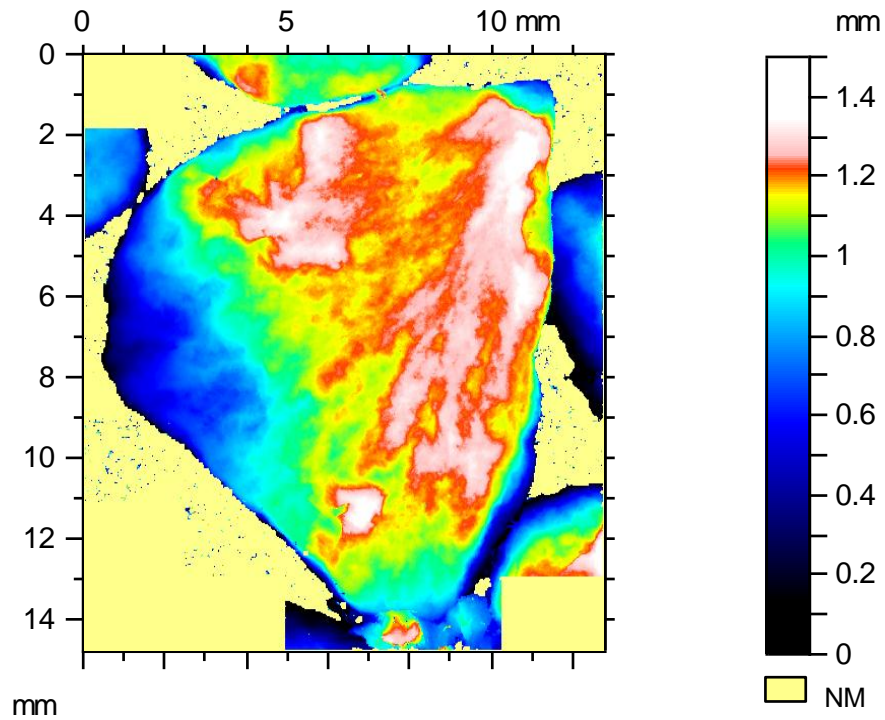
**Figure 5.11 Diagram of specimen alignment**

Once this broad alignment had been undertaken, the microscope's electronically moving stage and its control software were used to record the coordinates of particle extremes and then the coordinates of the areas that were scanned in more detail. Figure 5.12 shows the outline of limestone particle 1, with the (x, y) coordinates, in millimetres, of its extremities marked. The most distinctive or well defined corner of the aggregate particle was set as the origin and all other measurements are relative to that position.



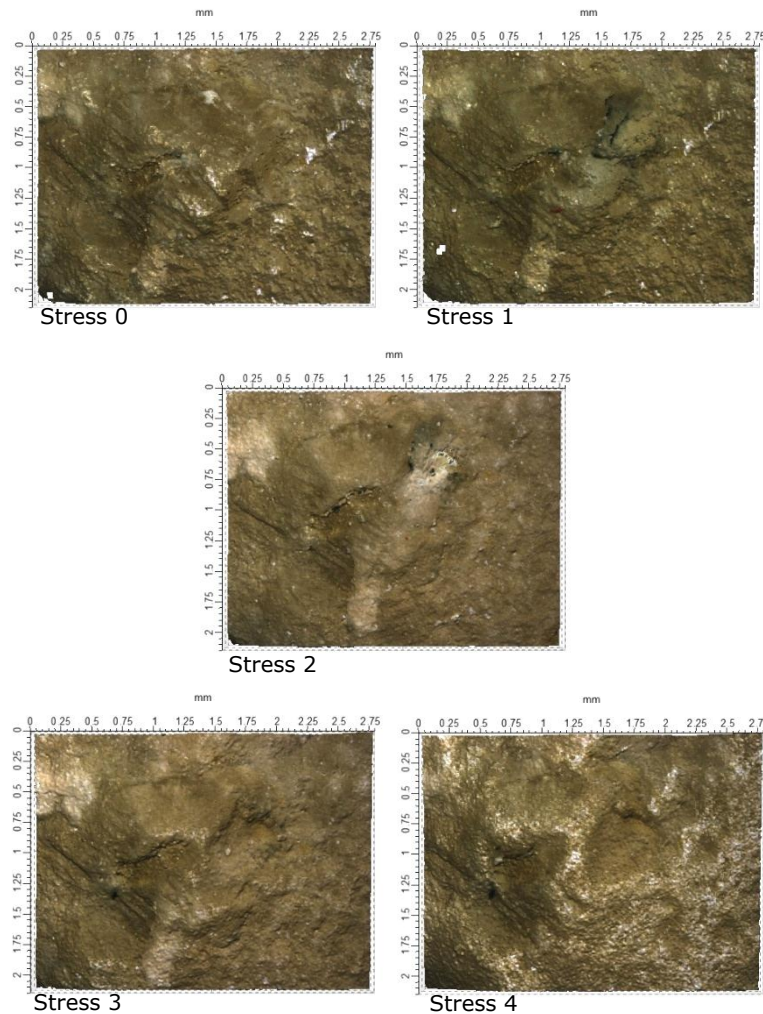
**Figure 5.12 Outline of limestone particle 1 with coordinates of extremities marked**

The coarse resolution texture map of the whole particle surface revealed which points were highest and it was assumed that it would be these points that would be most affected by the action of polishing in the W-S machine. The approximate location of the three highest points are marked on the outline in Figure 5.12 and the pseudo-coloured image in Figure 5.13 indicates height variation across the particle surface – it can be seen that the three points chosen for closer inspection correspond to the highest points on the surface. The use of this sort of pseudo-coloured topographical map is explored in more detail in later sections.



**Figure 5.13 Topographical map of limestone particle 1, before polishing**

The coordinates of the three highest points on each aggregate particle were recorded. These coordinates were used to locate the same area again when measuring texture at the next stress level. Where possible, photographs of the surface taken by the microscope at the previous stress level were used to align measurements or to confirm the location determined by coordinates. The series of photographs in Figure 5.14 show the same area of limestone (the point marked '3' on the outline in Figure 5.12) at each of the stress levels. The photographs were taken by the microscope using its 5X objective lens.



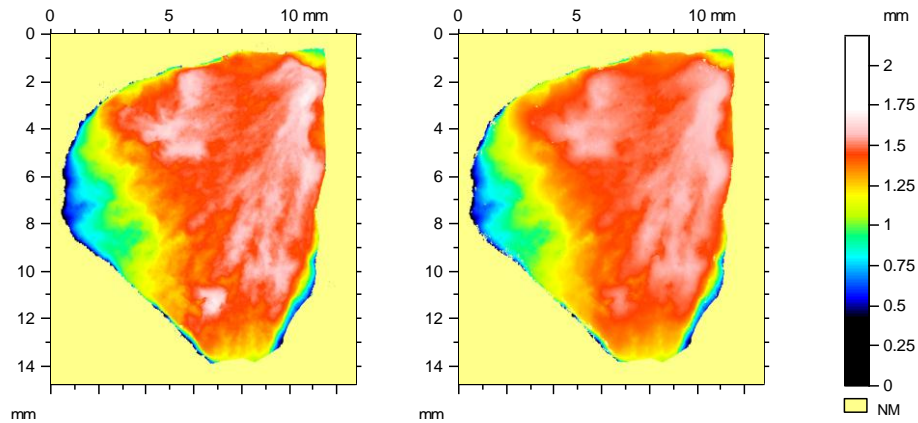
**Figure 5.14 Photographs of a specific area of limestone aggregate particle 1 at 5X magnification at five levels of polish showing associated changes in topography**

A useful tool provided by the Alicona microscope's analysis software allows automatic alignment of surfaces, after measurement, to assist with detection of changes to the surface caused by some external effect (polishing in this case, or, in the example given by the microscope, machine wear). The software uses a least squares best fit algorithm to determine the closest alignment and it can only work if there is a sufficient amount of surface that has remained unchanged. Note then, for example, it is not possible to align some of the surface areas measured at higher magnification because the whole area has changed significantly.

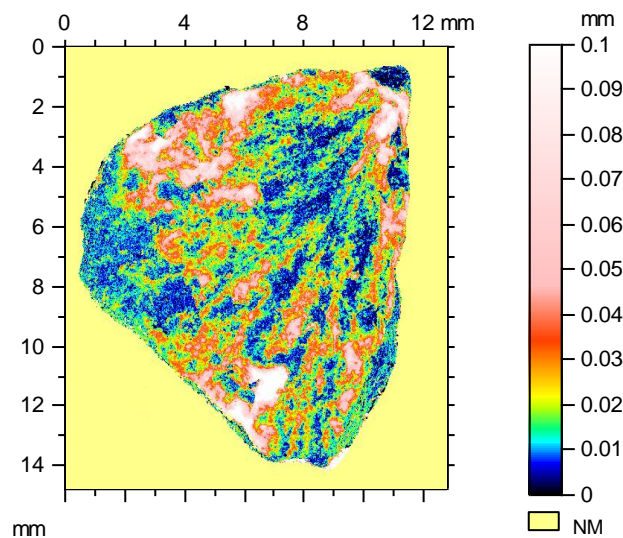
Figure 5.15, shows topographical maps of limestone particle 1 before and after polishing, while Figure 5.16 shows the difference between the two, as calculated by Alicona software. There are high planes and ridges fanning out from the top right of the stone surface before polishing; after polishing, these areas are less well defined and, in places, distinctly broader. The



largest changes in height indicated correspond to the highest points on the stone and there is little or no change in height in the lowest areas. Section 5.5 shows that the reason for this stasis, for some of the areas, is that there is no contact with the polishing rollers in the W-S machine. Qualitative analysis of changes caused by polishing are presented in more detail in Chapter 6.



**Figure 5.15 Topographical maps of limestone particle 1, before (left) and after polishing**



**Figure 5.16 Topographical maps showing calculated height differences caused by polishing**



## 5.4 Texture measurement

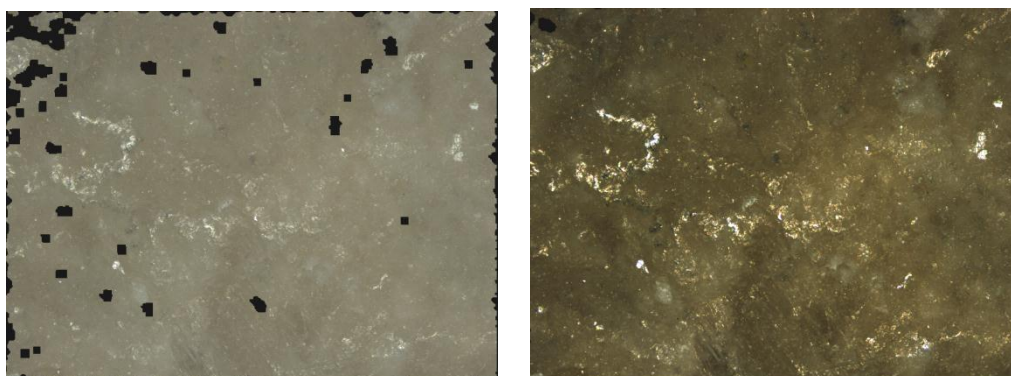
For all experiments, as mentioned, texture measurements were made using an 'InfiniteFocus' microscope made by Alicona housed and maintained by the National Physical Laboratory (NPL), Teddington. The principle of operation is outlined in Chapter 2; this section will describe the method of operation used for all experiments.

The measurement process is fast compared to other measurement techniques, such as line scanning profilometry, but still not fast enough to practically capture high resolution information for the entire specimen surface. This is the reason for selecting a number of areas on each of two aggregate particle surfaces, as described above. The low-resolution measurements made to assist with identification of the areas for closer study, made across the whole stone, use the microscope's 5X objective lens. In order to reduce the amount of time taken to make measurements over a large area, the resolution (stated by the control software) was reduced to 7  $\mu\text{m}$  laterally and 1  $\mu\text{m}$  vertically. The size of the area scanned varies according to the size of the aggregate particle but the number of measurement points on each particle surface, even at this reduced resolution, is around 20 million.

Having then chosen areas on the aggregate surfaces for closer inspection, the next measurements were also made using the microscope's 5X objective lens, but using higher resolution settings. Measurements were made of the same areas using 10X and 20X objective lenses which, because of a narrower field of view, result in higher resolution. According to the operating software, using the 5X objective lens achieves a resolution of 1.75  $\mu\text{m}$  laterally and 0.5  $\mu\text{m}$  vertically while the 10X objective lens achieves 881 nm laterally/124 nm vertically, and the 20X objective lens achieves 438 nm laterally/59 nm vertically. Note that doubling the magnification halves the field of view, and therefore doubles the resolution, as expected.

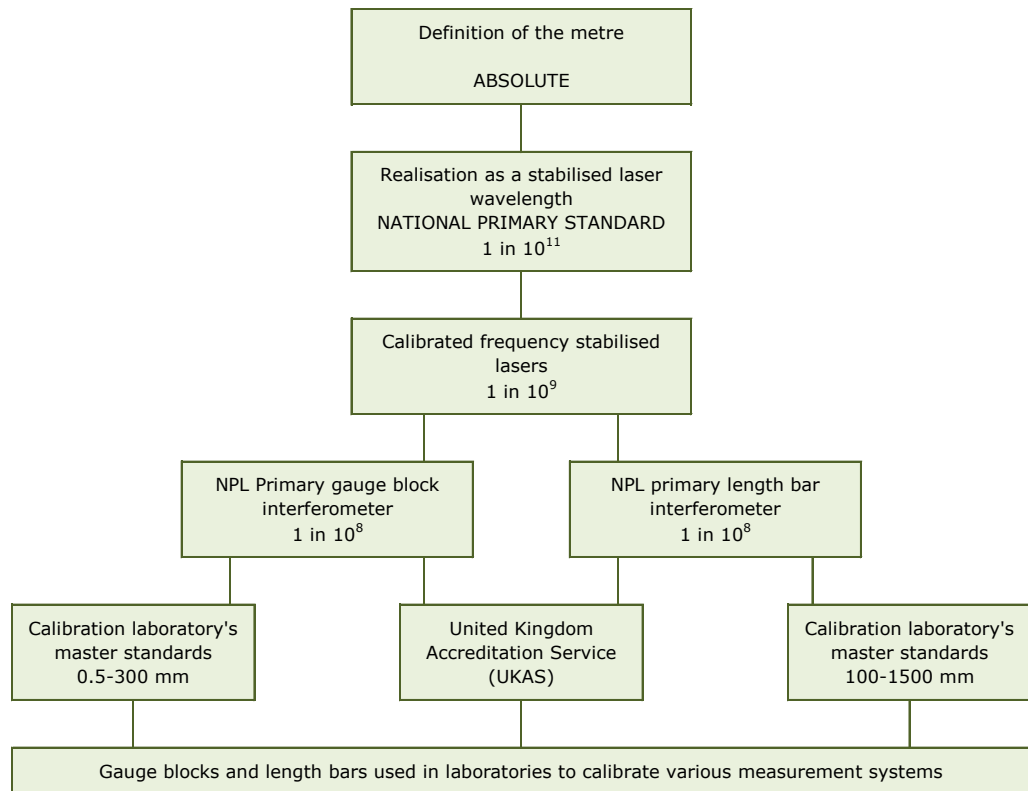
The practicalities of making measurements on aggregate surfaces are not straightforward and, by checking the data after each measurement, it was frequently found to be necessary to repeat measurements to achieve high quality data for later analysis. For example, the surface is not clean by any standard: sand (used in specimen preparation), dust, and miscellaneous fibres often obstructed the measurement view.

Another difficulty that presented itself was one of contrast. Since the microscope is an optical system, and measurements are made of a whole area (as opposed to a point), it is necessary to adjust lighting and exposure to make sure the whole area is correctly illuminated. Doing so, and checking the results, greatly improves the quantity and quality of data collected. Although the system has an auto-exposure function, which was always used before measurements were made, getting the correct contrast in each image was problematic, particularly for the limestone particle surfaces, which often had very bright and very dark spots within each area. The two images in Figure 5.17 show the photographic records of one of the areas on the surface of the first limestone aggregate particle, before polishing, at 5X magnification. The photograph on the left is over-exposed and, because of a limited range of contrast set in the measurement system, some of the darker areas of the surface were not measured – these show up as black polygons. The photograph on the right, of exactly the same area, is correctly exposed and, correspondingly, most of the area has been measured correctly.



**Figure 5.17 Area on limestone aggregate particle over-exposed (left) and correctly exposed**

There are several advantages to using the equipment at NPL including that the set up and calibration is independently and frequently checked and that these calibrations are 'traceable'. If a measuring device and its calibration are traceable then its operation has been calibrated, via an unbroken chain of comparisons, to national or international standards. As an example, for the case of gauge blocks and length bars (which may be used to calibrate various distance measurement tools and systems), a traceability chain is summarised in the diagram in Figure 5.18 (Flack & Hannaford, 2005), with an estimate of the uncertainty during the later stages.



**Figure 5.18 Traceability chain for gauge blocks**

## 5.5 Paint erosion

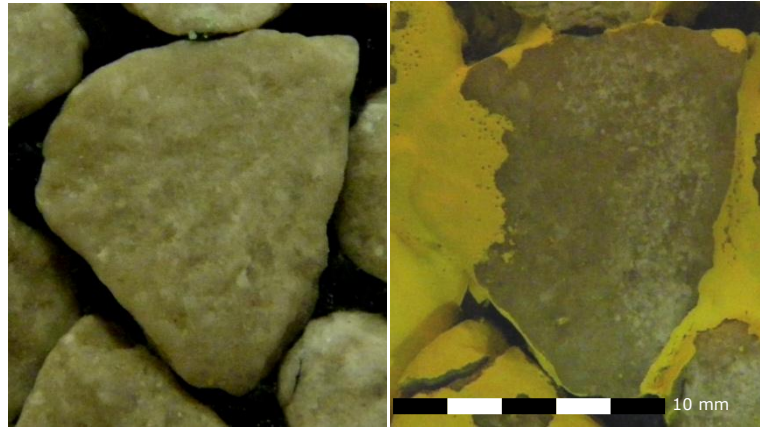
Before detailed analysis was carried out, a simple version of the paint erosion indication technique described by Parslow et al. (1997) was used to verify that the stones chosen at random had indeed come into contact with the polishing rollers. Following completion of the polishing experiment (and the associated texture measurement of the two randomly chosen stones), the whole specimen was coated with a single layer of road marking paint and then polished in the W-S machine for another 90,000 polishing roller passes. The resulting surface is shown in Figure 5.19; the stones previously chosen and characterized are highlighted with a black outline.



**Figure 5.19 Limestone test specimen after painting and polishing**

*The areas which have not been in contact with the polishing rollers are bright yellow (including a central zone over which the rollers do not pass) with the grey areas where the paint has been removed indicating that abrasion has occurred at these locations*

The centre of the specimen does not come into contact with the polishing rollers, which scribe an annulus 60 mm wide around the circumference of the specimen, but there are clearly parts of the 'polished' area that are still covered in paint. The aggregate particles are not completely flat and the polishing rollers are not flexible enough to conform to all the variations in the surface. The two photographs in Figure 5.20 show limestone particle 1 before and after painting/polishing, confirming that the majority of this stone's surface has been polished. The same is true for the second particle.



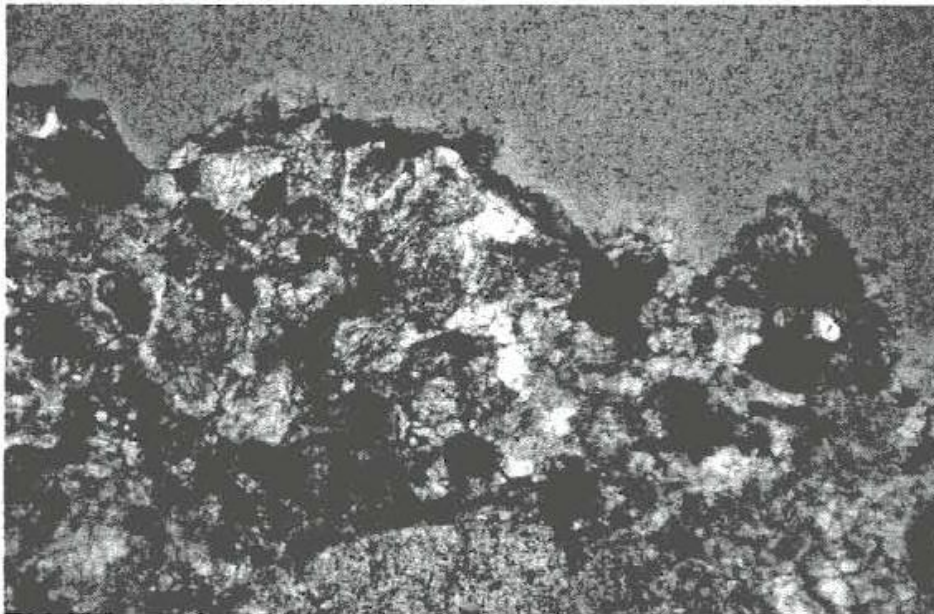
**Figure 5.20 Photograph of the surface of Stone 1 before and after painting and second polishing**

In principle, this technique could have been used throughout the experiment, and surface texture only measured on areas that were indicated as being in contact with the rollers. However, the presence of the paint may have influenced the polishing of the aggregate particle surfaces and thus altered the friction measurements.

## 5.6 Aggregates

As in the work of Do et al. (2009), limestone was chosen as the first subject aggregate. Limestone is rarely used as road surface course aggregate in the UK because it typically has a low resistance to polishing. As demonstrated, this is more evident when polished by traffic rather than in the laboratory (Figure 5.4). However, its low resistance to polishing, and therefore the wide range of friction levels observed when polished in the laboratory, makes limestone a good initial candidate for trial and development of the methodology.

Limestone is typically very homogenous, predominantly composed of a single mineral (calcite), with only small amounts of secondary minerals such as quartz or feldspars. A petrographic analysis of limestone taken from the same quarry as the limestone used in this experiment states that the "limestone is composed of robust fragments that resist breakage; pits and cavities are uncommon". Accordingly, the surface texture of limestone should be amongst the simplest to interpret of any aggregate type. A photomicrograph of limestone from the same quarry is shown in Figure 5.21: further notes from the petrographic analysis state that the image, taken in plane polarised light, shows irregular margins of the aggregate and minor surface indentations.



**Figure 5.21 Photomicrograph of limestone; width of field is 1.6 mm**

The second aggregate studied, a gritstone from the Yorkshire Dales, is used widely in road surface courses because of its high resistance to polishing. It is also a sedimentary rock and it comprises particles of size between 4 and 30 microns. A petrographic analysis of aggregate from the same quarry indicates that the rock type should more properly be called siltstone, which might be considered a subset of gritstone; the specimen will be referred to as gritstone for the remainder of this thesis. The particle shape is described as "Angular to Subrounded" and the surface texture of particles is "Rough to Moderately Smooth". This description is not particularly helpful for the purposes of this investigation but it is likely that the homogeneity of the structure and the particle size range will be useful information to assist with analysis of texture measurements.

For comparison with relative measurements of friction after polishing in the Wehner-Schulze machine, it is of interest to note that the approximate nominal PSV of the limestone is 40 while the nominal PSV of the gritstone is 65.

## 5.7 References

- Do, M. -T., Tang, Z., Kane, M., & de Larrard, F. (2009). Evolution of road-surface skid-resistance and texture due to polishing. *Wear* 266, 574-577.
- Dunford, A., & Roe, P. G. (2012). *PPR604. Use of the Wehner-Schulze machine to explore better use of aggregates with low polishing resistance. 1: Capabilities of the Wehner-Schulze machine.* Crowthorne: TRL.
- Flack, D., & Hannaford, J. (2005). *Measurement good practice guide no. 80. Fundamental good practice in dimensional metrology.* Teddington: National Physical Laboratory.
- Hosking, J. R. (1967). *LR81, An experiment comparing the performance of road stones in different bituminous surfacings: A.30 Blackbushe, Hampshire.* Crowthorne: RRL.
- Hosking, J. R., & Woodford, G. C. (1976). *LR738 Measurement of skidding resistance. Part II. Factors affecting the slipperiness of a road surface.* Crowthorne: TRL Ltd.
- Hushek, S. (2004). Experience with skid resistance prediction based on traffic simulation. *5th symposium of pavement surface characteristics.* Toronto.
- Parslow, G. I., Stephenson, D. J., Strutt, J. E., & Tetlow, S. (1997). Paint layer erosion resistance behaviour for use in a multilayer paint erosion indication technique. *Wear* 212, 103-109.
- Roe, P. G., & Dunford, A. (2012). *PPR564. The skid resistance behaviour of thin surface course systems. HA/MPA/RBA collaborative programme 2008-11: topic 1 final report.* Crowthorne: TRL.



## **6 Qualitative analysis of changes in texture during simulated polishing**

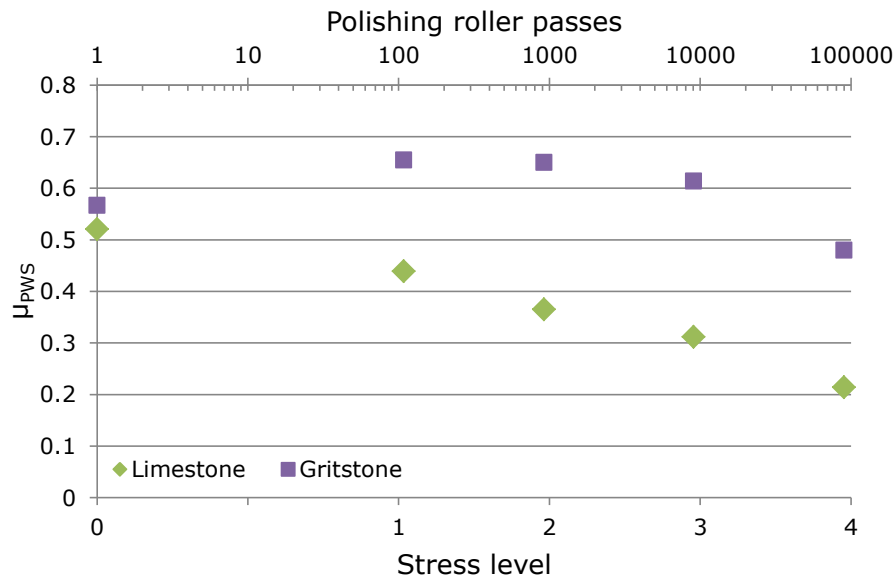
---

This chapter examines the visible changes that occur on the surfaces of limestone and gritstone aggregates, apparently as a result of polishing in the laboratory. Both aggregates are dealt with at the same time because, together, the range of friction measured on their surfaces after polishing approximately spans the maximum and minimum available from natural aggregates found in the UK. The long-term goal of this work, for the purposes of practical implementation, is a contiguous comparison of texture and friction that spans mineralogical differences.

The aggregates' different responses to polishing in the Wehner-Schulze machine, in terms of the friction measurements made on the surfaces, is perhaps the first indication that the mechanisms by which they polish are different. Qualitative analysis of changes in surface texture, in the following sections, reveals some of the differences between the polishing mechanisms and it is likely that quantitative analysis, in the next chapter, will need to account for these differences.

## 6.1 Friction measurements

Friction measurements made on the limestone specimen have already been presented to illustrate the polishing methodology (Figure 5.6). The graph in Figure 6.1 shows that information (green diamonds) and adds those measurements made on the gritstone specimen (purple squares).



**Figure 6.1 Friction measured on limestone and gritstone test specimens as a function of polishing in the W-S machine**

Whereas friction on the limestone specimen reduced linearly with polishing, change in friction on the gritstone specimen was more complicated. There is an initial increase in friction followed by a much more gradual decline. The initial increase may be as a result of a change in the form of the surface texture – the initial texture resulting from crushing at the quarry. The gradual decline in friction, to a still relatively high level, is to be expected of a 'high specification aggregate'. This sort of aggregate is used on the road network because of its ability to resist the polishing action of traffic (or polishing rollers in this case).

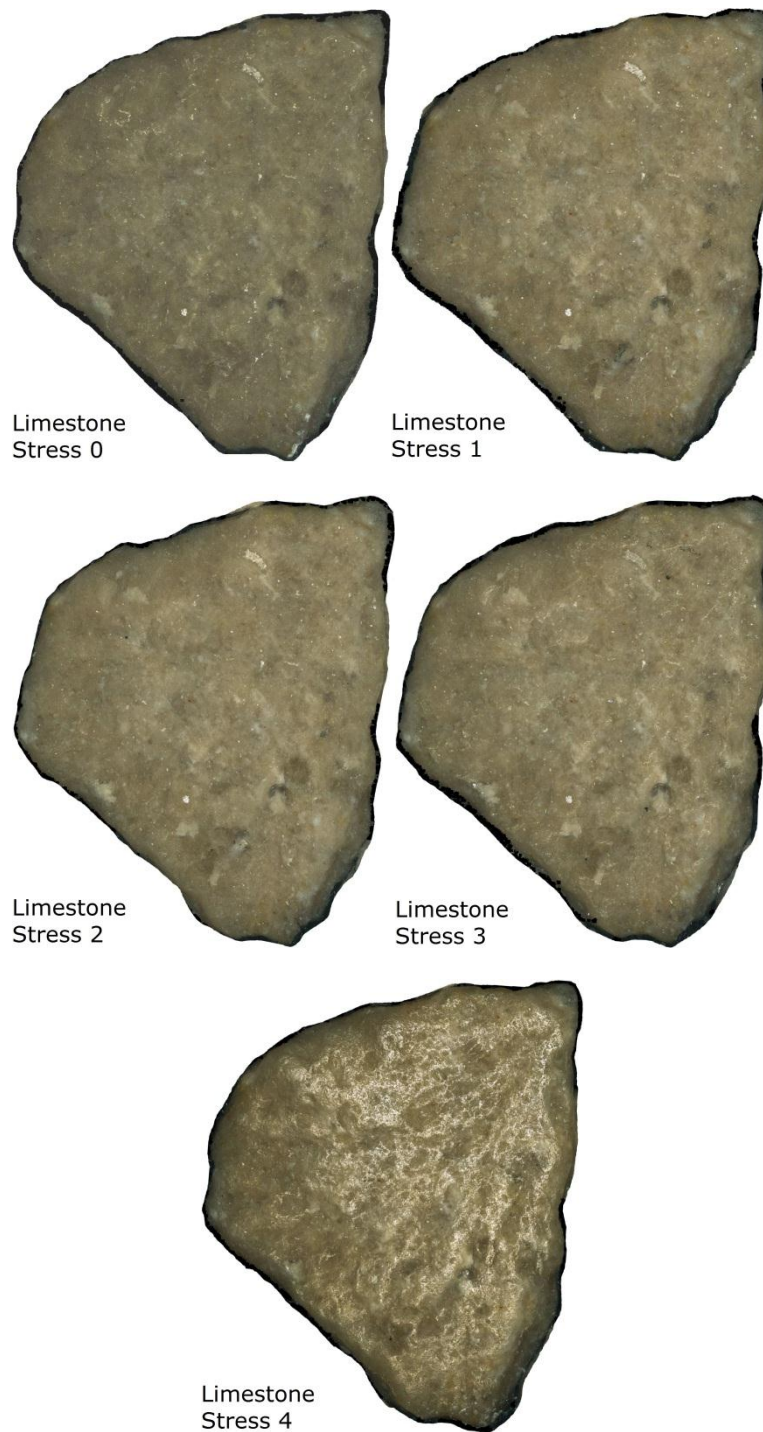
## **6.2 Changes observable on whole stone faces**

Some changes in surface texture on the surfaces of individual aggregate particles are visible to the naked eye. The simplest tool for recording these changes is photography; variation in texture can be apparent because of differences in the reflectivity of the surface (diffuse or specular) or the homogeneity of pixel intensities (see Section 3.2). Alternatively, changes in texture can be analysed qualitatively by converting texture measurements into topographical maps of surface height.

### **6.2.1 Photographic evidence**

The five photographs in Figure 6.2 show the surface of limestone particle 1 at each of the five polishing “stress levels”. The photographs were produced by the Alicona microscope, which records an image of each measured area. Contrary to the linear change in friction, almost no change is apparent until Stress 4 when the surface has become noticeably smoother, and therefore more reflective.

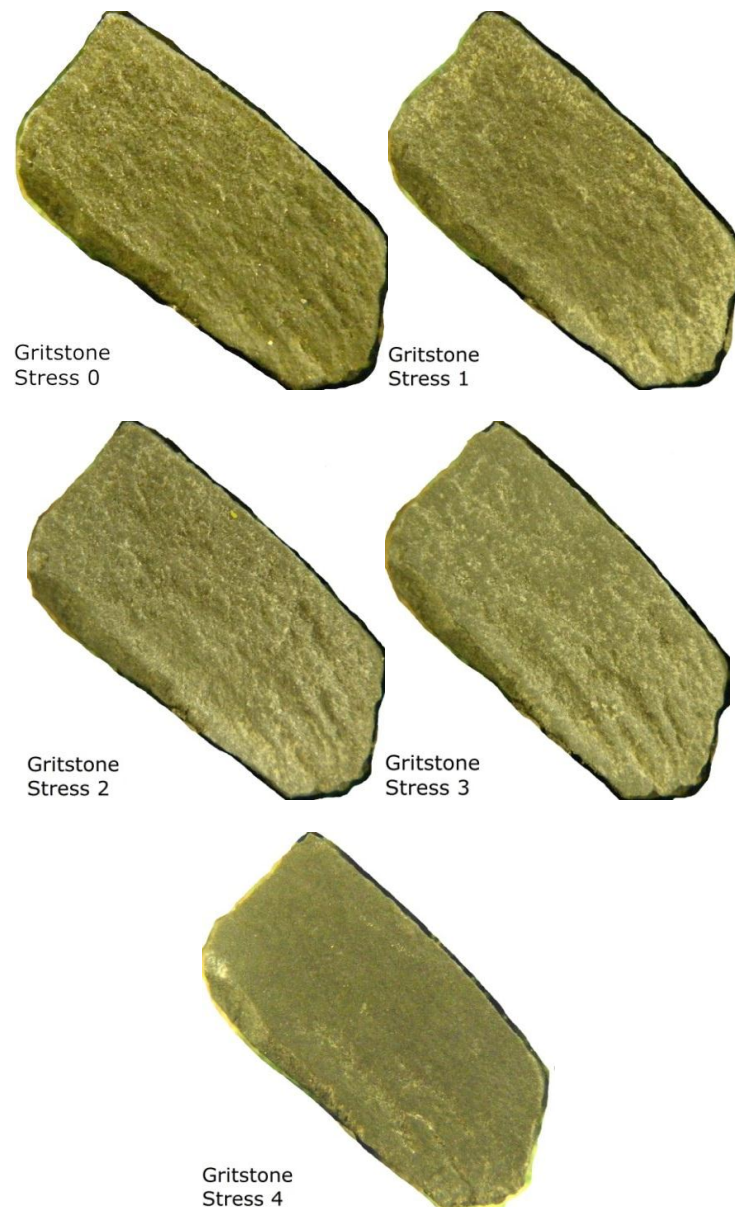
This contradicts the findings presented in Section 3.2, which demonstrated that image analysis methods could be used to detect gradual changes in surface texture, occurring due to polishing, on a limestone aggregate. The difference may be due to the way in which the photograph has been taken. The Alicona builds up a photograph from ‘image slices’ taken of a relatively small area (2.85 mm by 2.16 mm in this case, using the 5X objective lens) and then stitches them all together, both in the x-y plane, and in the z-direction. The resulting photograph is always uniformly, perpendicularly, lit and is exactly in focus throughout its depth. Although this yields a good image, the features required for analysis of texture changes may not be reproduced. Unfortunately no photographs of the surface were taken, using conventional photography, throughout the polishing process for the limestone specimen.



**Figure 6.2 Photographs of limestone particle 1 at each stage of polishing (from Alicona microscope)**

For comparison, therefore, Figure 6.3 shows five photographs of gritstone particle 1, taken using a compact digital camera (Pentax W60, macro mode). These photographs were only intended to record the experiment and, although they are not ideally composed, they are of just high enough resolution for useful observations to be made.

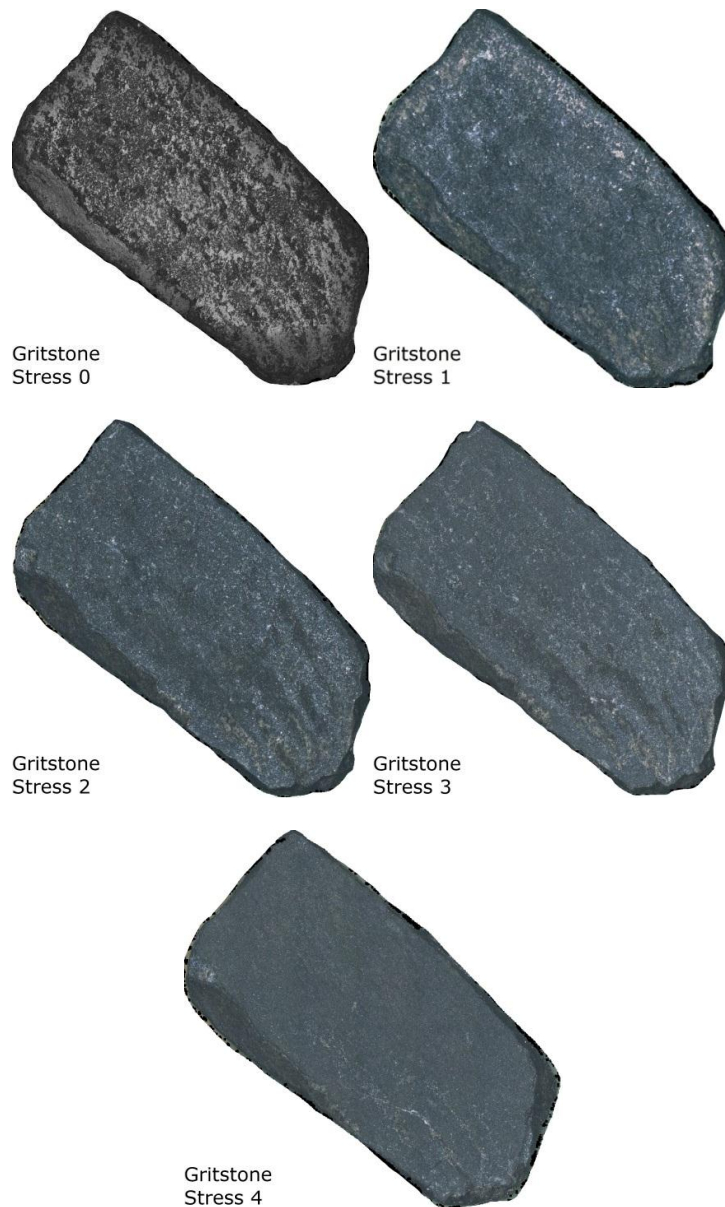
Changes due to polishing are apparent slightly sooner in the polishing process, matching more accurately with the pattern of changing friction. For example, by Stress 3 the top right region of the aggregate particle has become more homogenous, and presumably smoother. The surface has not become shiny and reflective as with the limestone, and this probably highlights a difference in the form of texture on the surface – producing diffuse rather than specular reflection.



**Figure 6.3 Photographs of gritstone particle 1 at each stage of polishing (from compact camera)**

Photographs of the same stone, produced by the Alicona microscope, Figure 6.4, demonstrate the theory that gradual changes in surface texture are not so apparent in images of this type. They are more uniformly lit and the colour reproduction is more accurate (the gritstone is grey, rather than

yellow). If this experiment is repeated, the standalone photography of the earlier experiment with dolerite aggregate (Chapter 4) might be revisited because the images from the microscope are not as useful for qualitative analysis as had been hoped.



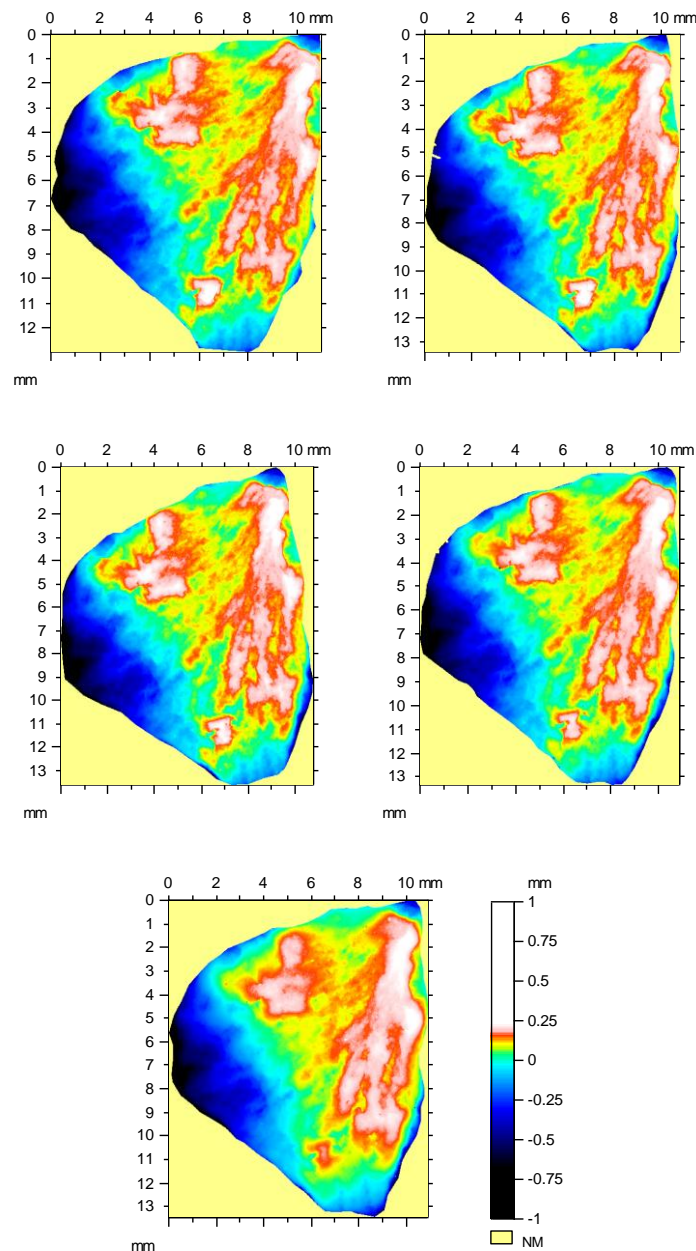
**Figure 6.4 Photographs of gritstone particle 1 at each stage of polishing (from Alicona microscope)**

A particular feature of the gritstone surface, when viewed through the microscope's lens, is a swift change in colour between Stress 0 and Stress 1. The white substance is probably some detritus or dust that has subsequently been removed by the first stage of polishing. The fact that this white substance shows up in Alicona images but not in the compact camera images may be due to the angle of lighting and therefore a change in the amount of light reflecting directly from the surface.



### 6.2.2 Topographical evidence

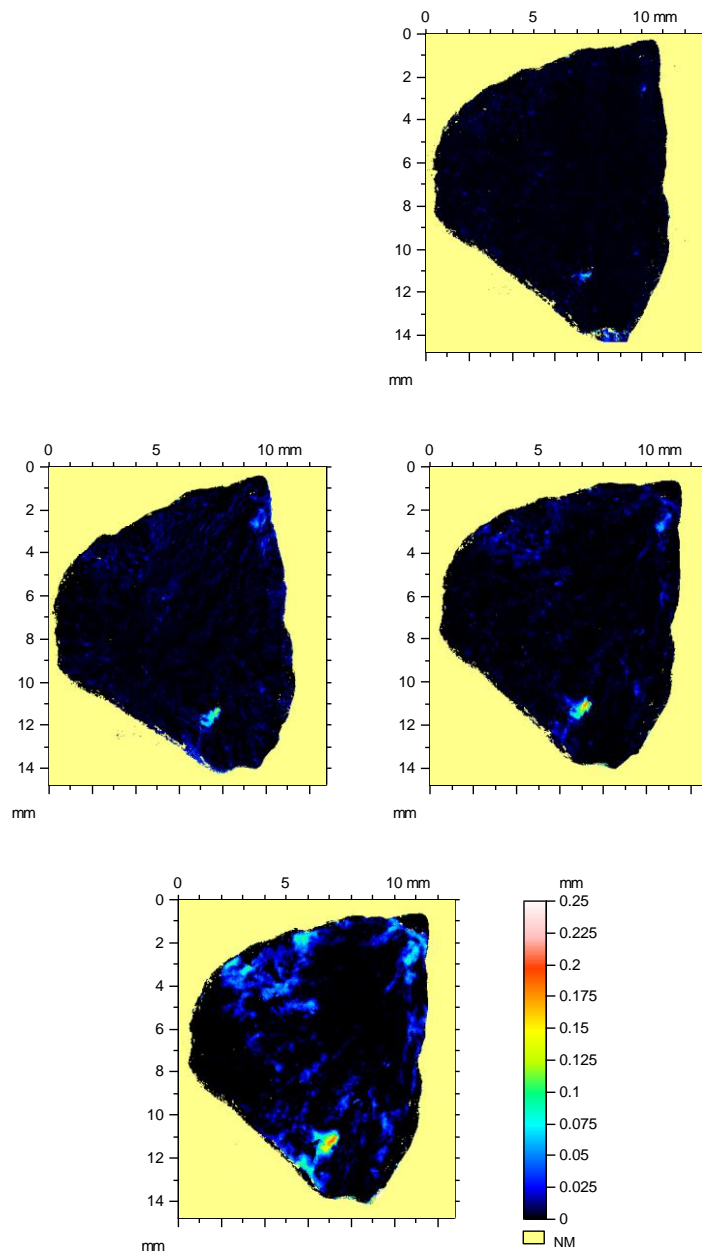
Analysis of topographic maps of height distribution at each stress level is almost analogous. In particular, for limestone only small changes are apparent until the transition between Stress 3 and Stress 4, when the uppermost parts of the surface (shown in red and white) become significantly more blurred, indicating a smoothing of the surface. This is shown the topographical images in Figure 6.5.



**Figure 6.5 Topographical maps of limestone particle 1 at each stage of polishing**

Even though the changes are small and difficult to observe, if the surfaces at each polishing stage are compared to the initial condition, macroscopic differences do become apparent. Figure 6.6 shows the topographic maps

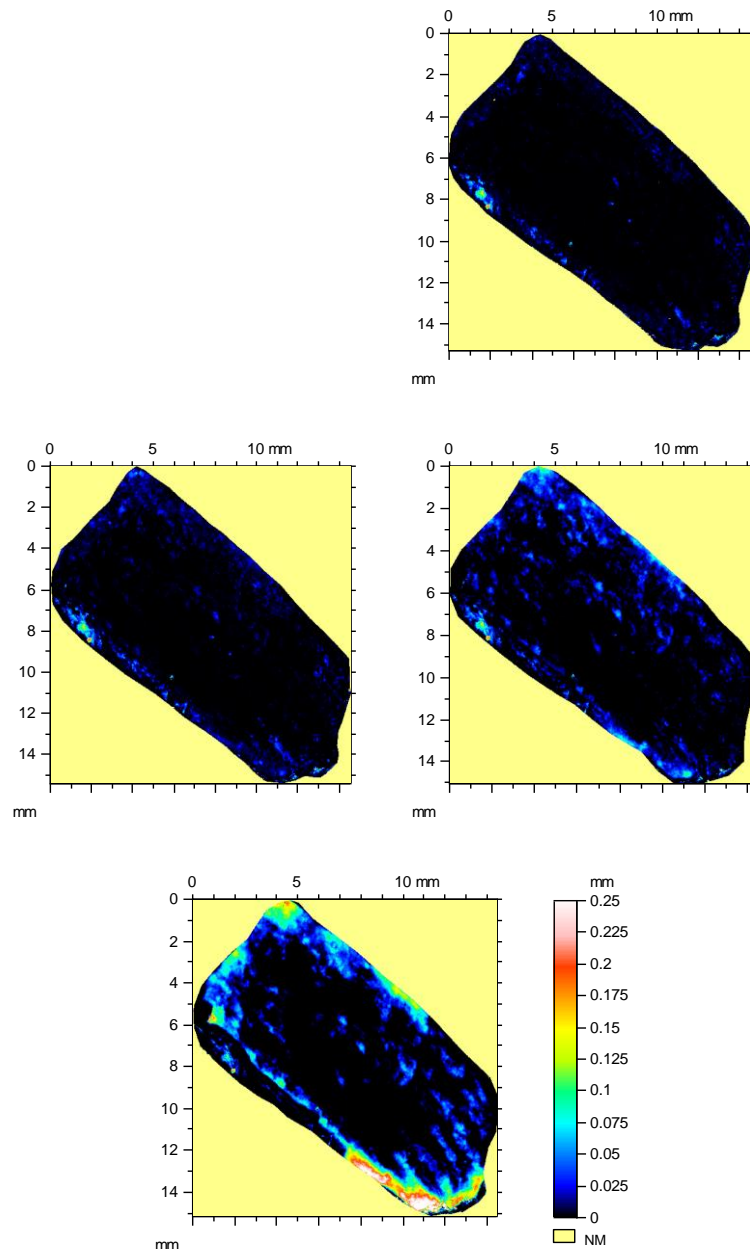
resulting from taking the point heights measured at Stress 0 from the heights measured at subsequent stress levels. To do this, a surface differences tool embedded in the Alicona microscope's software was used; provided its algorithms can align the majority of the surface, it can credibly highlight height variation.



**Figure 6.6 Topographical change from Stress 0, limestone particle 1**

It is clear that on limestone particle 1 there are high points that are worn down, even by only a small amount of polishing. The same treatment on gritstone particle 1 reveals a similar story except that changes in height from the initial surface condition are greater in places and generally more widespread.





**Figure 6.7 Topographical change from Stress 0, gritstone particle 1**

This is a good indication that the polishing mechanism for gritstone is probably different from the polishing mechanism for limestone. There is more material lost from the gritstone surface. This contradicts the expectation given by typical aggregate abrasion values (AAV - see Section 2.6) for these aggregates: gritstone 6 and limestone 10, which suggest that, by mass, the percentage loss after abrasion of limestone is almost twice that for gritstone. However, the Wehner-Schulze test is not designed to be as aggressive as the AAV test and so the comparison is perhaps not fair. Indeed, the expected polishing mechanism for high specification aggregates is that the surface texture is renewed by removal of mineral grains (see Figure 2.31).

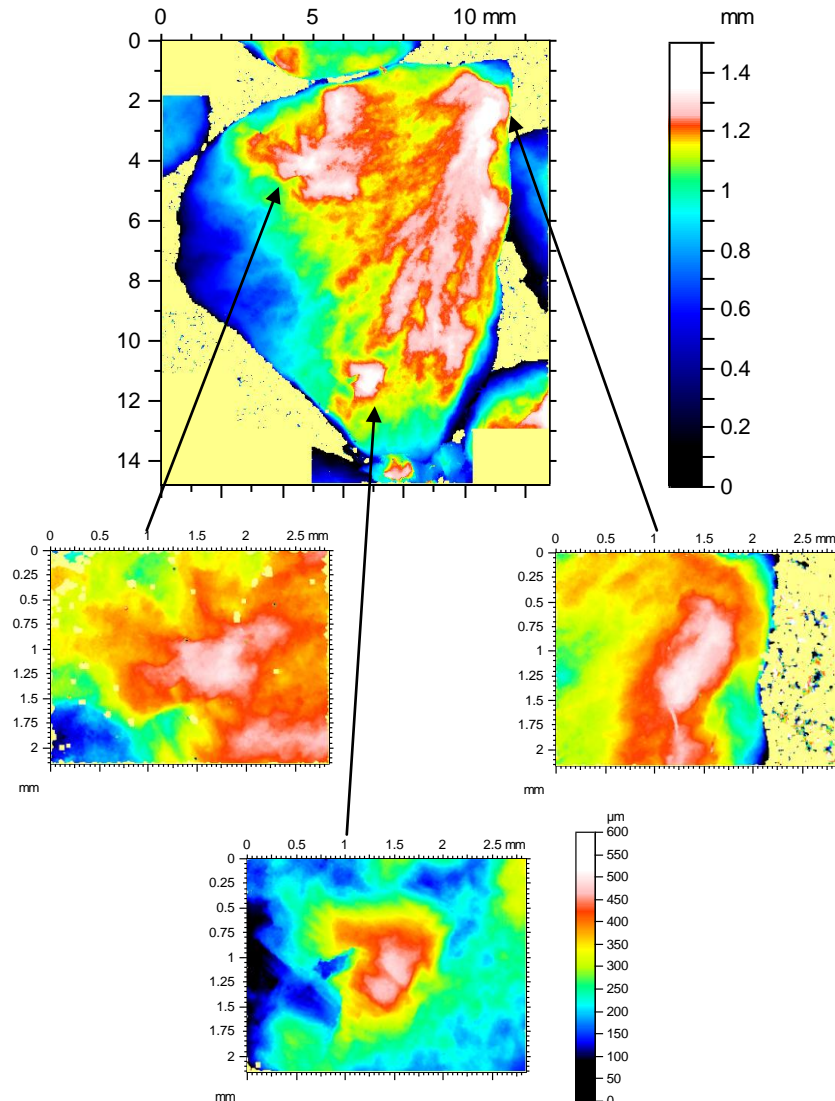
The areas that appear to be most worn are also highlighted by paint erosion. Figure 6.8 shows the limestone aggregate particle surfaces after it had been painted and then polished again in the W-S machine. Areas that are still painted yellow have not come into contact with the polishing rollers, and these correspond to black areas on the topographical maps of changes in Figure 6.6. It is clearly not possible to track removal of paint during the main polishing process because the presence of paint would influence both polishing and friction measurement. However, if this experiment is repeated, photographing intermediate stages of polishing (as opposed to just one photograph after an hour of polishing and complete paint erosion) may highlight any points of the surface that are still prominent.



**Figure 6.8 Limestone aggregate particle after painting and subsequent polishing**

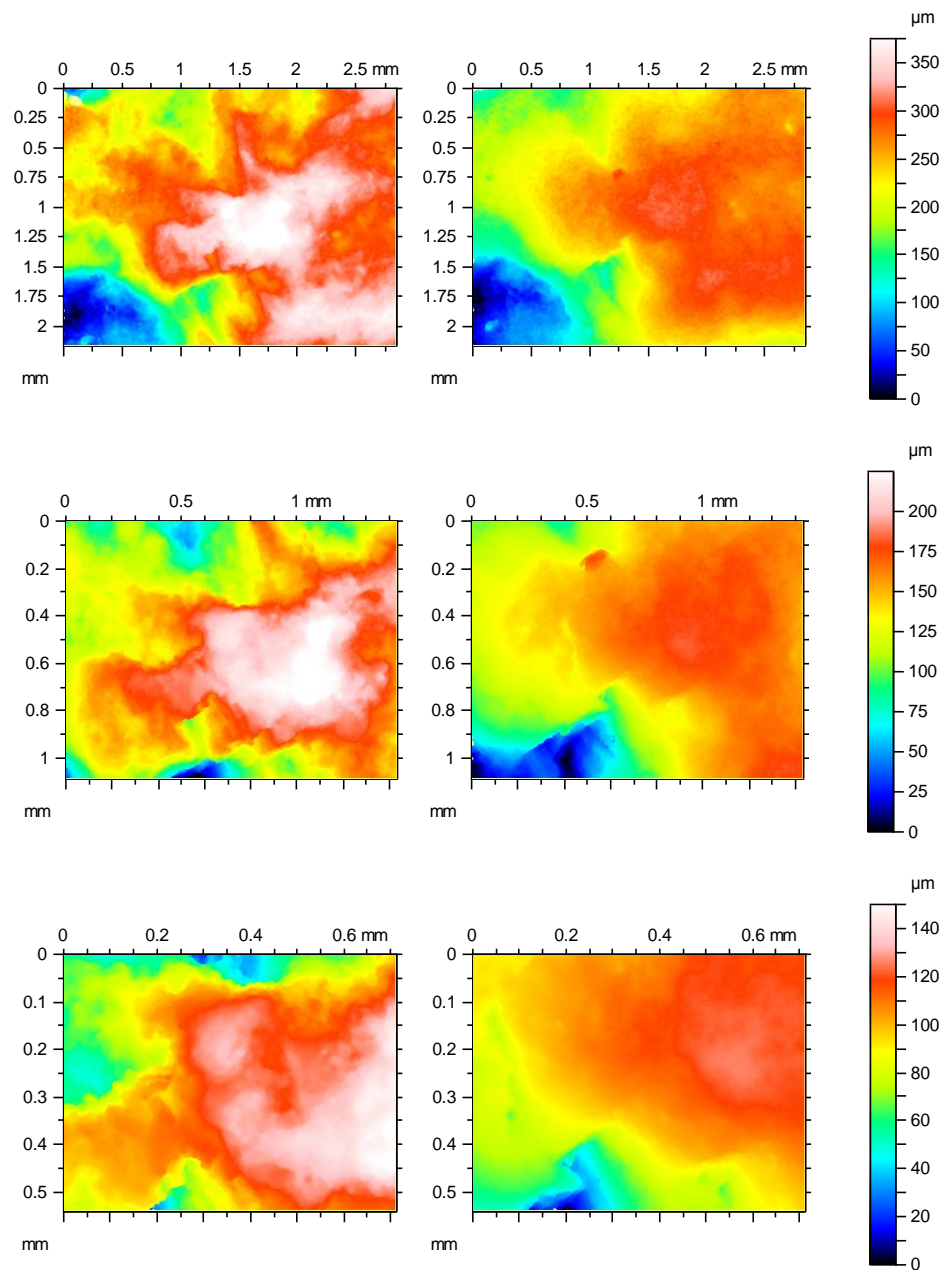
### 6.3 Changes that become apparent when considering smaller areas of surface

Figure 6.9 shows the height variation across the surface of limestone particle 1 and the three areas selected for closer inspection are indicated.

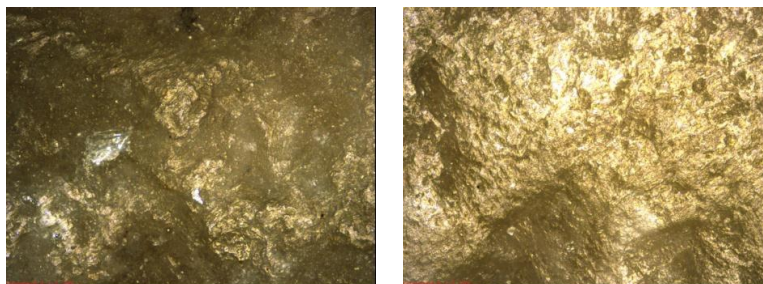


**Figure 6.9 Topographical map of limestone particle 1 and three areas selected for closer inspection, Stress 0, 5X magnification**

The surface texture for each of these areas, on each particle surface, was measured using the microscope's 5X, 10X and 20X objective lenses. Photographs and topographical information obtained using the higher magnification lenses reveal more detail about the forms of surface texture present on the limestone and gritstone aggregates. Figure 6.10 shows topographical maps of one of the areas at all three magnifications before and after polishing; Figure 6.11 shows photographs of the same area at 20X magnification before and after polishing.



**Figure 6.10 Topographical height maps of an area on limestone particle 1 at (top to bottom) 5X, 10X and 20X magnification at Stress 0 (left) and Stress 4**

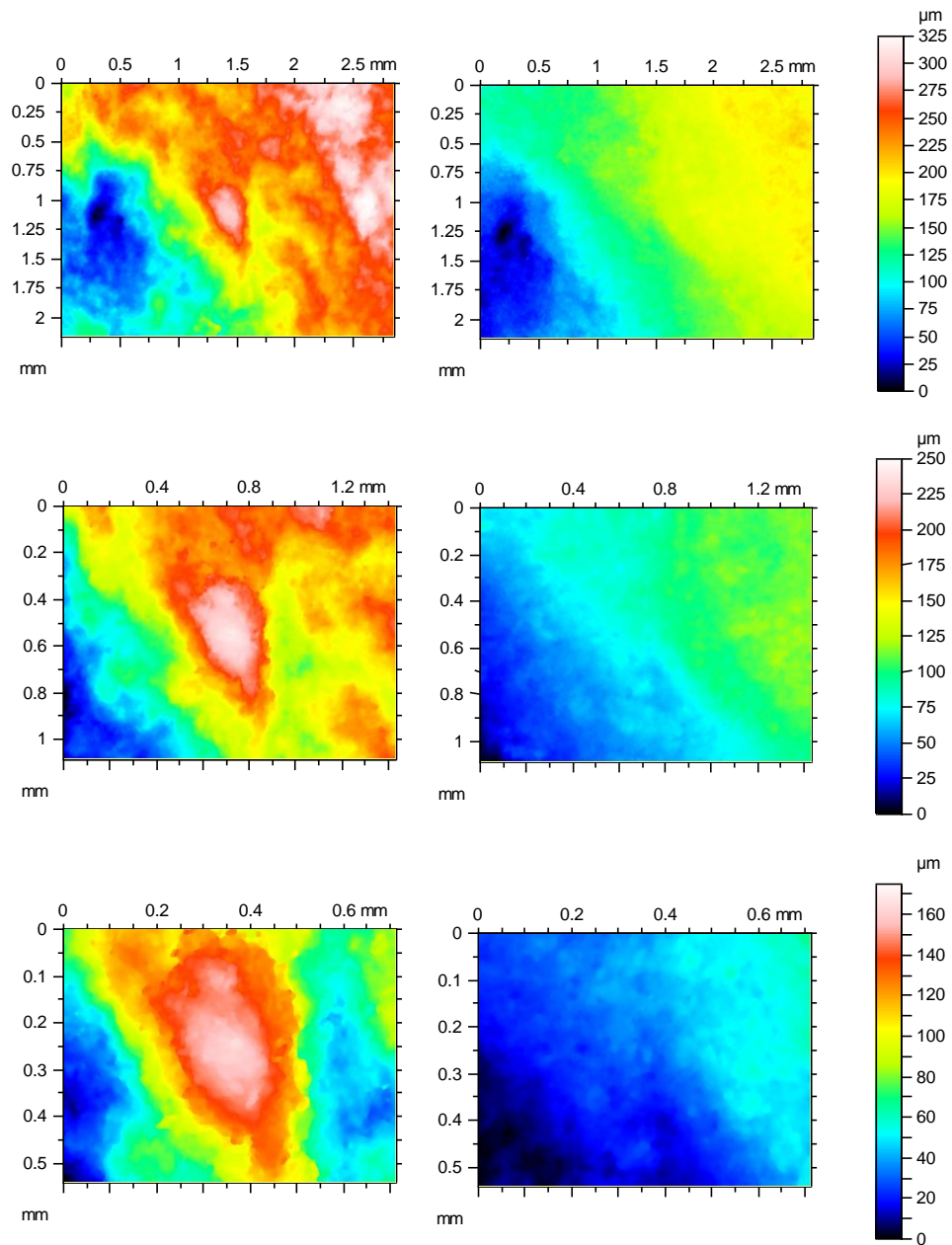


**Figure 6.11 Photographs of limestone area at 20X magnification, Stress 0 (left) and Stress 4**

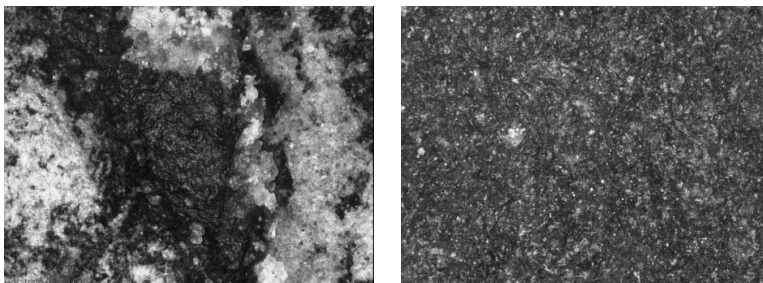
It is clear, as before, that the highest protrusion has been worn down. However, the remaining surface is not simply flat and smooth; the form of the texture has changed significantly as a result of polishing. After polishing, the surface of the limestone has a pock-marked appearance and there is still texture at various wavelengths. Again, a comparison can be made with the gritstone surface. Figure 6.12 and Figure 6.13 show the same information for one of the areas on gritstone particle 1. After polishing, the surface is almost unrecognisable; only the general slope and a characteristic feature on the lowest portion of the surface (see two dark blue depressions on the left of the images at 5X magnification approximately, 1.25 mm from the tops of the images) identify it as the same area. The photographs illustrate the same point, that polishing has had a significant effect on surface texture, and after polishing there is almost no apparent relief except for the relatively uniform low wavelength texture.

To complete the comparison between limestone and gritstone, the photographs in Figure 6.14 show all three measured areas on particle 1 of each aggregate type, after polishing, at 20X magnification. On all three areas there is evidence that the limestone has retained some texture at slightly higher wavelengths (greater than 0.5 mm), but relatively little low-wavelength (less than 0.5 mm) texture. In contrast, the gritstone is flat on the scale of the whole area (at 20X magnification the photographs are 0.7 mm wide) but does clearly have a significant amount of texture at shorter wavelengths.

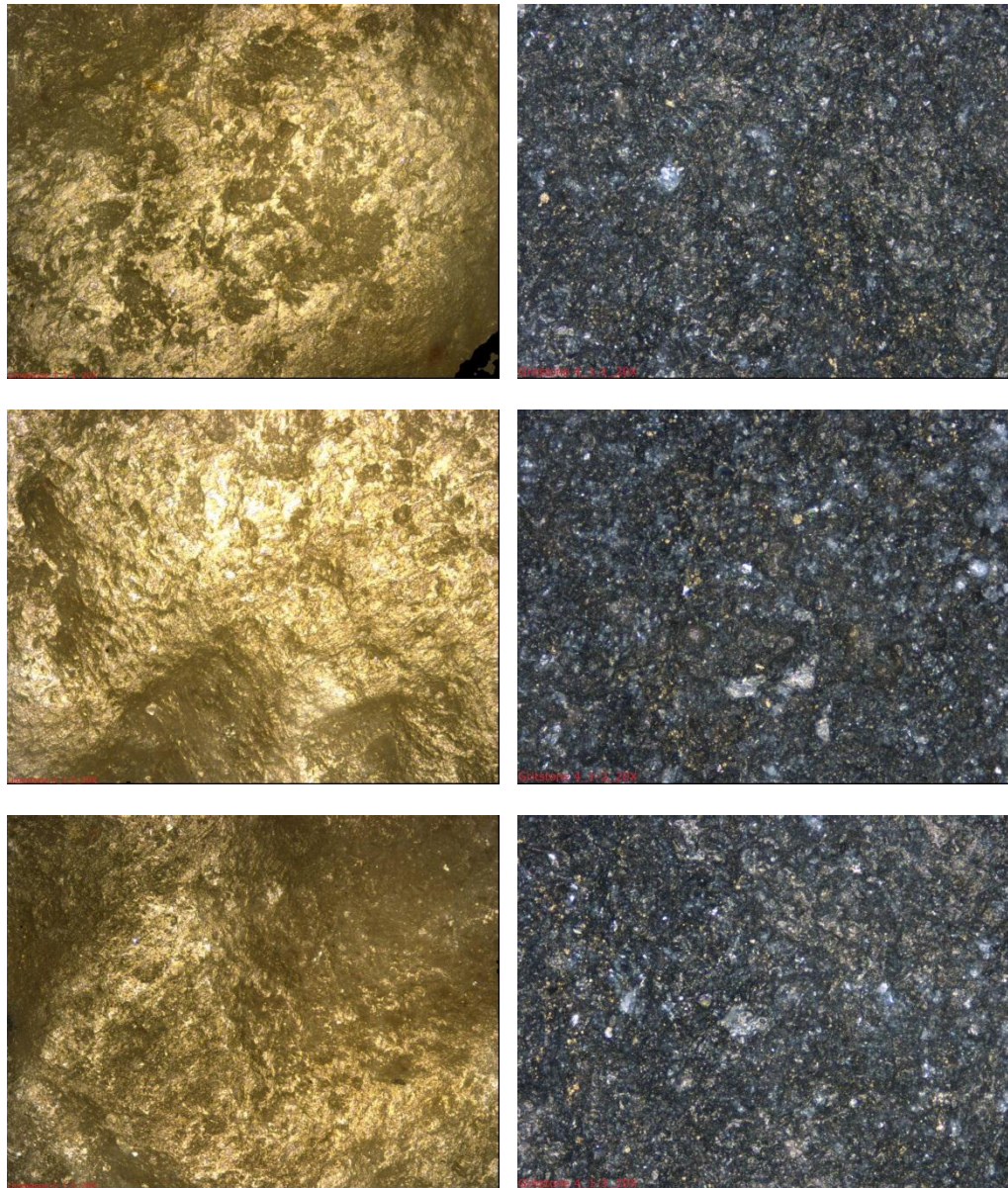




**Figure 6.12 Topographical height maps of an area on gritstone particle 1 at (top to bottom) 5X, 10X and 20X magnification at Stress 0 (left) and Stress 4**



**Figure 6.13 Photographs of gritstone area at 20X magnification, Stress 0 (left) and Stress 4**

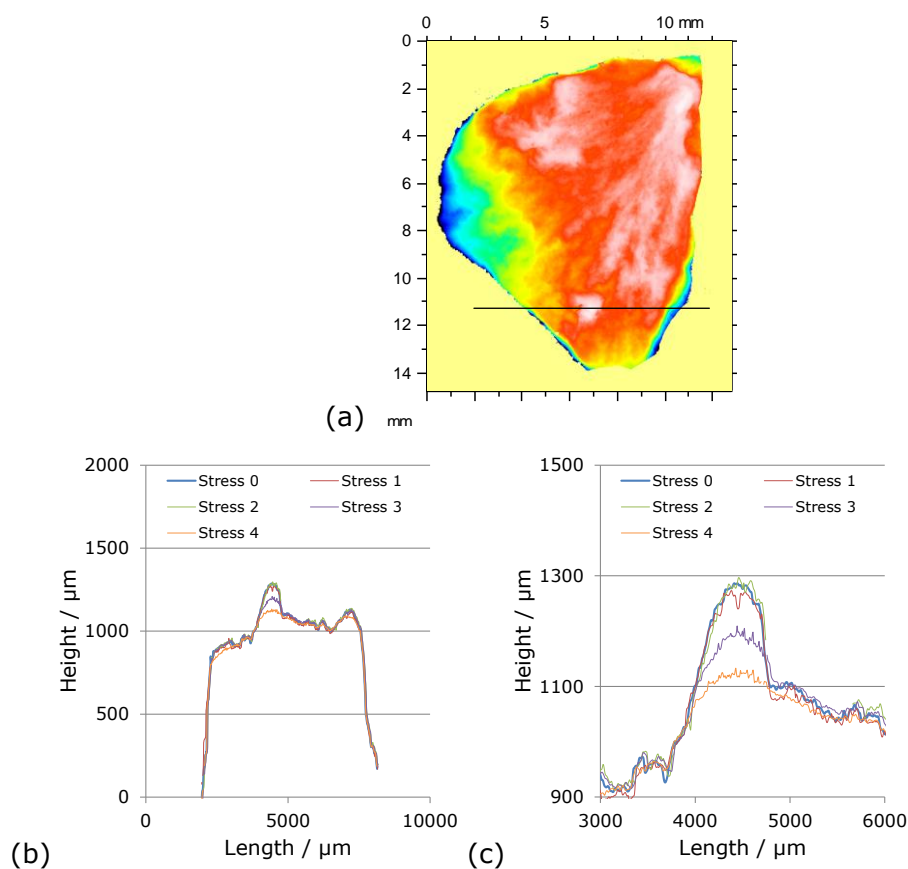


**Figure 6.14 Photographs of limestone (left) and gritstone areas, after polishing, at 20X magnification**

## 6.4 Analysis in two dimensions

Other researchers have conducted experiments using only profile information in two dimensions and some of the changes observed on the stone surfaces above can be seen quite clearly in cross section.

Taking a section through limestone particle 1, at the position indicated by the horizontal line drawn onto the topographical map in Figure 6.15 (a), surface profiles are shown in Figure 6.15 (b) and (c) using the data collected from measurements made of the whole stone surface at each stress level.

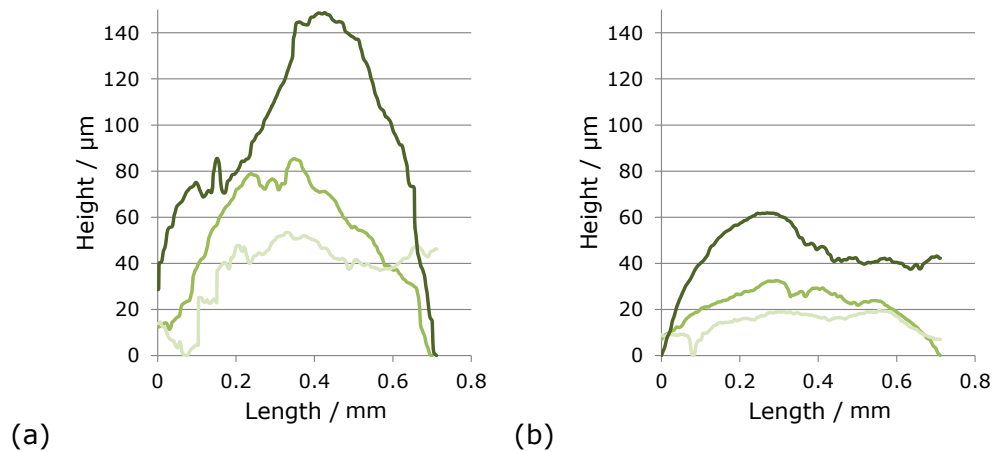


**Figure 6.15** Line profiles at each stress level along horizontal line in (a), across whole stone (b) and highlighting changing features (c)

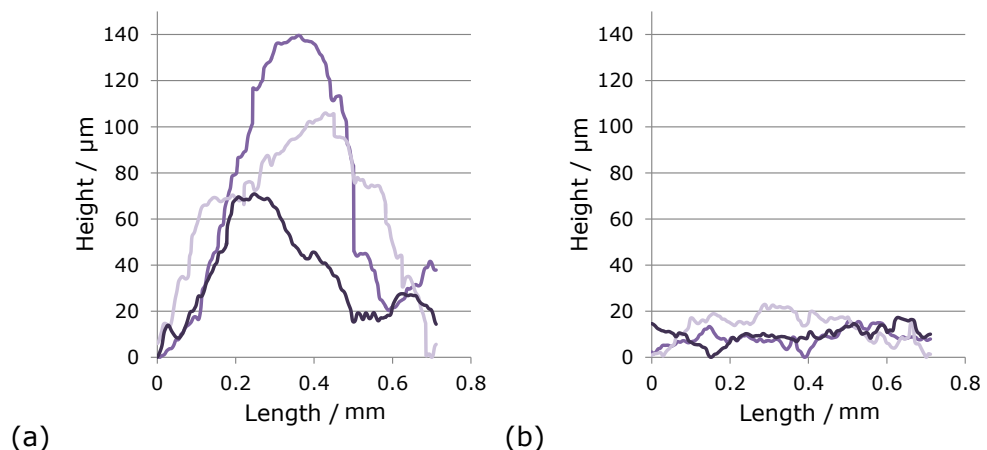
The two-dimensional line profiles show a clear change in the surface along the selected line. The advantages of making measurements in three dimensions before extracting this information in two dimensions include the increased confidence that the measurement line is identically located at each stress level and that, although the profiles show a protrusion wearing down with polishing, only the three-dimensional information indicates that it is an individual peak rather than a ridge.



Figure 6.16 (a) shows a line profile taken, horizontally, from the centre of each of the three surface areas inspected on limestone particle 1, at 20X magnification before polishing (Stress 0). Figure 6.16 (b) shows profile lines taken from the centre of each area after polishing (Stress 4). The surfaces were levelled before profiles were extracted (using Digital surf's Mountains software) and the heights are adjusted so that the lowest point on each profile is set at 0  $\mu\text{m}$ . Profiles from Stress 0 and Stress 4 are taken from corresponding regions of each surface but they are not precisely aligned. Figure 6.17 (a) and (b) shows profiles before and after polishing, respectively, for gritstone particle 1, again using measurements made at 20X magnification.



**Figure 6.16 Profile lines extracted from three surface areas on limestone particle 1 (20X magnification) before (left) and after polishing**



**Figure 6.17 Profile lines extracted from three surface areas on gritstone particle 1 (20X magnification) before (left) and after polishing**

Before polishing, the amplitude of the texture across the whole measured surface (0.7 mm) is similar for both limestone and gritstone: compare

Figure 6.16 (a) with Figure 6.17 (a). Also, before polishing the texture at shorter wavelengths is similar for both aggregates. After polishing, however, the limestone profiles are taller and smoother than the gritstone profile: compare Figure 6.16 (b) with Figure 6.17 (b). This reiterates the observations made at the end of Section 6.3, that polishing affects the two aggregates in different ways. When polished, limestone appears to lose texture at short wavelengths, but retain texture at long wavelengths whereas gritstone loses almost all texture at long wavelengths whilst retaining (or, probably, regenerating) texture at shorter wavelengths. These different polishing mechanisms will be explored further in the quantitative analysis presented in the next chapter.

## 6.5 Discussion

Measurements of surface texture were made using the Alicona InfiniteFocus microscope on limestone and gritstone surfaces as they were polished using the Wehner-Schulze machine. Photographs of the aggregate surfaces taken by the microscope do not show the same changes observed in earlier work, possibly because the lighting and depth of focus is too idealised. However, qualitative analysis, by topographical examination of the measurements, indicates without any doubt that the surface of some parts of the inspected aggregate particles is changing as a result of polishing (e.g. Figure 6.6). Furthermore, more detailed measurements have been taken of those parts of the aggregate that come into contact with the W-S machine's polishing rollers and surface texture in these areas is definitely changing as a result of polishing (e.g. Figure 6.10). This is an important observation because concerns were raised that, after earlier analysis of measurements on a dolerite specimen failed to show a trend for changing texture with polishing, effects might be masked by consideration of portions of the surface that had not been affected by the polishing rollers of the W-S machine.

Qualitative analysis has also confirmed that the same area of each surface has been measured at each stage, demonstrating that the careful specimen alignment procedure included in the experimental methodology has worked satisfactorily. This answers concerns that changes in orientation throughout the experiment could result in anomalous results and partly mitigates the risk that insufficient data is taken to characterise the surface.

Finally, qualitative analysis has confirmed that the two aggregates, limestone and gritstone, polish via different mechanisms. Use of surface profiles in two dimensions, whilst primitive, demonstrates that with polishing:

- Limestone becomes smoother – short wavelength height variation is reduced but some long wavelength amplitude is retained.
- Gritstone remains rough – long wavelength features are completely removed but short wavelength texture is still present.

Quantitative analysis, and selection of appropriate characterising parameters, will have to take account of these observations.



## **7 Quantitative analysis of changes in texture during polishing**

---

In this chapter, the measurements of surface texture made on the limestone and gritstone aggregates, using the robust methodology developed, will be analysed in a more quantitative manner. Measurement in three dimensions increases the amount of data available for manipulation (by a factor of more than 1000 compared with some of the experiments reported in the literature). Careful locational referencing, which has been confirmed through qualitative analysis, should give confidence that any changes in characterising parameters result from the action of polishing and, by extension, may be linked with changes in friction.

In the following section, changes in surface texture resulting from the polishing process are examined in several ways:

- Manual analysis of data, using Microsoft Excel, allows consideration of the polishing mechanisms that may be occurring.
- PSD analysis, as described by several researchers (Chen & Wang, 2011), (Himeno, Nakamura, Kawamura, & Saito, 2000) allows inspection of the surfaces wavelength by wavelength and should identify any features that are particularly affected by polishing.
- Fractal analysis is, again, a popular technique used by several researchers (Carr, Norris, & Newcomb, 1990), (Chen & Wang, 2011), (Ganti & Bhushan, 1995), (Radó, 1996). It can, in theory, be used to characterise the complexity of the surfaces throughout the polishing process.
- Characterisation of surface roughness using standardised parameters. Several sections are devoted to characterisation in this way. Three dimensional or 'areal' parameters are discussed, two dimensional equivalents of which have been investigated elsewhere (Do, Tang, Kane, & Larrard, 2009), (Shaw, 2007).

In each section, having established that a method for characterising texture responds to changes in the surface, presumably caused by

polishing, parameters derived from that characterisation method are compared with measurements of friction associated with the surface. Also, attempts are made to compare texture characterisation parameters with physical changes that appear to be occurring on the aggregate surfaces (i.e. qualitative analysis). It should be noted, however, that quantifiable changes in surface texture, occurring as a result of polishing, do not necessarily affect the friction of the surface. Furthermore, while a paint removal technique showed that the areas scanned came into contact with polishing rollers, no attempt has been made to show that every part of those areas comes into contact with the friction measuring sliders in the W-S machine.

At the end of this chapter, results from earlier feasibility studies using a third aggregate type (dolerite) are re-analysed and included for comparison.

All measurements of surface texture on the aggregates were made using the Alicona InfiniteFocus microscope. Throughout this chapter the objective lens used to make the measurements is noted (i.e. 5X, 10X or 20X magnification); further details of the equipment and settings can be found in Section 2.3. Unless otherwise stated (such as where manual manipulation has been carried out using Microsoft Excel), all analysis and calculation was achieved using Digitalsurf's Mountains software.

### **7.1 Development of model profiles against which to examine the surface characterisation techniques**

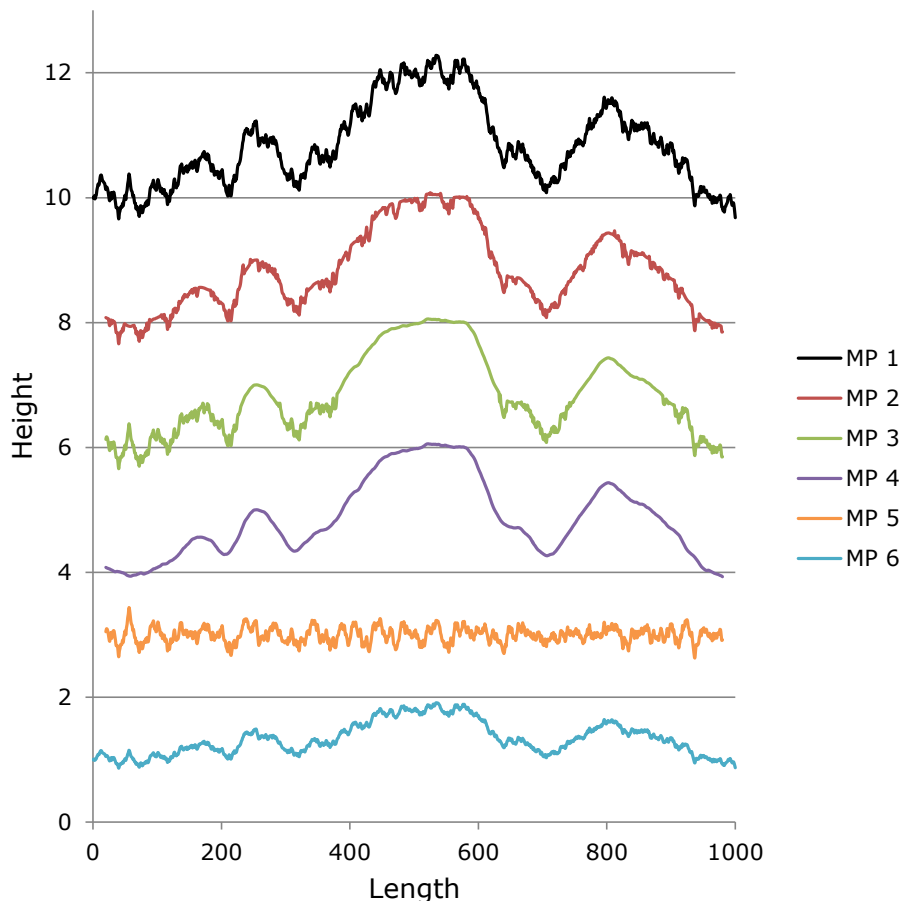
To assist with the understanding of the characterisation methods and, possibly, the changes in the aggregate surfaces that are being observed, some random profiles were generated and then altered by application of various operators. The random profiles are designed to represent the initial condition of the aggregate surfaces, and the altered profiles are designed to represent the surfaces after they have changed, due to polishing, via various possible mechanisms. These model profiles will be used throughout this chapter for illustration purposes.

A random profile was generated using Microsoft Excel and five different artificial profile altering effects were then applied, all shown in Figure 7.1 with an offset so they can be easily distinguished, labelled Model Profile (MP) 1 to 6 as follows:

1. Random profile – shown in black. Generated by repeatedly adding a random value (determined by Microsoft Excel) between -0.1 and 0.1 to an initial value, 10 in the example in Figure 7.1, or to the previous value.
2. Smoothed above a local threshold – shown in red. If an individual point on the profile was higher than the median of the surrounding 40 points then it was replaced by the average height of the same surrounding 40 points. This represents a situation where the polishing rollers come into contact with a large proportion of the surface and the tops of local peaks are worn regardless of whether they, in turn, are part of global peaks or troughs.
3. Smoothed above a global threshold – shown in green. If a point on the profile was higher than the median of the entire profile then it was replaced by the average height of the surrounding 40 points. This represents a situation where the polishing rollers only come into contact with the highest parts of the measured area with the resulting wear only occurring on global peaks.
4. Smoothed – shown in purple. All points were replaced by the average height of the surrounding 40 points. This represents the situation where the polishing rollers come into contact with the whole area and the surface is worn evenly regardless of height.

5. Long wavelengths removed – shown in orange. The smoothed profile (40 points moving average) was removed from the original profile. This profile represents abrasion of the surface and the leaving behind of a surface with similar fine texture.
6. Amplitude reduced – shown in light blue. All points on the random profile were multiplied by 0.4. This represents a situation where the surface polishing wears away material at all wavelengths.

Ten sets of profiles were generated in the same way. To reduce noise in the data, average results from characterisation of all ten sets of data will be used. Note that this is similar to analysing profiles that are ten times longer, but the data is easier to handle and present when it is split into lengths of 1000 units.



**Figure 7.1 Randomly generated and artificially smoothed profiles**

Qualitative analysis in Chapter 6 suggests that the limestone surfaces lose texture at short wavelengths but retain some texture at higher wavelengths, although this is also reduced. The first three artificial polishing mechanisms (smoothed above a local threshold, smoothed above



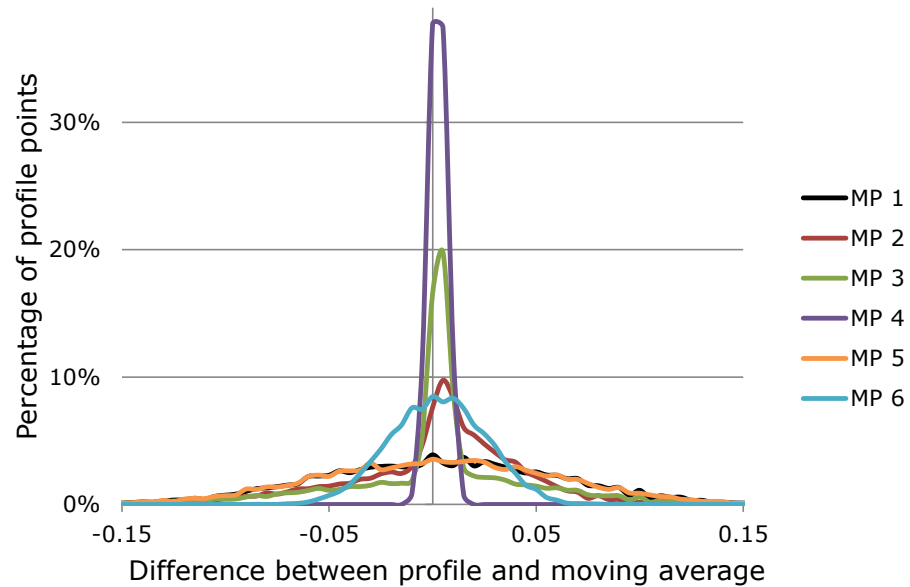
a global threshold, smoothed), or a combination of them, might represent the way in which limestone changes as it is polished. Gritstone surfaces retain a large amount of texture at short wavelengths while losing most of the texture at longer wavelengths and so might be best represented by the artificial polishing mechanism that removes long wavelengths.

## 7.2 Manual analysis

Following from the simple analysis carried out in the feasibility studies (Section 3.3), some manipulation of the raw data recorded by the Alicona system was carried out. Each measured surface can be exported as a matrix (1628 by 1236 points) of heights. By comparing the height of each point to its neighbours, it was hoped that an assessment of the behaviour of the surface during the polishing process could be achieved.

This simple method for characterisation was based on the roughness parameter  $R_a$ , as had been used in the feasibility studies. For ease of calculation, using Microsoft Excel, the height of each point was compared to the average height of the surrounding 11 points (five points before and five points after, and itself) along profiles taken from the surface parallel to the x-axis. The difference between the profile height and this moving average was recorded for every point on each surface profile. Unlike for  $R_a$ , the values were not made absolute. Positive values result from the original surface being higher than the 11 point moving average and negative values result from the surface being lower than the 11 point moving average.

To illustrate the results that can be generated by this sort of analysis, the graph in Figure 7.2 shows histograms of the calculated differences for the six model profiles (Section 7.1). Bin size for calculation of frequency was 0.005 and, as for the model profiles, the units are arbitrary.

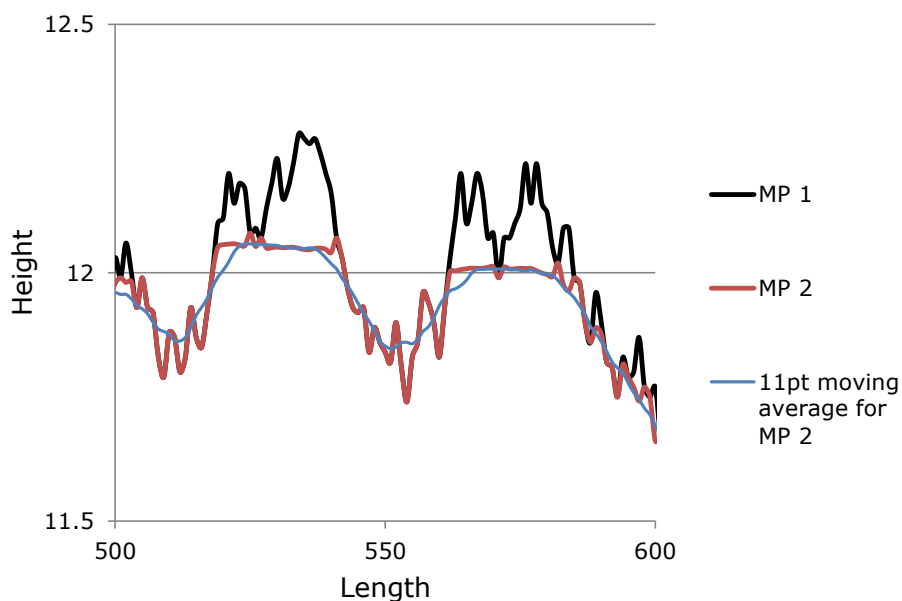


**Figure 7.2 Histograms of difference between profile and a local moving average**

For the random profile (MP 1), the distribution of values is symmetrical about zero and is approximately normal (the black line is just visible at the bottom of the graph behind the orange line). For the smoothed profile (MP 4), there are lots of points that are very similar to the surrounding moving average, which is reasonable because the artificial smoothing applied is longer than the wavelength examined. When the random profile is smoothed above a global threshold (MP 3), the distribution of values is somewhere between the two – half of the values are similar to the smoothed profile, being close to zero, and the remaining values are distributed symmetrically to an extent similar to that of the original profile. The distribution for the profile with long wavelengths removed (MP 5) is very similar to that for the original profile because variations on the wavelength examined (11 points) remain relatively unchanged even though longer wavelengths (40 points and above) are no longer present. When the amplitude of the random profile is reduced (MP 6) the distribution is narrower because the range of heights in the profile, and therefore the range of differences, is smaller.

When the profile is smoothed above local thresholds the distribution is skewed towards positive values: points on the 'smoothed above a local threshold' profile tend to be higher than the average of the surrounding points on that profile. This can be explained by comparison with the original random profile. On the peaks in the original profile, where they were still locally rough, the difference between the profile and an 11 point

average could still be positive or negative. After the localised smoothing had been applied, on the same peaks the difference between the profile and an 11 point average can only be positive (at the edges of the smoothed region) or close to zero (at the centre of the smoothed region). This is easier to see by examining a section of the two profiles when they are overlaid (black and red lines again) with the 11 point moving average of the locally smoothed profile shown in blue, as in Figure 7.3. Where MP 1 and MP 2 differ, the red profile is always higher than its blue moving average.



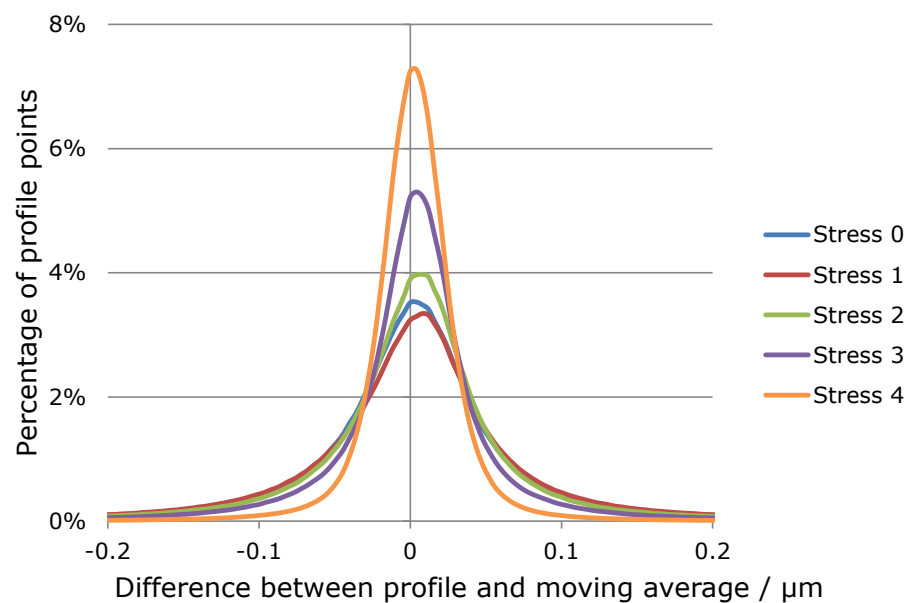
**Figure 7.3 Randomly generated profile (MP 1, black), locally smoothed profile (MP 2, red) and 11 point moving average for MP 2**

The same simple analysis was applied to the raw data collected at each stress level, for each aggregate. Each line of the surfaces was treated as a separate profile and the results were averaged over the surface and then over all of the surfaces measured at each stress level. The graphs in Figure 7.4 and Figure 7.5 show histograms of measured differences between profile heights and 11-point moving average height for limestone and gritstone respectively, measured using the 20X objective lens. Bin size for calculation of frequency was  $0.004\ \mu\text{m}$  and, for the 20X objective lens, 11 points equates to approximately  $5\ \mu\text{m}$ .

The analysis was carried out for longer moving average lengths (124-, 250- and 500-points) and, although the results are similar, the difference between histograms for the five stress levels was most striking for an 11-point moving average. In principle, use of different moving average

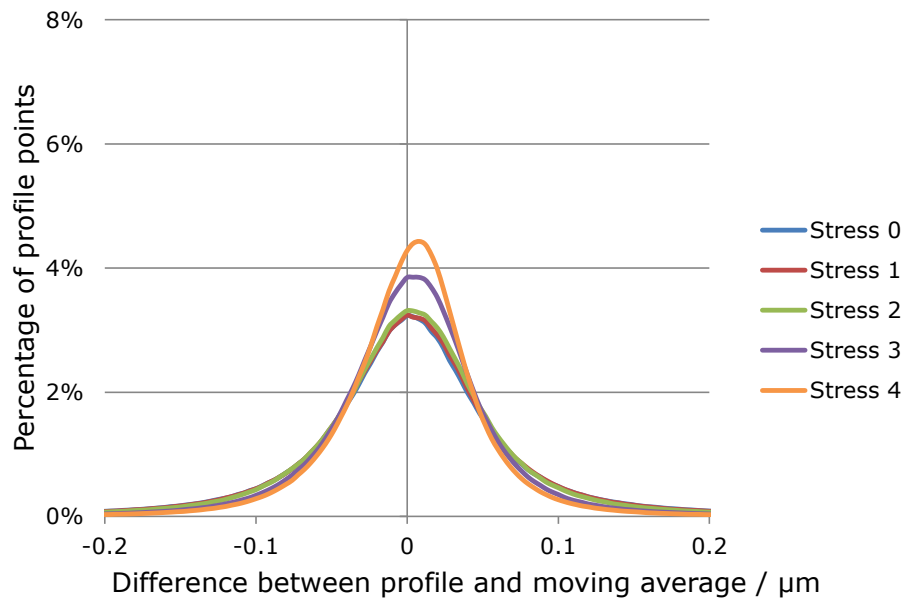
lengths could be used to examine the response to polishing of different wavelengths. More conventional methods for wavelength examination and filtering are explored further in later sections.

For limestone, polishing appears to produce an effect on the results of this analysis that is similar to either general smoothing (MP 4) or reducing amplitude (MP 6). The difference between the height of each point and the average height of its neighbours tends towards zero. The surface is becoming smoother or its amplitude is reducing or probably both, as a result of the action of polishing.



**Figure 7.4 Histograms of the difference between measured height and a local moving average for limestone, measured using 20X objective**

For the gritstone, the results are more difficult to interpret because they could be generated in a number of different ways (or a combination of several). If the polishing mechanism followed is just removal of wavelengths longer than the filter (5  $\mu\text{m}$ ) then, as shown using the model profiles in Figure 7.2, the histograms of differences would not change at all. In fact, for gritstone the distribution of differences remains quite similar throughout the polishing process but there is some change during the last two stages of polishing. There may also be some general smoothing or reduction in amplitude (the histograms suggest that profile differences tend towards zero for the last two stress levels) and there may be some localised smoothing (there is a slight skew towards positive profile differences in the last two stages of polishing).



**Figure 7.5 Histograms of the difference between measured height and a local moving average for gritstone, measured using 20X objective**

For both aggregates, that the effect of polishing is so apparent in values calculated by analysis of the measurements of surface texture suggests that the measurements are meaningful and that the methodology has been successful in generating useful data. However, the polishing mechanisms for the two aggregates are probably different and this will require further exploration.

Although the calculations above were made using macros programmed in Visual Basic, processing is slow and collation is laborious. For the remaining analysis, the bespoke software MountainsMap, that has already been used throughout this work, and that is well regarded in the texture measurement industry, will be used.

The importance of filtering wavelengths from a surface under inspection has already been mentioned. A commonly used method for determining the appropriate filters or, in this case, the wavelengths that appear to change due to polishing, is by inspection of power spectral density, autocorrelation or Fourier transform (see Section 2.4). This is explored in the next section.

### 7.3 Power Spectral Density

Inspection of power spectral density (PSD) has been carried out by several researchers (Chen & Wang, 2011), (Himeno, Nakamura, Kawamura, & Saito, 2000). Results presented in the literature have been difficult to interpret and conclusions drawn from them do not always appear robust (see Section 2.4). However, the theoretical basis for attempting to identify important frequencies or wavelengths is sound, and so some brief analysis has been applied to the measurements made on the limestone and gritstone aggregates.

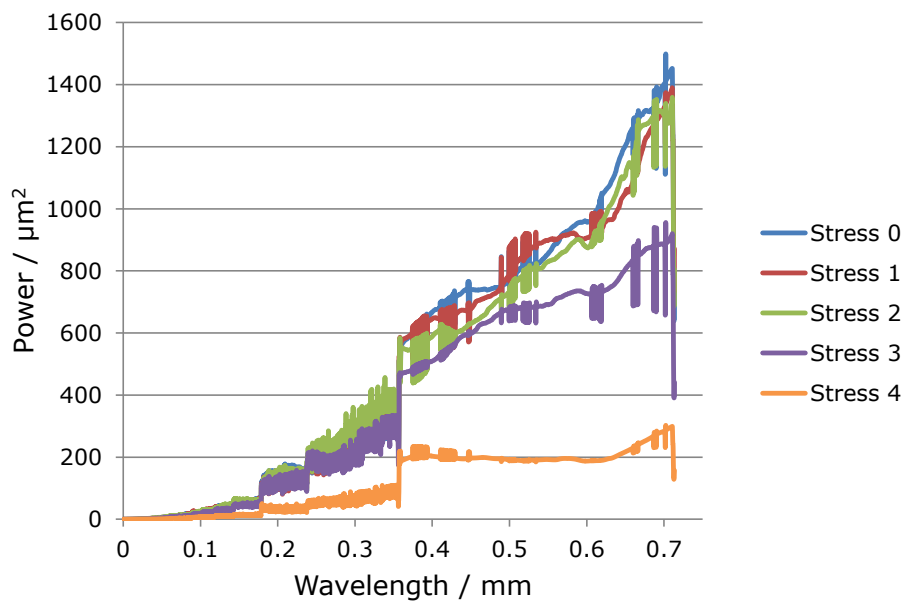
It is somewhat more intuitive to search for dominant or changing wavelengths, rather than frequencies. Mountains PSD analysis calculates a Fourier transform for each horizontal line on the measured surface, adds these functions together for the whole surface and displays the resulting curve against wavelength (i.e.  $1/\text{frequency}$ ). The software actually splits the surface into packets of wavelengths and applies the Fourier transform on each one separately so that the curve can be as detailed for high wavelengths as for low wavelengths. The consequence of this calculation method is that there are apparent step-changes in the PSD curves at a few wavelengths corresponding to the width of the measured area ( $714\text{ }\mu\text{m}$  for the 20X objective lens) and fractions of that width ( $357\text{ }\mu\text{m}$ ,  $237\text{ }\mu\text{m}$  and  $180\text{ }\mu\text{m}$  for the 20X objective). Calculating PSD along horizontal lines means that only periodicity in the X-direction is examined; the aggregate surfaces being examined should be isotropic and so this should not affect the outcome.

Before calculation of PSD curves, the surfaces were levelled to remove some of the slope of the surface resulting from orientation of the specimen on the microscope stage. To do this, the software calculates and subtracts an average plane by minimising the sum of the squares of the distances from the plane at each point on the actual surface.

Conceptually, the PSD curve is similar to the autocorrelation function plotted against wavelength shifts. Peaks in the curve indicate periodicity in the surface and, when comparing curves for each stress level, changes in power at any particular wavelength would indicate wavelengths that are particularly affected by polishing and that are perhaps, therefore, responsible for loss of friction. For display purposes, the PSD curves for each surface have been averaged for each stage of polishing to provide a single PSD curve to characterise each stress level.

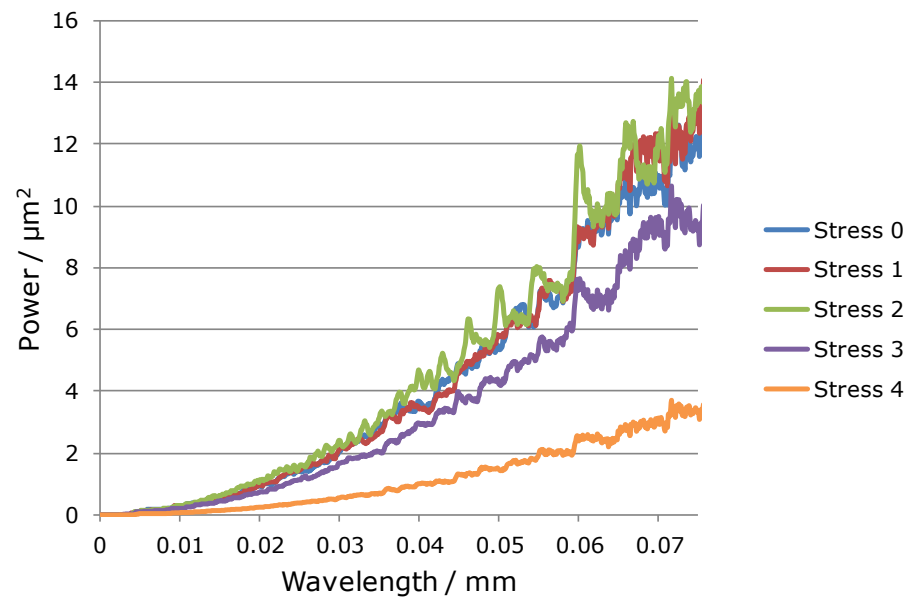
The graph in Figure 7.6 shows the PSD curves, averaged across all six areas measured at each stress level, for the limestone specimen, for measurements made using the 20X objective lens. The graph in Figure 7.7 shows the same curves using a shorter X-axis so that changes in shorter wavelengths are highlighted.

In general, there are no obvious peaks in the average PSD curves indicating that there is no systematic periodicity in the aggregate surface before or after the polishing process. However, the surface texture does clearly change with polishing: changes are moderate for the first stages of polishing, notable for the penultimate stage of polishing and then considerable for the final stage of polishing (i.e. Stress 3 to Stress 4). For all wavelengths, the curve representing PSD at Stress 4 has approximately 25 % of the power (i.e. amplitude squared) of the previous stress level. A reduction to 25 % power corresponds to a reduction to approximately 50 % height on the actual surface – discussed further at the end of this section.



**Figure 7.6 Average PSD curves for measurements made on limestone using the 20X objective lens**

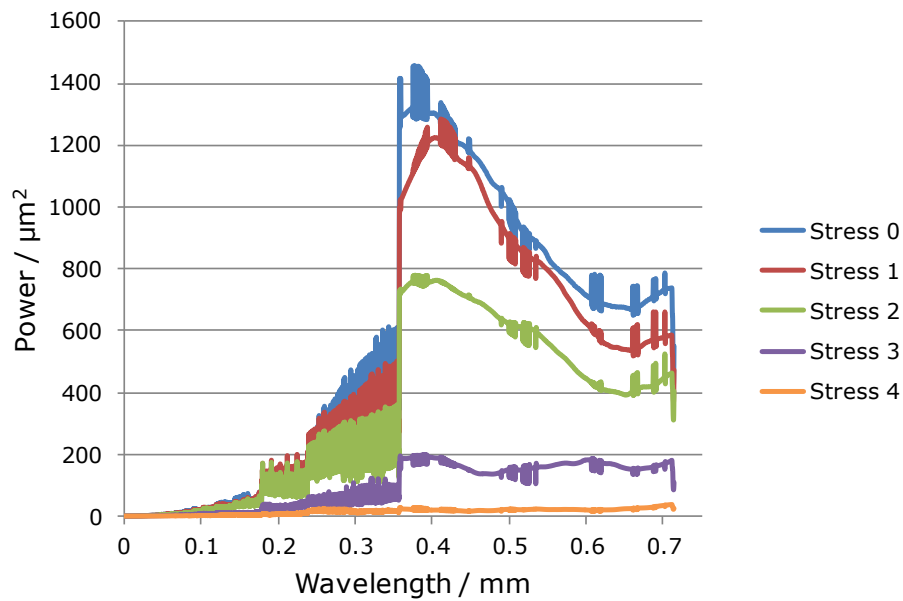




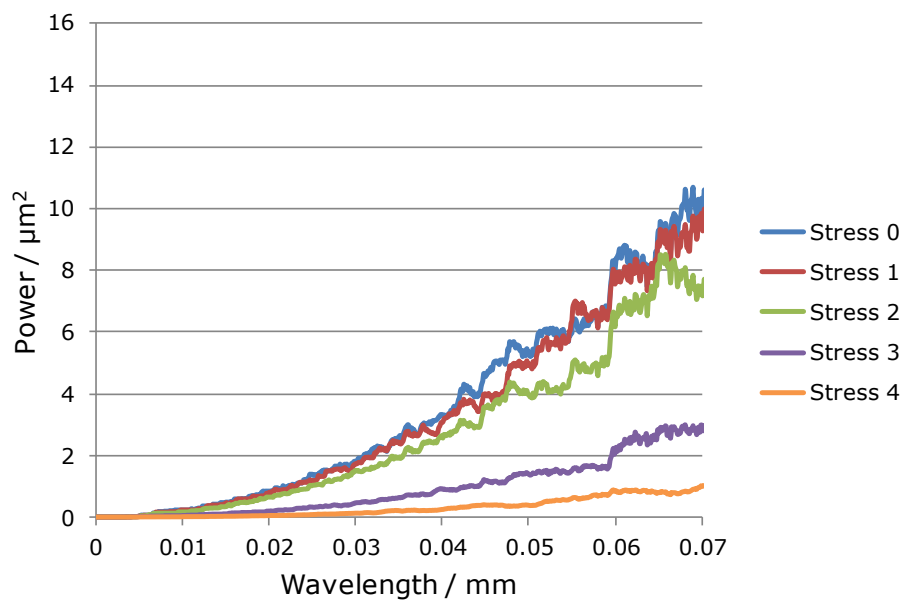
**Figure 7.7 Average PSD curves for limestone – reduced axes scales**

The graphs in Figure 7.8 and Figure 7.9 show the average PSD curves for each stress level, calculated using measurements made with the 20X objective lens on gritstone surfaces. Again, there are step changes corresponding to fractions of the width of the scanned area because of the calculation method employed by the software. The apparent changes in power between stress levels are more evenly spaced – for all wavelengths there is more power (and therefore more surface height) in Stress 0 than Stress 1 and more power in Stress 1 than Stress 2 and so on. There are two very striking features of the curves:

- There is, comparatively, very little power for all the wavelengths in Stress 4 – the curve is almost flat and close to zero
- The absolute drop in power for wavelengths between 357  $\mu\text{m}$  and 600  $\mu\text{m}$  is more significant than for other wavelengths.



**Figure 7.8 Average PSD curves for gritstone**



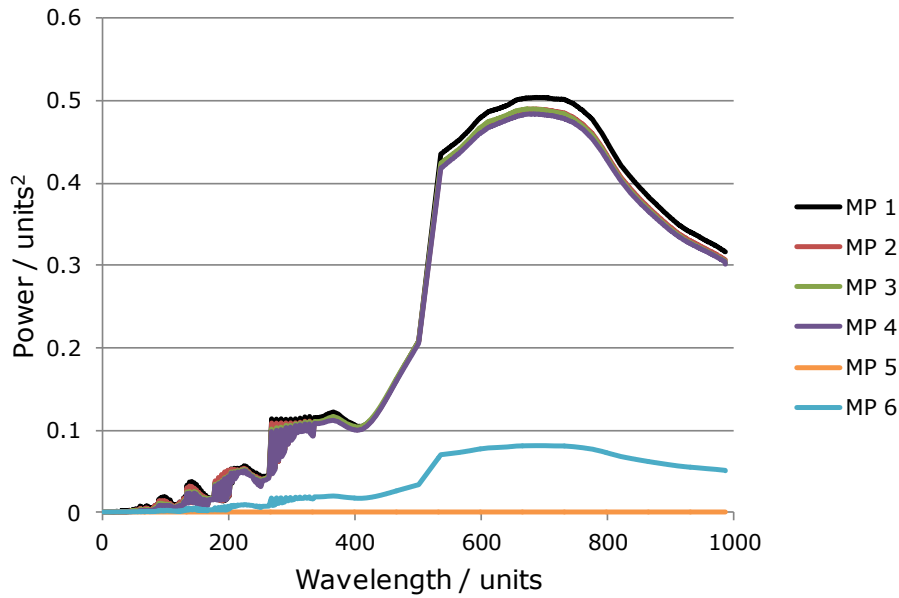
**Figure 7.9 Average PSD curves for gritstone – reduced axes scales**

Qualitative analysis suggested that, during polishing, the limestone surface tends to retain some of its long-wavelength texture while losing texture at shorter wavelengths. The PSD analysis does not reflect this situation well. This may be because, although long-wavelength features were retained, their heights were significantly reduced. It is possible that the PSD curves reflect the fact that the reduction in height of long-wavelength features, due to polishing, is much larger than the reduction in height of shorter-wavelength features because the shorter-wavelength features are initially smaller anyway.

The PSD analysis for gritstone is also difficult to rationalise in terms of qualitative observation of changes in surface texture. While the reduction in surface height (and therefore power) for the longest wavelengths does correspond well to the removal of long wavelength features, the retention or regeneration of surface texture at shorter wavelengths does not seem to be apparent in the PSD analysis.

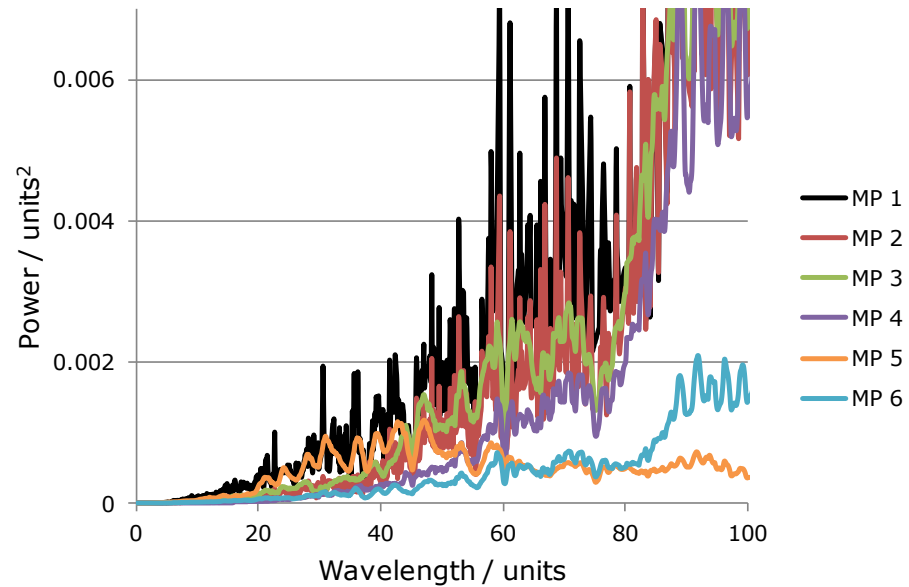
Chen and Wang (2011) analysed PSD for a number of two dimensional profiles measured on three different aggregates (basalt, gabbros and greywacke, the latter being similar to the gritstone used here). They suggest that "changes of PSD occur mainly at wavelengths shorter than 150  $\mu\text{m}$ , and significant variances of surface PSD can be observed below wavelength of 40  $\mu\text{m}$ ". The PSD curves above demonstrate changes at all wavelengths, not just those below 150  $\mu\text{m}$ , and so the explanation of physical changes occurring to the aggregates as they are polished (i.e. that asperities with wavelengths less than 150  $\mu\text{m}$  are removed) are not appropriate in this case. The researchers do go on to suggest that the analysis is complicated and should be further explored.

For comparison, PSD analysis on the model profiles (Figure 7.1) is presented below. Again, the software has split the analysis into packets of wavelengths. At long wavelengths (Figure 7.10), the first four model profiles are very similar, with a slight reduction in power: smoothing above local and global thresholds and smoothing in general does not affect the amplitude of long-wavelength features. As might be expected when long wavelengths are removed from the random profile (MP 5), the PSD analysis shows little or no power at long wavelengths. When the amplitude of the random profile is reduced to 40 %, the power shown in the PSD analysis is reduced to 16 % (i.e.  $0.4^2$ ).



**Figure 7.10 Average PSD curves for model profiles**

At shorter wavelengths (Figure 7.11 shows the same information on shorter scales), PSD curves for the three smoothing operations (MP 2, MP 3 and MP 4) are very similar to the PSD curve for the random profile for wavelengths greater than 40 units, as before, but are shallower for wavelengths shorter than 40 units. This is expected because the smoothing operation, whether smoothed above a global or local threshold or smoothed generally, was applied using a 40 point moving average. Conversely, removing long wavelengths from the original random profile, i.e. wavelengths longer than 40 points, means that PSD curves for MP 1 and MP 5 are similar for wavelengths shorter than 40 units. The curve for MP 6, for which the amplitude of the random profile was reduced to 40 %, still has approximately 16 % of the power in the PSD curve for MP 1.



**Figure 7.11 Average PSD curves for model profiles – reduced axes scales**

PSD analysis on the model profiles highlights the fact that the qualitative observations about the changes occurring, due to polishing, on the surfaces of the limestone and gritstone aggregates is probably over-simplified compared with the polishing mechanisms occurring. Qualitative analysis would predict a greater reduction in power for short wavelengths than for long wavelengths for limestone and a greater reduction in power for long wavelengths than for short wavelengths for gritstone. If this were the case, average PSD curves for limestone and gritstone surfaces would resemble PSD curves for model profiles 4 and 5, respectively. However, for both aggregates, the change in PSD curves is dominated by a general, and almost uniform, reduction in power for all wavelengths, making the curves most similar to that for MP 6, the 'reduced amplitude' operation.

Comparing Stress 0 to Stress 4, power in the PSD curves is reduced to approximately 25 % for limestone and to approximately 5 % for gritstone. These reductions in power correspond to reductions in profile amplitude to 50 % and 20 % respectively. Although this does agree with observations about material loss (see Section 6.2), analysis using PSD is not as revealing as would be ideal.

The main purpose of carrying out analysis of PSD was to ascertain whether some wavelengths change more than others due to polishing. Apart from the packet of wavelengths that appears to be more affected by polishing on the gritstone surfaces (between 357  $\mu\text{m}$  and 600  $\mu\text{m}$ ), there is no other

clear indication that some wavelengths are more affected than others. Therefore, when analysing and attempting to characterise the texture data, it will be important to consider a range of filter lengths. In addition to the natural filtering that occurs by use of lenses of different magnification, the Mountains software allows the application of a Gaussian filter with a standard set of cut-off lengths (also called nesting indices): 0.8 mm, 0.25 mm, 0.08 mm, 0.025 mm, 0.008 mm and, for the highest resolution data, 0.0025 mm.

Before moving on to consider filter lengths and roughness parameters, it is worth investigating another popular technique found in the literature. Fractal analysis should give an indication of the complexity of a surface and may provide information as to the way the aggregates polish, and the features that control friction.

## 7.4 Fractal analysis

Fractal analysis is an iterative process. For analysis in three dimensions the software uses an enclosing boxes method: each section of the surface is enclosed by a box of side  $\epsilon$  and the number of boxes required to enclose the whole surface is counted. The procedure is repeated for smaller and smaller  $\epsilon$  so a natural log-log graph of the number of enclosing boxes against box width can be drawn – this is the 3D equivalent of the method presented in Section 2.4. As before, the slope of the plotted curve indicates the fractal dimension of the surface.

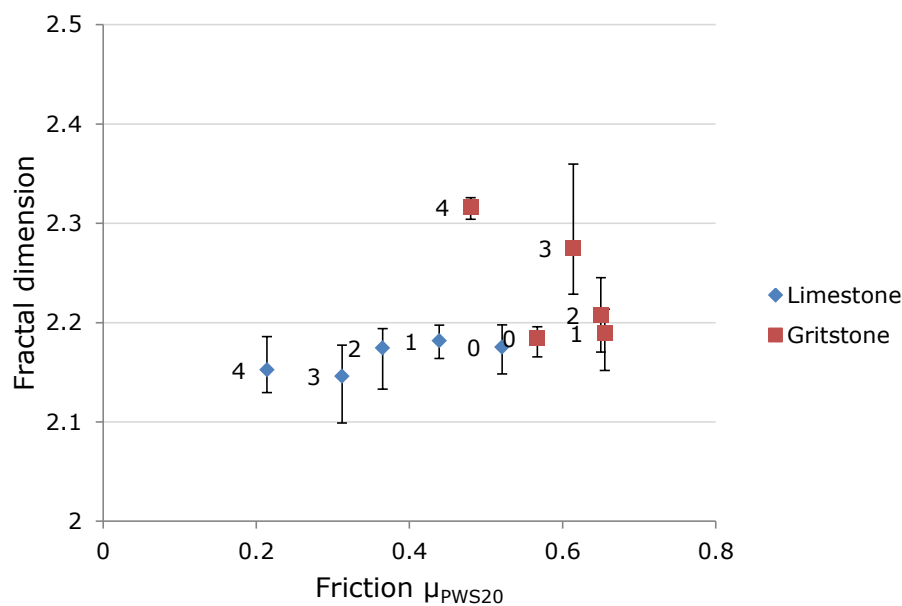
Table 7.1 shows the average fractal dimension calculated by the software for all levelled surfaces, at each stress level, for measurements made on the two aggregates using the 5X, 10X and 20X objective lenses. For limestone there is no obvious pattern of changing fractal dimension with increased polishing. This is counterintuitive compared to the qualitative and previous quantitative analysis which suggests that the surfaces become smoother when they are polished: smoother surfaces should have lower fractal dimension. For gritstone, the fractal dimension increases with increased polishing; this accords with the qualitative observation that gritstone retains some considerable roughness when it is polished.

**Table 7.1 Fractal dimensions for levelled limestone and gritstone surfaces**

Stress level	5X	Limestone 10X	20X	5X	Gritstone 10X	20X
0	2.18	2.20	2.18	2.25	2.24	2.18
1	2.18	2.20	2.18	2.25	2.24	2.19
2	2.17	2.20	2.17	2.25	2.25	2.21
3	2.17	2.18	2.15	2.27	2.30	2.27
4	2.19	2.19	2.15	2.37	2.38	2.32

Figure 7.12 shows average fractal dimension plotted against friction measured on the aggregate surfaces, for measurements made using the 20X objective lens. Error bars show the range of fractal dimension from the six areas measured at each stress level and the points are labelled to their left with the stress level to which they correspond. It is clear that fractal dimension is unlikely to be a very good indicator of surface friction for limestone. For gritstone, if the average fractal dimension of Stress 0 is

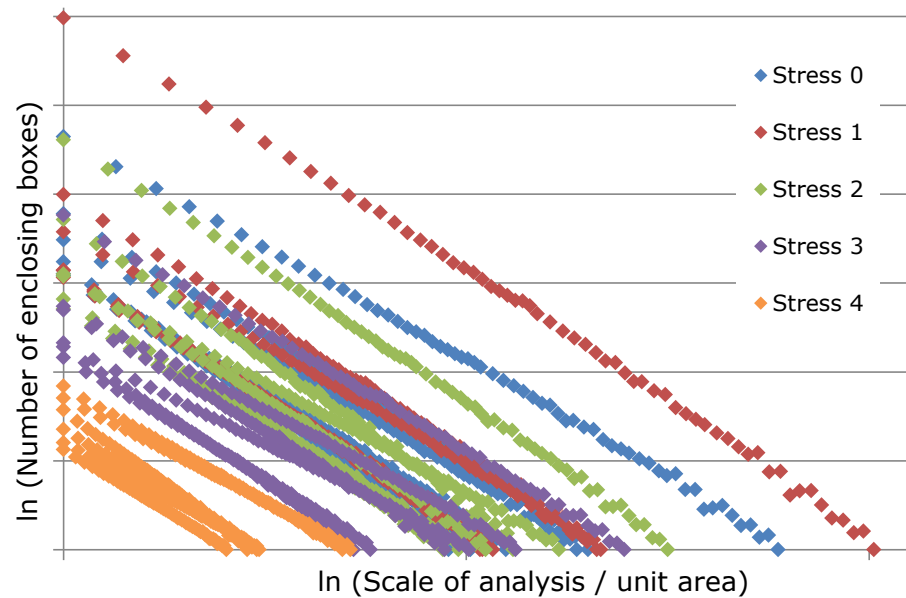
ignored, the trend for increasing fractal dimension with decreasing friction is apparent. Discounting the measurement made on the aggregate surface before polishing is justified by reasoning that the form of the surface at that stage is that of a quarried and crushed stone rather than that of a polished stone. An increase in fractal dimension with polishing would not be expected if the aggregate surfaces were getting smoother; fractal dimensions ought to decrease if the surface is becoming less complicated. However, it has already been postulated that the gritstone aggregate surface, in particular, does not simply get smoother as it is polished.



**Figure 7.12 Fractal dimension against friction for limestone and gritstone surfaces measured at 20X magnification**

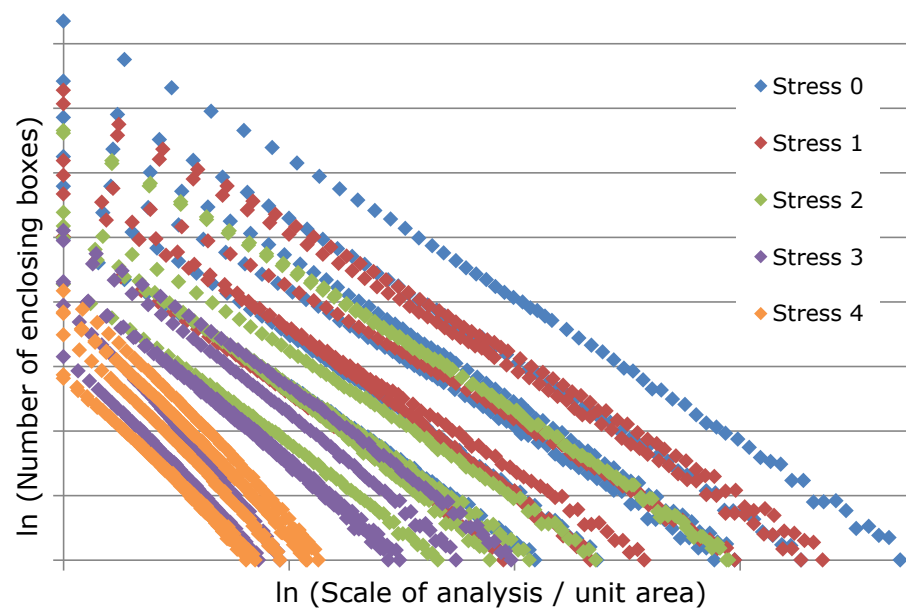
If the number of enclosed boxes is plotted against the scale of analysis (i.e. the size of the box) for each surface in turn, some additional information can be gained. The graph in Figure 7.13 shows the natural log of the number of enclosing boxes against the natural log of box area used for calculation for limestone surfaces at 20X magnification – measurements are in surface points rather than lengths and are not shown on the graph for clarity. It is clear that the slope of the curves remains similar throughout, confirming that fractal dimension does not change with polishing. It is possible that the smoothing process occurs at a lower wavelength than can be picked up by the fractal analysis. However, the PSD curves suggest that surface heights change just as much for long wavelengths as for short wavelengths and the fractal curves do not give any sign that a limit of resolution has been reached (see discussion in Section 2.4).





**Figure 7.13 Results from fractal analysis of measurements made on limestone surfaces using the 20X objective lens**

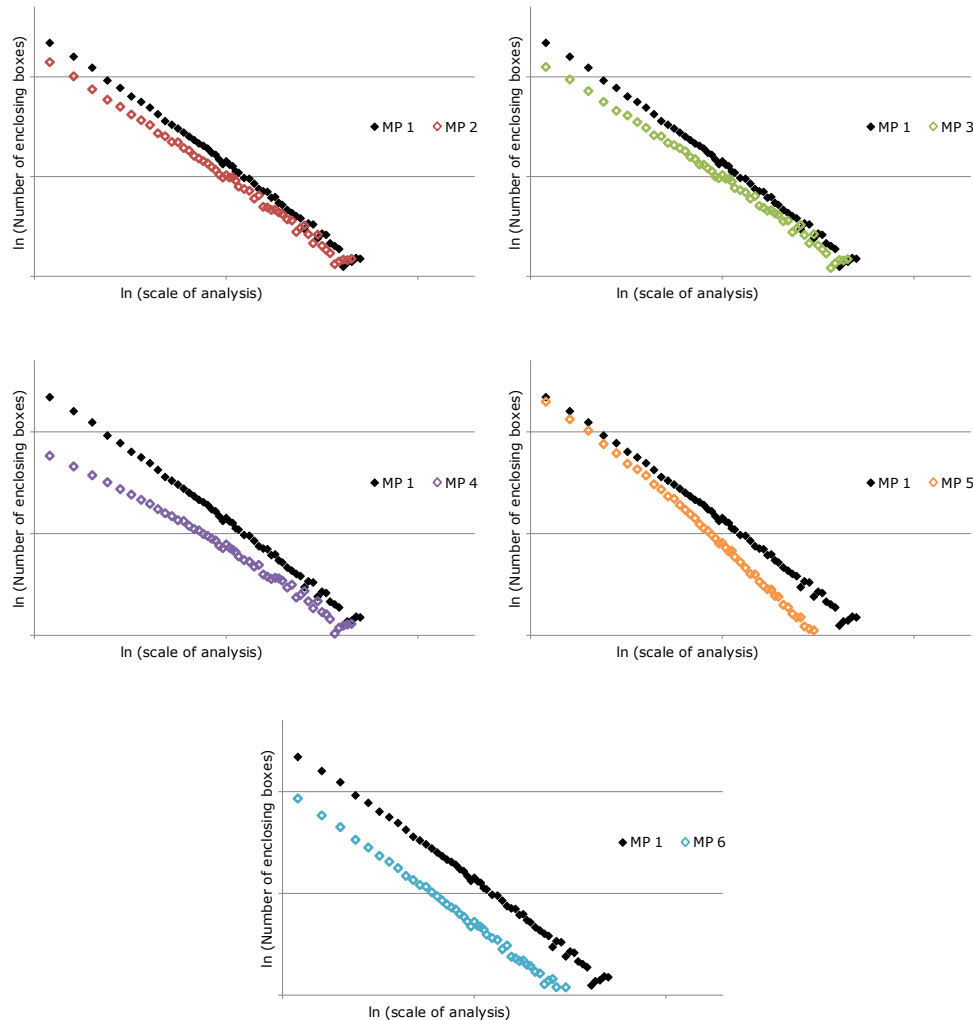
For gritstone, the plotted curves (Figure 7.14 shows curves for surfaces at 20X magnification) confirm that fractal dimension increases with polishing.



**Figure 7.14 Results from fractal analysis of measurements made on gritstone surfaces using the 20X objective lens**

For comparison, the graphs in Figure 7.15 show curves from fractal analysis, in two dimensions, of the model profiles (Figure 7.1), compared to the original random profile in each case. It can be seen that the quantitative changes observed for gritstone surfaces most resemble a combination of the removal of long wavelength features (MP 5) and a

reduction in amplitude (MP 6). For limestone, the response to fractal analysis is most similar to a reduction in amplitude (MP 6) but could also incorporate some smoothing, either above a global or local threshold (MP 2 or MP 3). This follows the qualitative analysis well.



**Figure 7.15 Fractal analysis of randomly generated profiles**

When long wavelength features are removed from the surface, the fractal dimension increases. The change in gradient is driven by a reduction in the size of the largest boxes required to encompass the length of the profile i.e. the profile line is shorter after long wavelength features have been removed.

When the profile is generally smoothed, the change in gradient is driven both by a reduction in the size of the largest boxes required to encompass the whole profile and, mostly, by a reduction in the number of boxes required to enclose the profile's whole length when those boxes are very small i.e. the profile line is shorter and smoother after removing short wavelength features. However, if only a portion of the surface is

smoothed, then the smoothed portion will require a smaller number of small boxes but the still-rough portion will respond to further reduction in box size.

Aside from fractal dimensions, the curves from fractal analysis of the aggregate surfaces indicate a change with polishing for both aggregates: the curves move towards the origin. The area under the curves is related to the area of the surface (box size multiplied by the number of boxes). The projected area (i.e. the size of the measured rectangle seen in plan view) is constant when the same objective lens is used, so a change in surface area also relates to a change in material volume. This does correspond to qualitative observations that polishing resulted in significant material loss for both aggregates (see Figure 6.6 and Figure 6.7, which show topographical changes for limestone and gritstone respectively). MP 6, where the random model profile has been reduced in amplitude for all wavelengths, generates a similar response to fractal analysis.

Manual analysis highlighted the importance of filtering data, PSD analysis suggested that all wavelengths change due to polishing and fractal analysis has emphasised the different polishing mechanisms in the two aggregates and further suggested that surface volume is an important characteristic. All of these findings can be used when selecting appropriate filters and characterisation parameters, which is explored in more detail in the following sections.

## 7.5 Introduction to roughness parameters

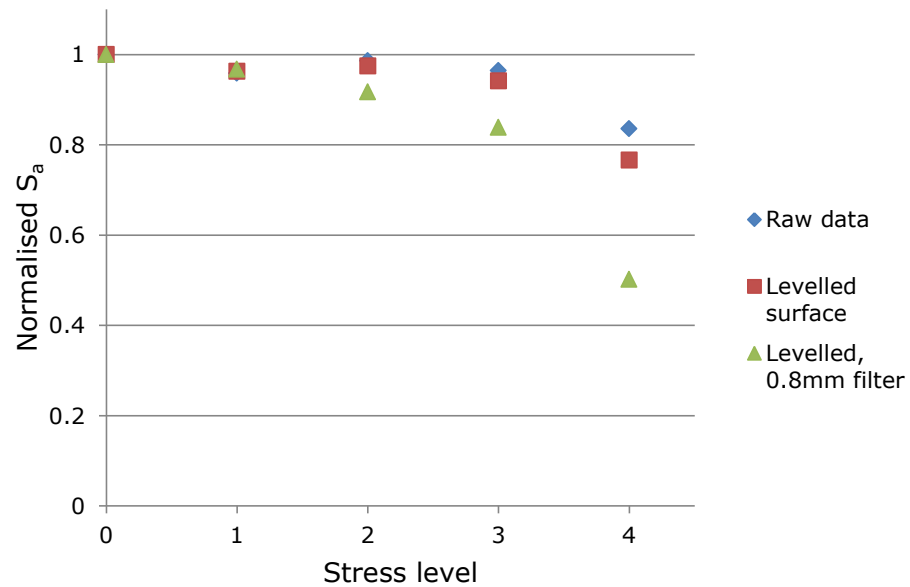
A large amount of work has been carried out investigating the characterisation of roughness (see Section 2.4). It would be useful to characterise the roughness of aggregate surfaces, preferably in such a way that relates to the friction they offer, using an existing parameter or set of parameters. Standard roughness parameters may not be an exhaustive set of characterisation tools. However, a lot of the methods used so far can be considered as similar: the asperity sharpness measurement proposed by Do et al (2009), the compound height/spacing parameter used by Shaw (2007) and the descriptors proposed by Forster (1989). They, in turn, might be related to standard parameters that measure peak height, density and gradient. The difficulty will be in finding the best parameter, not forgetting the appropriate filtering that is likely to be necessary.

Automatic analysis using the software does, in principle, allow a structured approach to finding parameters that change with polishing – i.e. batch processing all measurements to generate parameter values for all parameters implemented in the software under ISO25178 (British Standards, 2012). However, it is more informative to first consider those parameters that physically accord with the preceding qualitative and quantitative analyses. For clarity, one parameter (or set of associated parameters) is presented in each of the following sections, first giving a standard description and suggestions for how it might physically respond to changes in surface texture (using the model profiles already introduced - Figure 7.1), then using it to characterise the effect of polishing on each of the two aggregates and finally using it to compare surface texture with friction.

When trends in changing parameter values are inspected, especially when comparing the effect of different filtering, normalised measurements are presented. This obviates the need for multiple axes or multiple graphs. However, when considering a single set of data (or a set of data for each of the aggregates), average values for all surfaces measured at each stress level are presented with error bars showing the range of measurements made for each of the six measured areas.

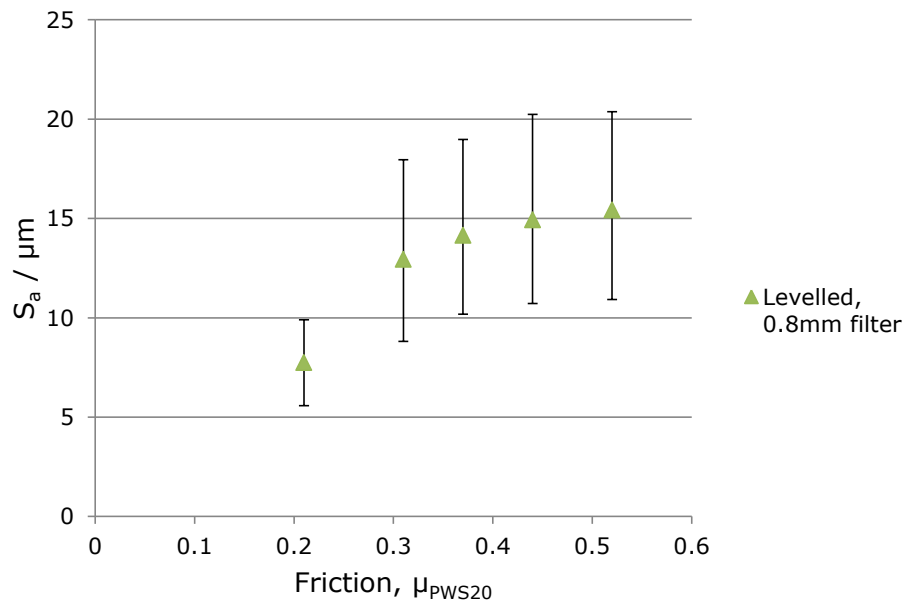
For example, the graph in Figure 7.16 compares the trend for reduction in  $S_a$  when it is calculated using raw data, after the data has been levelled using the software's least-squares levelling algorithm, and after further

filtering using a 0.8 mm Gaussian filter. The data used to calculate the values shown in this graph was measured on limestone surfaces at 5X magnification. The Gaussian filter is described in Section 2.4; this type of filter will be used extensively throughout the following sections. Unless otherwise specified, the filter is low-pass in terms of wavelength i.e. its application will effectively remove features longer than the specified wavelength.



**Figure 7.16 Average  $S_a$  calculated for limestone surfaces at 5X magnification using raw data, levelled data and levelled and filtered data, normalised to the highest value**

Having observed that a more significant response to polishing can be found by levelling and filtering the surfaces, average measured values are plotted against friction with error bars indicating the range of measurements from the six measured areas. The graph in Figure 7.17 shows average  $S_a$  calculated for levelled limestone surfaces, measured using the 5X objective lens, after application of a 0.8 mm Gaussian filter.



**Figure 7.17 Average  $S_a$  calculated for limestone surfaces at 5X magnification using levelled and filtered data**

Note that levelling is a commonly used first stage in handling data from surface profile measurement. It is considered to be a correction to the data to account for changes in surface form and general alignment during measurement. The software's levelling algorithm has been applied to all data before calculation of roughness parameters and before application of any further filtering.

Qualitative analysis has suggested that limestone gets smoother as it is polished, and this is confirmed to a certain extent by the manual analysis that approximated the roughness parameter  $R_a$ . PSD analysis did not indicate any particularly important wavelengths. Fractal analysis suggested that the volume of the surface changes and confirmed qualitative analysis, which suggested that gritstone loses some of its long-wavelength features but retains roughness at short wavelengths. PSD analysis suggested a significant change in a specific band of wavelengths and this will need to be considered when applying filters. It should be borne in mind throughout that if the long term goal of this work remains a comparison between roughness characterisation and measured friction for both aggregates, as a continuum, there is no point in dwelling on parameters that work for one aggregate and not the other, except to elucidate the polishing mechanisms involved.

The following types of parameter have been considered first:

- Height parameters,  $S_a$  and  $S_q$ , because they should be affected by the changing roughness of the surface if the correct wavelengths are examined. They are amongst the simplest standard parameters and they (or two dimensional equivalents  $R_a$  and  $R_q$ ) have been used by other researchers (Do, Tang, Kane, & Larrard, 2009).
- Peak height and peak density, similar to an analysis of peak height divided by peak spacing, shown to be effective in other studies (Shaw, 2007).
- Peak gradient, which should be affected by smoothing of the surface and by changing peak shapes. This should be similar to the indenter angle parameter developed by Do et al. (2009).
- Volumetric parameters calculated from Abbott-Firestone curves, because qualitative analysis and fractal analysis suggested surface volume changes with polishing.
- Surface height distribution because it transpired, from inspection of Abbott-Firestone curves, that the distribution of surface heights appears to change shape with polishing.

Apart from the specific set of wavelengths identified for gritstone, PSD analysis did not suggest any particular wavelengths for investigation so the standard set of filter lengths recommended in ISO25178 have been applied to start with and the effect on the results is presented for characterisation using  $S_a$ .

## 7.6 Height parameters

$S_a$ , the arithmetical mean height is calculated using Equation 7.1 and  $S_q$ , its root mean squared equivalent is calculated using Equation 7.2.

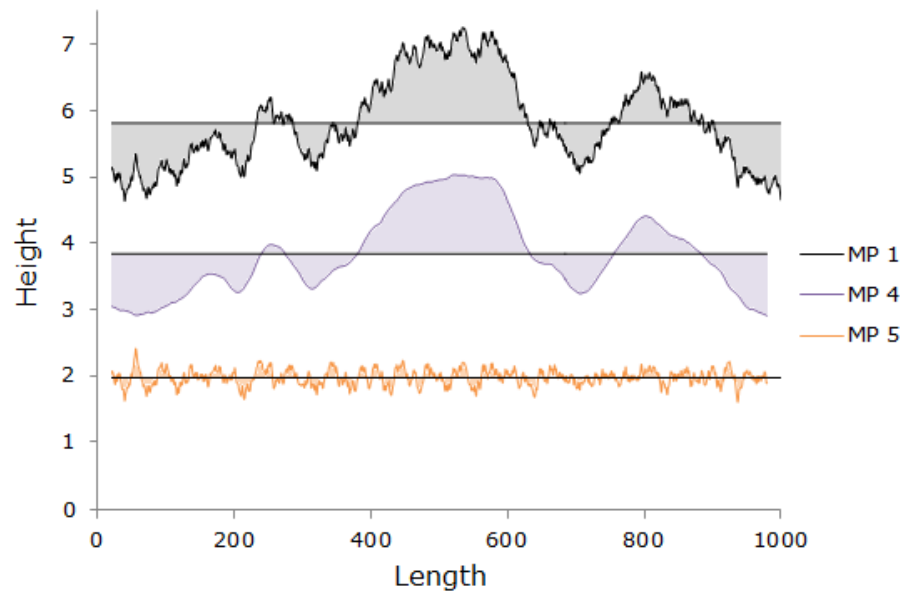
$$S_a = \frac{1}{A} \int_A |z(x, y)| dx dy \quad 7.1$$

$$S_q = \sqrt{\frac{1}{A} \int_A z^2(x, y) dx dy} \quad 7.2$$

In both cases, the height of the surface,  $z$ , is measured from a mean plane within the area  $A$ . If the surface deviates less from its mean plane then the value returned for the height parameter will be lower. However, the magnitude of the parameter will depend on the filtering applied to the measured data.

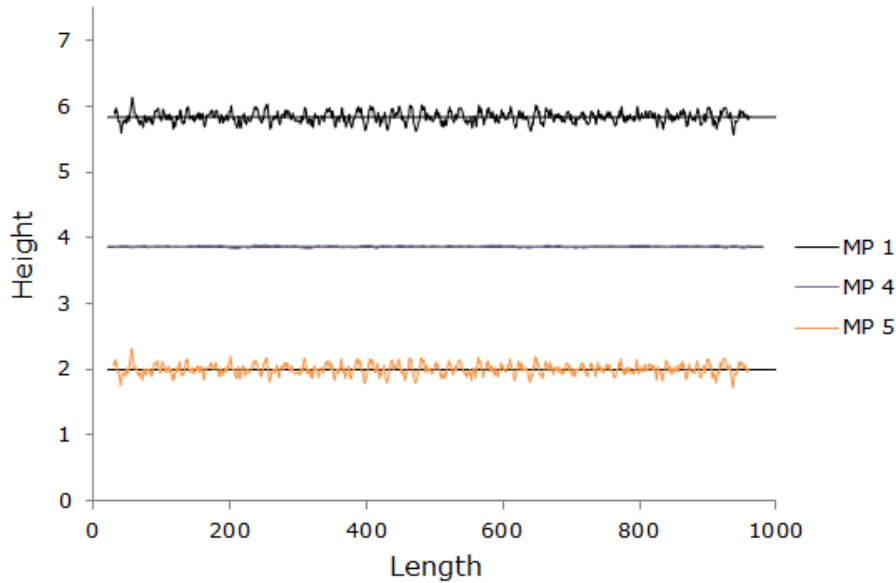
For example, if no filtering is applied to the random model profile from Figure 7.1 (also shown in black in Figure 7.18 below) then general smoothing (MP 4) only results in a reduction in  $R_a$  from 0.55 units to 0.53 units whereas removal of long wavelengths (MP 5) results in a reduction from 0.55 units to 0.10 units. This is because average deviation from the mean line includes the height of long wavelengths still present in the smoothed profile (MP 4) which are no longer present in MP 5. The random model profile is shown in black in the graph in Figure 7.18 and the shaded area represents the value of  $R_a$ . The purple and orange lines and shading show the equivalent values for MP 4 and MP 5, respectively.





**Figure 7.18 Model profiles shaded to show values of  $R_a$  calculated if no filtering is applied**

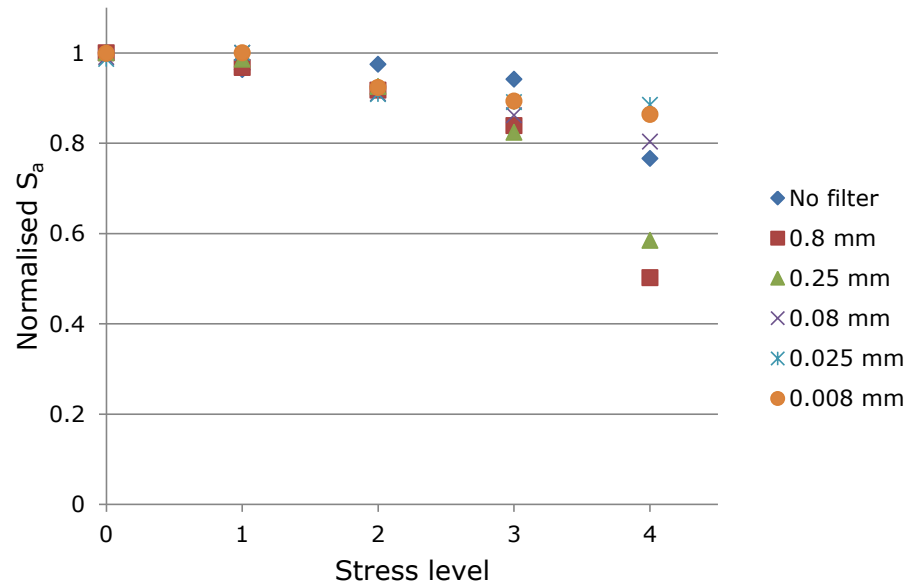
If the surfaces, or profiles, are filtered first then the form can be removed and different wavelengths can be inspected for their reaction to polishing or for their effect on friction. To complete the comparison, the graph in Figure 7.19 shows the random profiles, with shading to indicate  $R_a$ , after application of a 20 point low pass (wavelength) filter – note that the deviation of the smoothed profile from its mean line is almost nil. The values of  $R_a$  for the random profile, smoothed profile and the profile with long wavelength features removed (MP 1, MP 4 and MP 5), after application of a low pass filter, are 0.19 units, 0.09 units and 0.11 units respectively.



**Figure 7.19 Sections of a random profile and artificially smoothed profiles, shaded to show values of  $R_a$  calculated after a low pass (wavelength) filter has been applied**

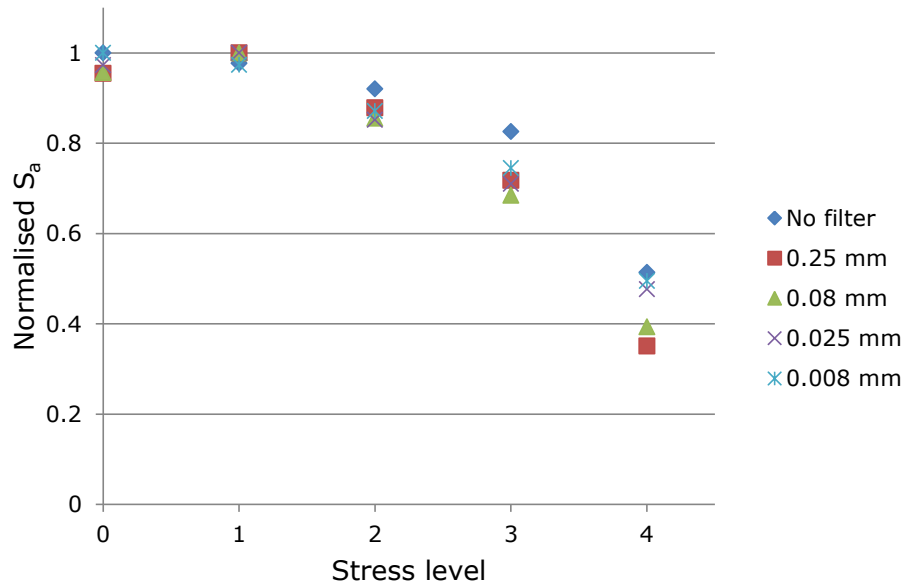
For measurements made on aggregate surfaces, the filter lengths applied are limited by the properties of the scanned data. The maximum filter length is limited by the size of the area because the filter can only be applied to data that is more than one filter length from the edge. For example, the width of a surface after application of a 0.8 mm filter is 1.6 mm shorter. The minimum filter length is limited by the resolution of the data – it is not possible to apply a filter of 2.5  $\mu\text{m}$  to data where the measurement point size is 1.75  $\mu\text{m}$  (as it is with the 5X lens).

The graph in Figure 7.20 shows the average values of  $S_a$  for each stress level on limestone surfaces measured using the 5X objective lens. Shorter filters result in smaller values of  $S_a$  but, to compare trends, values have been normalised to the maximum value in each series (generated in this case by measurements made at Stress 0) and plotted on the same graph.

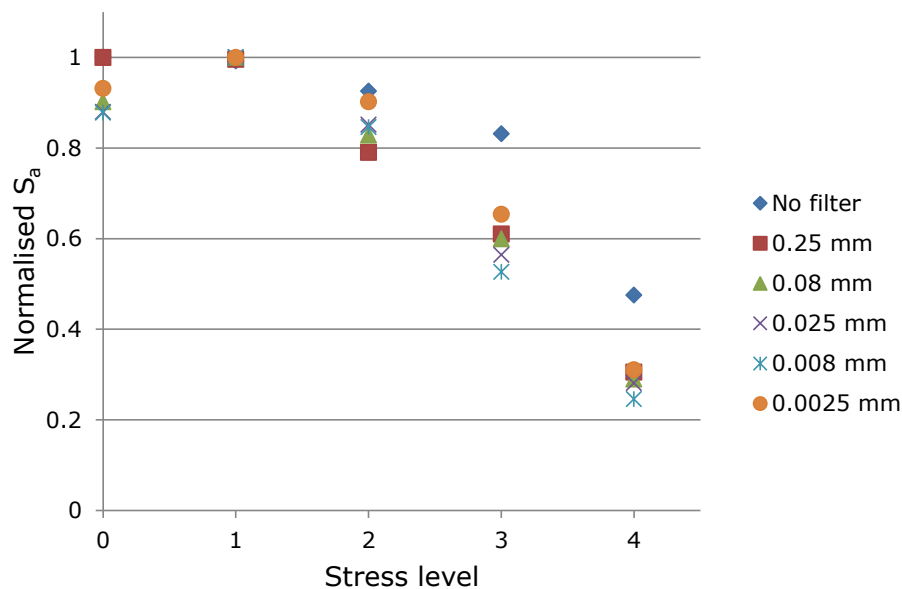


**Figure 7.20 Average  $S_a$  calculated from limestone surfaces at 5X magnification after application of different Gaussian filters, normalised to the highest value**

Use of a higher magnification objective lens is in itself a form of filtering – as magnification increases, the size of the scanned area reduces and so the variation in height across it also reduces (except for surfaces that are flat). So, just as the use of levelling and filtering improves the reaction of the parameter to polishing so does use of higher magnification lenses. The graphs in Figure 7.21 and Figure 7.22 show normalised average values of  $S_a$  for each stress level after application of the filter lengths allowed by the scanned area properties (size and resolution) for measurement made with the 10X and 20X lenses respectively.



**Figure 7.21 Normalised  $S_a$  for measurements of limestone surfaces at 10X magnification**

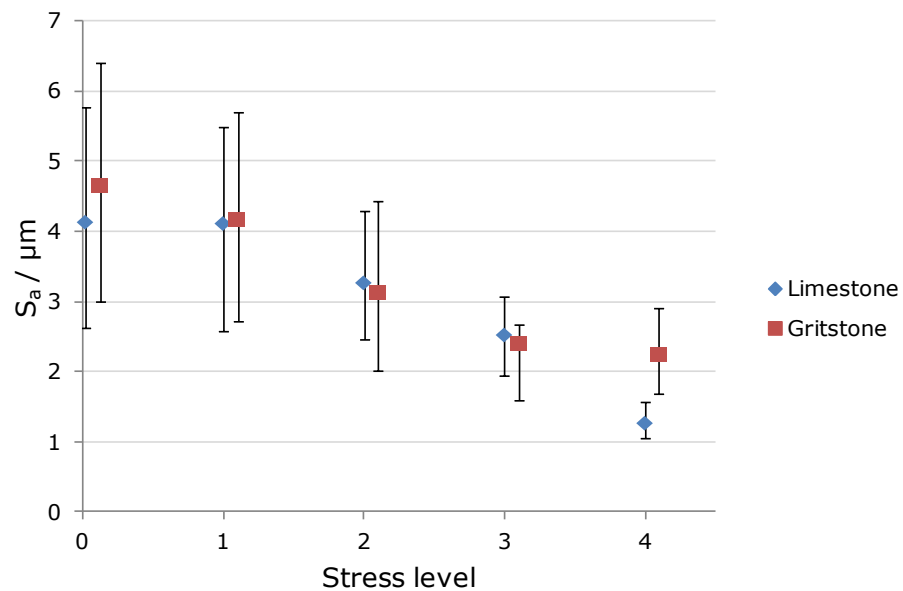


**Figure 7.22 Normalised  $S_a$  for measurements of limestone surfaces at 20X magnification**

For limestone,  $S_a$  changes with polishing at all magnifications and for all filter lengths. The pattern is most obvious for the longest filters and for data collected at higher magnifications. Interestingly, when short wavelength filters are applied to the data collected at higher magnifications, the value of  $S_a$  for Stress 0 is no longer the highest value in the series. The effect is not due to outlying data for the six measured areas. It could be either (or both) an effect generated because the surface texture on the aggregate at Stress 0 has a different form (it is in the state

it left the quarry as opposed to being polished) or because some important features of the surface at this stress level are masked by filtering.

For gritstone, the most significant changes in  $S_a$  are also calculated using data from measurements made at 20X magnification, after application of relatively long-wavelength filters. The trend has a slightly different form, however; instead of a gradual reduction throughout the whole polishing process, the values measured for the last stress level suggest an approach to an asymptote. The graph in Figure 7.23 shows values of  $S_a$  calculated for surfaces measured using the 20X objective lens, after application of a 0.25 mm Gaussian filter, for both limestone and gritstone.

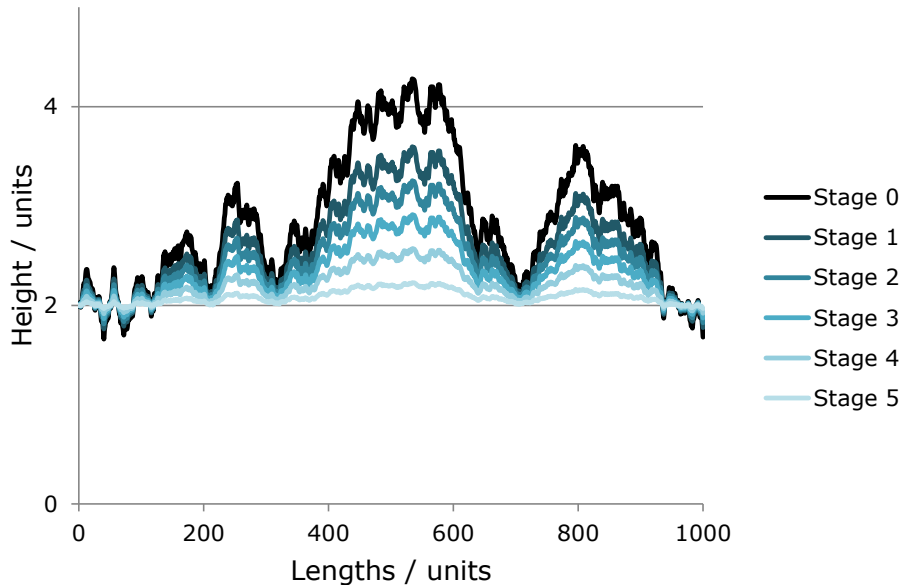


**Figure 7.23 Average  $S_a$  for measurements on limestone and gritstone surfaces at 20X magnification after application of a 0.25 mm Gaussian filter**

Although the trend for gritstone is driven by a single point it does correspond well to previous qualitative comparison with removal of long wavelengths, as can be demonstrated using sets of model profiles, as before.

If some intermediate stages are generated for each of the model profiles (Figure 7.1) they can be used to compare the trend for changing  $R_a$ , the two-dimensional equivalent of  $S_a$ , with the trends observed using measurements from limestone and gritstone. For example, to generate a set of model profiles to represent a gradual change as for MP 6, where amplitude is globally reduced, stage 0 is the random profile, stage 1 is the

same profile reduced to 70 % amplitude, stage 2 is 55 % amplitude, stage 3 is 40 % (equivalent to the model profile shown in Figure 7.1), stage 4 is 25 % and stage 5 is 10 %. This series of model profiles is shown in Figure 7.24.

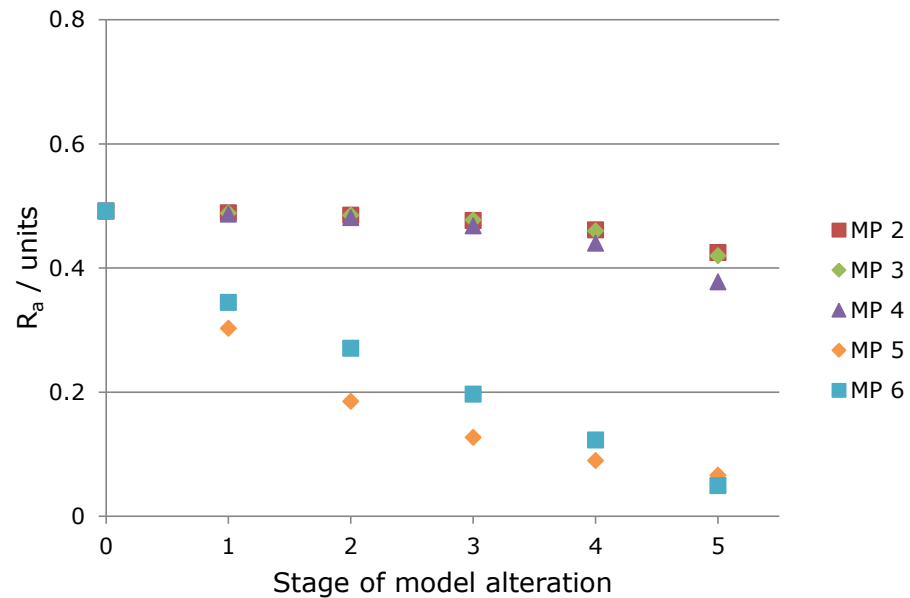


**Figure 7.24 Intermediate stages of the operation 'amplitude reduced' applied to model profiles**

For MP 2, where local peaks have been smoothed, stage 0 is the random profile, stage 1 is generated when points higher than the median of the surrounding 10 points are replaced by the average of the surrounding 10 points, stage 2 is generated when points higher than the median of the surrounding 20 points are replaced with the average of the surrounding 20 points, and so on until stage 5 where points higher than the median of the surrounding 160 points are replaced by the average of the surrounding 160 points. For MP 3, when global peaks have been smoothed, points higher than the median of the entire profile have been replaced by the average of the surrounding 10, 20, 40, 80 or 160 points to generate stages 1 to 5 respectively. Similarly, for MP 4, when the entire profile has been smoothed, moving averages of lengths 10, 20, 40, 80, 160 have been used. For MP 5, moving averages of lengths 320, 160, 80, 40 and 20 have been removed from the original random profile.

For each stage of these newly generated sets of model profiles a value of  $R_a$  can be calculated, and this is shown in Figure 7.25. The three smoothing operations (local or global peaks or general, MP 2, MP 3 or MP 4) behave similarly with a gradual decrease in  $R_a$  that accelerates

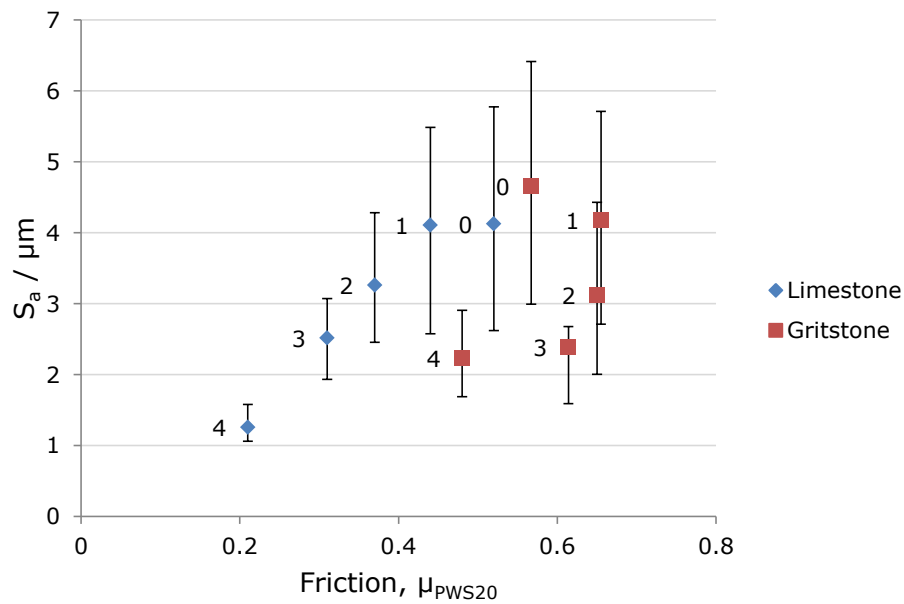
towards the end of the sequence. When long wavelengths are gradually removed (MP 5), the value of  $R_a$  decreases towards an asymptote and when profile amplitude is generally reduced (MP 6) the decrease in  $R_a$  is linear with the stage of operation (remembering that the reduction in profile amplitude between stage 0 and 1 is twice the reduction between stage 1 and 2, 2 and 3 etc.).



**Figure 7.25 Average  $R_a$  calculated for sets of model profiles where a random profile has been gradually altered**

Once again, the limestone behaves most like profiles being gradually smoothed by removing short wavelength features while the behaviour of gritstone is best represented by removal of long wavelength features, probably in conjunction with a reduction in profile amplitude in both cases.

The graph in Figure 7.26 shows average  $S_a$  values for levelled surfaces measured using the 20X objective lens, after application of a 0.25 mm Gaussian filter, against friction measured on the surfaces of both aggregates. Following the method summarised in the introduction to this section, this combination of magnification and filter length is shown here against friction because the normalised values (shown in Figure 7.22 for limestone, for example) suggested that it gives the best response to polishing.

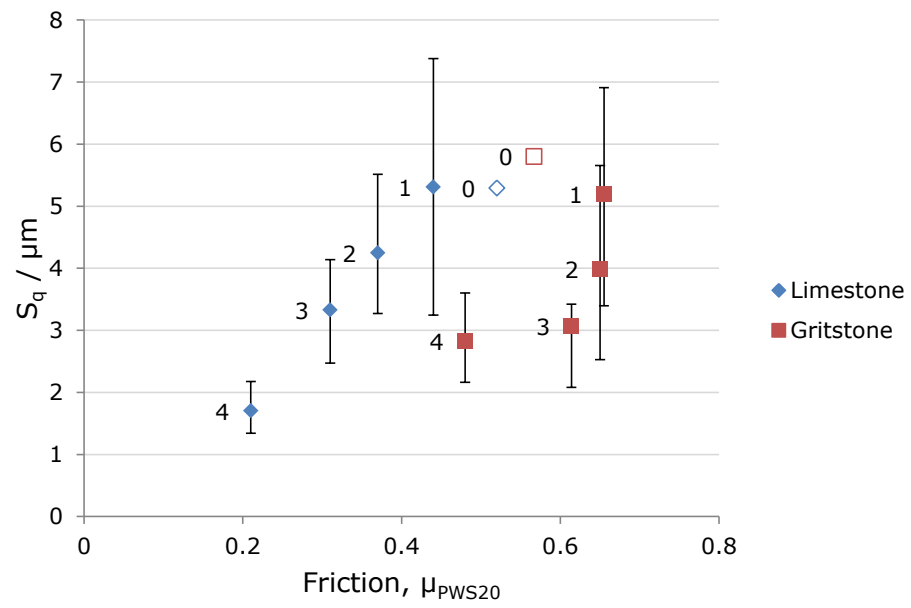


**Figure 7.26 Average  $S_a$  against friction for limestone and gritstone surfaces measured at 20X magnification, after application of a 0.25 mm Gaussian filter**

Clearly  $S_a$  will not be a good common predictor of friction for both of these aggregates and variation in  $S_a$  for the six areas (shown using error bars) is larger than would be ideal. If the measurements made on the surfaces before polishing (Stress 0) are ignored again, on the basis that the differing form of an unpolished surface is a complicating factor, it might be considered that there are two separate trends for the two separate aggregates. The relationship for limestone is linear while the relationship for gritstone has an exponential form, although this is driven primarily by a small change in  $S_a$  corresponding to a relatively large change in friction between Stress 3 and Stress 4.

The trends for  $S_q$  are very similar, as shown in Figure 7.27 where the values calculated for the initial before-polishing state of the aggregate surfaces are shown without error bars using open symbols.



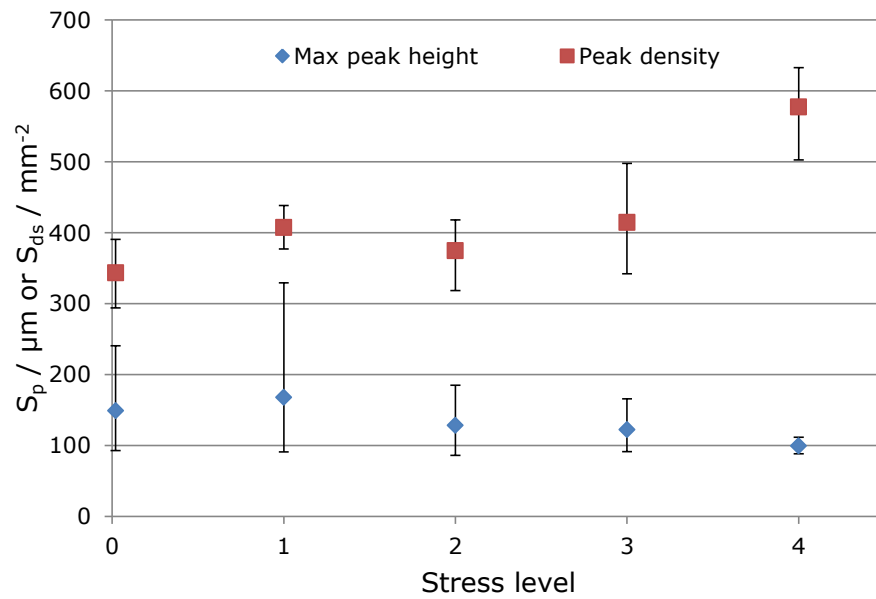


**Figure 7.27 Average  $S_q$  against friction for limestone and gritstone surfaces measured at 20X magnification, after application of a 0.25 mm Gaussian filter**

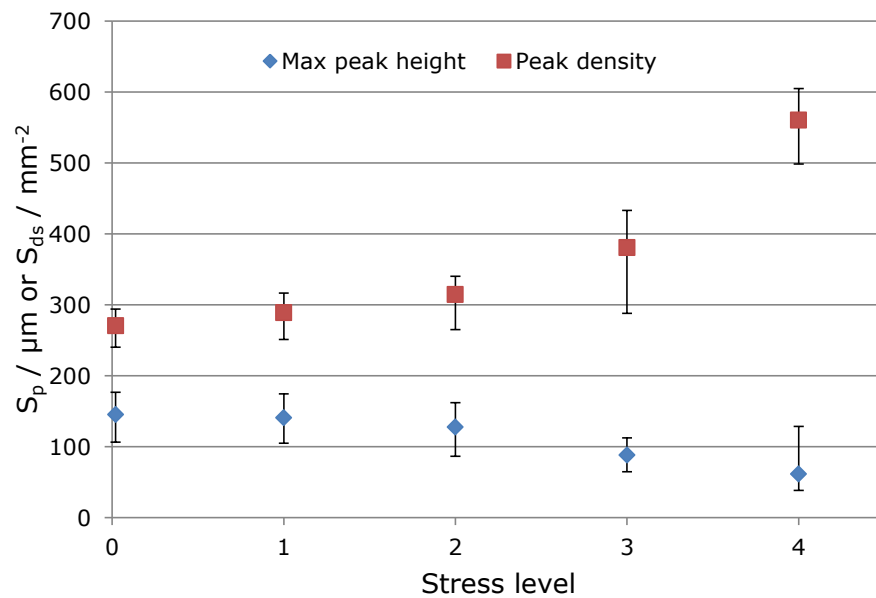
## 7.7 Peak height and peak density

Work at the Health and Safety Laboratory compared slip resistance with roughness characterised for profiles measured on a variety of floor samples (Shaw, 2007). They found a good, positive, correlation between slip resistance and peak height divided by peak spacing. The relationship makes physical sense: higher and/or more dense peaks results in higher friction, perhaps by increasing hysteretic loss as rubber deformation is increased by taller asperities and/or by increasing adhesion because there is more contact with a larger number of peaks.

There is no direct areal equivalent of the profile spacing parameter RS but there are parameters that describe the density of peaks. For example,  $S_{ds}$  is defined by EUR15178 documentation, which was the outcome of the European "SURFSTAND" project (Blunt & Jiang, 2003) and this calculates the peak density (in peaks per  $\text{mm}^2$ ). The calculation depends on the definition of a peak, which is discussed further later in this section. The Mountains software is unable to calculate  $S_{ds}$  for surfaces containing non-measured points and so the average values calculated below omit those surfaces that are on the edge of the aggregate particle (the portion of the measured area not on the particle having been designated as 'non-measured'). The graph in Figure 7.28 shows average  $S_p$ , the maximum peak height, and average  $S_{ds}$  for limestone surfaces measured with the 5X objective lens, after levelling. Figure 7.29 shows the same information for gritstone surfaces. It can be seen that maximum peak height does indeed reduce with polishing (and therefore with decreasing friction). However, if this analysis were to follow the HSL experiment and the resulting logical explanation, then average peak density should also decrease with polishing (density should be proportional to one over the square of spacing) but, for both aggregates, it increases.



**Figure 7.28 Peak height and peak density for four levelled limestone surfaces at 5X magnification**

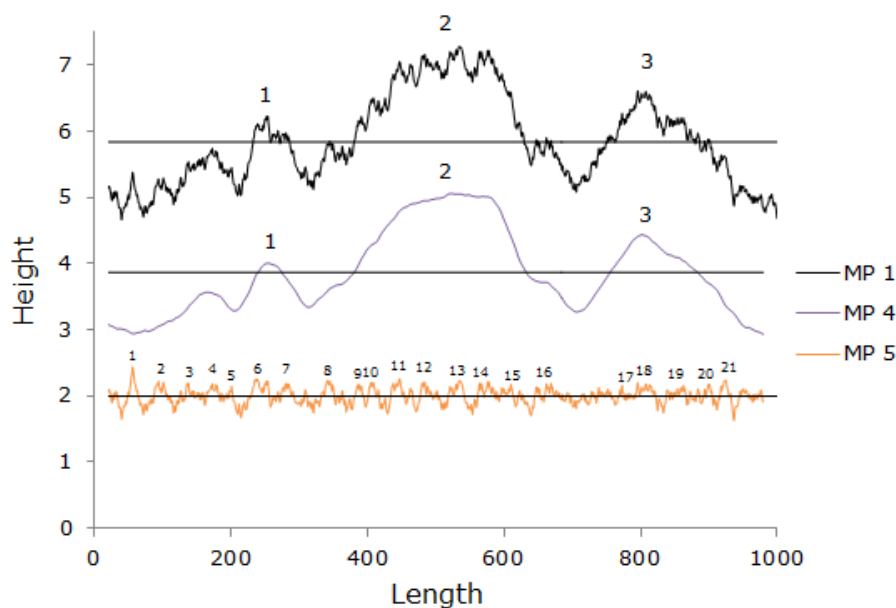


**Figure 7.29 Peak height and peak density for four levelled gritstone surfaces at 5X magnification**

As discussed in Section 2.5, the HSL experiment used acid etching to artificially increase friction on sample surfaces, in contrast to the methodology used here to reduce friction by polishing. This may result in a bias towards a reduction in peak spacing (and therefore increase in peak density) being related to an *increase* in friction, acid etching having the effect of decreasing peak spacing but not much affecting peak height.

It is conceivable that a surface with a small number of large peaks could result in higher friction than a surface with a large number of small peaks. If the force generated by hysteretic friction is the dominant mechanism of friction generation, compared to adhesion, then a reduction in peak height may indeed be more important than a change in peak density.

If the polishing mechanism for gritstone does resemble a removal of long wavelength features, which is supported by qualitative analysis, then an increase in peak density does make physical sense assuming a peak is defined as the highest point between crossings of the mean plane (with some restrictions on height relative the surface – see Section 2.4). Three of the model profiles are shown in Figure 7.30; the profile peaks are numbered. If limestone is likened to the smoothed profile, or even to locally smoothed profiles, there is no explanation from qualitative analysis so far for an *increase* in peak density for limestone.



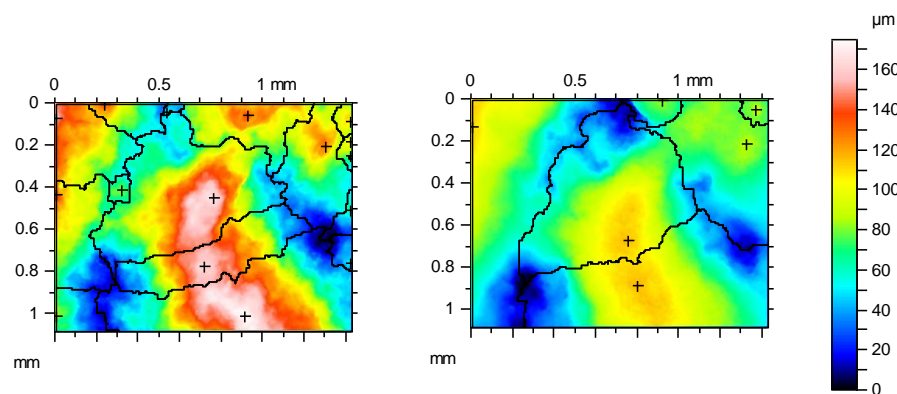
**Figure 7.30 Random model profile (MP 1), smoothed profile (MP 4) and profile with long wavelengths removed (MP 5), with peaks numbered**

It should be noted that the same approximate trends are apparent for both aggregates regardless of the magnification or filter lengths applied. The apparent increase in peak density on limestone is emphasised only by measurements at Stress 4, it having stayed moderately consistent until that point.

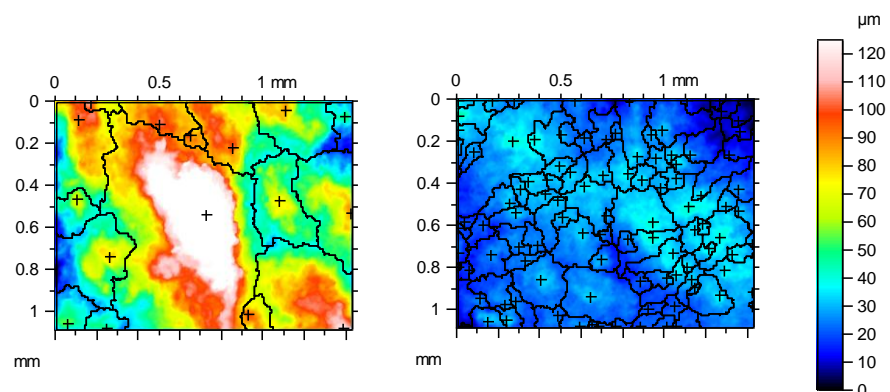
The increase in peak density with polishing could be a result of the way in which the EUR15178 parameter defines a peak (the highest point between

successive crossings of a mean plane). Feature characterisation might be employed to better distinguish peaks in a surface. The process is described in Section 2.4 and it allows surfaces to be segmented into specific features (peaks in this case), using a pruning algorithm so that small features that might normally be counted, but which might have little effect on the functional characteristics of the surface (i.e. friction) are combined with larger features that probably have a larger effect. The Mountains software uses Wolf-pruning to segment each surface into a number of 'motifs'.

The images in Figure 7.31 show one area of the limestone surface (levelled) at Stress 0 on the left and at Stress 4 on the right, both measured using the 10X objective lens, this magnification having given the clearest results. In both states the surface has been segmented and the lines drawn onto the images represent boundaries between segments, or motifs, and crosses mark peaks or valleys. An equivalent pair of images is shown for gritstone in Figure 7.32.



**Figure 7.31 Topographical maps of limestone before (left) and after polishing with segmented motifs marked, 10X magnification**

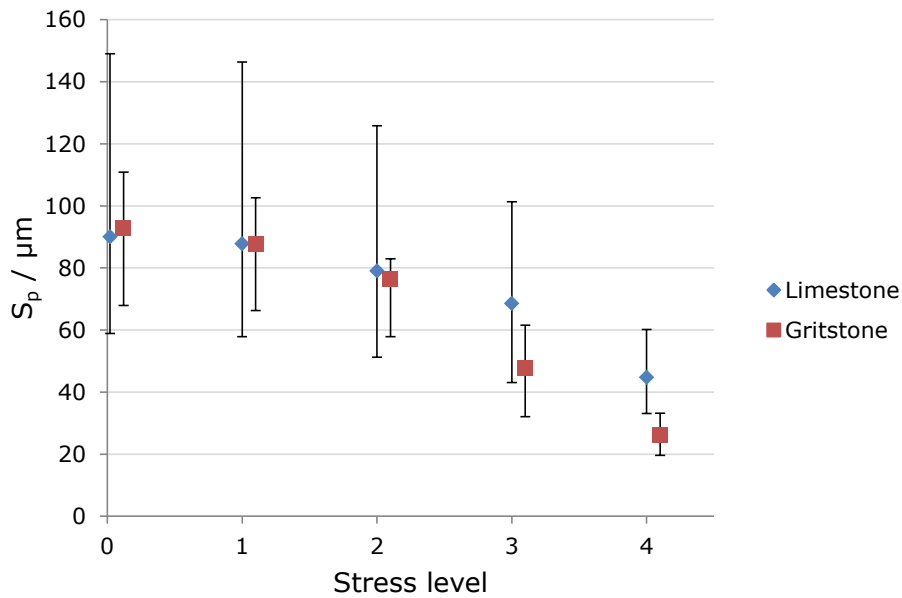


**Figure 7.32 Topographical maps of gritstone before (left) and after polishing with segmented motifs marked, 10X magnification**

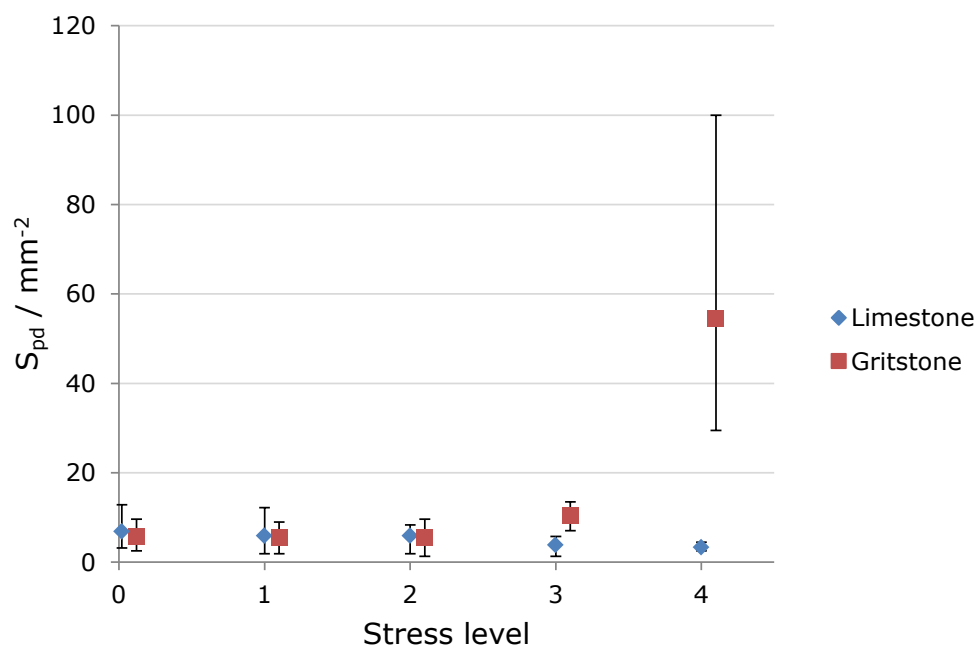
If segmentation and wolf pruning is used then polishing results in a reduction in the number of segments on limestone and an increase in the

number of segments on gritstone. This corresponds to a decrease, and increase, in peak density for the limestone and gritstone, respectively, and accords much more closely with the qualitative description of the polishing mechanisms for the two aggregates: smoothing and removal of long wavelengths.

The graphs in Figure 7.33 and Figure 7.34 show the maximum peak height and peak density, respectively, for both limestone and gritstone. The peak density parameter implemented in ISO25178, which requires prior segmentation, is labelled as  $S_{pd}$ .

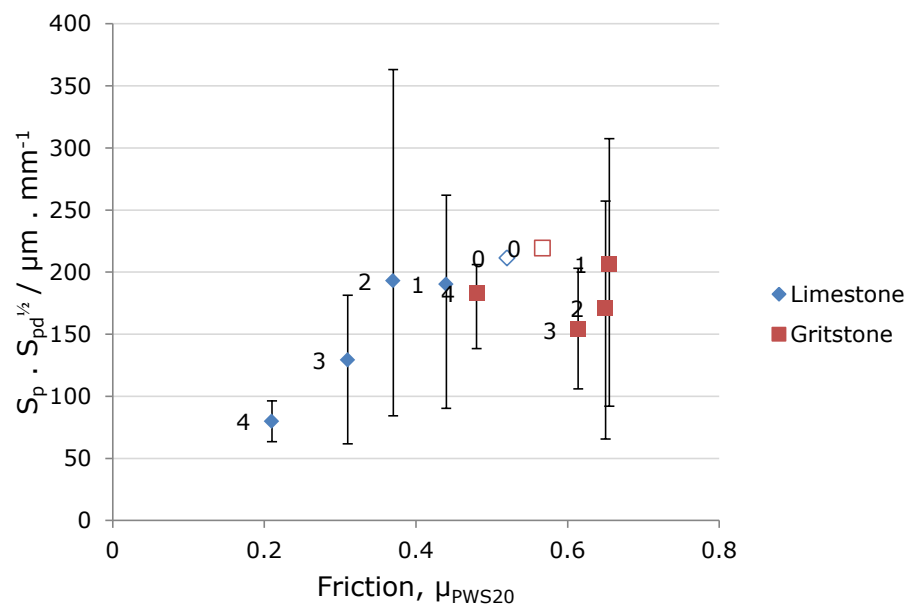


**Figure 7.33 Peak height for levelled limestone and gritstone surfaces at 10X magnification**



**Figure 7.34 Peak density for levelled limestone and gritstone surfaces at 10X magnification**

Finally, using the post-segmentation parameters for peak height and peak density, the graph in Figure 7.35 shows the compound parameter,  $S_p * S_{pd}^{1/2}$ , which is a combination of parameters approximately equivalent to the ratio of peak height to peak spacing used by Shaw (2007), against friction. It can be seen that there is a reasonably strong positive correlation, as in Shaw's work, for limestone but the correlation for gritstone is much less convincing, even if the outlying and variable measurements at Stress 4 are ignored.

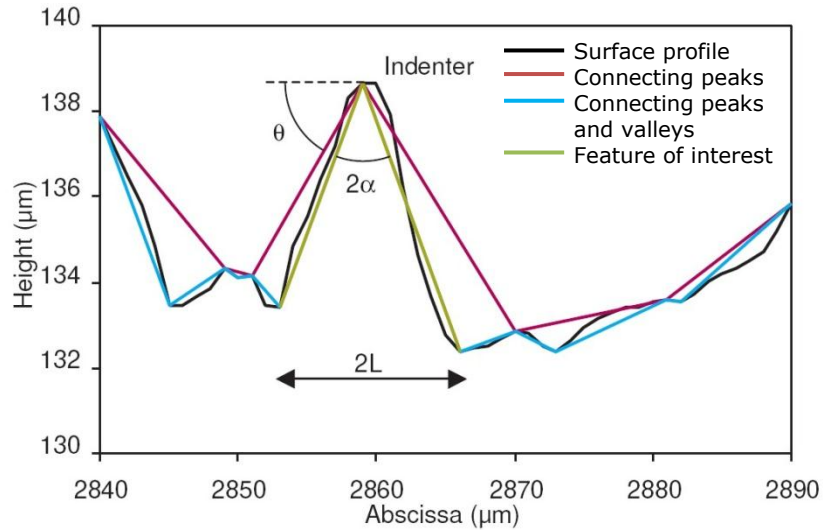


**Figure 7.35 Average  $S_p$  multiplied by average  $S_{pd}^{1/2}$  against friction for limestone and gritstone surfaces measured at 10X magnification**



## 7.8 Peak gradient

Researchers in France have had some success relating friction to roughness measured using a so-called indenter angle to characterise surface profiles (Do M. T., 2005), discussed in Section 2.4. The parameter's description is illustrated again in Figure 7.36.

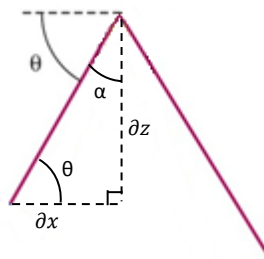


**Figure 7.36 Shape measurements made to correlate with friction reproduced from (Do M. T., 2005)**

There is a parameter defined within the ISO25178 standard called  $S_{dq}$ , the root mean square gradient, given by Equation 7.3 for definition area A.

$$S_{dq} = \sqrt{\frac{1}{A} \iint_A \left[ \left( \frac{\partial z(x,y)}{\partial x} \right)^2 + \left( \frac{\partial z(x,y)}{\partial y} \right)^2 \right] dx dy} \quad 7.3$$

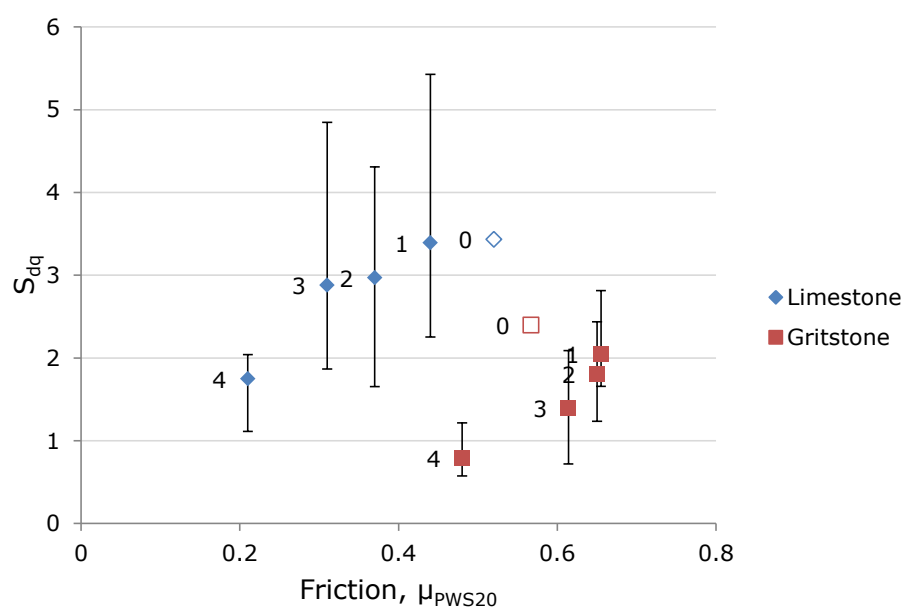
If the illustration in Figure 7.36 is considered as a profile along the x-axis then the tangent of the angle  $\theta$  might be approximated by the ratio represented by the gradient in that direction and the inverse of that gradient might approximate the tangent of the angle  $\alpha$ . For clarity this is illustrated in Figure 7.37.



**Figure 7.37 Approximating indenter angle using profile gradient**

The parameter decreases with polishing for both limestone and for gritstone and this does make physical sense: as the surfaces polish, their peaks become flatter and so the gradient parameter decreases. The trend remains the same regardless of magnification or filtering. It is surprising that, in general, the average gradient of the gritstone surfaces is lower than the average gradient of peaks on the limestone surfaces. However, it should be noted that where this parameter differs from the indenter angle parameter is that the  $S_{dq}$  is calculated for all points and not just for the peaks.

Figure 7.38 shows average RMS gradient against friction for the two aggregates.

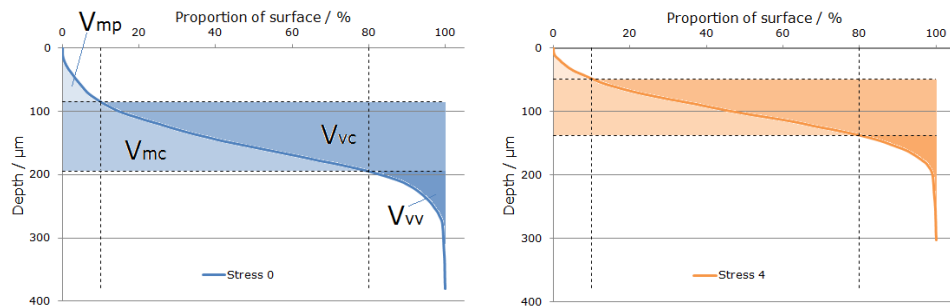


**Figure 7.38 Root mean square gradient for levelled limestone and gritstone surfaces at 20X magnification**

It may be possible to segment the surface so that only peaks are used for calculation of  $S_{dq}$  and a suitable process for doing so could be developed in future work.

## 7.9 Volumetric parameters

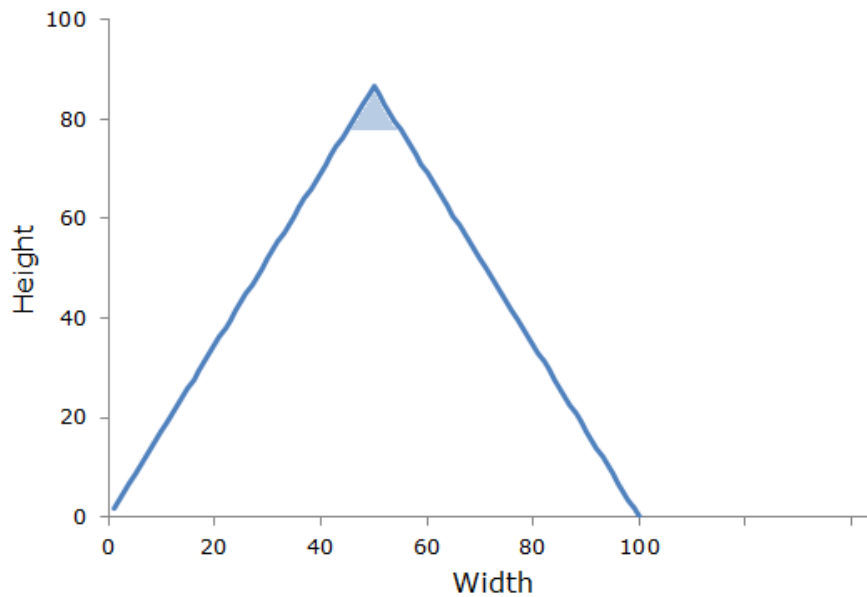
Fractal analysis suggested that the volumes of both limestone and gritstone surfaces were reduced by polishing. There are a number of volumetric parameters, defined in ISO25178, used to describe the shape of the Abbott-Firestone curve (see Section 2.4). The curve presents the cumulative distribution of surface height, or depth, against the proportion of the surface with that height. The graphs in Figure 7.39, show the Abbott-Firestone curves for one of the limestone areas at Stress 0 (left) and Stress 4 (right). Four volumetric parameters are marked on the curve for Stress 0 and shaded areas represent the magnitude of those parameters.



**Figure 7.39 Abbott-Firestone curves for one limestone area at 5X magnification**

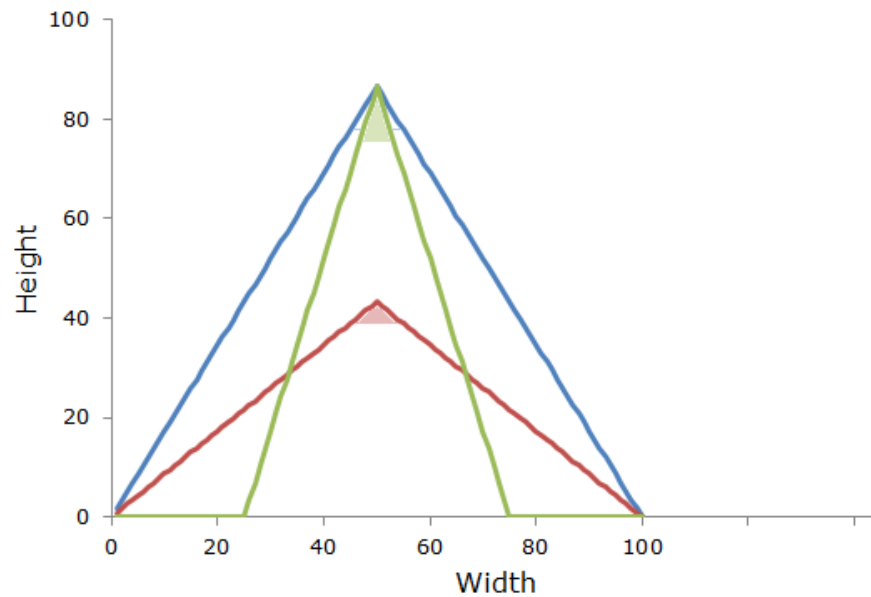
The height of the surface (measured between the highest and lowest points) has clearly been reduced by polishing: before polishing 100 % of the surface area is contained within approximately 380  $\mu\text{m}$  on the z-axis and after polishing 100 % of the surface is contained within approximately 300  $\mu\text{m}$ . The shape of the curve has also changed: for example, before polishing the highest 10 % of the surface had a height within 85  $\mu\text{m}$  of the very highest peak, whereas after polishing the tallest 10 % of the surface had a height within 50  $\mu\text{m}$  of the very highest peak. It is this portion of the surface that appears to be most affected by polishing.  $V_{\text{mp}}$  describes the peak material volume; it is defined here as the volume of material contained within the top 10 % of the surface. Once again, this is difficult to describe in three dimensions but a simple analogy in two dimensions follows.

The single peak represented by the blue line in Figure 7.40, has a total length of 200 (it's an equilateral triangle) so 10 % of its length is 20. The top 10 % of its length can be found within 9 units of the peak and the area within the profile bounded by this length is shaded in blue.



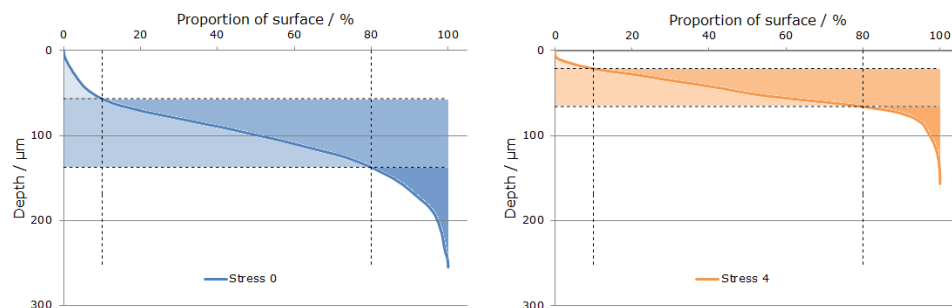
**Figure 7.40 Profile peak; top 10 % peak area shaded**

A reduction in the peak's height or its width would result in a reduction in the area contained within the profile. The area bounded by the highest 10 % of the profile length is shaded in red and green, respectively, for each of these two situations, in Figure 7.41. Both the red and green areas are smaller than the blue area in Figure 7.40 but the top 10 % of the red profile's length is within 4 units of the red summit whereas the top 10 % of the green profile's length is within 11 units of the green summit. The effect of polishing on limestone, characterised by a reduction in the peak material volume  $V_{mp}$  is therefore probably caused by a reduction in peak height.



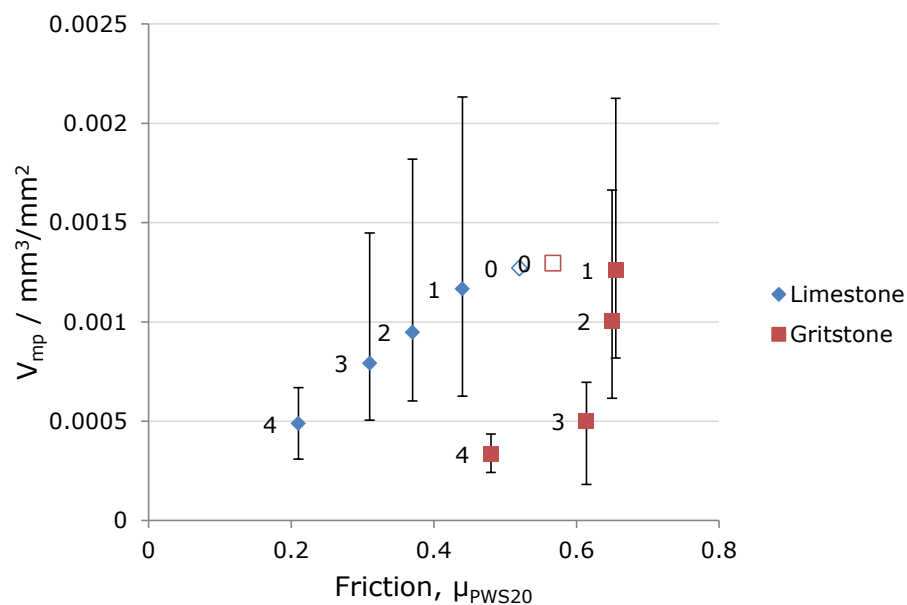
**Figure 7.41 Shortened and narrowed profile peaks; top 10 % peak area shaded**

For gritstone, Abbott-Firestone curves also demonstrate a significant reduction in overall surface volume. The graphs in Figure 7.42, show the Abbott-Firestone curves for one of the gritstone areas at Stress 0 (left) and Stress 4 (right).



**Figure 7.42 Abbot-Firestone curves for one gritstone area at 5X magnification**

As before, an average parameter can be calculated for all measured areas on each of the aggregates. Generally, there is a pattern that appears to relate to the polishing applied; average values for the four parameters,  $V_{mp}$ ,  $V_{mc}$ ,  $V_{vc}$ ,  $V_{vv}$ , decrease with increased polishing. One of the strongest trends can be found using levelled surfaces measured using the 10X objective lens. The graph in Figure 7.43 shows  $V_{mp}$  against friction for limestone and gritstone. There is a very good positive correlation for limestone and a reasonable, but completely separate, positive correlation for gritstone.



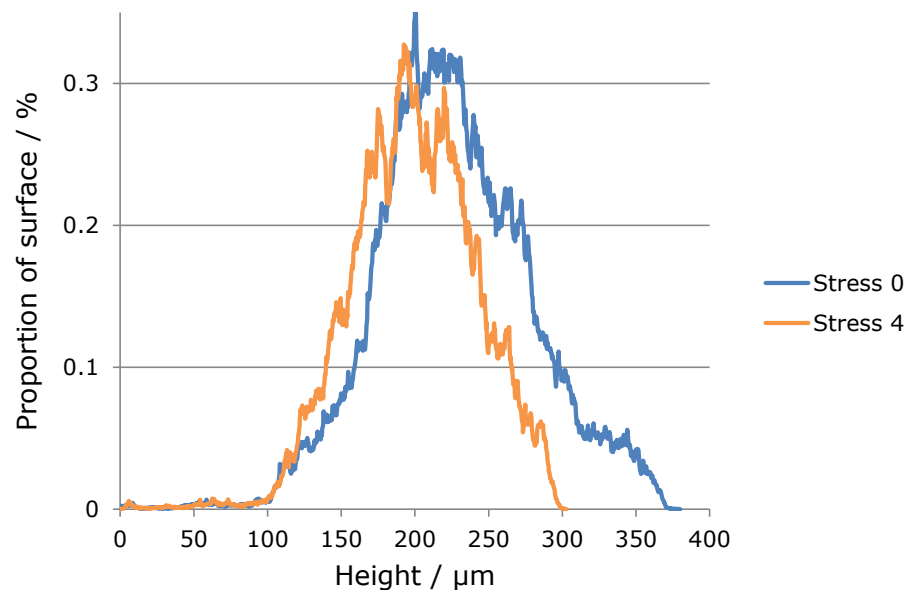
**Figure 7.43 Average  $V_{mp}$  against friction for limestone and gritstone surfaces measured at 10X magnification**

For both aggregates, the volumetric parameters suggest that as the surfaces are polished, there is less material, peaks become less tall, and valleys become less deep. Since the height of a peak and the depth of a valley are, in this case, relative and related, because the heights are measured from the lowest point and vice versa, the implication is that the distribution of heights across the surface is changing. Height distributions and parameters that describe the shape of the height distributions are inspected more closely in the next section.

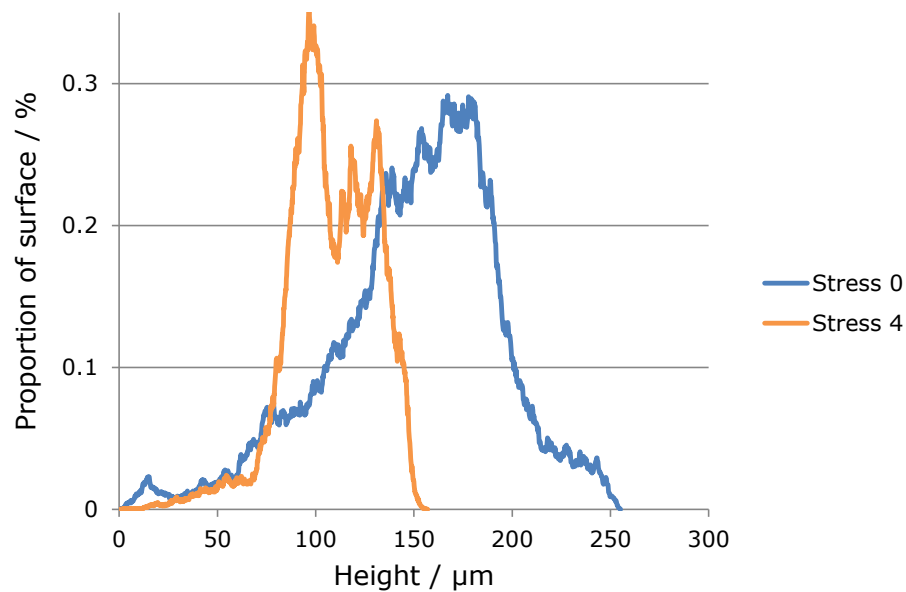
## 7.10 Height distribution

The Abbott-Firestone curve is a cumulative histogram of surface heights. It can be easily manipulated to show histograms in a more conventional format. The graphs in Figure 7.44 and Figure 7.45 show histograms of surface heights for the same single areas represented by the Abbott-Firestone curves above, on limestone and gritstone aggregates respectively. For both aggregates, polishing causes a shift towards shorter heights and a reduction in the range of heights measured. The effect is particularly apparent for the single gritstone surface shown; it should be noted that the trend is similar but less dramatic for the other five gritstone areas.

A reduction in the range of heights measured is in line with previous observations that material is being worn away. A skew towards shorter heights implies that it is the top of the surface that is being lost and this corresponds well to the change in peak material volume discussed in the previous section, and to the comparison with the behaviour of model profiles (Figure 7.47).



**Figure 7.44 Histogram showing height distribution for one limestone area at 5X magnification before and after polishing**



**Figure 7.45 Histogram showing height distribution for one gritstone area at 5X magnification before and after polishing**

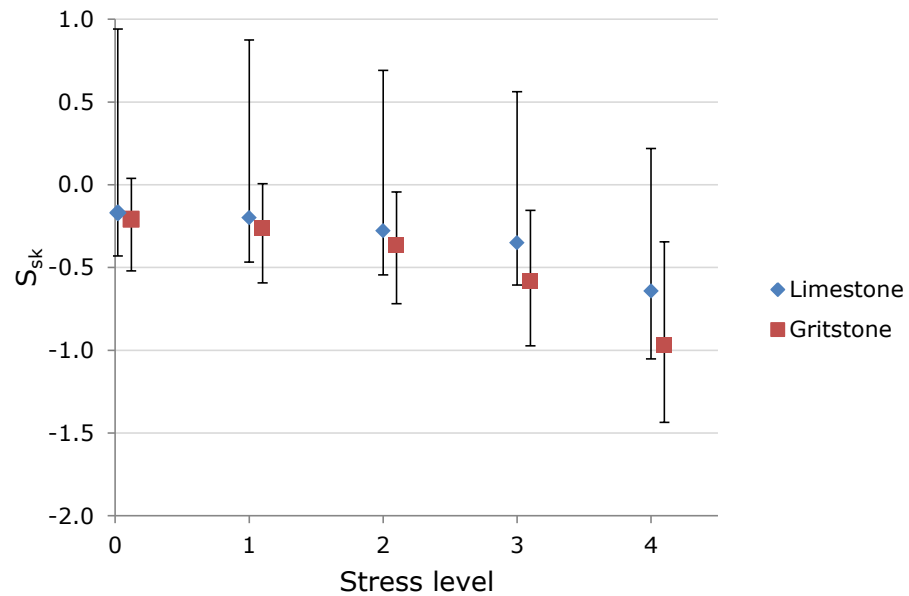
It may be possible to deduce more information about physical changes occurring in the areas represented by the height distributions above. For the limestone surface, the height distributions before/after polishing are very similar up to approximately 120  $\mu\text{m}$ . Although it is known (by paint removal) that the whole area came into contact with the W-S machine's polishing rollers, it might be the case that this lowermost portion of the surface is being affected to a lesser degree. The range of heights measured within the area reduces from 380  $\mu\text{m}$  to 300  $\mu\text{m}$ ; these are the values of  $S_z$  for this area before/after polishing. For gritstone, the height distribution is only similar for the lowest 70  $\mu\text{m}$  and only that if the small peak in the distribution at 20  $\mu\text{m}$  for Stress 0 (the cause for which is not clear) is ignored.  $S_z$  for gritstone (the range of heights measured) reduces from 250  $\mu\text{m}$  to 150  $\mu\text{m}$  corresponding to a much larger, relative, loss of material.



There are two height parameters defined by ISO25178 that deal with skewness and kurtosis in surface height distributions. The skewness parameter  $S_{sk}$  is calculated using Equation 7.4.

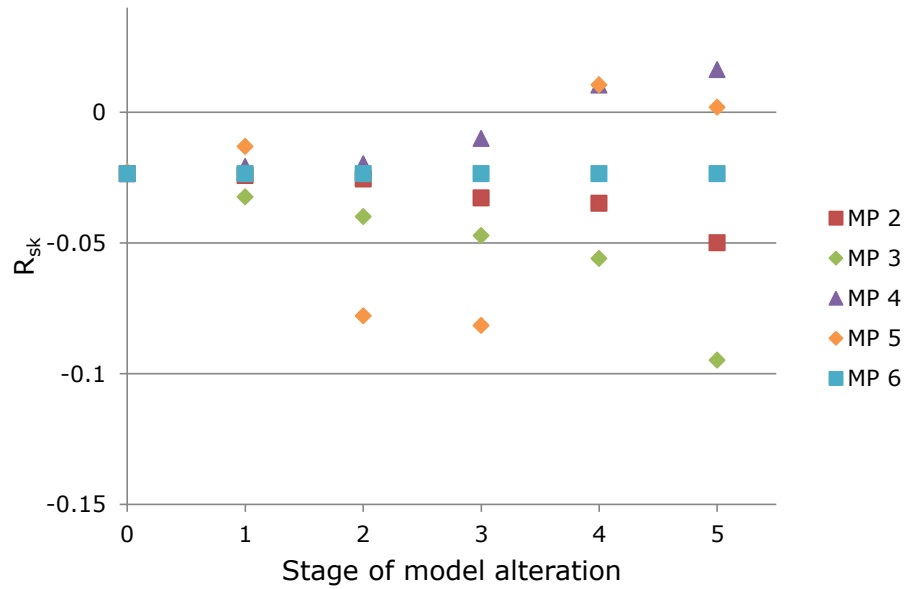
$$S_{sk} = \frac{1}{S_q^3} \left[ \frac{1}{A} \iint_A z^3(x, y) dx dy \right] \quad 7.4$$

where  $S_q$  is the root mean square mean height of the surface (see section 7.6). The graph in Figure 7.46 shows the average skewness of all surfaces, measured at each stress level for the two aggregates, against stress level, using measurements made with the 5X objective lens. Skewness becomes more negative with polishing (note that the x-axis in the graph crosses at -2 instead of 0).



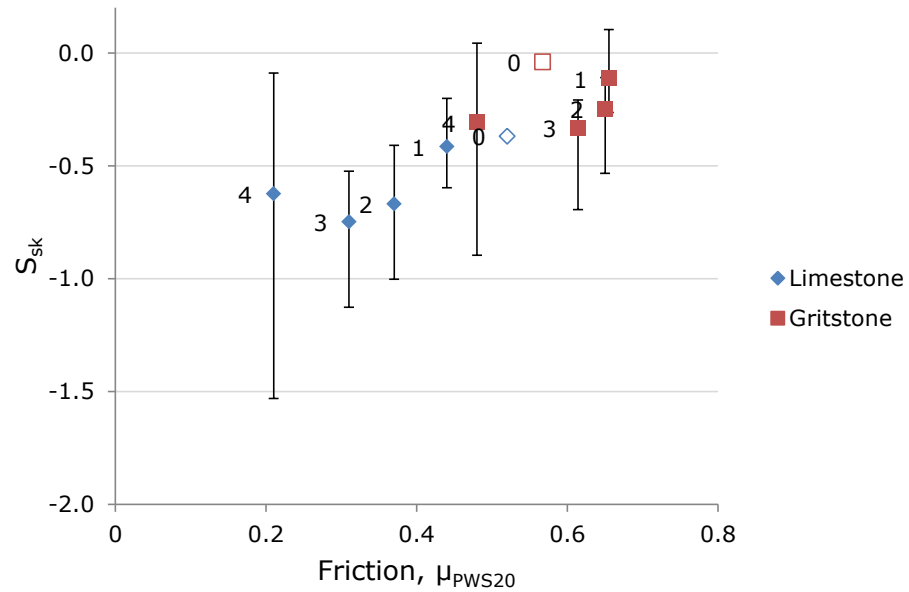
**Figure 7.46 Skewness of height distributions for levelled surfaces at 5X magnification**

Using the sets of model profiles introduced in Section 7.6, it is possible to demonstrate that polishing of the peaks of the surface (either locally or globally) would result in increasingly negative skewness. The graph in Figure 7.47 shows the average value of  $R_{sk}$ , the two dimensional equivalent of  $S_{sk}$ , for the five sets of model profiles (including their intermediate stages of alteration).



**Figure 7.47 Average  $R_{sk}$  calculated for sets of model profiles where a random profile has been gradually altered**

Application of filters on the data collected from the aggregate surfaces or use of higher magnification lenses does not change the response of the parameter  $S_{sk}$  to polishing (i.e. skewness always becomes more negative with increased polishing) but, in one case, what would otherwise be two separate relationships with friction appear to overlap. The graph in Figure 7.48 shows average skewness against friction for levelled and filtered (using a 0.25 mm Gaussian filter) measurements made using the 5X objective lens.



**Figure 7.48 Skewness of height distributions for levelled surfaces at 5X magnification after application of 0.25 mm Gaussian filter**

That skewness correlates with friction as a continuum for both aggregates may simply be a coincidence caused by an increase in negative skew for limestone surfaces and significantly less negative skew for gritstone surfaces. However, the latter might occur when the average reduction in height for peaks at this wavelength is less than the average reduction in height when longer wavelengths are included, which is commensurate with the polishing mechanisms proposed for gritstone. Furthermore, if it is more than a coincidence, it might suggest that it is the peaks at wavelengths shorter than 0.25 mm that affect friction: loss of the tops of these peaks, signified by increasingly negative skewness, results in a loss of friction. To examine this further a larger amount of data, perhaps from an increased range of aggregates would be useful.

### **7.11 Correlation between roughness parameters and friction**

To ensure that all combinations of magnification, filtering and characterisation parameter have been considered, a systematic search for correlation with friction was undertaken. Results from calculation of all the parameters output by the Mountains software, for every combination of magnification and filter length, were tabulated against the friction measured at each stress level. Microsoft Excel was then used to return a Pearson correlation coefficient,  $r$ , and an approximation to Spearman's rank correlation coefficient. The Pearson correlation coefficient (often given as  $r^2$  when fitting trend lines to data) varies between -1 and 1 and is absolutely greater when two variables are more linearly dependent, i.e. when there is a linear correlation between roughness and friction. Spearman's coefficient highlights non-linear correlations; it also varies between -1 and 1 and is absolutely greater when the relationship between the two variables is monotonic, e.g. when an increase in friction always results in an increase in roughness.

For example, Table 7.2 shows the results for all values of  $S_{sk}$  calculated on levelled surfaces at 5X magnification.

**Table 7.2 Average  $S_{sk}$  for all levelled surfaces after application of various Gaussian filters, 5X magnification**

	Filter: (mm)	None	0.8	0.25	0.08	0.025	0.008
	Friction	$S_{sk}$ after filtering					
Limestone	0.52	-0.2	-0.3	-0.4	0.0	0.5	21.8
	0.44	-0.2	-0.3	-0.4	0.2	2.4	26.9
	0.37	-0.3	-0.4	-0.7	-0.6	0.1	25.3
	0.31	-0.4	-0.5	-0.7	-0.4	0.2	26.0
	0.21	-0.6	-0.6	-0.6	0.0	0.5	26.3
Gritstone	0.57	-0.2	-0.1	0.0	0.3	2.9	30.3
	0.66	-0.3	-0.2	-0.1	0.0	1.3	30.4
	0.65	-0.4	-0.4	-0.2	-0.1	1.1	29.6
	0.61	-0.6	-0.5	-0.3	0.0	1.2	29.6
	0.48	-1.0	-0.4	-0.3	-0.1	0.9	27.4
Pearson		0.20	0.59	<b>0.85</b>	0.34	0.45	0.55
Spearman		0.18	0.53	<b>0.84</b>	0.14	0.64	0.73

The correlation coefficients suggest that, after application of a 0.25 mm Gaussian filter,  $S_{sk}$  calculated on surfaces measured at 5X magnification correlates linearly and monotonically with friction. This relationship has already been shown in Figure 7.48.

This process highlighted several parameter/magnification/filter combinations that do correlate well with friction. The combinations shown in Table 7.3, for surfaces that have already been levelled, resulted in Pearson or Spearman coefficients greater than 0.75 in magnitude.

**Table 7.3 Parameters demonstrating correlation with friction**

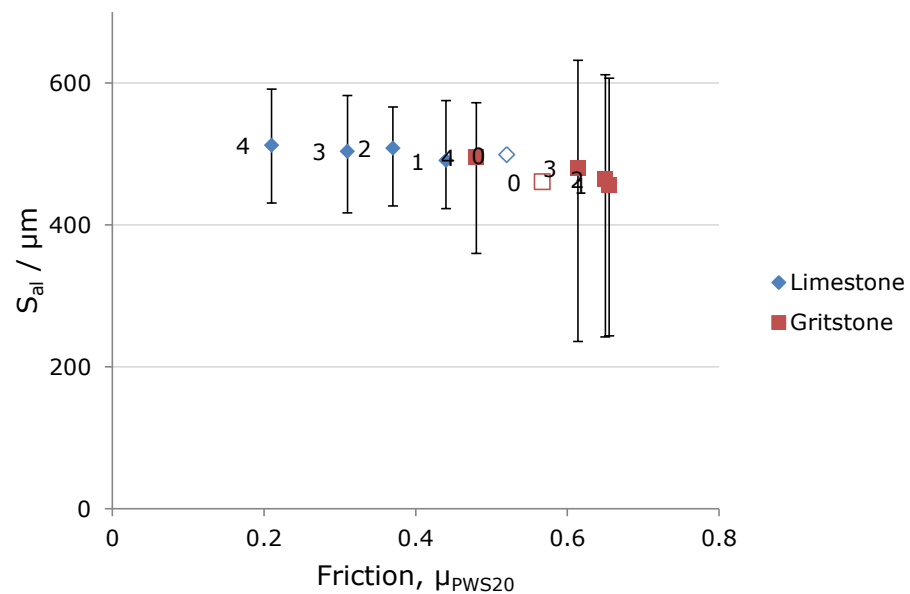
Magnification	Filter	Parameter	Pearson	Spearman
5	None	$S_{al}$	-0.9	-0.9
5	0.25	$S_{sk}$	0.85	0.84
5	0.25	$S_{ku}$	-0.8	-0.8
5	0.08	$S_{ku}$	-0.7	-0.9
5	0.08	$S_{al}$	-0.8	-0.6
5	0.008	$S_{al}$	-0.8	-0.7
10	0.25	$S_{ku}$	-0.9	-0.8
10	0.25	$S_{sk}$	0.82	0.7
10	0.025	$S_{al}$	-0.8	-0.8
20	None	$S_{ku}$	-0.8	-0.8
20	0.25	$S_{ku}$	-0.8	-0.8
20	0.008	$V_{mc}$	0.77	0.62
20	0.0025	$V_{mc}$	0.85	0.7

$S_{sk}$  describes the skewness of the distribution of measured heights. This parameter has been discussed and, because measured heights are relative, it can be attributed some physical sense.

$S_{ku}$  was not discussed in detail but is also related to the distribution of surface heights, giving the kurtosis of the distributions. Again, this makes some physical sense – more positive kurtosis means that the distribution is sharper and the range of heights measured is smaller.

$V_{mc}$  has already been discussed and apparently only correlates well with friction, across both aggregates, if very short wavelength filters are applied. This might imply that it is the shortest wavelengths measured that are important for friction and, since 0.0025 mm is at the limit of the resolution measured, it may be necessary to make measurements using a higher magnification objective lens.

$S_{al}$  is the autocorrelation length; according to the description in Mountains software this parameter has a high value if the surface has mainly high wavelengths. If that is the case, increasing values of  $S_{al}$  might suggest that the surface is increasingly composed of high wavelength features as it is polished, which is the exact opposite of the polishing mechanism proposed for gritstone. The results are shown in Figure 7.49; it can be seen that the change in  $S_{al}$  with changing friction is very small compared to the range of values calculated for the six areas measured at each stress level (error bars).



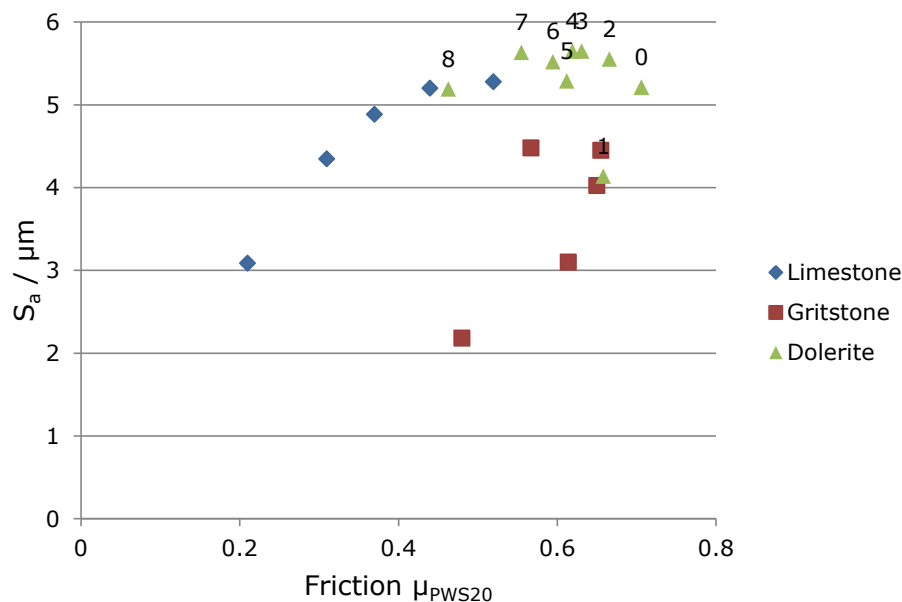
**Figure 7.49 Average autocorrelation length,  $S_{al}$ , for levelled surfaces at 5X magnification**

The systematic search for parameters that characterise texture in such a way as to correlate well with friction has not revealed a panacea. Qualitative analysis has indicated that the two aggregates polish via different mechanisms. Quantitative analysis supports those observations and suggests that the different mechanisms result in different relationships between surface texture and friction. However, the relationships investigated so far have been for limestone, which is rarely used in the road surface course, and for gritstone, which is. It may be informative to add data from the dolerite used in feasibility studies before going on to repeat the experiment, having developed and demonstrated the methodology, using a larger range of aggregates that are commonly used in the road surface course.

## 7.12 Inclusion of results from dolerite surfaces

In this section, the average values of roughness parameters calculated using measurements of surface texture made on replicas of the dolerite specimen, used during the feasibility study (Chapter 4), will be compared with the parameter values already presented for limestone and gritstone.

For some parameters there is some coincidence between those values calculated using measurements made on the replicas of dolerite surfaces and on the limestone and gritstone surfaces. For example, the graph in Figure 7.50 shows average values of  $S_a$  calculated for levelled surfaces at 5X magnification, after application of a 0.25 mm Gaussian filter. Apart from a single outlying point (for stress level 1), the values calculated for replicas of the dolerite aggregate fall in line with the trend for changing  $S_a$  shown by limestone.



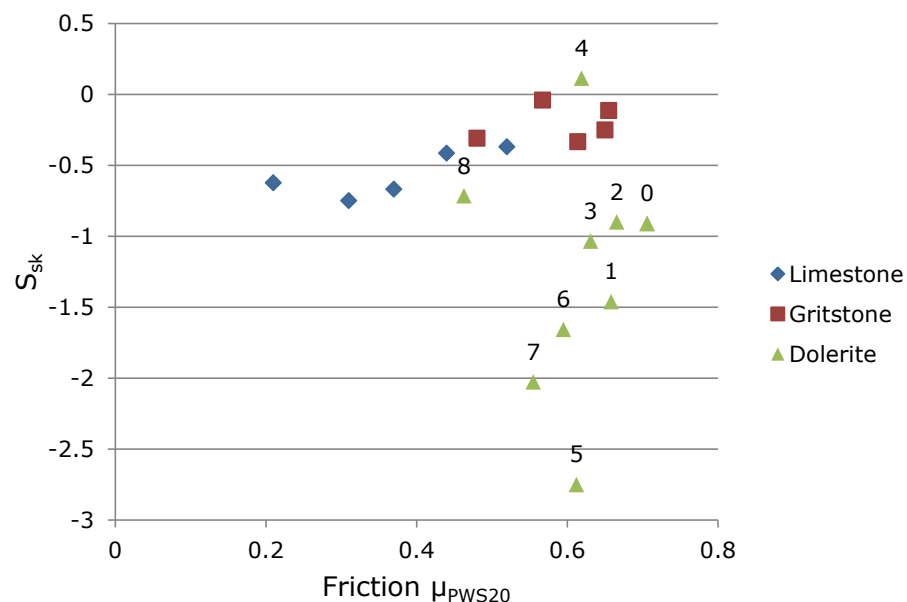
**Figure 7.50 Average  $S_a$  for limestone and gritstone aggregate surfaces and dolerite replica surfaces after application of 0.25 mm filter, 5X magnification**

For some of the parameters discussed, the values calculated using measurements made on the dolerite replicas do not necessarily make physical sense without further manipulation. For example, peak material volume,  $V_{mp}$ , of the replicas is not the peak material of the aggregate because the replica is in inverse relief. Similarly, whereas for the aggregate surfaces it has been noted that the highest portions of the surface are most affected, thereby making skewness increasingly negative, for the replicas, it would be the lowest portions of the surface that are



affected. Using the value of skewness calculated on the replicas, but with the opposite sign, should compensate for this difference.

The graph in Figure 7.51 shows average skewness,  $S_{sk}$ , calculated for levelled surfaces, at 5X magnification, after application of a 0.25 mm Gaussian filter. The stress level from the progressive polishing regime employed is shown above each point for the dolerite only and these values have the opposite sign to the actual values calculated. The patterns for changing skewness on limestone and gritstone have already been presented (Figure 7.48). There is no clear pattern for skewness changing with polishing (or change in friction) for the dolerite specimen; nor do the values align well with those calculated using measurements made on the limestone or gritstone surfaces.



**Figure 7.51 Skewness of limestone and gritstone aggregate surfaces and dolerite replica surfaces after application of 0.25 mm filter, 5X magnification**

When all combinations of magnification, filter length and parameter are considered, a coincidence between the values calculated on all three aggregates is not a common occurrence. A new set of data for dolerite surfaces should be collected, using the robust methodology developed, before a complete comparison of behaviour for the different aggregate types can be carried out.

### 7.13 Discussion

Measurements of surface texture can be characterised in such a way that changes due to polishing in the laboratory can be quantified. The robust methodology for polishing and examination of aggregate surfaces has allowed unprecedented confidence that parametric changes are due to changes in surface texture caused by polishing. Each element of the methodology has contributed to confidence in the results:

- A logarithmic pattern of polishing, spread over 5 levels of applied stress, providing a series of surfaces with a range of levels of friction, means that trends in data are more easily spotted. A trend demonstrated through five points is more convincing than one demonstrated through three points (Do M. -T., Tang, Kane, & de Larrard, 2009).
- Measurement of texture in three dimensions not only allows better qualitative analysis (Chapter 6), but also increases the amount of data collected that can be used for quantitative analysis. Compared with recent work using 2D measurements (Chen & Wang, 2011), where three 100 mm profiles were examined at each polishing stage, providing approximately 100,000 height measurements, measurement of six areas in three dimensions provides approximately 12,000,000 height measurements at each polishing stage. Measurement in three dimensions also allows use of areal (as opposed to profile) roughness parameters, which are rapidly becoming the default choice for surface characterisation in industry (Giusca, Evans, McDonald, & Leach, 2012), (Leach, 2011).
- Careful location referencing and the use of the paint removal technique (Chapter 5) means that the same area is analysed at each stress level and there is no doubt that that area is being affected by contact with the polishing rollers of the Wehner-Schulze machine. Again, this helps with qualitative analysis because changes in surface appearance are easier to spot. It also means that there is more control over other factors, such as locally variable topography, that might affect characterisation of roughness.

It has been possible, using a set of model profiles, to compare quantitative changes in surface texture with qualitative observations, thereby proposing polishing mechanisms for limestone and gritstone aggregates. It is

indicated that the polishing mechanisms are different. Fractal analysis and volumetric parameters indicate that both aggregates lose material as they are polished and the changing skewness of measured height distributions suggests that material is lost from the highest portions of the surfaces. Fractal analysis, changing height parameters and feature characterisation suggest that, while limestone polishes smooth in terms of short wavelength features, gritstone retains some fine-scale roughness throughout the polishing process.

The different polishing mechanisms make it difficult to compare roughness with friction in a single continuum. This difficulty was observed by Yandell (Yandell, 1970) and it has been suggested that complete harmonisation of characterisation across such different mineralogies may not be possible. This work is worth pursuing further – it may be possible to harmonise roughness/friction relationships for more similar mineralogies. There are, for example, a large number of different gritstone aggregates quarried in the UK, with a range of resistances to polishing (and therefore a range of friction after polishing). The analysis presented in this chapter and further work, such as might be carried out using a range of gritstone aggregates, will be discussed in more detail in the next chapter.

## 7.14 References

- Blunt, L., & Jiang, X. (2003). *Advanced Techniques for Assessment Surface Topography: development of a basis for 3D surface texture standards "surfstand"*. London: Kogan Page Science.
- British Standards. (2012). *BS EN ISO 25178-2:2012. Geometrical product specifications (GPS) - Surface texture: Areal. Part 2: Terms, definitions and surface texture parameters*. London: BSi.
- Carr, J. R., Norris, G. M., & Newcomb, D. E. (1990). Characterisation of aggregate shape using fractal dimension. *Transportation Research Record 1278*, 43-50.
- Chen, X. H., & Wang, D. W. (2011). Fractal and spectral analysis of aggregate surface profile in polishing process. *Wear 271*, 2746-2750.
- Do, M. T. (2005). Relationship between microtexture and skid resistance. *BLPC 255*, 117-136.
- Do, M. -T., Tang, Z., Kane, M., & de Larrard, F. (2009). Evolution of road-surface skid-resistance and texture due to polishing. *Wear 266*, 574-577.
- Do, Tang, Kane, & Larrard. (2009). Physical model for the prediction of pavement polishing. *Wear 267*, 81-85.
- Forster, S. W. (1989). Pavement microtexture and its relation to skid resistance. *Transportation Research Record 1215*.
- Ganti, S., & Bhushan, B. (1995). Generalised fractal analysis and its application to engineering surfaces. *Wear 180*, 17-34.
- Giusca, C. L., Evans, A. A., McDonald, D., & Leach, R. K. (2012). *The effect of use duration on surface roughness measurements of stone tools*. Teddington: National Physical Laboratory.
- Himeno, K., Nakamura, Y., Kawamura, A., & Saito, K. (2000). Skid resistance of asphalt pavement surfaces related to their microtexture. *Proceedings of the international symposium on pavement surface characteristics of roads and airfields*. Nantes: PIARC.
- Leach, R. (2011). *Optical measurement of surface topography*. Berlin: Springer.
- Radó, Z. (1996). Fractal characterisation of road surface texture for analysis of friction. *International symposium on pavement surface characteristics* (pp. 101-132). Christchurch New Zealand: ARRB.

Shaw, R. (2007). *An examination of novel roughness parameters to be used in conjunction with the HSE slips assessment tool (SAT)*.

London: Health and Safety Executive (HSE).

Yandell, W. O. (1970). *The measurement of surface texture of road stones with particular regard to the effect on the frictional properties of road surfaces*. University of New South Wales.



## 8 Summary and discussion

---

In this chapter a summary of all previous chapters is presented. The purpose and outcomes of the work undertaken is discussed and some of the points of discussion raised at the end of each chapter are repeated. the final section in this chapter raises some general points of discussion about the project as a whole.

This thesis has encompassed:

- A review of literature pertaining to friction theory, road surface texture, texture measurement and characterisation, attempts to relate texture to friction and, briefly, properties of aggregate that is used in the road surface.
- A description of feasibility studies carried out to examine whether traffic speed measurement of surface texture (of an appropriate scale) is, or will be, possible, and whether laboratory techniques could be used to accurately measure the surface texture of aggregate particles.
- The development of a robust methodology for examination of surface texture throughout a laboratory polishing regime. An initial, less successful first attempt, using surface replication and measurement of texture in three dimensions was followed by further development that included experiments designed to show the suitability of the laboratory polishing and friction testing mechanisms and a novel technique for determining polishing contact.
- Qualitative analysis, which clearly demonstrated that texture on the surface of two different aggregate types had changed as a result of polishing and also allowed polishing mechanisms for the two aggregates to be proposed.
- Quantitative analysis, which has suggested that the surface texture of aggregate particles can be numerically described and that the polishing mechanisms of the aggregates can be seen in the characterisation parameters' response to polishing.

## **8.1 Introduction**

The introduction to this thesis briefly outlined a *raison d'être*: the need for a road to provide adequate skid resistance and the probable link between skid resistance and accident risk. The skid resistance of the road is monitored and maintained by highway authorities. Measurement is undertaken using various devices, all of which operate on the principle of measuring forces acting on a rubber tyre or slider when it is forced to slip against the road surface. The desire to improve or enhance the speed, accuracy and volume of data collected when measuring skid resistance is the point of germination of the research that is described in the rest of this thesis. Determination of skid resistance by measurement of surface texture is the method proposed to achieve this goal.

In order to determine skid resistance from measurements of surface texture it is important to better understand the interaction between surface texture and a sliding tyre (in the case of a vehicle attempting to stop), the form and scale of texture that is important, and a method for characterising this texture. The work presented in this thesis is the first step on a path leading to this understanding. The aim of the research was to develop a methodology that allowed observation of changes in surface texture on the surfaces of aggregates as they polish, propose mechanisms for the way the aggregates polish and evaluate numerical methods that might characterise the texture on aggregate surfaces.



## **8.2 Literature review**

A review of available literature indicated that friction interactions involving rubber are complicated and fundamental research into the behaviour of viscoelastic materials is still ongoing. There are two primary mechanisms of friction generation that depend on the texture of the surface against which rubber is sliding: adhesion and hysteresis.

Road surface texture is frequently described and a popular theory is that road surface texture is needed for friction because of the likely presence of water. Texture both helps in the bulk removal of water from the interface between tyre and road and breaks through any remaining film of water. While measurement and characterisation of surface texture on many materials is a mature subject, largely because of its relevance in industry for efficiency gains from reduction machine wear, routine characterisation of road surface texture is restricted to large features. It is generally accepted that it is the road surface's microtexture (wavelengths shorter than 0.5 mm) that contributes to friction at low speeds.

Attempts have been made to characterise the microtexture of aggregates used in the road surface. Research presented in the literature has certainly helped to inform the methodology proposed in this thesis and some of the characterisation techniques used. There is a divergence in the literature when it comes to surface texture characterisation. While the science of texture measurement appears to be progressing towards measurement and parameterisation in three dimensions, a trend which has been followed by the machine industry, even the most recent attempts to describe texture for road surface applications have used only two dimensions.

The advantages of measurement and characterisation in three-dimensions are several-fold. Some of the studies presented in the literature have suffered from a deficit of data and others from a difficulty in interpretation of forms of texture measured (and the way texture changes when aggregates are polished). The review of literature therefore confirms that the research aims have not already been reached. There is a need for development of a robust methodology for measurement, in three-dimensions, of aggregate surfaces.

### **8.3 Feasibility studies**

The development of a robust methodology for aggregate texture measurement and characterisation, the main body of this thesis, was part of a wider range of experiments, all carried out since the outset of the PhD study. In particular, three experiments help to inform that methodological development. In turn, they demonstrated that:

- It is theoretically possible to capture high resolution information about the road surface, either now or at least in the near future. This is an important consideration because the possibility of practical implementation not only provides a *raison d'être* but has made possible the funding and interest for more laboratory studies to come.
- The information collected, in the form of high resolution photographs, should enable some characterisation of the surface in a way that relates to friction. The experiments carried out in the laboratory to investigate the changing appearance of the surface have developed appropriate methods for polishing and friction testing that allow investigation of discrete friction levels and have highlighted the importance of polishing mechanisms and aggregate mineralogy.
- It is possible to make meaningful measurements of surface texture on specimens of aggregate, which are generally much rougher than would normally be examined in the laboratory. Experience with the measurement technique has given confidence that, in general, texture measurements are accurate, but that a large number of measurements should be made in order to properly characterise the surface.

#### **8.4 First attempts at an improved methodology**

Following from the feasibility studies, a structured method for examining the surface texture of aggregate particles as they were polished in the laboratory was developed. The polishing regime applied polishing stress, using the Wehner-Schulze machine, in a logarithmic fashion so that an evenly distributed range of levels of friction could be achieved on the same aggregate surface. As well as taking photographs of the surface at each stage of polishing, replicas of the aggregate surfaces were made so that texture measurements could be made in a separate laboratory.

Scanning electron microscopy was used to examine the texture of the aggregate particles, and to compare the texture found in the replica with that of the aggregate itself. A technique for location referencing, by using prominent features of the surface (such as stone edges or distinctive ridges), was developed so that exact locations could be compared (either stone to replica or before- to after-polishing). Qualitative observations of changes to surface texture before and after polishing are the most compelling outcome from this work.

Quantitative measurements of surface texture were made on replicas of the aggregate surfaces using a focus variation measurement microscope. A large number of discrete areas were scanned and characterisation was attempted using various standard roughness parameters and data filtering techniques. It was assumed that some trend would be immediately apparent in any measure of surface roughness, but this was not the case.

It was concluded that elements of the methodology may have masked changes that would otherwise have been observed. No record was kept of the exact location in which texture measurements were made and it was not possible to verify that those areas were likely to have been affected by contact with the polishing rollers of the Wehner-Schulze machine. For the same reason, because the location was not recorded as it had been for SEM inspection, it was not possible to observe changes occurring to the surface throughout the polishing process. The replication process, although ostensibly of sufficient fidelity (according to observations made using scanning electron microscopy), may have led to some error in texture measurement and, in particular, to changes in texture at each stage of polishing. And the mineralogy of the aggregate used is complex, probably leading to complicated texture forms that would be difficult to characterise even with greater confidence in the data.

## **8.5 Development of a robust methodology**

Experience from the first attempt to improve the collection of data led to some specific refinements being made, allowing further development and collection of data that could be analysed qualitatively and quantitatively with some confidence. The experiment was carried out using aggregates with simpler mineralogies (namely limestone and gritstone), location referencing was used to make measurements of texture in the same position at each stage of polishing, measurements were made on the aggregate rather than on replicas and a paint removal technique was used to identify the areas of aggregate surface that came into contact with the Wehner-Schulze machine's polishing rollers.

The relevance of the use of the Wehner-Schulze machine is also presented in this chapter. The relationship between the polishing applied by its rollers to aggregate specimens and the polishing applied by vehicles to in-service roads is explored. The relationship between friction measured in the laboratory and skid resistance measured by full-scale devices on the road is also presented.

Development of this methodology for measurement of surface texture of aggregate particle surfaces is, arguably, the most important part of the research described in this thesis. Although an exploration of methods for surface texture characterisation (Chapter 7) is probably a more intellectual element of the overall study, neither that nor the qualitative examinations that precede it (Chapter 6) would have been possible without confidence in the data. Even after those analyses, the exact data requirements for texture characterisation in relation to friction generation are not clear, but the robust methodology developed can be adapted accordingly, allowing future work to progress.

## **8.6 Qualitative analysis of changes in texture**

Topographical examination of measurements of surface texture indicates without any doubt that the surfaces of the inspected aggregate particles are changing as a result of polishing, especially in the areas that come into contact with the machine's polishing rollers (verified by paint removal indication). This is an important observation because it confirms that refinements in the data collection techniques allow concerns, raised after earlier analysis of measurements on a dolerite specimen (Chapter 4), that the effect of polishing could be masked by consideration of portions of the surface that had not come into contact with the polishing rollers of the W-S machine, can be allayed. Qualitative analysis also confirmed that the same area of each surface was measured at each stage of polishing, demonstrating that the careful specimen alignment procedure included in the experimental methodology worked satisfactorily.

Qualitative analysis suggests that the two aggregates, limestone and gritstone, polish via different mechanisms. Limestone becomes smoother, short wavelength height variation is reduced but some long wavelength amplitude is retained and gritstone remains rough, long wavelength features are completely removed but short wavelength texture is still present.

## 8.7 Quantitative analysis of changes in texture

Analyses of surface texture measurements were made using a number of different methods. To assist with interpretation of the results, a set of model profiles were generated to explore the reaction of the characterisation method to several potential polishing mechanisms. Following from qualitative analysis, the polishing action of limestone was likened to a surface that had been smoothed by removing short wavelength features (either generally or above local or global height thresholds) and the polishing action of gritstone was likened to a surface that had lost long wavelength features.

Power Spectral Density analysis was undertaken with the aim of revealing which wavelengths, if any, were most affected by the polishing action of the Wehner-Schulze machine. As had been shown in the literature, the results from PSD analysis are difficult to interpret, possibly due to the complicated nature of the surface texture (in comparison with machined surfaces). Although, for gritstone, one packet of wavelengths (357  $\mu\text{m}$  to 600  $\mu\text{m}$ ) did appear to be more affected than others, it was not possible to corroborate aspects of the qualitative analysis using PSD. Using the model profiles, it was suggested that the PSD analysis was dominated by a global reduction in surface height for all wavelengths, which may have masked more subtle changes that would allow comparison between changes in short- and long-wavelength features.

Fractal analysis of the surfaces measured at each stage of polishing suggested that fractal dimension (and therefore the complexity of the surface) does not change with polishing for limestone, and increases with polishing for gritstone. Using the model profiles it was possible to show that these responses might be compatible with a loss of low wavelength texture above a local or global threshold and loss of long wavelength texture, respectively. In both cases, plotting fractal curves for each stage of the polishing process also demonstrates the loss of material, or reduction in amplitude at all wavelengths, occurring throughout the polishing process.

Standard areal surface roughness parameters were used to characterise, on average, the state of the surfaces at each stage of polishing. Those parameters that can be supported by likely physical changes in the surface were presented in some detail. For example, height parameters  $S_a$  and  $S_q$ , the three dimensional equivalents of  $R_a$  and  $R_q$  that have been used by

other researchers (Do, Tang, Kane, & de Larrard, 2009), change with polishing on both aggregate types. Because the methodology developed allowed measurement of surface texture at five discrete stress levels, the trend for changing average  $S_a$  (or  $S_q$ ) is very clear – in both cases it reduces with polishing. Some correlation with friction could be demonstrated for each aggregate individually, but it was not possible to generate a single correlation encompassing both aggregates. It is suggested that this is because of the different polishing mechanisms exhibited by the two different aggregates.

Other areal surface roughness parameters were investigated, such as peak height and peak density, following from work by Shaw (2007), peak gradient, following from work by Do (2005), surface volume and surface height distribution, both following from observations made after fractal and PSD analyses. In every case, a trend for changing surface texture with polishing could be clearly identified, and some correlation with friction could be seen for the individual aggregates, but a single correlation could not be generated.

The effect of filtering the surface before calculation of roughness parameters was explored; it was found that, in general, removing the longest wavelength features from the measured surface improved the parameter's response to polishing for both aggregates and for all types of roughness parameter. This remained true for measurements made with each of the three objective lenses (5X, 10X and 20X) even though the longest wavelength measured was different in each case by virtue of a smaller area being measured at higher magnification. Filtering by selection of the packet of wavelengths that PSD analysis indicated should change more than others for gritstone (357  $\mu\text{m}$  to 600  $\mu\text{m}$ ) did not provide any additional benefit over removal of the longest wavelength.

For completeness, all roughness parameter and filter length combinations were inspected for correlation with changing friction, as a continuum across both aggregates. Only one additional roughness parameter was suggested by this method ( $S_{al}$ , the autocorrelation length) and, given the average values presented, it was reasoned that the correlation was likely to have occurred by chance rather than for physical reasons, although it should be considered during further work (see Chapter 9).

## 8.8 General discussion

It has already been stated that the (continuing) development of a robust methodology for inspection of aggregate surfaces is the most important part of the work undertaken so far. Measurement in three dimensions has greatly improved the ease with which qualitative analyses can be made. Throughout, it has been possible to compare likely polishing mechanisms for the two aggregates with surface texture measurements and numerical characterisation of those measurements.

The proposed polishing mechanisms can be compared with the theories of friction (Section 2.1) as follows.

When limestone is polished, the amplitude of short wavelength features is reduced but some of the long-wavelength texture is retained. Friction reduces as the surface is polished because there are fewer points of contact with the sliding rubber, the rest of the surface having been obscured by a film of water.

When gritstone is polished, the amplitude of long wavelength features is greatly reduced but some of the short-wavelength texture is retained. Friction reduces because the long-wavelength texture is being removed, probably reducing the contribution to friction from hysteretic loss, but it reduces less quickly than for limestone because short wavelength texture is still present to break through the water film ensuring friction via adhesion.

It appears that a loss of amplitude at any wavelength results in a reduction in friction. However, that reduction is greater when shorter wavelength features are removed. Referring back to qualitative analysis, the differentiation between short and long wavelengths in this context can be compared to the appearance of the aggregate surfaces at 20X magnification (Figure 6.14). On the scale of that field of view, 0.7 mm wide, limestone still retains some texture, but gritstone does not. During quantitative analysis it was noted that parameters generally gave a better response to polishing when the longest wavelengths present were filtered out. These filter lengths were 0.8 mm, 0.25 mm and 0.08 mm.

The definition of 'microtexture', wavelengths shorter than 0.5 mm, asserted by PIARC (1987) as being the scale of texture important for friction at low speeds, has therefore been confirmed by the experiments presented in this thesis.



## 8.9 References

- Do, M. T. (2005). Relationship between microtexture and skid resistance. *BLPC 255*, 117-136.
- Do, M. -T., Tang, Z., Kane, M., & de Larrard, F. (2009). Evolution of road-surface skid-resistance and texture due to polishing. *Wear* 266, 574-577.
- Shaw, R. (2007). *An examination of novel roughness parameters to be used in conjunction with the HSE slips assessment tool (SAT)*. London: Health and Safety Executive (HSE).



## **9 Conclusions and recommendations for further work**

---

As with the introduction to this thesis, the conclusions presented below are simple. The research aims set at outset have been met and it can be reasonably argued that the work presented in the preceding chapters has advanced the field of friction/texture comparison for road stones. Recommendations are made for further work.

## 9.1 Conclusions

The research questions posed at outset are shown below in red italics. Possible answers to the questions, where the work described in the preceding chapters has offered a solution, are suggested with each question.

- *Which wavelengths of texture are important?*

All of them. Actually, it has only been possible to show that all wavelengths of texture are affected by polishing limestone and gritstone surfaces. Just because a wavelength of texture has been changed by polishing and that polishing has brought about a change in friction does not, from a causality point of view, necessarily mean that particular wavelength affects friction. However, because of the different polishing mechanisms exhibited by the aggregates, it has been shown that a loss of short-wavelength texture (on limestone) is associated with a decrease in friction and a loss of long-wavelength texture (on gritstone) is also associated with a decrease in friction.

- *What form does the texture take?*

That depends on the stone. Texture form before polishing is not totally dissimilar but once polished, which is an important state in terms of an in-service road, limestone comprises large smooth asperities while gritstone comprises flat rough surfaces. The texture is related to the mineralogy of the aggregate and other aggregate types will be different.

- *How can the relevant texture be numerically characterised?*

Using roughness parameters. Hypotheses proposed after early work in the study of friction and texture for road stones, for example by Yandell (1970) and Forster (1989), that numerical characterisation required measurements of asperity height, density or shape, or a combination of them, have been confirmed. It seems sensible to make use of parameters that already exist; amongst those described in ISO25178 (British Standards, 2012) it is possible to find parameters that make use of these measurements. It is, of course, more complicated than simply measuring asperities: data handling and filtering is important and this question has not yet been fully satisfied by the work presented.

- What is the link between texture and skid resistance?

It is complicated. As mentioned, it is not possible, using the methodology developed, to determine whether the changes in surface texture resulting from polishing are causally linked to the resulting reduction in friction. However, it does seem to be true that high amplitude texture is required for high friction and that it is beneficial if that texture is spread over a range of wavelengths. Given that friction on gritstone is higher than friction on limestone, it may also be reasonable to suggest that the lower wavelength texture found on gritstone, even after polishing, is more important than higher wavelength texture retained by limestone. Other factors should not be forgotten though – the literature, and accepted theory, suggests that the rate of change in friction with increasing speed is also related to texture at higher wavelengths than is found on the surface of gritstone aggregate particles (Section 2.5).

The more specific aims of the research have all been demonstrably met:

- Develop a methodology that will allow observation of changes in surface texture on aggregate surfaces as they are polished in the laboratory.

The development of a robust methodology has been the major part of the work presented in this thesis. It is the most novel element of the work and, hopefully, will be used in further work at TRL and adopted by other researchers as a method for exploring the polishing mechanisms and texture of aggregate surfaces with a view to further clarifying the enigmatic relationship between texture and friction.

- Observe changes in texture on more than one type of aggregate and compare the forms of the texture present and the mechanisms by which texture changes.

This aim can be simply summarised. Limestone loses low wavelength texture when it is polished but retains some long-wavelength texture. Conversely, gritstone predominantly loses long-wavelength texture while retaining short-wavelength texture.

- Evaluate several numerical methods for their ability to characterise the texture found on aggregate surfaces.

The most successful techniques found in the literature (peak height, peak density and peak angle) and more abstract techniques tried before (PSD and fractal analysis), were supplemented with an exploration of the effect and necessity of data filtering and some alternative parameters looking at volume and height distribution. Changes in surface texture due to polishing in the laboratory could be observed, quantified and compared with likely polishing mechanisms. However, the next logical step in the process, correlation with friction, was probably confounded by the different polishing mechanisms exhibited by the two aggregate types.

The germination of the project was in attempts to improve the practical measurement of road surface skid resistance without the need for contact. It seems fitting to conclude with the impact of the results of the work presented in this thesis in the context of that long term objective. That there appears to be a different relationship between texture and friction for the two aggregates (as a result of polishing mechanisms and mineralogy) is a complicating factor but not necessarily an impediment. The source and mineralogy of the coarse aggregate used in the road surface in a particular location could be recorded. This is, in fact, both currently possible, using pavement management systems, and frequently contractually required. And so texture measurements of aggregates on the road surface could be compared with a specific texture/friction relationship, suitable for the type of aggregate in use, to determine the probable friction provided.

Aside from the technical difficulty of making sufficiently high resolution measurement of surface texture, further work is required before this can be practically implemented.

## **9.2 Recommendations for further work**

Although the methodology has allowed, or will allow, considerable advancement in understanding of the relationship between friction and the texture of road stones, further development would be valuable. High resolution photography, which was included in the first attempts at methodology development, should be reincorporated to assist with qualitative analysis. The possibility of using replicas of the aggregate surface should be assessed more thoroughly. The use of replicas would improve the speed at which experiments could be carried out because the whole of the polishing part of the experiment could be carried out in advance of making all texture measurements (although this is mostly relevant while the polishing equipment and measurement equipment are in different locations). The use of surface replication has the potential for provision of a permanent record of the surfaces measured. It was noted during quantitative analysis that because the initial state of the aggregate surface results from a crushing process at the quarry, rather than a polishing process in the laboratory, its characteristics may not fit with a developing trend. It may therefore be worth considering the first after-polishing stage (Stress 1) as a starting point, adding one or more additional polishing stages so that a minimum of five levels of friction is maintained.

Improvements to the methodology notwithstanding, this work could be progressed by repeating the experiment with alternative specimens. The next two experiments might use:

- A number of different gritstone aggregates. According to Thompson et al. (2004), there were 110 quarries producing aggregate classified as gritstone, greywacke, or siltstone at the time of writing. These types of rock will have mineralogies similar to the gritstone used in the work presented here. The polished stone values (PSVs), a measure of resistance to polishing, range from 58 to 75. The PSV of the gritstone used here was 63 and use of a range of other aggregates will allow a broader range of friction levels.
- A number of dolerite aggregates, including the one used in the initial stages of methodology development. There were reported to be 63 dolerite quarries in 2005, with PSV ranging from 50 to 67.

Within each of these two sets of specimens, the effect of different polishing mechanisms should be minimised. Additional factors, such as mineral composition and grain size might also be explored. Comparing the two sets of specimens will probably allow comparison of different polishing mechanisms and the feasibility of a single friction/texture relationship could be revisited.

Further in the future, if replication of surfaces can be vindicated then it could be used to easily inspect the polishing action of traffic rather than that of laboratory-based equipment. This sort of experiment has been carried out before (Neville, 1974), where a dental amalgam was used to make replicas of the surface. Texture of areas of road surface could be inspected, measured and characterised at intervals throughout the life of a surface material. The effects on texture of other factors such as seasons, road geometry and traffic density (see Section 2.5) might also be explored in this way.



### 9.3 References

- British Standards. (2012). *BS EN ISO 25178-2:2012. Geometrical product specifications (GPS) - Surface texture: Areal. Part 2: Terms, definitions and surface texture parameters*. London: BSi.
- Forster, S. W. (1989). Pavement microtexture and its relation to skid resistance. *Transportation Research Record* 1215.
- Neville, G. (1974). *A study of the mechanism of polishing of roadstones by traffic*. Crowthorne: TRL.
- Thompson, A., Burrows, A., Flavin, D., & Walsh, I. (2004). *The Sustainable Use of High Specification Aggregates for Skid Resistant Road Surfacing in England*. East Grinstead: Capita Symonds Ltd.
- Yandell, W. O. (1970). *The measurement of surface texture of road stones with particular regard to the effect on the frictional properties of road surfaces*. University of New South Wales.